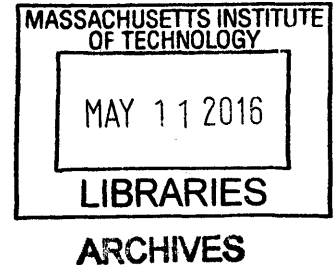# Application of Advanced Fuel Concepts for use in Innovative Pressurized Water Reactors

by
Nathan Christopher Andrews

B.S. Nuclear Engineering
The Pennsylvania State University, 2010

M.S. Nuclear Science and Engineering
The Massachusetts Institute of Technology, 2012

SUBMITTED TO THE DEPARTMENT OF NUCLEAR SCIENCE AND ENGINEERING
IN PARTIAL FULFILLMENT OF THE REQUIREMENTS FOR THE DEGREE OF

DOCTOR OF PHILOSOPHY IN NUCLEAR SCIENCE AND ENGINEERING
AT THE
MASSACHUSETTS INSTITUTE OF TECHNOLOGY

JUNE 2015

Signature of Author: **Signature redacted**

Department of Nuclear Science and Engineering
May 2015

Certified by: **Signature redacted**

Mujid S. Kazimi
TEPCO Professor of Nuclear Engineering
Thesis Adviser

Certified by: **Signature redacted**

Benoit Forget
Associate Professor of Nuclear Science and Engineering
Thesis Reader

Accepted by: **Signature redacted**

Mujid S. Kazimi
TEPCO Professor of Nuclear Engineering
Chairman, Committee for Graduate Studies

1

Application of Advanced Fuel Concepts for use in Innovative Pressurized Water Reactors

by Nathan Christopher Andrews

This work addresses several specific knowledge gaps that exist in the use of alternative fuel and cladding combinations in a pressurized water reactor (PWR) environment. In the switch from a UO_2 with zirconium-based cladding to any other combination, there is a multitude of questions that need to be answered. This work examines three of these knowledge gaps: (1) the disposition of weapons-grade plutonium in thorium and silicon carbide cladding, (2) economics of accident tolerant fuel (ATF) claddings and (3) breeding of plutonium in uranium nitride fuel.

Burning weapons-grade plutonium in a standard pressurized water reactor (PWR) using thoria as a fuel matrix has been compared to using urania. Two cladding options were considered: a 0.76 mm thick silicon carbide ceramic matrix composite (SiC CMC) and 0.57 mm thick standard Zircaloy cladding. A large benefit was found in using thoria compared to urania in terms of plutonium percentage and mass burned. A slightly smaller mass of plutonium is required in a core with SiC CMC cladding, due to its lower neutron absorption compared to Zircaloy. The thorium system was also better from a non-proliferation viewpoint, resulting in less fissile mass at discharge and more fissile mass burned over an assembly's lifetime. A limited safety comparison was made for two reactivity insertion accidents: (1) highest worth rod ejection accident (REA) and (2) main steam line break (MSLB). The MSLB accident demonstrated a safe value for the minimum departure from nucleate boiling ratio. The maximum enthalpy added to the fuel during the REA was also below current regulatory limits for PWRs. This indicates that the more negative moderator temperature coefficients of thoria-plutonia and urania-plutonia fuel, compared to a typical PWR design, were not limiting.

For an ATF cladding to replace zirconium alloys, it must be economically viable by having similar fuel cycle costs to today's materials. Four proposed materials are examined: stainless steel (SS), FeCrAl alloy, molybdenum (Mo) and SiC CMC, each having its own development time and costs. The chosen cladding thicknesses were dependent on strength and manufacturing constraints. It was found that all options may end up requiring higher enrichment than zirconium-based claddings for the same fuel cycle length. If the present value of avoiding a reactor accident with a large radioactivity release is estimated using past experience for LWR large accidents and if it is assumed that ATF cladding is able to prevent such release, there is a definite net economic benefit relative to typical Zircaloy cladding only in using SiC, since it only results in a small fuel cycle cost increase. There is only a marginal benefit in using SiC to prevent a core-only loss without radioactivity release (TMI-type) accident and a large loss using metallic ATF concepts.

The thermal hydraulic and neutronic feasibility of a nitride fueled pressurized water reactor (PWR) breeder design were examined. Because of its higher fuel density, nitride fuel would be preferable to traditional oxide fuel in attempting to achieve breeding in a PWR. The design chosen uses large hexagonal assemblies with 14 inner seed pin rows and 4 outer blanket pin

rows. In this design, reactor grade plutonium of 12.75 wt%HM was used as fuel. Nitride was also simulated as being 100% N-15, to limit neutronic penalties and C-14 production. The as-specified assembly model only achieved a fissile inventory ratio (FIR) value above 1.0 when the thimble regions were assumed to be voided, which lowers the H/HM ratio in the assembly. This led to FIR values above 1.0 for the oxide, 85% theoretical density nitride (N85) and 95% theoretical density nitride (N95). All were at an FIR of 1.03 at 35 MWd/kgHM. However, the single batch discharge burnup of the voided assembly in MWd/kgHM was 32.2 for N95, 24.5 for N85, while only 15.6 for the oxide.

Thesis Adviser: Mujid S. Kazimi
                              TEPCO Professor of Nuclear Engineering

Thesis Reader: Benoit Forget
                              Associate Professor of Nuclear Science and Engineering

Acknowledgements

Contents

List of Figures

List of Tables

15

1. Introduction

1.1 Motivation

Currently, there are over 300 pressurized water reactors (PWRs) operating in the world. Given the large number of operating PWRs and the large amount of institutional knowledge that has been created in their operation and construction, it is desirable to harness this knowledge for several missions, including both the disposition and breeding of plutonium. Currently operating PWRs use a uranium oxide, UO_2, fuel or a mixed uranium and plutonium oxide fuel in the form of 1cm long pellets stacked within a long and thin zirconium alloy cladding. However, this combination of fuel and cladding has several distinct limitations. In order to best achieve goals other than the generation of electricity in a once-through cycle, the fuel form and cladding combination itself needs to be reexamined to correctly select the best to meet the relevant goal. Particular goals of interest are the burning of weapons-grade plutonium for proliferation issues, breeding of reactor-grade plutonium for increased uranium utilization and fuel cycle economics, and the economic mitigation of severe accident through using accident tolerant fuel (ATF). This work addresses the neutronic, thermal-hydraulic and safety analyses supporting the selection of the best fuel-clad combination for various PWR design missions.

Zirconium based claddings, such as Zircaloy (which combines Zr with a variety of minor-element compositions), undergo autocatalytic reactions in water-based systems at the high temperatures found in some accident scenarios. The pickup of hydrogen on the exterior of zirconium alloy cladding is currently the primary limiting factor in keeping fuel discharge burnup below 62 MWd/kg. Higher burnups could result in both economic and proliferation benefits for the nuclear fuel cycle. Since Fukushima, in March 2011, there has been an increased interest in ceramic multilayer composite silicon carbide (SiC) as a potential accident tolerant fuel cladding. Given its lower corrosion rate, high melting point, insensitivity of its strength to irradiation and lower neutron absorption, it might allow higher fuel burnups.

Using UO_2 also presents several issues in relation to other fuel options. The presence of uranium-238 in enriched UO_2 fuel results in the generation of plutonium-239, which makes it less

desirable for use in the disposition of plutonium. In comparison to uranium nitride, uranium carbide, thorium oxide and metallic nuclear fuel, the thermal conductivity of uranium oxide is significantly lower. A higher thermal conductivity reduces fuel temperature, which limits fission gas release and provides increased margin in accidents. The relatively low heavy metal density of UO_2 in comparison to other fuel material options limits the maximum attainable burnup of a given fuel geometry and results in a higher H/HM in a water cooled reactor. The higher H/HM leads to a softer spectrum, which makes breeding in a light-water environment more difficult.

While UO_2 fuel has been shown to be very effective as a standard fuel for use in PWRs, it is not clear that it is the best fuel material for either the disposition of plutonium or for use as a breeder fuel. Several alternative fuel types offer clear advantages. The use of thoria (ThO_2) in lieu of urania (UO_2) as a fuel matrix has been investigated in the past for disposition of excess weapon plutonium. Using thorium would reduce the production of transuranics during the burning of excess weapons grade plutonium or that from spent fuel. [Lombardi et al., 2001] The majority of the previous investigations focused on a traditional fuel design with zircaloy cladding, and reactor grade plutonium fuel. [Mittag et al., 2011] However, much less work has been done looking at the disposition of weapons grade plutonium in thoria and in the use of the silicon carbide cladding with this fuel.

The concept of a light water reactor (LWR) breeder reactor has been examined for a long period of time, with extensive research going back into the 1970s. While the thorium fuel cycle was the main choice in the 1970s, currently, there is more interest in reduced moderation boiling water reactors (RBWR) for breeding. Multiple Japanese investigations and US Department of Energy (DOE)-sponsored university research programs have addressed these breeding BWR reactors. Prior to current LWR breeder research, much more work was performed into the possibility of using a pressurized water reactor (PWR) in order to breed, yet none of this work took an in-depth look at the use of uranium nitride (UN) as fuel for this purpose. Since the heavy metal density of nitride is higher than oxide, the hydrogen to heavy metal (H/HM) ratio is decreased in the core. This skews the energy spectrum to a higher energy, making breeding easier. Previous work by Feng (2011) examined the use of a uranium nitride fuel in a boiling water reactor and performed preliminary evaluations on the behavior of nitride fueled, reduced moderation PWR. However,

this work did not examine a design of the fuel assembly other than that of the boiling water reactor. For the proposed concept a variety of analyses need to be performed.

Since Fukushima, there has been increased interest in accident tolerant fuel (ATF) as a way to prevent both reactor loss and the large early release of fission products in case of severe accidents. Many different ATF claddings have recently been proposed, including stainless steel (SS), an alloy of iron-chromium and aluminum (FeCrAl), a tri-layer zirconium, molybdenum and FeCrAl composite (Zr-Mo-FeCrAl) and silicon carbide with a ceramic composite (SiC-CMC), which is a three layer composite. However, the economics of accident tolerant fuel is in question because the primary options have a long development time and a possible enrichment penalty. An economic assessment of the benefit to the nuclear industry from different ATF cladding materials needs to be performed, based on the net present value (NPV) of any future fuel cladding changes. In order to determine the overall cost of any fuel cladding changes, cladding development, manufacturing cost and enrichment savings/penalty need to be considered. These costs need to be evaluated against how much could be saved in the prevention of various accidents.

1.2 Objective

This work seeks to address several specific knowledge gaps that exist in the use of alternative fuel and cladding combinations in a pressurized water reactor environment. In the switch from a UO_2 with zirconium-based cladding to any other combination, there is a multitude of questions that need to be answered. Here, neutronic and thermal-hydraulic modeling of alternative core and assembly designs is performed. Such designs are then evaluated in transient and accident scenarios.

The first question addressed is how the use of thorium as a fuel material impacts the plutonium burning characteristics, steady-state behavior and core transient behavior of a pressurized water reactor system. Using weapons-grade plutonium as a fuel, the behavior of a thoria-plutonia

20

system is compared to a urania-plutonia system. This is done to determine just how much a thoria fuel with weapons grade plutonium would differ from one based on typical urania fuel, where the majority of previous experience exists. Both thoria-plutonia and urania-plutonia fuel are examined with typical zirconium cladding and thee layer silicon carbide cladding. The effect of silicon carbide cladding on the plutonium burning characteristics and core behavior in both steady state and transient conditions is also assessed in the same way the change in fuel is. A literature review is provided covering the use of thorium as a fuel, the disposition of plutonium in urania and thoria based fuel, relevant core designs, and background information on the use of silicon carbide as a cladding.

Secondly, the effect of changing the fuel from uranium oxide to uranium nitride in a PWR breeding system is examined. Because of the increased heavy metal density of UN, it is believed that the fuel will provide a benefit to plutonium breeding. However, previous research has indicated that tight-lattice PWRs have problems maintaining a negative void coefficient of reactivity. [Shelley, 2003] This problem could be further exacerbated by the increased heavy metal content of uranium nitride fuel. This work examines how switching to nitride fuel from oxide fuel impacts the breeding characteristics of a tight-lattice reduced moderation PWR system. Additionally, it examines the effect of this switch on the thermal-hydraulic characteristics and accident performance of the system. An in-depth literature review is not included for uranium nitride fuel or tight-lattice breeding PWR designs since this was previously performed by Feng (2011).

The third objective of this thesis is to examine how economic multiple accident tolerant fuel cladding options fare when both the cost of implementing the option and its potential accident prevention benefits are assessed. Essentially this work is an attempt to answer whether or not the accident prevention benefit is worth the increased cost. To this end, stainless steel (SS), FeCrAl, a tri-layer molybdenum composite and silicon carbide with a ceramic composite design are all examined. These results are then compared to the results obtained by other researchers in the field.

1.3   Literature Review

1.3.1   Background on Weapons-Grade Plutonium Disposition in Thoria and Urania with Silicon Carbide Cladding

As a result of the Cold War weapons activities and subsequent agreement to gradually reduce the nuclear weapon warheads, there are significant amounts of excess weapons-grade plutonium in multiple countries, including the United States. The amount of plutonium stockpiled by selected countries can be seen in Table 1-1. The US and Russia agreed to burn the excess plutonium in their reactors, thus benefiting from the material while altering its isotopic content and embedding it in a highly radioactive spent reactor fuel. Recently, the NRC approved the use of mixed oxide (MOX) as fuel in TVA reactors to burn this plutonium. Additionally, in all the listed countries in the Table except for the US, there is interest in burning transuranics from spent nuclear fuel, using reactor designs similar to currently operating LWRs. [Broeders et al, 2000] Since such reactors can be loaded periodically with fresh fuel, on the order of half a ton of plutonium may be used as the fissile per reactor per year (when one third of the fresh fissile is assumed to be mixed Pu-U oxide).

Table 1-1: Plutonium stockpiles of selected countries [IPFM, 2014]

Country	Non-civilian Pu MT	Civilian Pu MT
United States	87.0	0
Russia	128.0	50.1
France	6.0	57.5
United Kingdom	3.5	91.2
China	1.8	0.014
Japan	0	47.1

Similar to most previous investigations, this work will focus on pressurized water reactors (PWR) since both the United Kingdom and United Stated governments have expressed interest in disposing of weapons material in PWRs. [Worrall and Grove, 2005] Designs of advanced fuel

containing the weapons grade plutonium are evaluated based on their effectiveness in burning the plutonium and the non-proliferation benefit in the fuel cycle involved.

A comparison of the typical isotopic composition of weapons grade plutonium compared to reactor grade plutonium can be seen in Table 1-2. Among the isotopes listed, Pu-239 is the principal fissile isotope. As listed, Pu-239 concentration by weight is 50% greater in weapon grade plutonium compared to reactor grade. For the same mass of total Pu, this results in a larger amount of reactivity in the core due to fewer neutron absorptions that do not cause fission. In order to control the excess reactivity and avoid high peak-to-average fuel pin power ratios, a higher degree of neutron absorbers (e.g. "poisons") are needed in the core for the same Pu loading in wt%HM. These neutron absorbers help to dampen local power peaking and reduce the amount of soluble boron in the coolant. Due to deviations in core design and delayed neutron characteristics from U235 fission compared to plutonium fissions, it is necessary to perform transient safety analysis and compare UO_2 -PuO_2 and ThO_2 -PuO_2 core performance to traditional low enriched UO_2 core. Of particular interest are accidents that result in reactivity insertion in the core.

Table 1-2 : Isotopic composition (wt%) of typical weapons grade plutonium and reactor grade plutonium [Chodak, 1996]

Isotope	Weapons Grade	Reactor Grade At 50 MWd/kg
Pu-238	0.012	1.3
Pu-239	93.8	60.2
Pu-240	5.8	24.3
Pu-241	0.23	8.3
Pu-242	0.022	5.1
Am-241	0.13	0.8

A potential benefit to fuel switch from urania to thoria lies in the material properties of a thoria-plutonia fuel, which may allow a higher burnup than urania based fuel types. [Cozzo et. al., 2005] [Karam et. al., 2008] The ability to achieve higher burnups could result in both economic and proliferation resistance benefits, but is currently limited by the zirconium based cladding. If

a material can function as a fuel cladding with less tendency to corrode, particularly at somewhat elevated temperatures, higher fuel burnup may be possible. In 2005, Westinghouse announced to the NRC that it is considering SiC as a cladding material for LWR fuel. However, SiC is brittle which has led designers to propose a three layer ceramic matrix composite (CMC) as a cladding. Due to current manufacturing constraints, CMC has to be thicker than current zirconium based cladding. This three layer CMC consists of a ceramic inner monolith, surrounded by interwoven SiC threads which is then coated with a SiC layer, to act as an environmental barrier to limit corrosion of the load carrying composite layer. To keep the hydraulic diameter of the fuel assembly the same as currently operating reactors, the larger cladding thickness implies a smaller pellet thickness (assuming the same gap thickness). A comparison of the CMC to Zircaloy cladding pin dimensions can be seen in Table 1-3.

Table 1-3: Geometry of Zircaloy and "medium-thickness" SiC fuel pins for a typical 17x17 Westinghouse 4-Loop PWR fuel assembly [Westinghouse, 2014]

Geometry	Zircaloy	SiC
Fuel Pellet Outer Diameter (cm)	0.819	0.781
Cladding Inner Diameter (cm)	0.836	0.798
Cladding Outer Diameter (cm)	0.950	0.950
Fuel Rod Pitch (cm)	1.26	1.26
Clad Density (g/cm^3)	6.55	2.85

Another concern that arises with SiC is its lower thermal conductivity, after irradiation, in relation to metallic zirconium. Due to its higher modulus of elasticity (E=stress/strain in the elastic region), SiC cladding also does not creep down onto the fuel, as the zirconium cladding does early in operation. This results in a larger fuel-cladding gap size that lowers the gap conductance, which increases the fuel temperature. This higher temperature leads to an increase in fission gas release, which increases the internal pressure of the fuel pin, potentially leading to increased chance of failure. In an effort to increase the gap conductance and lower the fuel temperature, different materials are examined as clad-gap fillers.

1.3.2 Thorium as Nuclear Fuel Material

Thorium was one of the original nuclear fuel materials examined at the inception of the nuclear reactor program in the United States. A proof of concept demonstration was performed in the final core of the Shippingport Atomic Power Station (APS), which was a Department of Energy owned plant. [Olsen et. al, 2002]. The Shippingport Light Water Breeder Reactor (LWBR) was a pressurized water cooled reactor that utilized a U-233 and Th-232 fuel cycle. [Olsen et. al, 2002] The fuel itself was 1 to 5% uranium in a Thoria matrix, with the uranium more than 98% enriched with U-233. [Olsen et. al, 2002] The reactor core was developed by Pittsburgh Naval Reactors beginning in 1965, and fuel fabrication was finished in 1976. [Olsen et. al, 2002] The LWBR operated from 1977 to 1982 at the APS and generated over 29,000 effective full power hours (EFPH) or energy. [Worrall et. al., 2012] Additionally, the Elk River and Indian Point reactors also used a solid fuel solution of UO_2 and ThO_2, as highly enriched uranium oxide in a thorium oxide matrix [Chodak, 1996]

Work at MIT conducted in the 1980s by Kamal et. al. (1982) focused on the use of thorium for improved uranium utilization, by using thorium fuel for breeding. The thorium was examined both interspersed in assemblies as single pins and in full thorium assemblies on the core exterior. In the early 2000s, there was renewed interest in Thorium. Wang (2003) examined a seed and blanket thorium-uranium fuel cycle for PWRs. Included in the work was the modification of the fuel performance code FRAPCON. Shwageraus (2003) examined the neutronic behavior of a thorium-based PWR nuclear system.

In addition to being proposed as a breeding material, when being used with U-233; thorium has also been examined as a fuel matrix for burning of plutonium. A thorium and plutonium fuel would produce no new plutonium during irradiation, increasing the net consumption rate of plutonium. Lombardi, et. al. (1995) discussed the possible use of thorium in this manner. An in-depth review of plutonium-burning PWR designs is discussed in a later section.

The thorium fuel cycle and/or plutonium disposition in thorium have been examined in depth by the United States, the United Kingdom and India among other countries. [Worrall et. al., 2012]

In India, thorium in conjunction with the U-233 it produces is being examined for a future self-sustaining nuclear fuel cycle. This fuel cycle work has governmental support, with thorium-based reactors and fuel currently being designed by national labs in India. Fuel assemblies manufactured out of U-233 and thorium will be irradiated in the planned Advanced Heavy Water Reactors (AHWR). Work at Idaho National Laboratory by Herring et. al. (2000) discussed the uranium-thorium based fuel, concluding that there was both an economic and proliferation benefit to its adoption. However, subsequent research by AREVA puts the economic conclusions of this study in doubt. [Worrall et. al., 2012] The United States and Germany examined thorium as a breeder material in the High Temperature Reactor (HTR) designs. This is because the very high burnups in the HTR resulted in more U-233 production. [Worrall et. al., 2012] The United Kingdom has recently been examining thorium-based fuels for the disposition of excess weapons materials and the adoption of a thorium-based fuel cycle. [Worrall et. al., 2012]

Research at companies such as LightBridge and Thor Energy into thorium as a fuel is also being performed. LightBridge has been working on a two-part fuel assembly for PWRs, containing a central seed and an outer blanket region. [Worrall et. al., 2012] Thor Energy is currently designing and testing thorium-plutonium fuel pellets in the Halden reactor in Norway. [Bjork (b), 2013]

1.3.3 Plutonium Disposition in Thorium

Uranium has often been explored as the fuel of choice for the disposition of plutonium in LWRs. Mixed UO_2 and PuO_2 fuel is most commonly referred to as mixed-oxide fuel (MOX). This term is only used in this paper for uranium-plutonium oxide fuel and not thorium-plutonium oxide fuel. France, the UK, Russia and Japan have MOX fuel fabrication plants. The United States was constructing a fuel fabrication plant in Savannah River that is currently on hold due to cost overruns. Using a thorium-plutonium oxide fuel to dispose of plutonium has a significant advantage over uranium in that more plutonium cannot be produced in the fuel. Both Th-232, the primary isotope of thorium, and U-238 are fertile isotopes. After Th-232 captures a neutron and

becomes U-233, while U-238 become Pu-239 after neutron capture. These neutron capture and decay chains can be seen in Figure 1-1.
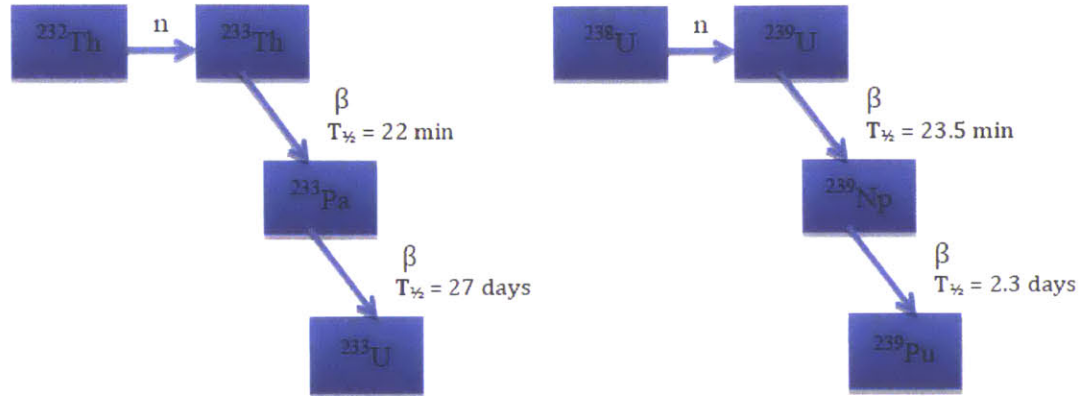
Figure 1-1: Neutron capture and decay chains of fertile isotopes U-238 and Th-232 [US NRC, 2013]

To measure the effectiveness of any burning reactor design and fuel management strategy, one of the most important parameters is the conversion ratio. This is the ratio of the neutron capture rate of fertile isotopes over that in fissile isotopes. It can be seen in Equation 1-1. In this work, the goal is to minimize this ratio so as to minimize amount of fissile material remaining at fuel discharge.

$$CR = \frac{\int \Sigma_c^{fertile}(E) \cdot \phi(E) dE}{\int \Sigma_c^{fissile}(E) \cdot \phi(E) dE} \cong \frac{gains}{losses} \qquad (1\text{-}1)$$

Previous work at MIT by Shwageraus et. al. (2003) demonstrated theoretically the viability of using ThO_2-PuO_2 fuel to dispose of reactor-grade plutonium. The analysis considered thorium-plutonium fuel of varying compositions placed in assemblies with different hydrogen-to-heavy metal (H/HM) ratios. It was concluded that such a system had a Pu destruction rate of ~1000 kg of transuranics (TRU) per GWe-yr. [Shwageras et. al., 2003] It was also shown that denaturing the resultant U-233 with U-238 reduces the plutonium destruction rate by roughly 20%. An equilibrium core study performed by Lombardi et. al. (2001) compared thorium oxide to uranium oxide fuel, to see which fuel type was more preferable for burning plutonium. It was shown that with the same fuel geometry, 47% of initial plutonium remained at discharge when using thorium, while 59% of initial plutonium remained when using uranium. [Lombardi, 2001]

27

Previous research into mixed thorium and plutonium fuel has defined both assembly-level and full core designs. Four previous design studies are presented in this section so that the current design can be placed in the context of other work. These studies all use Zircaloy as fuel cladding.

Dziadosz et. al. (2004), designed an assembly fueled with weapons grade plutonium and thorium. The assembly showed advantageous behavior for plutonium disposition over similar uranium-plutonium assemblies. From this design, core-level behaviors were inferred and a preliminary qualitative safety analysis of a core was performed. Four main safety conclusions were reached. First, the behavior of the core during an anticipated transient without scram (ATWS) needs to be more thoroughly analyzed to ensure a thorium core would meet current licensing procedures. Second, the material properties of a thorium-plutonium mixture are not well known and need to be improved. (Current work along this front is being performed by Thor Energy, which is irradiating such fuels at the Halden Reactor in Norway.) Third, boron is less effective as a neutron absorber than in similar uranium cores. Finally, it was recommended that a broader range of transient analyses be performed, especially loss of coolant accidents (LOCAs). The assembly used for this analysis is shown in Figure 1-2.
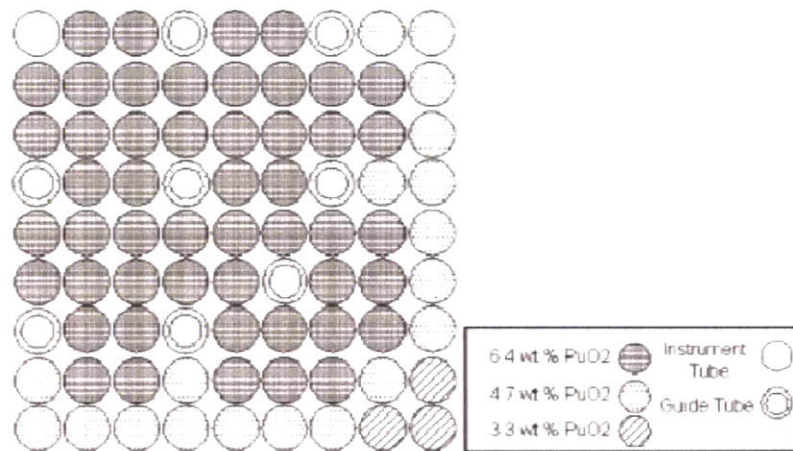
Figure 1-2: Southeast quadrant of the Westinghouse 17x17 fuel assembly designed [Dziadosz et. al., 2004]

Fridman and Kleim (2010) presented a full-core model of an equilibrium core, which used thorium mixed with reactor-grade plutonium as fuel. For burnable poison in the core, wet annular burnable absorber (WABA) rods were used. The core simulation showed a delayed neutron

fraction (β) two times smaller than a traditional enriched uranium core. Additionally, because of the reduced effectiveness of burnable poisons to control excess reactivity, B_4C was needed in the control rods instead to the AgInCd, which is currently used in PWRs. The loading pattern developed was for a typical 4-loop Westinghouse PWR, with 17x17 fuel assemblies. It can be seen in Figure 1-3.
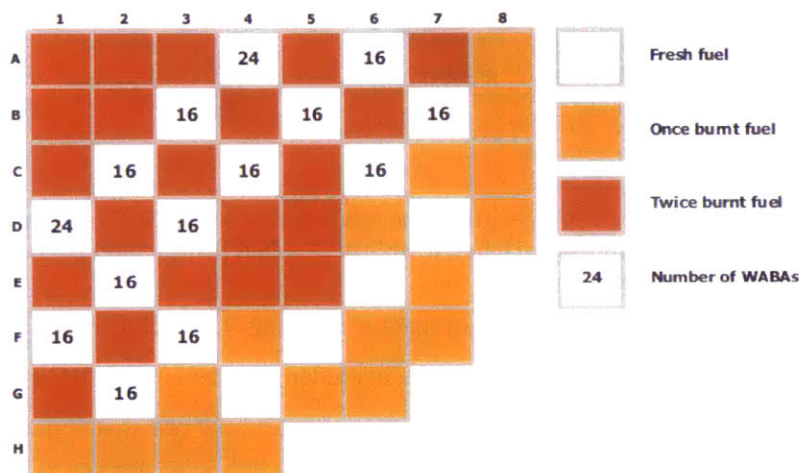
Figure 1-3: Low leakage core loading pattern (southeast quadrant) showing the location of the burnable poison WABA rods used in the core [Fridman and Kleim, 2010]

Mittag and Kleim (2010) created a core design loaded with ~1/3 of thorium-plutonium, which contained 5% reactor grade plutonium. The remainder of the fuel was enriched uranium. The core was a typical Westinghouse 4-loop PWR, and the assembly had a 17x17 fuel array. This can be seen in Figure 1-4. This work computed the reactivity coefficients of moderator temperature, moderator density, fuel temperature and boron concentration of the mixed core described previously. It was found that these reactivity coefficient values were similar to cores with uranium-plutonium (MOX) and enriched uranium.

29
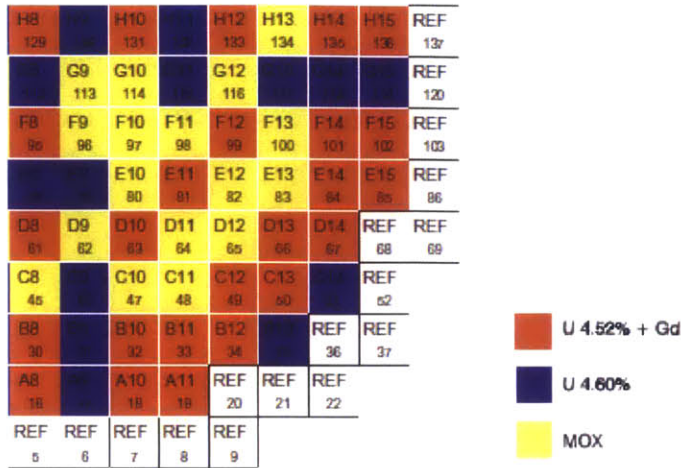
Figure 1-4: PWR loading pattern showing thorium-plutonium fuel labeled as yellow "MOX", blue and red assemblies both use enriched uranium as a fuel [Mittag and Kleim, 2010]

Bjork et. al. (a) (2013) simulated the Swedish reactor Ringhals 3, which is 3135 MW_{th}. For the design, a 3-batch reload scheme was used and the cycle length was 12 months. The core was simulated using the CASMO/SIMULATE code package; the same one that is used in this analysis. The assemblies modeled had a 17x17 fuel array and contained reactor grade plutonium, using IFBA as a burnable poison. Fuel rods contained 9.0% to 13.7% reactor grade plutonium mixed with thorium. Since the shutdown margin for the reactor was negative when the typical AgInCd was used, the control rods were switched to enriched B_4C that had 60% boron-10 instead of the natural composition of 19.8%. Additionally, safety coefficients and accident scenarios were evaluated. The loading pattern and assembly design for this work can be found in Figure 1-5.
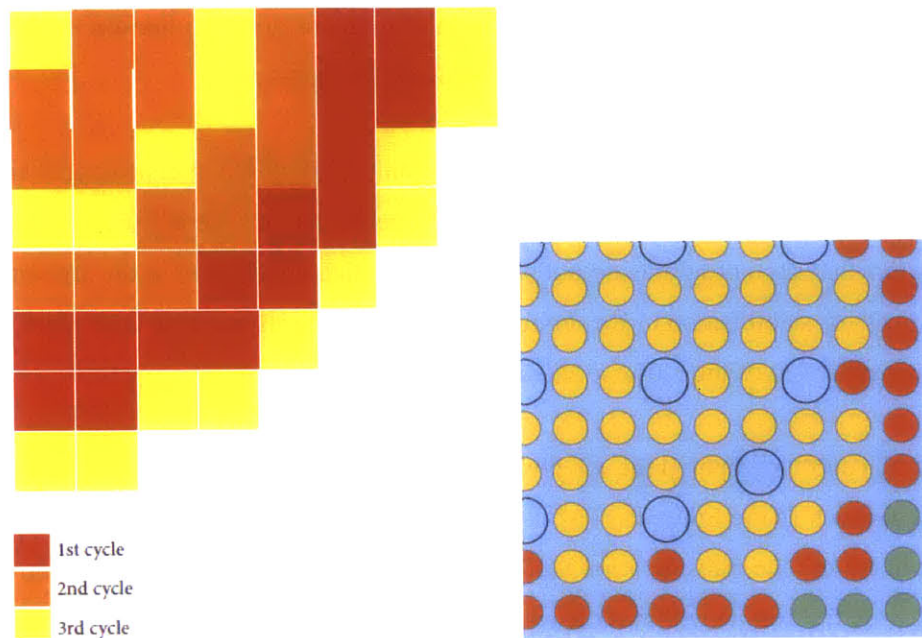
Figure 1-5: Core loading pattern (left) developed by Bjork et. al. (a) (2013), and corresponding assembly design (right)

Shwageraus and Feinroth (2010) discussed the potential of silicon carbide cladding for thorium-plutonium fuel for extended burnups up to 126MWd/kg. Current fuel performance results, however, place doubts on the ability of the fuel rod to survive to this burnup point. This work was continued by Bloore (2013), who created designs for pressurized water reactor cores using reactor-grade plutonium-thorium fuel with thick silicon carbide cladding.

1.3.4   Mixed Oxide Plutonium Disposition in PWRs

The use of a mixed uranium-plutonium oxide fuel form to burn plutonium, either from spent fuel or weapons activity, had been applied in reactors in Europe for decades. It has also been demonstrated by multiple researchers that while a LWR system and uranium-based fuel can be used to dispose of excess plutonium, it is less effective than fast reactors or thorium. [Broeders et. al., 2000] Mittag and Kleim (2010) developed such a core for comparison with thorium-based fuel. The shared loading pattern for these designs can be seen in Figure 1-4. Work has also been

performed to create core designs for the disposition of weapons grade plutonium in currently operating TVA reactors, with multiple designs available in literature.

Haas and Hamilton (2000) indicated that at that time only LWR MOX fuel programs are sufficiently technologically mature to be completely operational in several European countries. They also argue that such programs do not allow for significant reduction in the amount of plutonium, only for stabilization of the amount. This is particularly the case with reactor grade plutonium, where much of the plutonium is fertile.

Broeders et. al. (2000) compared the effectiveness of burning transuranics in LWRs to other reactor systems such as the European Fast Reactor and SNR-300, both of which are oxide-fueled sodium fast reactors. The transmutation half-lives, which are an indicator of the effectiveness of burning any specific isotope within these systems, can be seen in Figure 1-6. While the difference between several of the isotopes is high, the transmutation half-life of Pu-239 is similar for both fast and thermal systems. A clear advantage can be seen for all isotopes though in using a fast reactor system when the fission to capture ratio is considered, which is shown in Figure 1-7. These two plots indicate that while a thermal-spectrum PWR system is capable of disposing of tranuranics, it is not as effective as a fast-spectrum reactor for burning of the minor actinides and Pu isotopes other than Pu-239. On the other hand, LWRs exist today and their industrial needs are supplied by an existing industry. Any non-commercial type of reactor will lack the extent to which its needs of equipment already exist in the market place.
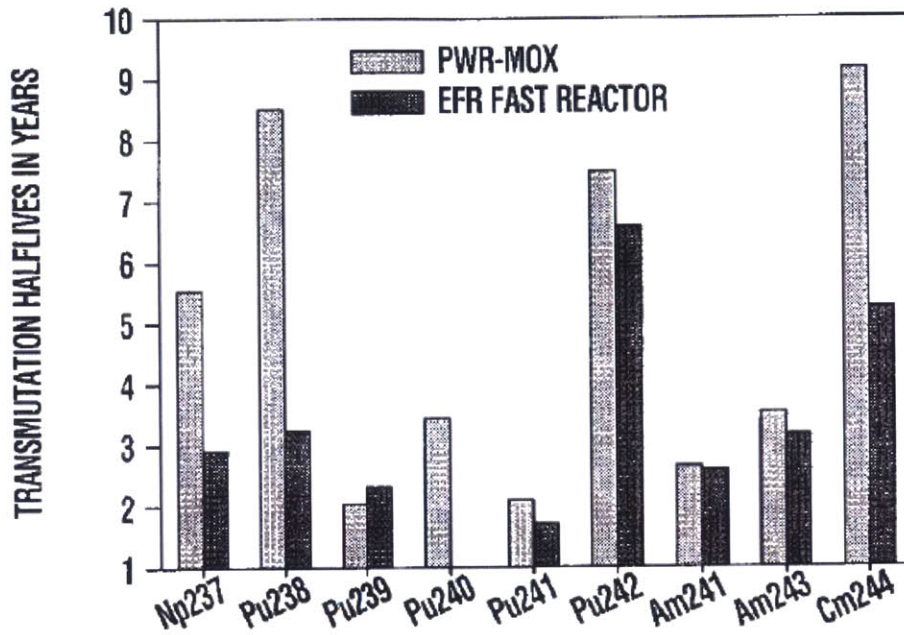
Figure 1-6: Typical transmutation halflives for transuranic nuclides in a thermal reactor (PWR MOX) and in a reactor of European Fast Reactor (EFR) type both operated on plutonium- bearing mixed oxide fuel. Short transmutation halflives have a positive impact on transuranic burning [Broeders et. al, 2000]
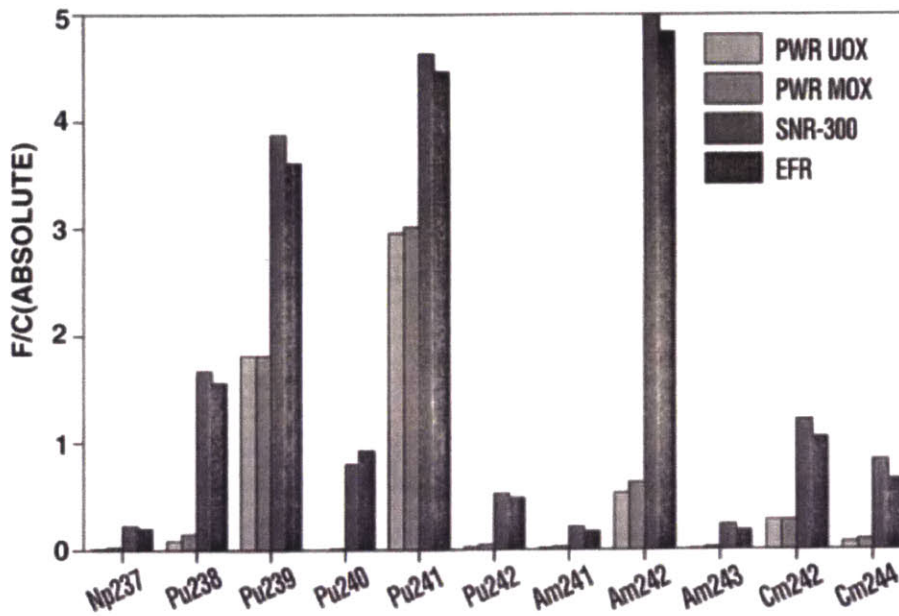
Figure 1-7: Ratio of fission to capture reaction rates (F/C) in thermal and fast reactors. High F/C ratios are favorable for burning long-lived nuclides. [Broeders et. al, 2000]

1.3.5 Design Considerations for a Typical PWR fuel with Weapons-grade Plutonium and Thorium, using SiC Cladding

When switching fuel in a typical PWR from low-enriched uranium to weapons-grade plutonium, the transient behavior of the reactor can be expected to change. This is best represented by the reduction in the delayed neutron fraction and the prompt neutron lifetime. The delayed neutron fraction is the fraction of neutrons that is not emitted immediately after fission. Neutrons that are emitted immediately are known as "prompt neutrons." The lower the delayed neutron fraction, the less time you have to control a fission chain reaction. The delayed neutron fraction of a thorium and weapons grade plutonium fuel system is less than 50% of typical uranium fueled PWR. This can be seen in Table 1-4. The prompt neutron lifetime is also roughly halved for a thorium system compared to a typical PWR. This indicates the necessity of performing transient analysis, particularly for reactivity initiated accidents, such as control rod ejection and main steam line break.

Table 1-4: Core-averaged delayed neutron fraction and prompt neutron lifetime for different reactor fuel types, values are shown at hot full power and beginning of cycle

Parameter	Typical PWR	Thorium - Plutonium	Uranium - Plutonium
Delayed Neutron Fraction	0.0061	0.0029	0.0033
Prompt Neutron Lifetime *seconds*	16×10^{-6}	7.9×10^{-6}	7.3×10^{-6}

In comparison to uranium-235 and reactor grade plutonium, weapons grade plutonium, when used as a fuel, results in a larger amount of excess reactivity in the core for the same enrichment. In order to control the excess reactivity and keep local peaking below safety limits, higher amounts of burnable poison are needed in the core. Soluble boron, dispersed gadolinium in the fuel matrix and a thin coating on the exterior of the fuel pellet, known as integral fuel burnable absorber (IFBA), are all commonly used in the United States and Europe. All PWRs use soluble boron to maintain the value of the multiplication constant (k_{eff}) at unity during operation. This boron is diluted out as the cycle proceeds. In the United States, the pellet coating IFBA is used in fresh assemblies to limit reactivity. Gadolinia (Gd_2O_3), most commonly used in BWRs in the

United States, is also used in Europe to serve the same purpose for PWRs. One of the main goals of burning plutonium is the minimization of proliferation risk. The mass of fissile material that is contained in an assembly, is the metric commonly used to characterize the proliferation attractiveness of the fuel.

An additional concern that affects all calculations is that thorium nuclear data is very sparse, especially in the epithermal region. This can lead to increased uncertainty in the computed reaction rates. The thermo-physical characteristics of thorium fuels at high burnup are also not well known. In order to reduce these uncertainties, it is necessary to perform additional experiments to obtain such data.

1.3.6 Design Considerations for a Nitride-fueled Tight-lattice Plutonium Breeder

For a reactor to be considered a breeder, the conversion ratio (CR) must be greater than one. Conversion ratio is defined in Equation 1-2. [Ronen, 1990] The term breeding ratio (BR) is used when the conversion ratio is greater than one.

$$CR = \frac{\int \Sigma_c^{fertile}(E)\cdot\phi(E)dE}{\int \Sigma_c^{fissile}(E)\cdot\phi(E)dE} \cong \frac{gains}{losses} \qquad (1\text{-}2)$$

Another measure that can be used to determine if a reactor is breeding is the Fissile Inventory Ratio (FIR). This term is the ratio of final fissile mass to initial fissile mass; its definition for this analysis is shown in Equation 1-3. [Ronen, 1990] For this application, the isotopes of interest are plutonium 239 and plutonium 241, since they are the primary fissile isotopes from which power is extracted during operation.

$$FIR \cong \frac{(M^{Pu239}+M^{Pu241})_{final}}{(M^{Pu239}+M^{Pu241})_{initial}} \qquad (1\text{-}3)$$

35

A more in-depth review of conversion ratio calculation and approximations that can be made in its calculation can be seen in the work by Feng (2011). The text by Ronen (1990) on LWR breeding technology also contains more information on conversion ratio calculation.

Feng (2011) contained preliminary analysis of a nitride-fueled PWR breeder. However, the simulation was performed primarily for the purpose of scoping. The conditions of the simulation run were not the same as an operating PWR. The simulation had the geometry of an RBWR assembly and had single phase liquid at 7.2 MPa. [Feng, 2011] Since significant research has been performed previously on the optimum assembly and core design for a PWR breeder, additional work was required to determine the impact of switching from oxide fuel to nitride fuel in relation to conversion ratio. The work by Feng also indicated that the conversion ratio of a pressurized water RBWR was just below one. It was concluded in this work that by examining a PWR assembly optimized for breeding, CR should be pushed above one. [Feng, 2011]

This work identifies a promising breeding PWR design and then examines the effects on conversion ratio by switching the fuel from mixed oxide (MOX) to nitride. Also a significant literature review was performed, and is presented in Section 2.2, to determine the most appropriate critical heat flux (CHF) correlation to predict the departure from nucleate boiling ratio (DNBR) for a tight-lattice breeding PWR. The CHF and DNBR are geometry-dependent parameters

In order to obtain sufficient breeding in a LWR, the amount of moderation in the core needs to be significantly decreased in comparison to a standard PWR design. This decrease in the amount of coolant relative to the amount of fuel leads to different core cooling conditions. Accordingly, a valid correlation for DNB needs to be found. This correlation needs to match the parameters of a tight lattice PWR core. A literature review of relevant correlations is presented to determine the best correlation for use in this unique operating regime.

In comparison to a liquid metal fast reactor (which is the standard technology used for breeding), it is much more difficult for a LWR to meet the necessary conversion ratio. This is due to the increased slowing down caused by the water in the core, which acts as a moderator. To obtain

the necessary ratio, core designers introduce additional heterogeneity on both the core-wide level and the assembly level. This high degree of heterogeneity makes modeling difficult since at the bare minimum either a full core 2D model or a 3D assembly model is needed. In fact, many breeding LWRs require a full core 3D analysis. While the conversion ratio could easily be determined at the beginning of life with a full core 3D model, it becomes difficult to determine the conversion ratio at depletion points due to the computational cost to reach higher burn-ups.

While the high hydrogen to heavy meatal ratio (H/HM) that results when using uranium nitride fuel can aid in boosting the CR, other design barriers arise when using the fuel. The increased heavy metal loading makes maintaining a negative void coefficient of reactivity harder. Nitride fuel itself also presents unique fuel performance issues. Swelling, thermal and fission gas release behaviors are significantly different than oxide fuel. Nitride fuel has increased swelling in relation to uranium oxide. [Feng, 2011] Fuel performance analysis by Feng (2011) indicated that the seed region of any core should not exceed a theoretical density of 85% to maintain fuel survivability. When heated water vapor comes into contact with the UN, the following reaction occurs, forming ammonia and UO_2. [Sunder, 1998]

$$2UN + 4H_2O \rightarrow 2UO_2 + 2NH_3 + H_2$$
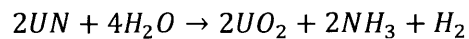
The formed ammonia also is then free to react with other metals in the system. Because of the pervasiveness of this reaction it is seen as one of the major challenges for UN being used as a fuel in an LWR. Research into how this reaction would proceed in an LWR environment has been performed by multiple national labs, vendors and many universities. It is not covered in this work.

1.4   Scope

In the second chapter of this work, methods, codes and design metrics used in this work are presented. Included are descriptions of Studsvik deterministic reactor analysis code package of CASMO4E, CMSLINK, SIMULATE-3 and SIMULATE-3K, and the continuous energy

probabilistic (Monte Carlo) code Serpent. [Studsvik, 2009] [Mielosyzk, 2013] [Leppänen, 2012] Benchmarks used to perform rod ejection and main steam line break transient safety analyses are also presented.

Presented in chapters three through five are the evaluations of potential pressurized water reactor core designs using weapons grade plutonium as a fuel with a thorium oxide matrix and with CMC SiC as a fuel cladding. Neutronic, thermal hydraulic, safety and fuel performance analyses are performed. Thoria-plutonia core and fuel designs are then compared to the results obtained from similar analyses using urania-plutonia and conventional low enriched uranium fuels in zirconium alloy cladding.

The third chapter covers three separate thorium core designs with different poison options for reactivity hold down. The designs were derived with SiC as a cladding. These options are enriched soluble boron in the coolant, dispersed gadolinium in the fuel matrix and a thin coating on the exterior of the fuel pellet, known as integral fuel burnable absorber (IFBA). The IFBA design is chosen as the best and a Zircaloy cladding version of this core is also presented.

In chapter four The IFBA thoria-plutonia designs are compared to ones using a urania-plutonia fuel. The effects of thorium as a fuel and SiC as a cladding are presented. The designs are evaluated based on safety, proliferation benefit and plutonium burning efficiency. For safety analysis, theses designs and a typical PWR are evaluated against two benchmarks for PWR accidents: rod ejection and main steam line break. These transient safety analyses are presented in chapter five.

Chapter six covers the final objective of this thesis, assessing the overall net economic benefits of accident tolerant fuel cladding options. Using the net present value of different cladding options over the projected lifetime of operating reactors, the increased costs of proposed cladding options are evaluated against the net economic benefit of severe accident prevention.

Chapter seven addresses the use of uranium nitride as opposed to uranium oxide in a tight-lattice PWR breeder reactor. Chapter six covers how switching to uranium nitride fuel affects, breeding

characteristics, thermal-hydraulic conditions and neutronics. Safety analyses are also performed, including coefficients of reactivity. These analyses are performed using the Monte Carlo neutronic code Serpent.

2. Models and Methods

This Chapter contains the design parameters and information on the codes used for core analysis and design. An introduction to these codes and their physics is contained in this chapter. Included are benchmarks of the codes and models developed for use in design and analysis. In particular there is a benchmark of the lattice physics code CASMO4E, which uses multi-group ENDF/B-VI library, against the continuous energy Monte Carlo code Serpent with ENDF/B-VII libraries. [Studsvik, 2009] [Leppänen, 2012] Operational limits that need to be met are presented. For safety analyses, moderator temperature coefficients and shutdown margins were evaluated. The metrics used for core design and safety analysis by which the designs are compared are also included.

2.1 Design Methods

2.1.1 Typical PWR used for Plutonium Burning

In this analysis a typical 4-loop Westinghouse PWR is simulated to determine the effectiveness of current PWRs at burning weapons-grade plutonium in thorium. This reactor type uses a 17x17 RFA fuel assembly type [Westinghouse, 2014] with 193 assemblies in a core. All the final cores shown and developed in this work are equilibrium cycle cores. The cores developed were depleted to the point when the core boron concentration became 0 ppm, which was reached very near 492 EFPDs, which correlates to one and a half years of full power operation, with a capacity factor of 90%. In each new cycle, 85 new assemblies are loaded into the core. 84 of these remain into the second cycle and 24 remain for a third cycle in the core. The central assembly of the core is replaced every cycle to limit maximum burnup and maintain core symmetry. Work by Bloore (2013) compared an 84 assembly reload core, to a 64 assembly reload core for designs with silicon carbide cladding and uranium fuel. The cores were designed to similar cycle burnups, as is the desire here. The 84 assembly reload core showed a lower initial fissile composition, discharge burnup and initial boron concentration. All three of these are desirable, so an 84

assembly reload scheme, with an additional fresh central assembly every cycle, was adopted in this work. A typical core and a typical assembly for this reactor type can be seen in Figure 2-1.
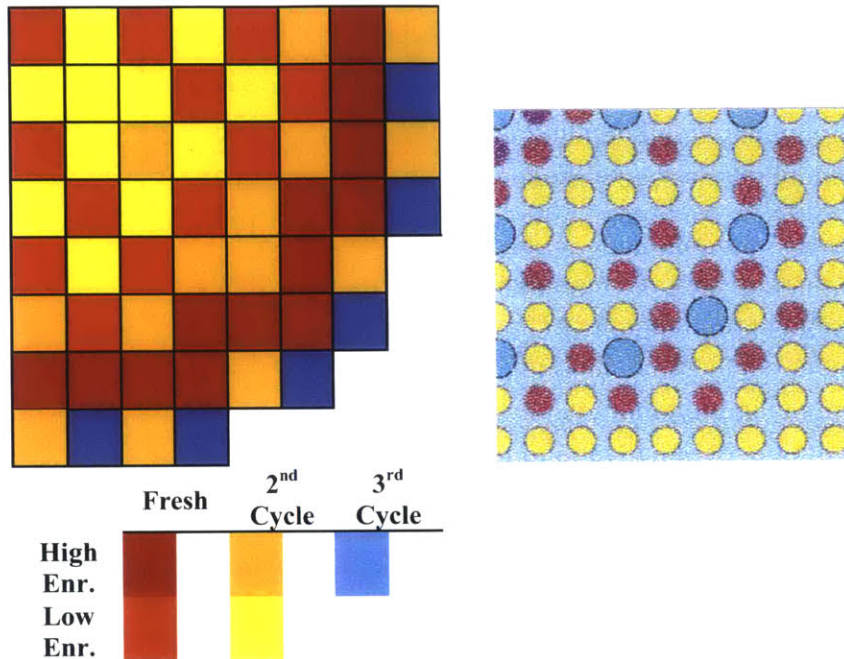
Figure 2-1: Sample ¼ core loading pattern, showing southeast quadrant (left) and sample 17x17 fuel assembly showing the southeast quadrant (right)

For the IFBA (both SiC and Zircaloy cladding) and enriched boron cores, ten cycles are run to equilibrium and the 11th cycle is used to represent an equilibrium cycle. For the Gd core, the 25th cycle is used. The higher number of cycles needed to reach equilibrium for the Gd core is due to the reactivity changes that occur during the depletion of the Gd assemblies. The typical operating parameters of a Westinghouse 4-loop PWR are shown in Table 2-1. These parameters are taken as inputs to the codes CASMO4E and SIMULATE-3.

Table 2-1: Operating parameters of a typical Westinghouse 4-loop PWR. [Westinghouse, 2014]

Parameters	4-Loop PWR
Core thermal power (MW)	3587.0
Power density (kW/L)	109.9
Core flow rate (MT/hr)	67047.0
System pressure (MPa)	15.5
Core inlet temperature (K)	565.71
Number of fuel assemblies	193
Active Fuel height (m)	3.66

The general design process is summarized in Figure 2-2. The design process begins with material and geometry specification, which then informs assembly and core-level design. Fully developed cores are then evaluated to make sure they meet design limits and shutdown margins. Then transient and fuel performance analyses are performed. This process is iterative, so the failure at any point in the process to meet design criteria leads to a new iteration in the process.

#	Step	Code
1	• Generate geometry parameters and material composition	
2	• Fuel temperature relations	*FRAPCON-MIT*
3	• Assembly level design	*CASMO4E*
4	• Develop full core loading pattern	*SIMULATE3*
5	• Check steady-state design limits	*SIMULATE3*
6	• Evaluate core for shutdown margin	*SIMULATE3*
7	• Perform transient analysis	*SIMULATE3K*
8	• Fuel performance analysis	*FRAPCON-MIT*

Figure 2-2: Overall design process of a PWR core, showing the relevant code for each design step

In this analysis, there are three primary metrics that are used to evaluate and compare the cores developed against one another. These are the fissile mass remaining at discharge, the discharged

plutonium isotopic vector and the net fraction of Pu remaining in discharged assemblies. The discharge vector is checked to ensure that the plutonium is no longer weapons grade. The mass of plutonium in a single assembly is calculated for each core type. Since Thorium breeds U-233 under irradiation, it is also necessary to track this isotope since it is also fissile.

2.1.2   Uranium Nitride Fueled Tight-Lattice PWR Assemblies

Similar to the design of a typical PWR assembly, a tight-lattice design begins with material and geometry specification. In a tight-lattice assembly, instead of the typical square array a triangular pin array is used. A triangular pin array and a rod gap near 1.0 mm lead to a very low H/HM ratio. In order to analyze such an assembly design, a model is created for the Monte Carlo neutronics code Serpent. The output returned isotopic composition and k_{eff} at specified burnups. From the isotopic information, the FIR was calculated. Additionally, the single batch discharge burnup was set at the point when keff=1.0. If the simulation did not run until this burnup point, linear reactivity theory (LRT) was used to determine when the keff=1.0 line would be crossed. [Leppänen, 2012] A sample assembly geometry from Serpent can be seen in Figure 2-3.
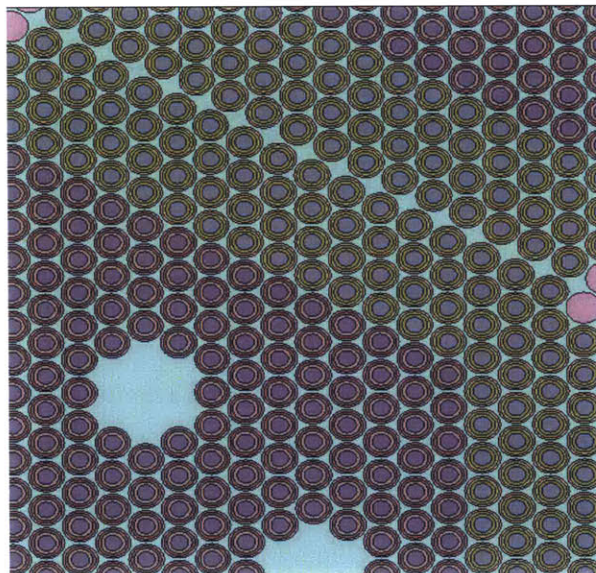
Figure 2-3: Quarter assembly, showing the seed region, blanket region and thimble tubes

After an assembly design has been verified to have a conversion ratio above 1.0 for its lifetime, the thermal hydraulic conditions of the assembly need to be evaluated. The maximum allowable power of an assembly is dictated primarily by the flow conditions. In particular, mDNBR, pressure drop and vibration limit all need to be met. They are calculated using a single-channel model. After the maximum allowable power for an assembly is calculated, the assembly design is re-depleted using this new power. Then safety parameters are calculated. This process can be seen in Figure 2-4.
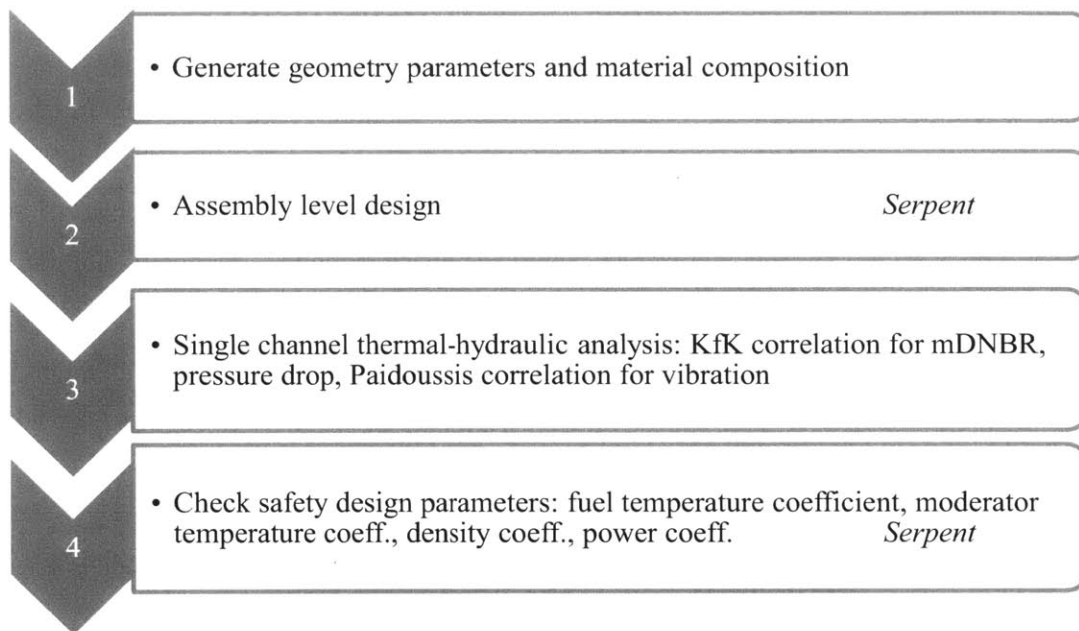
Figure 2-4: Overall design process and safety analysis of a tight lattice PWR for breeding, showing the relevant code for each design step

This design process is repeated for three separate fuels. The first is typical UO_2; the second two are both UN, one with 85% theoretical density and one with 95% theoretical density. While the 95% theoretical density is not expected to meet fuel performance limits, it provides an upper limit to breeding. These three fuel types are then evaluated against one another for their thermal-hydraulic and breeding performance.

2.2   Design Limits

2.2.1   Steady-State Design Limits and Burnable Poison Options for Typical PWR Cores

As mentioned previously, thermal and safety limits both need to be met. In a PWR, the primary thermal design condition is to prevent departure from nucleate boiling (DNB). If boiling in a PWR moves from nucleate boiling to the vapor film boiling regime, then the heat removal capacity of the coolant is significantly reduced. This could result in cladding overheating and fuel melt. Two design parameters that are used to prevent this from occurring are the hot channel enthalpy peaking factor and a pin peaking factor. The hot channel enthalpy peaking factor ($F_{\Delta H}$) is a measure of the relative amount of thermal energy added to any fuel rod subchannel in the core, shown in Equation 2-1.

$$F_{\Delta H} = \frac{Maximum\ Enthalpy\ Added\ in\ a\ Fuel\ Rod\ Subchannel}{Average\ Enthalpy\ Addition\ in\ a\ Fuel\ Rod\ Subchannel} \qquad (2\text{-}1)$$

The peaking factor (F_Q) is the heat generation rate of the single hottest location (e.g. Node) on a pin within the core, relative to the core-averaged pin heat generation rate. It is shown in Equation 2-2.

$$F_Q = \frac{Maximum\ Linear\ Heat\ Generation\ Rate\ at\ a\ Node}{Average\ Linear\ Heat\ Generation\ Rate} \qquad (2\text{-}2)$$

In order to meet neutronic safety limits, the moderator temperature coefficient (MTC), which is a measure of the core's neutronic reactivity response to changes in coolant temperature, needs to be maintained at a negative value when the reactor is operating at hot full power (HFP). This can be seen in Equation 2-3. Changes in the coolant temperature leads to changes in the moderator density which leads to a different moderation level by the coolant, resulting in a change in power. Additionally, at hot zero power (HZP), the value of this coefficient should be maintained below +5pcm/°F.

45

$$Moderator\ Temp.Coefficient = \frac{Reactivity\ Change\ due\ to\ Moderator\ Temp.Change}{Moderator\ Temperature\ Change} \qquad (2\text{-}3)$$

Another important parameter is the Doppler temperature coefficient that is required to be negative. This is a measure of the negative neutronic feedback that enters into the system when the fuel temperature is raised. As the fuel temperature rises, Doppler broadening of cross-section resonances occurs causing more non-fission absorptions to occur, leading to the negative feedback. The formula for this can be seen in Equation 2-4.

$$Doppler\ Temp.Coefficient = \frac{Reactivity\ Change\ due\ to\ Fuel\ Temp.Change}{Fuel\ Temperature\ Change} \qquad (2\text{-}4)$$

The power coefficient of reactivity, in a reactor must be negative so that the fission reactions are not self-reinforcing as power increases. The power coefficient is expressed in Equation 2-5.

$$Power\ Coefficient = \frac{Reactivity\ Change\ due\ to\ Power\ Change}{Core\ Power\ Change\ Change} \qquad (2\text{-}5)$$

Another neutronic design parameter that needs to be met is the shutdown margin (SDM), which is a measure of how effective the control rods are at shutting down the core. The SDM needs to be above 1300 pcm. Typically, a PWR uses AgInCd control rods. However, when using weapons-grade plutonium; these do not give a large enough shutdown margin. Therefore, B_4C rods, which are used in the control blades of BWRs are used in the core designed here instead. The calculation of the shutdown margin can be seen in Equation 2-6. The control rod worth, minus the highest reactivity worth rod cluster is calculated. This takes into account the possibility of a rod cluster being stuck and not scramming when needed. This worth needs to offset the core power defect, which is a measure of the reactivity added when the core is taken from a HFP condition to a HZP condition. There are also penalties for one control rod bank to be inserted 30% and a penalty for the collapse of any voids present in the core.

$$\textbf{SDM = (Full Core Rod Insertion Worth)} - \textbf{(Worst Stuck Rod)} -$$
$$\textbf{(Core Power Defect)} - \textbf{(Bank Insertion Penalty)} - \textbf{(50 pcm void penalty)} \qquad (2\text{-}6)$$

It is also necessary for the initial boron concentration in the coolant to be below 1500 ppm. This controls the reactivity swing that occurs as a result of fuel depletion.

While meeting all of the limits it is also important to limit the burnup of the fuel rod. Currently the NRC limit is 62 MWd/kgU for a fuel rod; however, with SiC as a cladding it is expected that this limit can be pushed higher. [Shwageraus and Feinroth, 2010]

A summary of these limits can be seen in Table 2-2. Additionally, the core needs to be designed to meet a 1.5 year cycle length with 90% capacity factor, which comes to 492 EFPD.

Table 2-2: Summary of design limits for a typical PWR

Parameter	Limit
Cycle Length	492 EFPD
FΔH	< 1.55
F$_Q$	< 2.0
Initial Boron Concentration	< 1500 ppm
SDM	> 1300 pcm
HFP MTC	< 0 pcm/°F
HZP MTC	< +5 pcm/°F

Currently, there are four main burnable poisons used for reactivity control in PWRs: soluble boron in the coolant, a thin fuel pellet coating call IFBA, gadolinia (Gd_2O_3) intermixed in the fuel matrix and wet annular burnable absorber (WABA) which is a removable poison rod. In this study enriched soluble boron, IFBA and gadolinia are all examined as possible burnable poison options for use with a mixed thoria-plutonia fuel. Boron-10 is a large thermal absorber that is the active absorber in both soluble boron and IFBA, which is a thin ZrB_2 coating. Gadolinium-157 has the largest thermal neutron cross section of any natural element; making it both good at lowering core excess reactivity and shaping power in the core.

2.2.2 Steady-State Design Limits for Tight-Lattice PWR Cores

For any design, the first metric checked is the fissile inventory ratio at high burnup points. This is an indicator that the conversion ratio is above 1.0. After this the thermal-hydraulic limits are evaluated. The first is the departure from nucleate boiling ratio (DNBR), which is expressed in Equation 2-7. After a departure from nucleate boiling occurs, the heat transfer properties of the coolant become significantly worse, because the fuel rod is not fully wetted. This can lead to cladding deformation and failure.

$$DNBR = \frac{Heat\ flux\ at\ which\ a\ departure\ from\ nucleate\ boiling\ occurrs}{Actual\ heat\ flux} \tag{2-7}$$

The DNB is evaluated at every point axially for every pin and is highly dependent on flow conditions and geometry. The minimum DNBR (mDNBR) is the minimum value of this ratio over the whole axial length of every pin examined. It is necessary for this value to remain above 1.44. The DNB correlation used in this analysis is covered in Section 2.4.4.

In addition to the mDNBR, the core pressure drop and vibration ratio also need to be calculated. The maximum allowable pressure drop is 400 kPa and is determined by maximum available pumping power. The vibration ratio is set to a value low enough to prevent grid to rod fretting in the core. The correlation used for this analysis is the Paidoussis (1998). Both the friction and vibration correlations used are presented in Appendix A.

Like a typical PWR, coefficients of reactivity need to maintain safe values. Here the fuel, power and moderator coefficients of reactivity are all of interest. However, two other coefficients that need to be actively examined at each design step are the density and void coefficient of reactivity

$$Density\ Coefficient = \frac{Reactivity\ Change\ due\ to\ Density\ Change}{Density\ Change} \tag{2-8}$$

$$Void\ Coefficient = \frac{Reactivity\ Change\ due\ to\ Void\ Change}{Void\ Change} \tag{2-9}$$

The limits for the density and void coefficients of reactivity, other reactivity design limits and thermal-hydraulic design limits can be seen in Table 2-3.

Table 2-3: Summary of design limits used for a tight-lattice PWR

Parameter	Limit
mDNBR	1.44
MTC	< 0.0 pcm/F
Density Coefficient	> 0.0 pcm/(g/cc)
Power Coefficient	< 0.0 pcm/%
Pressure Drop	< 400 kPa
Cycle Length	> 1 year
Fissile Inventory Ratio	> 1.0
Vibration Ratio (y/d)	0.021

2.3   Neutronic Codes and Benchmarks

2.3.1   Serpent

Serpent is a continuous-energy Monte Carlo reactor physics tool with ability to perform depletion calculations. Serpent development began in 2004 at the VTT Technical Research Centre in Finland. The code is capable of both two-dimensional and three-dimensional analysis. Serpent uses a universe-based combinatorial solid geometry model. Inputted geometry consists of material cells delineated by user-specified surfaces. The code has built in lattice geometries which makes modeling assemblies and reactors much simpler. Both hex-array and square arrays can be analyzed. By default the code uses the Woodcock delta-tracking model for all particles. This tracking method is well suited to calculations which have a long mean-free-path in relation to geometries, which is typically the case for light water reactor fuel assemblies. The main drawback to using this delta-tracking method is that it is restricted to collision estimators for reaction rate calculations. [Leppänen, 2010] In reactor calculations, this can be a concern, even though there are a large number of collisions estimators, since there are more neutron paths than

collision. This also limits the effectiveness of Serpent in shielding and detector calculations. [Leppänen, 2012]

Serpent utilizes continuous-energy cross sections which have ACE format data. For this analysis ENDFB/B-VII.0 was used. Data for 432 nuclides is used at 6 different temperatures from 300 K to 1800 K. The code broadens the cross-section from a next lowest data-point if the desired temperature is not one of the ones provided only in the resolved resonance range. Thermal bound-atom scattering data for light and heavy water and graphite is included. [Leppänen, 2012]

Serpent also has built-in burnup capability, so no external coupling is required. While the number of depletion zones is not limited, the memory requirement of the depletion calculations can become restrictive. Reaction rates are normalized to the power produced and the isotopic change over a given burnup interval is calculated. The burnup mode takes into account fission products that are created and decays that occur over a specified interval. Created output files, because of the high number of isotopes and regions, quickly become large in size. Serpent has two separate models to solve the Bateman depletion equations. The first is the Transmutation Trajectory Analysis (TTA) which is based on the analytical solution of linearized depletion chains. The second is the Chebyshev Rational Approximation Method (CRAM), which is an advanced matrix exponential solution method. CRAM is used in this analysis. [Leppänen, 2012]

2.3.2 CASMO-SIMULATE Code Package

The CASMO/SIMULATE code package was developed by Studsvik for use with conventional BWRs and PWRs. In this study, the lattice code CASMO4E is used for pin and assembly level analysis to develop homogenized assembly cross sections. [Studsvik, 2009] The resultant cross sections from CASMO4E are then sent to the full-core nodal diffusion code SIMULATE3. [Studsvik, 2009] In order to link the codes, CMSLINK is used to rewrite CASMO4E outputs into a form readable by SIMULATE3. [Studsvik, 2009] Then a full-core loading pattern is developed using SIMULATE3.

CASMO4E is a two-dimensional deterministic transport solver which is based on the Method of Characteristics; nuclear data for the code is represented using a 70 energy group library developed for light water reactors, covering energies from 0 to 10 MeV. The code automatically corrects for thermal expansion effects on the input geometry. Assembly depletions are performed on a microscopic level for each fuel and burnable absorber pin. These assembly depletions also include branch cases that involve fuel and coolant temperature, coolant density, boron concentration and control rod perturbation and histories used for core-wide calculations. The CASMO4E cross-section library, E6LIB, is based on the ENDF/B-VI data file developed at Brookhaven National Nuclear Data Center. This library was then adapted for use in CASMO4E by the program NJOY-94.105. [Studsvik, 2009]

SIMULATE3 is a two-group nodal diffusion code for use with LWRs. It is based on the QPANDA (Quartic Polynomial Analytic Nonlinear Diffusion Accelerated) neutronics model, which uses fourth-order polynomial representation of intranodal flux distributions for both the fast and thermal groups. The code allows for pin power reconstruction, which is important for determining the limiting fuel pin in the core. [Studsvik, 2009]

In SIMULATE3, the equation that is used to determine the fuel temperature is user-defined, and is controlled by Equation 2-10. These terms are dependent on the fuel, cladding and gap thermo-physical evolution as a function of core residence time and are thus different for each design.

$$T_{AVE} = T_{MOD} + C_0 + [C_1 + b]P + C_2 \times P^2 \qquad (2\text{-}10)$$

where b is a function of burnup and is user-defined based on Figure 2-5, T_{MOD} is the moderator temperature and P is the fraction of rated node-average power. C_0, C_1 and C_2 are fitting parameters. C_0 was set to 0 for all cases. The other two parameters were calculated using the fuel performance code FRAPCON-MIT and are shown in Table 2-4. The burnup dependent value, b, is shown in Table 2-5. [Mielosyzk, 2013]
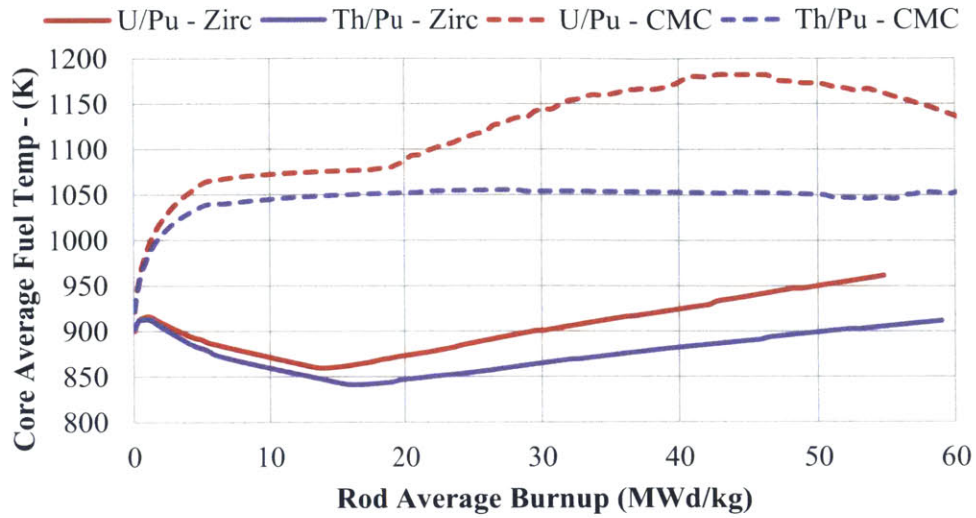
Figure 2-5: Core average fuel temperature for different fuel assembly types through cycle

Table 2-4: SIMULATE3 temperature relation coefficients

Fuel	Clad	Linear Term (C_1)	Binomial Term (C_2)
Th – Pu	Zircaloy	366.43	-19.55
	SiC CMC	345.47	-14.34
U – Pu	Zircaloy	326.39	-12.24
	SiC CMC	339.11	-8.29
Typical PWR – Enriched U	Zircaloy	316.25	-12.33

Table 2-5: SIMULATE3 burnup dependent temperature relation coefficient, "b"

Burnup *MWd/kgHM*	U/Pu SiC CMC	U/Pu Zircaloy	Th/Pu SiC CMC	Th/Pu Zircaloy	PWR
0.0	5.0	3.0	5.0	2.0	0.0
5.0	146.0	-6.5	118.0	-19.0	21.7
7.2	152.5	-16.0	123.0	-31.0	8.9
21.5	183.2	-20.7	136.0	-50.3	-8.0
45.0	266.0	43.0	135.0	-10.0	-18.6
54.0	250.0	62.0	129.0	4.0	-3.3
60.0	220.0	78.7	140.0	12.8	11.0
69.0	180.0	104.0	145.0	32.3	33.0

Typical volume averaged fuel temperature that results from these correlations can be seen in Figure 2-6 for all of the four fuel assembly types at end of life. It can be seen that the fuel temperature in cases with SiC cladding have a roughly 250 K higher temperature than with zircaloy. Additionally, it can be seen that, as result of the increased thermal conductivity and higher gap conductance, the thoria-plutonia cases have lower average fuel temperature than corresponding urania-plutonia cases.
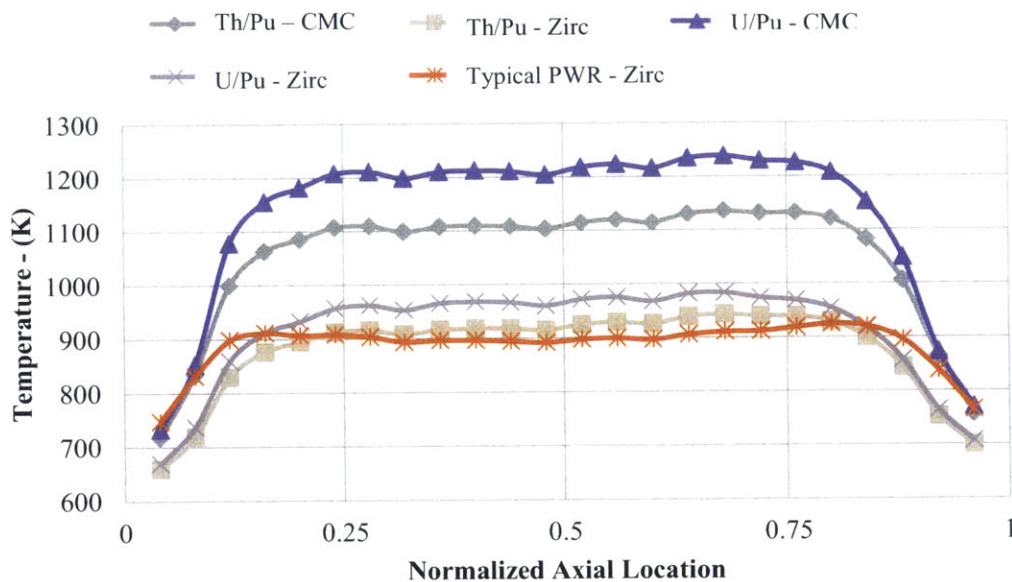
Figure 2-6: Volume averaged fuel temperature for different fuel assembly types at cycle EOL

2.3.3 Thorium Neutronic Modeling Benchmarks

Since the majority of codes developed for light-water reactor analysis have been written and optimized to work with reactor designs similar to those currently deployed, it is necessary to benchmark the behavior of these codes when they are being used with thorium. Any time fuel composition differs significantly from <5% enriched uranium, or the H/HM ratio departs from typical values seen in LWRs, a benchmark needs to be performed. Several of these benchmarks have been performed for thorium in previous research and they are either comparisons against

experimental data or a Monte Carlo code, which will converge on the solution after enough distinct neutron histories. This work presents a benchmark of CASMO4E against the continuous energy Monte Carlo code Serpent. [Studsvik, 2009] [Leppänen, 2012]

Kloosterman and Damen (1999) performed an initial benchmark of reactor grade and weapons grade plutonium fuel in thorium. This was done to examine the reactor physics aspects of a mixed plutonium thorium fuel and to assess the viability of thorium in burning plutonium. In this benchmark, burnup calculations have been performed with the OCTOPUS burnup and criticality code system, the BONAMI-NITAWL-XSDRNPM codes were used for resonance shielding and 1-D spectrum calculations and ORIGEN-S for burnup calculations. From the reactor physics standpoint, they concluded that the irradiation of plutonium in thorium oxide seemed feasible.

The International Atomic Energy Agency (IAEA) compiled an international benchmark and comparison of thorium nuclear data and modeling methods, which was performed between 1995 and 2001. [IAEA, 2003] Contributions from the United States, Russia, India and China among other countries were included. The neutronic benchmark contains both information on nuclear data and the resultant impact on lattice calculations of a PWR. Also, there is a waste toxicity benchmark in the study.

Mittag and Kliem (2010) performed a benchmark of the FZD HELIOS code package against the benchmark previously created and performed by the IAEA, showing acceptable agreement. The lattice depletion code was applied to produce diffusion and kinetics parameters, which are used as input data for the nodal diffusion code DYN3D. DYN3D is a reactor dynamic code capable of modelling LWR core transient behavior.

Bjork et. al. (b) (2013) performed experiments and analysis of a thorium-plutonium oxide fuel rodlet that was irradiated to a burnup of 37 MWd/kg. The rodlet contained 2.28% weapons grade plutonium, with the remainder being thorium. The codes MCBurn, HELIOS, CASMO5 and EET were all benchmarked against the experimental results. It was concluded that the codes showed a general ability to simulate thorium-plutonium fuel in an LWR environment. Given the uncertainties in the system and lack of knowledge regarding thorium nuclear data, the results

showed acceptable agreement, with two exceptions. MCBurn predicted a higher relative power of the thorium-plutonium pin compared to the surrounding MOX pins, and CASMO5 predicted a comparatively flat radial concentration profile of Th-232 and related isotopes. [Bjork et. al. (b) 2013]

2.3.4   Benchmark of CASMO4E against Serpent

Since CASMO4E is typically used with either <5% enriched uranium or uranium-plutonium mixed oxide, it needed to be benchmarked for use with weapons-grade plutonium and thorium. CASMO4E was benchmarked for use with thorium and reactor-grade plutonium by Bjork et. al (2013). For this benchmark, CASMO4E was benchmarked against Serpent. For this benchmark, a more conservative fuel composition was used than the assemblies used in the full core study. A thoria-plutonia pin cell with SiC as a cladding which had a fissile composition of 12.75% was analyzed to a burnup of 100 MWd/kg. The pin cell geometry can be found in Table II. A specific power of 50.0 W/g-HM was used for the analysis. In this benchmark both the fuel and moderator temperature were 600 K and there was 800 ppm boron in the coolant. The benchmark includes an analysis of both k_{eff} and the isotopic composition of the pin cell. The k_{eff} comparison can be seen in Table 2-5. It can be seen that the difference between the criticality constants calculated in the two codes increases with burnup.   This indicates that uncertainties increase in the system as the cycle progresses. Differences are mainly due to the two different cross-section libraries that the codes used. Using the values of k_{eff} shown in Table 2-6 and the reactivity difference between the two codes, the difference in burnup for the pin to have the same reactivity is 0.23 MWd/kgHM at a burnup of 60 MWd/kgHM. This places uncertainty on cycle length. The cycle burnup is 23.5 MWd/kgHM calculated for the thoria-plutonia core, the core average burnup is 40.2 MWd/kgHM and peak assembly burnup is 57.6 MWd/kgHM. Applying the 100 pcm difference at 60 MWD/kg burnup to the cycle burnup would result in an uncertainty of 1.0% in cycle length. A full core or multi-assembly model would provide a more accurate assessment of the uncertainties in the data and codes. This would take into account spatial self-shielding effects.

Table 2-6: Benchmark of CASMO4E against Serpent keff

Burnup	k_{eff}			Difference
MWd/kgU	Serpent	Uncertainty	CASMO	*pcm ρ*
0.1	1.37625	0.00079	1.37697	-38
60	1.11653	0.00089	1.11529	100
100	0.98427	0.00101	0.98065	375

The isotopic benchmark can be seen in Table 2-7 for a burnup of 60 MWd/kg and also a burnup of 100 MWd/kg. The largest difference between the two codes can be seen in Th-232, with a difference 0.08 wt% at 60 MWd/kg and 0.16 wt% at 100 MWd/kg. We believe that the agreement between the two codes is close enough for CASMO4E to be used as an analysis tool for weapons-grade Pu in Th with both SiC and Zircaloy. Since the power distribution and core neutron spectrum will be similar to current LWRs, the nodal diffusion code SIMULATE3 will also be valid for the analysis of such reactor types.

Table 2-7 : Benchmark of CASMO4E against Serpent isotopic composition at 60 MWd/kg and 100 MWd/kg

Isotope	60 MWd/kgH Burnup Isotopic Weight Percent (%)			100 MWd/kgH Burnup Isotopic Weight Percent (%)		
	CASMO	Serpent	Difference	CASMO	Serpent	Difference
Th – 232	74.08	74.00	-0.08	72.56	72.40	-0.16
U – 233	1.16	1.20	0.04	1.56	1.60	0.04
U – 234	0.101	0.110	0.009	0.216	0.235	0.019
U – 235	0.020	0.020	0.001	0.058	0.060	0.002
Pu – 238	0.017	0.017	0.000	0.050	0.047	-0.002
Pu – 239	4.521	4.489	-0.032	1.634	1.642	0.008
Pu – 240	1.610	1.619	0.009	1.443	1.447	0.004
Pu – 241	0.812	0.786	-0.027	0.940	0.888	-0.052

CASMO4E used the ENDF/B-VI nuclear data library, while Serpent used ENDF/B-VII.0 nuclear data library. The total cross section for both of the data libraries for Th-232 can be seen

in Figure 2-7. The difference in the two cross sections can be seen especially in the residence region.
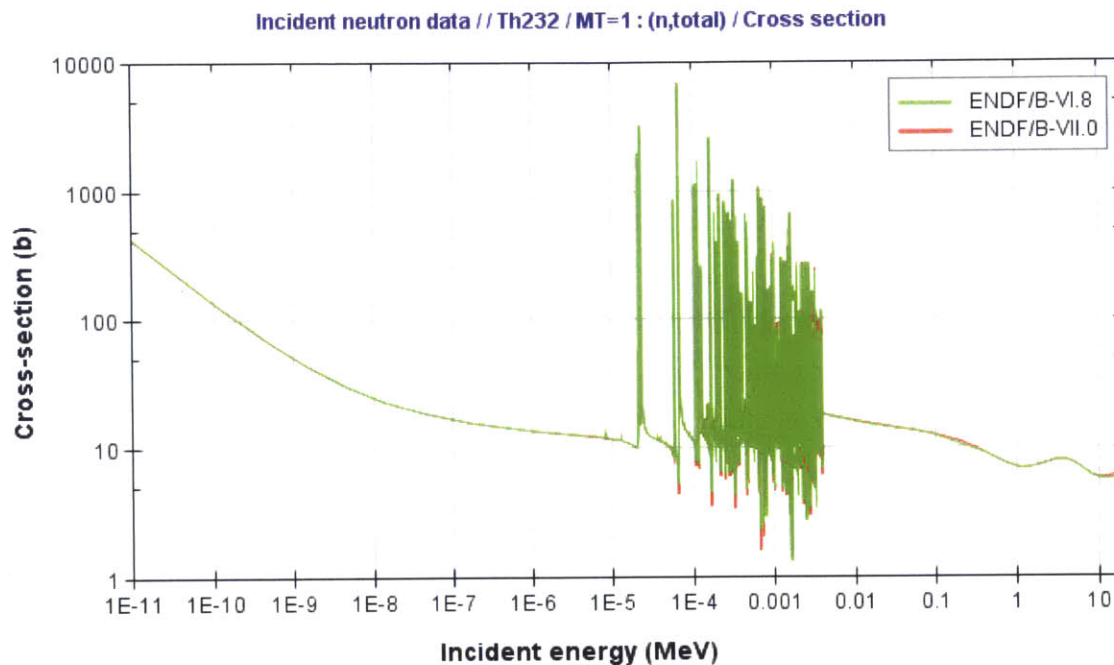
Figure 2-7: Thorium-232 total cross section for ENDF/B-VI.8 and ENDF/B-VII.0 nuclear data libraries [Janis 4.0, 2013]

2.3.5 Transient Analysis Limits and Methods – SIMULATE-3K

For transient analysis, the Studsvik developed code SIMULATE-3K is used. This code is a transient version of the code SIMULATE-3. [Studsvik, 2009] The diffusion equation is solved in the same way, and the frequency transform method is used to solve the transient problem. In SIMULATE-3K, the flux is separated into two components an exponential time dependent component and a spatial component that has weak time dependence. At each time step, the cyclic Chebyshev semi-iterative method is used to determine the flux. By default, the code uses material properties from MATPRO. Both the thermal conductivity and gap conductance are functions of temperature and burnup. While the code includes both UO_2 and MOX thermo-

mechanical properties, for thoria-plutonia fuel, it is necessary to user- input the fuel thermal conductivity and gap conductance.

In any transient, it is necessary for the core to maintain safe behavior. This includes maintaining a safe mDNBR, fuel temperature and core power response. Rod ejection and main steam line break are the transient accidents of interest. In a rod ejection accident, the maximum enthalpy that can be added to a fuel node is the limit of interest. In order to find the most limiting condition, the rod cluster which results in the highest power spike is assumed ejected. In a main steam line break accident, the driving factors for the core response are the inlet moderator temperature and the core pressure. These were shown in the previous chapter for a typical Westinghouse reactor and are used as boundary conditions in this analysis. In this transient, there is an initial increase in power and then a rapid decrease after the 114% overpower is reached, which is the SCRAM set point.

2.4 DNBR Determination for Tight Lattice PWRs

In previous experimental work, five different correlations were examined as possible candidates for use to determine the DNBR of tight-lattice fuel assemblies. These efforts were part of larger design projects, since without an accurate DNB correlation the maximum power in an assembly cannot be determined. Because few correlations are developed specifically for tight-lattice fuel assemblies, the typically used correlations need to be validated against separate sets of tight-lattice data. These experiments are summarized in Section 2.1. They were performed by Mitsubishi, Bettis Atomic Power Lab, the Japanese Atomic Energy Agency and Karlsruhe. Five separate correlations are examined here against the tight lattice experiments previously summarized. They are WSC-2, KfK, EPRI-1, EPRI B&W and W3. It is important that any correlation which is used for reactor design to be validated against operating parameters similar to that of the reactor in question. Of particular importance are the equivalent hydraulic diameter, mass flux and pressure. Other important parameters are inlet enthalpy conditions, spacer-grid effects and local heating conditions.

These evaluations cover a wide range of important operations parameters such as hydraulic diameter, mass flux and pressure. The geometry and test conditions of multiple tight-lattice DNB experiments were examined: Cheng et al. (1998), Iwamura et al. (1991), Iwamura et al. (1994), BAPL and Akiyama et al. (1991).

In order to determine the validity of the different CHF correlations, the critical heat flux was evaluated against experimental data points. The validity of each CHF correlation was evaluated according to the CHF ratio, shown in Equation 2-11. A value below 1.0 indicates that the correlation under predicts, while a value above 1.0 indicates that the correlation over predicts.

$$CHF\ ratio = \frac{Predicted\ CHF}{Measured\ CHF} \quad (2\text{-}11)$$

2.4.1   W-3 Correlation

The first DNB correlation examined is the W-3 correlation. Examination of this correlation was done by Akiyama et al. (1991). It can be seen in Figure 2-8 that this correlation begins to over-predict the actual DNB value as the heat flux increases. The over-prediction is large and has a large spread. Accordingly, this correlation is not examined in-depth or presented, since it clearly is not capable of accurate predictions of tight lattice geometry.

Predicted DNB Heat Flux (kW/m²)
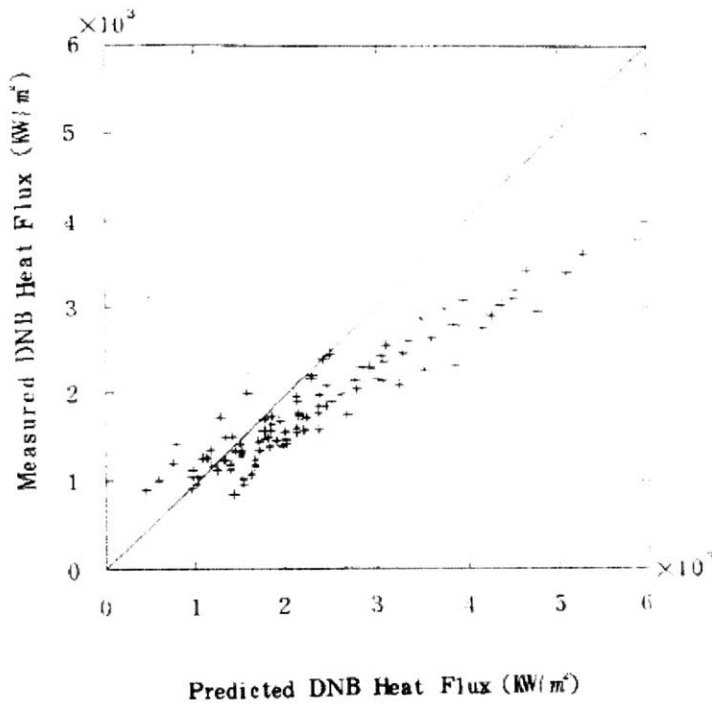
Figure 2-8: Comparison of water DNB data with the W-3 correlation for the Akiyama et al. (1991) experiments

2.4.2 EPRI B&W Correlation

This correlation is based on energy balance consideration and was developed by Uotinen et al. (1981), and was optimized for tight lattices using triangular and square arrays.

$$q_0'' \left(10^6 \frac{Btu}{hr \cdot ft^2} \right) = A_1 \left[\frac{D_h G}{h_z - h_i} \cdot \frac{\partial h}{\partial z} \right]^{A_2} + A_3 \left[\frac{D_h G}{h_z - h_i} \cdot \frac{\partial h}{\partial z} \right]^{A_4} \left[A_5 (\Delta H_i) + \frac{\partial h_f}{\partial P} (2000 - P) \right] \quad (2\text{-}12)$$

D_h: Heated equivalent diameter (in.)

G: Mass flux $\left(\frac{10^6 lb}{hr \cdot ft^2} \right)$

h_z: Local enthalpy (Btu/lb)

h_i: Inlet enthalpy

$\frac{\partial h}{\partial z}$: Local enthalpy gradient (Btu/lb·in.)

60

ΔH_i: Inlet subcooling (Btu/lb)

P: Pressure (psia)

$\frac{\partial h_f}{\partial P}$: Slope of saturated liquid enthalpy curve (=0.123)

Constant parameters:

$$A_1 = 2.8591, \quad A_2 = 0.51796, \quad A_3 = 0.023018, \quad A_4 = 0.63960, \quad A_5 = 1.2614$$

This correlation was examined by Iwamura et al. (1994). From these experiments, it was found that the correlation performed poorly in comparison to the WSC-2, KfK and EPRI-1 correlations. The ratio of predicted CHF to measured CHF showed a large under-prediction of the CHF. This was especially the case when the analysis was performed using local conditions; the CHF ratio was 0.656 ± 0.032 and 0.532 ± 0.121 for two separate tests. [Iwamura, 1994] This indicates that this correlation is not applicable in the relevant operating conditions. Tests by Iwamura et al. (1991) also have the same trend, where a CHF ratio value of 0.642 was found for four and seven rod bundle experiments.

2.4.3   EPRI-1 Correlation

This is the typical EPRI correlation normally used for LWR analysis. Modifications by Akiyama et. al. (1991) showed that this can be applied to a tight lattice triangular design.

$$q_0{''} \left(10^6 \frac{Btu}{h \cdot ft^2}\right) = \frac{A - x_{in}}{CF_g C_{nu} + \left[\frac{x_t - x_{in}}{q_l{''}}\right]} \qquad (2\text{-}13)$$

$$A = P_l P_r^{P_2} G^{(P_5 + P_7 P_r)} \qquad C = P_3 P_4^{P_4} G^{(P_6 + P_8 P_r)}$$

q_l: Local heat flux $\left(\frac{10^6 Btu}{hr \cdot ft^2}\right)$

x_{in}, x_i: Inlet and local qualities

G: Mass flux $\left(\frac{10^6 lb}{hr \cdot ft^2}\right)$

$P_r = \frac{P}{P_{crit}}$: Reduced pressure

Constant parameters:

$$P_1 = 0.5328, \quad P_2 = 0.1212, \quad P_3 = 1.6151, \quad P_4 = 1.4066, \quad P_5 = -0.3040,$$
$$P_6 = 0.4843, \quad P_7 = -0.3285, \quad P_8 = -2.0749$$

$F_g = 1.3 - 0.3C_g$: Grid spacer factor

C_g: Grid loss coefficient

$C_{nu} = 1 + \frac{Y-1}{1+G}$: Non uniform heat flux factor

Y: Axial heat flux profile parameter $= \dfrac{Average\ heat\ flux\ to\ Z}{Local\ radial-average\ heat\ flux\ at\ Z}$

This correlation was examined by Iwamura et al. (1994). The ratio of predicted CHF to measured CHF showed a large under-prediction of the CHF. This was especially the case when the analysis was performed using local conditions; the CHF ratio was 0.687 ± 0.079 and 0.980 ± 0.100 for the tests performed. [Iwamura, 1994] This indicates poor performance. The correlation also produced a CHF ratio of 2.023 ± 0.442 for a set of 7-rod experiments performed by Iwamura et al. (1990). Similar large over predictions were seen for several sets of BAPL CHF data. Three of the seven test sections have average CHF ratio values of 1.347, 1.430 and 1.567. Other tests performed by Cheng et. al. (1998) in Figure 2-9 show that the correlation produces results that begin to over predict the CHF at pressure near 3.0 MPa. However, this test does not expand to the actual operating pressure of a PWR.
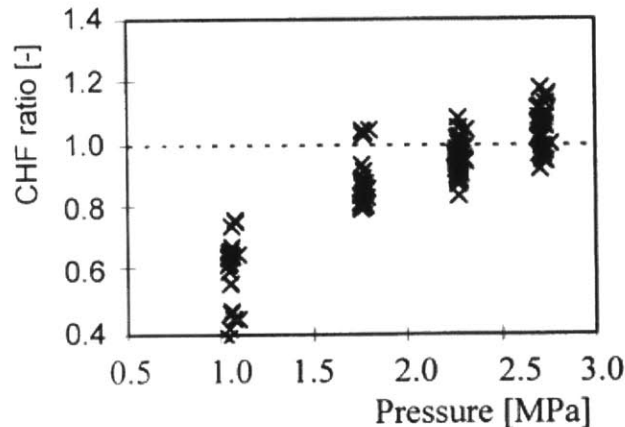
Figure 2-9: Comparison of water DNB data with the EPRI-1 correlation for the Cheng et. al. (1998) experiments

Tests performed by Akiyama (1991) show good correlation with a slightly modified EPRI-1 correlation (multiplied by a factor of 1.025) at PWR-relevant operating conditions, as shown in Figure 2-10.
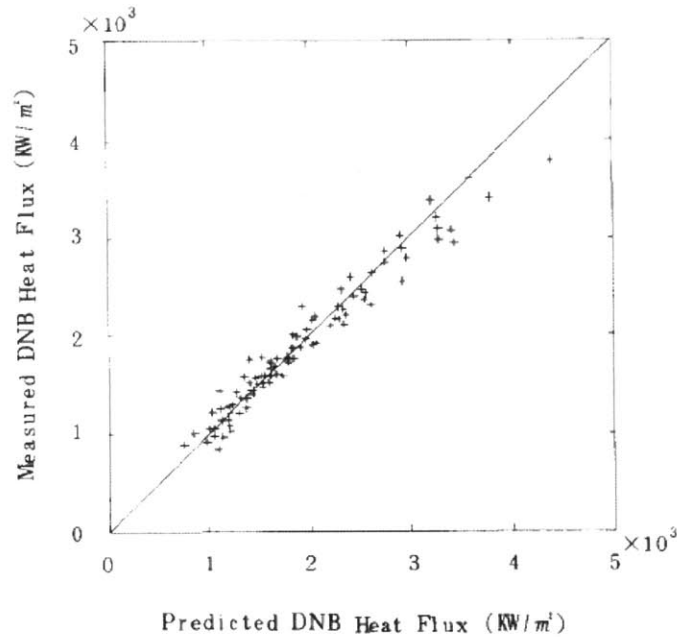
Figure 2-10: Comparison of water DNB data with a modified EPRI-1 correlation for the Akiyama et. al. (1991) experiments

Given the very large over-prediction seen in several tests performed by Iwamura et al. (1991), this correlation cannot be recommended.

2.4.4   KfK Correlation

The KfK correlation is a modified version of the WSC-2 correlation, which is shown next.. It was developed by Dalle Donne & Hame (1985) for tight lattice arrays. The heat flux of DNB is calculated in the following manner

$$q_0'' \left(10^6 \frac{Btu}{h \cdot ft^2}\right) = \frac{A+B\Delta H_i}{C+ZYY'} \qquad (2\text{-}14)$$

63

$$A = \frac{0.25GD\lambda F_1 Q_1}{1+Q_2 F_2 GD(Y')^{Q_3}} \qquad B = 0.25GD \qquad C' = \frac{Q_4 F_3 (CDY')^{0.5}}{D_w} \qquad C = C'V\left[1 + \frac{Y-1}{1+G}\right]$$

ΔH_i: Inlet subcooling (Btu/lb)

Z: Distance from channel inlet (in.)

Y: Axial heat flux profile parameter $= \dfrac{Average\ heat\ flux\ to\ Z}{Local\ heat\ flux\ at\ Z}$

Y': Subchannel imbalance factor $= \dfrac{Heat\ retained\ in\ subchannel}{Heat\ generated\ in\ subchannel}$

G: Mass flux $\left(10^6 \frac{lb}{h\cdot ft^2}\right)$

$$D = F_p D_h$$

F_p: Radial form factor

D_h: Heated equivalent diameter (in.)

λ: Latent heat of evaporation (Btu/lb)

D_w: Wetted equivalent diameter (in.)

$$P_r = 10^{-3}P$$

P: Pressure (psia)

$$F_1 = P_r^{0.982}\exp[1.17(1 - P_r)]$$

$$F_2 = P_r^{0.841}\exp[1.424(1 - P_r)]$$

$$F_2 = P_r^{1.851}\exp[1.241(1 - P_r)]$$

Geometry parameters:

$$Q_1 = 1.784, \quad Q_2 = 7.540, \quad Q_3 = -1.0, \quad Q_4 = 8.783$$

Grid spacer parameter:

$$V = -0.252 - 2.789\exp(-3.874G) + 1.915\exp(-0.234G)$$

The KfK correlation showed the closest result to experimental predictions for both Iwamura experiments and the BAPL experiment. [Iwamura, 1994] [Iwamura, 1991] Additionally the correlation shows acceptable behavior when analyzed against the Cheng et al. (1998), shown in Figure 2-11, experiment and the Akiyama et al. (1991) experiment, shown in Figure 2-12.
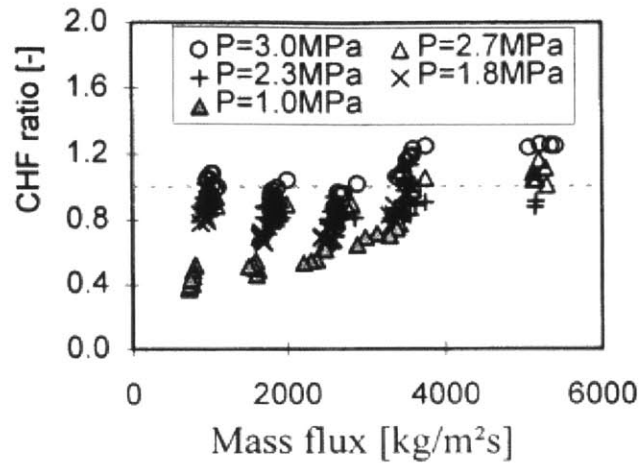
Figure 2-11: Comparison of CHF ratio results for the experiments by Cheng et al. (1998)
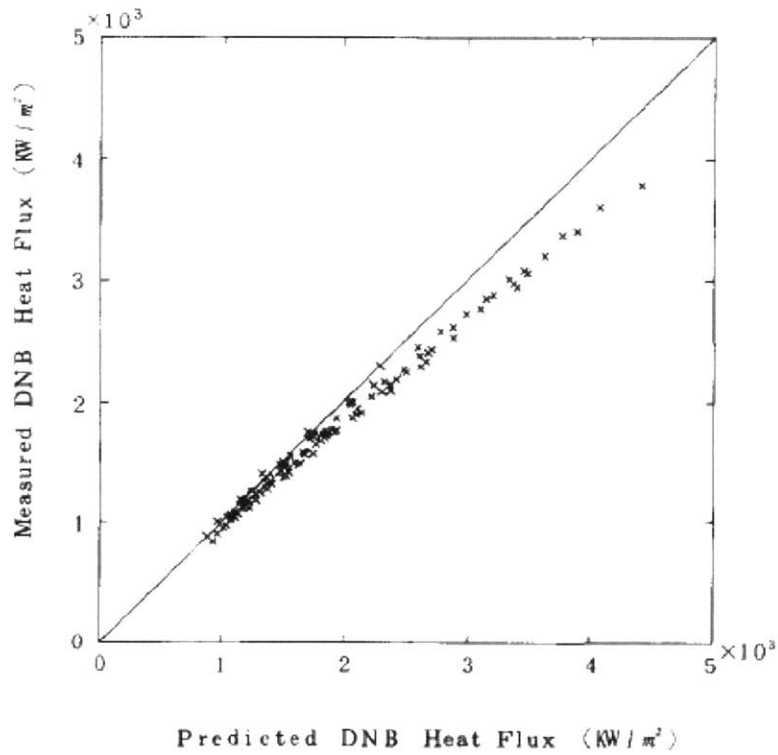
Figure 2-12: Analysis of KfK correlation using Akiyama et al. (1991) experiment

Because of these results, the KfK is the correlation which is recommended for use. The range of validity of the correlation is summarized in Table 2-8.

Table 2-8: Summary of flow conditions for KfK correlation examinations

Parameter	Minimum	Maximum
Pressure [MPa]	2.7	14.0
Mass Flux [Mg/m^{2}s]	None	5.4
Exit quality	-0.44	0.96

2.4.5 WSC-2

This correlation shares all parameters with the KfK correlation, with the exception of geometry and grid spacer constants. It is applicable to triangular rod pitch, but it was not developed specifically for tight lattices similar to high conversion PWRs. [Bowring, 1979]

$$q_0'' \left(10^6 \frac{Btu}{h \cdot ft^2} \right) = \frac{A + B \Delta H_i}{C + ZYY'} \qquad (2\text{-}12)$$

Geometry parameters:

$$Q_1 = 1.329, \quad Q_2 = 1.372, \quad Q_3 = -1.0, \quad Q_4 = 12.26$$

Grid spacer parameter:

$$V = 0.7$$

This correlation is presented here as a reference, since it is the basis of the KfK correlation. It gives large over-prediction of CHF than the KfK correlation and is therefore not used. This can be seen in tests by Akiyama et al. (1991), Iwamura et al. (1994) and BAPL.

2.4.6   Correlation Comparison and Recommendation

The correlation selected for use on the tight lattice PWR geometry is the KfK correlation. The correlation produces the best results when compared across the whole range of available data. This data includes six separate geometries, a wide range of pressures extending above a PWR's

operating pressure and a wide range of mass flux values. A summary of all of the results found, which examine the KfK correlation can be seen in Table 2-9. It should be noted that the Cheng correlation data is taken only from points above 2.7 MPa, since the correlation is not valid below this pressure.

Table 2-9: Summary of CHF ratio of the KfK correlation and associated standard deviation for validation when compared to experimental data for

Test	Sub-Test	Mean CHF ratio	Standard Deviation	Data Points
Akiyama (1991)	-	1.089	0.049	72
Cheng (1998)	-	1.028	0.121	41
BAPL [Iwamura, 1994]	A-5	0.902	0.041	5
	A-6	0.972	0.061	16
	A-7	1.088	0.114	23
	A-10	1.008	0.07	14
	A-11	1.143	0.126	20
	A-13	1.028	0.084	27
	A-14	0.907	0.056	22
Iwamura (1994) (Double Hump)	A	0.984	0.046	24
	B	1.088	0.042	43
Iwamura (1991)	A	0.867	0.045	73
	B	0.976	0.084	77
	C	0.905	0.104	62
	D	0.830	0.074	39
All Data:	Equal Importance	0.988	0.074	558
	Data Point Weighted	0.981	0.074	558

By looking at all of the data, we can see that the mean of all the data returns a CHF ratio value very near unity. This is very desirable. The highest single experiment average is 1.142 with a standard deviation of 0.126; this is highlighted in Table 2-9, coming from BAPL data. The Iwamura tests and BAPL tests do not give specific data points. However, the Akiyama and Cheng experiments do, for these the highest CHF ratio values are 1.17 and 1.26 respectively.

Based on this, it is reasonable and in fact conservative to propose designs with a mDNBR of 1.4 for tight lattice PWRs, taking into account only this data. For comparison, the results from EPRI-1 analyses are included in Table 2-10. It can clearly be seen that the mean and standard deviation are much higher, when looked at over the whole data set. The Cheng test was not included in this analysis because data points could not be distinguished.

Table 2-10: Summary of CHF ratio of the EPRI-1 correlation and associated standard deviation for validation when compared to experimental data

Test	Sub-Test	Mean CHF ratio	Standard Deviation	Data Points
Akiyama (1991)	-	1.028	0.098	72
Cheng (1998)	-	-	-	-
BAPL [Iwamura, 1994]	A-5	0.904	0.115	5
	A-6	1.065	0.139	16
	A-7	1.43	0.282	23
	A-10	1.199	0.163	14
	A-11	1.567	0.337	20
	A-13	1.347	0.241	27
	A-14	0.903	0.192	22
Iwamura (1994) (Double Hump)	A	0.687	0.079	24
	B	0.98	0.1	43
Iwamura (1991)	A	0.931	0.278	73
	B	2.023	0.442	77
	C	1.378	0.387	62
	D	0.896	0.158	39
All Data:	Equal Importance	1.167	0.215	517
	Data Point Weighted	1.229	0.245	517

Table 2-11 is also provided as a reference for comparisons of the EPRI B&W correlations and the WSC correlations.

Table 2-11: Summary of CHF ratio of the EPRI-B&W and WSC-2 correlation and associated standard deviation for validation when compared to experimental data

Test	Sub-Test	WSC-2 Correlation		EPRI-B&W Correlation		Data Points
		Mean CHF ratio	Standard Deviation	Mean CHF ratio	Standard Deviation	
BAPL [Iwamura, 1994]	A-5	0.863	0.124	0.904	0.115	5
	A-6	1.034	0.177	1.065	0.139	16
	A-7	1.163	0.198	1.43	0.282	23
	A-10	1.02	0.175	1.199	0.163	14
	A-11	1.212	0.254	1.567	0.337	20
	A-13	1.023	0.166	1.347	0.241	27
	A-14	0.906	0.135	0.903	0.192	22
Iwamura (1994) (Double Hump)	A	1.127	0.063	0.656	0.032	24
	B	1.233	0.046	0.532	0.121	43
Iwamura (1991)	A	1.334	0.057	0.638	0.07	73
	B	1.513	0.048	0.672	0.136	77
	C	1.249	0.07	0.615	0.124	62
	D	1.292	0.052	0.635	0.051	39
All Data:	Equal Importance	1.151	0.120	0.936	0.154	445
	Data Point Weighted	1.248	0.091	0.806	0.135	445

Table 2-12 has a breakdown of all the correlations examined. It can clearly be seen that the KfK correlation is the best, having the most accurate mean and the lowest standard deviation. This indicates that KfK correlation is the best for use in tight-lattice PWR assemblies. Currently there is no evidence that DNB is dependent on surface properties at high pressures. Therefore, cladding choice should have minimal effect on these correlations' accuracy.

Table 2-12: Data point weighted results for CHF ratio for all correlations examined

Correlation	Average CHF ratio	Standard Deviation
KfK	0.981	0.074
EPRI-I	1.229	0.245
EPRI-B&W	0.806	0.135
WSC-2	1.248	0.091
W-3	1.217	0.246

2.5 Reactivity Insertion Accident Benchmarks

2.5.1 Rod Ejection Accident and Benchmarks

First, the control rod ejection accident is discussed. In this accident, some control or safety rods that are fully inserted into the core are assumed to be ejected. This ejection inserts a large amount of reactivity into the core, causing a power spike for a time-period on the order of 0.1 seconds for typical LWRs at HZP. As the core power increases, the fuel temperature rises. When this occurs, there is negative reactivity feedback from fuel Doppler broadening. This feedback eventually fully dampens the initial power spike and core reactivity returns to its initial level. The initial core power and rod position determine the magnitude of the power increase. The most limiting condition typically occurs when all rods are inserted (ARI) into the core, as when the core is starting up, and the reactor is at hot zero power (HZP) condition. In this condition, the worth of a single control rod cluster for a typical PWR is often near or above 1.0 $, which is the amount of reactivity required for prompt criticality. In this accident sequence, there is a fear that the amount of energy added to the fuel rods would cause their failure. Adequate and safe performance has traditionally been measured by the fuel enthalpy. The limits can be expressed in terms of fuel coolability and rod failure. [Yang, et al., n.d.] The coolability limit decreases at higher burnups since fuel melting temperature decreases with increased burnup. [Yang, et al., n.d.] At low burnups, the fuel rod fails from high temperature processes; while at higher burnups, failure results from pellet cladding mechanical interaction. [Yang, et al., n.d.] The limits can be seen in Figure 2-14 (the NRC has recently revised the cladding strength to reflect hydrogen

concentration in the cladding, and this may change the limits at high burnups, i.e. make them more limiting). [Yang, et al., n.d.]
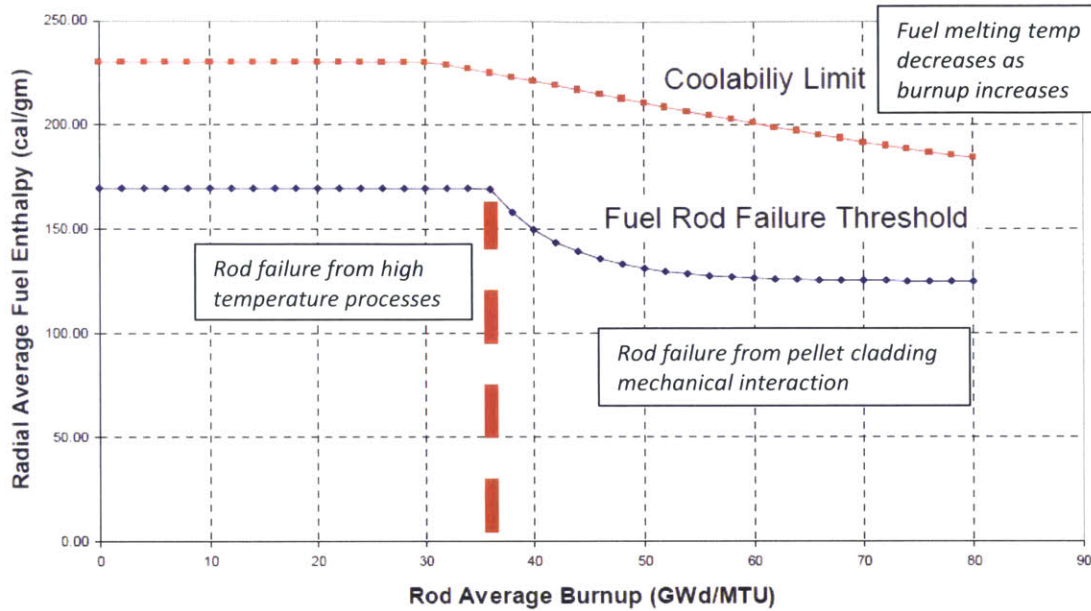
Figure 2-13: Enthalpy limits for fuel rod coolability and fuel rod failure, showing failure mechanisms [Yang, et al., n.d.]

A PWR MOX/UO$_2$ rod ejection benchmark was performed by Kozlowski and Downar (2007). The reactor was a Westinghouse 4-loop PWR, and it is thus similar to the reactors being proposed for use in plutonium disposition in the United States. The core contained a maximum of 1/3 core loading of weapons-grade MOX fuel assemblies; the core loading pattern can be seen in Figure 2-15.

	1	2	3	4	5	6	7	8
A	U 4.2% (CR-D) 35.0	U 4.2% 0.15	U 4.2% (CR-A) 22.5	U 4.5% 0.15	U 4.5% (CR-SD) 37.5	M 4.3% 17.5	U 4.5% (CR-C) 0.15	U 4.2% 32.5
B	U 4.2% 0.15	U 4.2% 17.5	U 4.5% 32.5	M 4.0% 22.5	U 4.2% 0.15	U 4.2% (CR-SB) 32.5	M 4.0% 0.15	U 4.5% 17.5
C	U 4.2% (CR-A) 22.5	U 4.5% 32.5	U 4.2% (CR-C) 22.5	U 4.2% 0.15	U 4.2% 22.5	M 4.3% 17.5	U 4.5% (CR-B) 0.15	M 4.3% 35.0
D	U 4.5% 0.15	M 4.0% 22.5	U 4.2% 0.15	M 4.0% 37.5	U 4.2% 0.15	U 4.5% (CR-SC) 20.0	M 4.3% 0.15	U 4.5% 20.0
E	U 4.5% (CR-SD) 37.5	U 4.2% 0.15	U 4.2% 22.5	U 4.2% 0.15	U 4.2% (CR-D) 37.5	U 4.5% 0.15	U 4.2% (CR-SA) 17.5	
F	M 4.3% 17.5	U 4.2% (CR-SB) 32.5	M 4.3% 17.5	U 4.5% (CR-SC) 20.0	U 4.5% 0.15	M 4.3% 0.15	U 4.5% 32.5	
G	U 4.5% (CR-C) 0.15	M 4.0% 0.15	U 4.5% (CR-B) 0.15	M 4.3% 0.15	U 4.2% (CR-SA) 17.5	U 4.5% 32.5		
H	U 4.2% 32.5	U 4.5% 17.5	M 4.3% 35.0	U 4.5% 20.0				

Assembly Type
CR Position
Burnup [GWd/t]

Fresh
Once Burn
Twice Burn

CR-A — Control Rod Bank A
CR-B — Control Rod Bank B
CR-C — Control Rod Bank C
CR-D — Control Rod Bank D
CR-SA — Shutdown Rod Bank A
CR-SB — Shutdown Rod Bank B
CR-SC — Shutdown Rod Bank C
CR-SD — Shutdown Rod Bank D
O — Ejected Rod

Figure 2-14: Loading pattern (southeast quadrant) of a Westinghouse 4-Loop PWR, with 1/3 MOX composition and a three batch equilibrium cycle. This loading pattern is taken from a rod ejection benchmark, so the maximum ejected rod is shown. [Kozlowski and Downar 2007]

Hot zero power (HZP) rod ejections were performed in the benchmark, since this is the most limiting condition for an equilibrium core, which is used in this analysis. The codes evaluated in the benchmark all showed, with the exception of BARS, a rod ejection worth near $1.1. When the rod was ejected, the core power increased from zero power to near 150% nominal power. [Kozlowski and Downar, 2007] Core power can be seen in Figure 2-16, while the core reactivity can be seen in Figure 2-17.
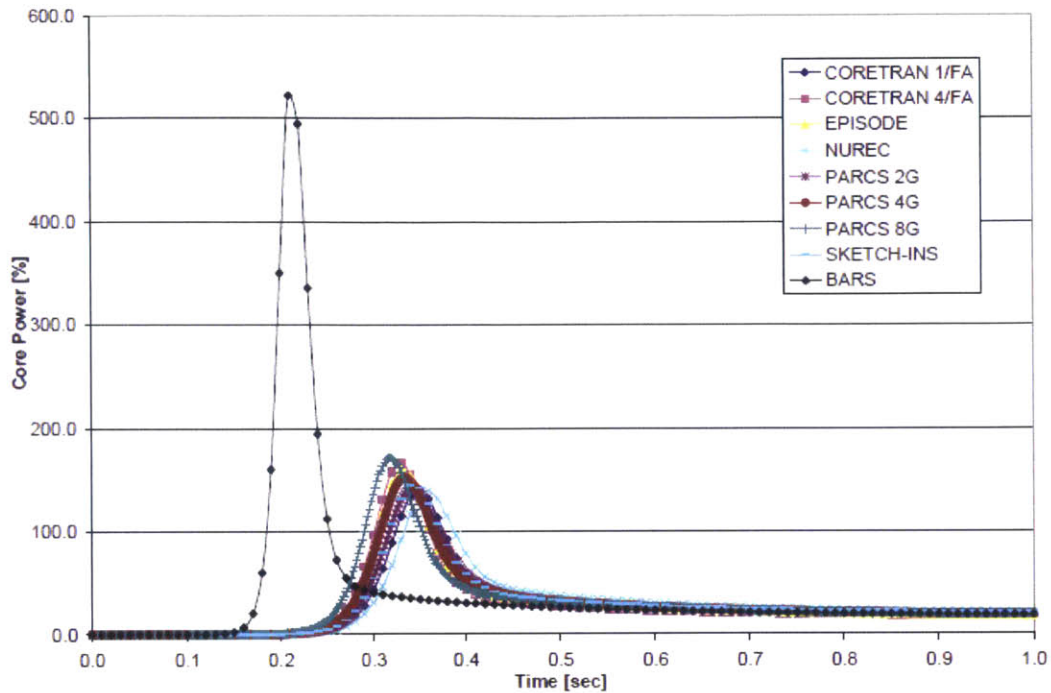
Figure 2-15: Core power response after rod ejection, showing the initial core power increase and subsequent drop after Doppler feedback increases [Kozlowski and Downar, 2007]
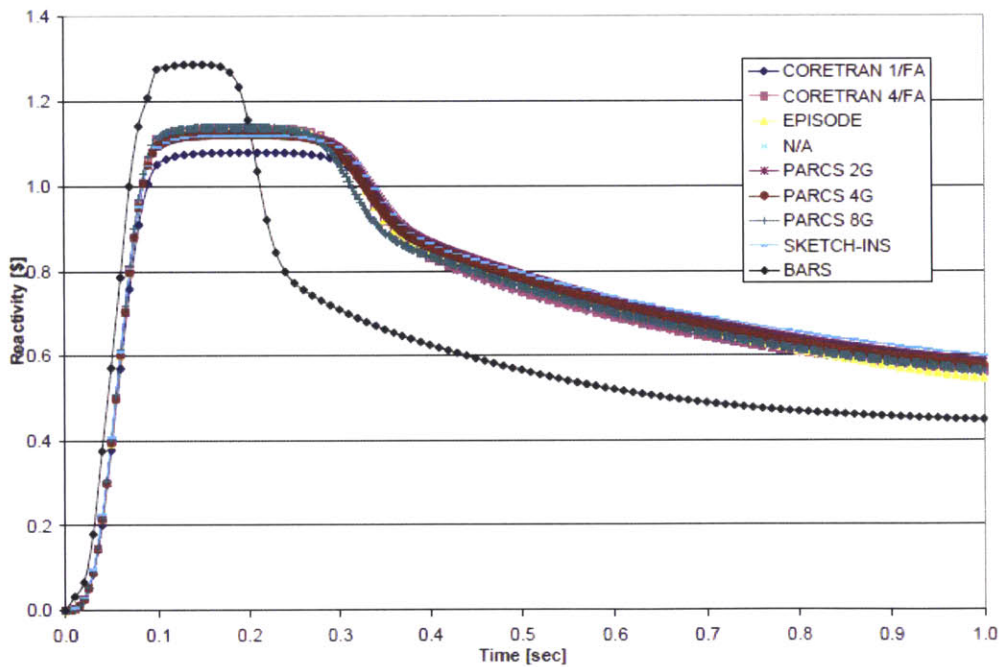
Figure 2-16: Total core reactivity during a rod ejection accident [Kozlowski and Downar, 2007]

2.5.2 Main Steam Line Break Accident and Benchmarks

The second reactivity insertion accident of interest is the main steam line break. In this accident scenario, a break in the main steam line of the secondary system occurs between the steam generator and the turbine. The location of the break can be seen marked on Figure 2-18.
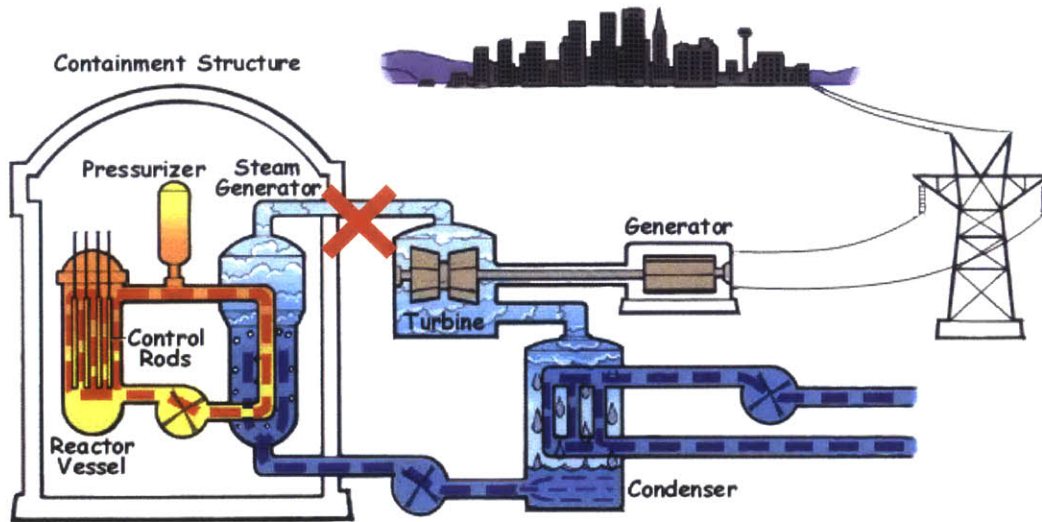
Figure 2-17: PWR primary and secondary systems showing the location of a main steam line break [US NRC, 2012]

The progression of the accident can be summarized as follows. After a break occurs in the steam line, the system depressurizes from steam escaping the system; and the water in secondary system boils off rapidly. This increases the cooling of the primary system water resulting in a lower core inlet temperature and a lower primary system pressure. The lower temperature that enters the core results in an increase in core reactivity. This increase in core reactivity causes the core to trip at a high power signal, usually near 110-118% of nominal. The core trip initiates a SCRAM, which results in an immediate decrease in core power since safety and control rods are inserted into the core (e.g. SCRAM).

This accident is of interest because a thorium-fueled core exhibits a more negative moderator temperature coefficient of reactivity than a typical uranium fueled core. As the core inlet coolant temperature drops, power rises more quickly in a thorium-fueled system than in a similar

74

uranium-fueled system. Multiple benchmarks have been performed for this accident. Two that were used as comparison points for this work are the US Nuclear Regulatory and OECD Nuclear Energy Agency joint benchmark of TMI, and work at the Korea Atomic Energy Research Institute (KAERI). [Jeong et. al., 2006]

The design presented in this study has the same primary and secondary systems as a typical operating Westinghouse 4-loop PWR, with the exception of the core itself. Therefore, it is sufficient to model only the core conditions that change during the transient, inlet coolant temperature and core pressure. For this analysis these parameters are taken from the Three Mile Island benchmark created by Ivanov et al. (1999). This benchmark coupled a point kinetics neutronics model with system-level thermal hydraulic codes such as RELAP. [Beam et. al., 2000] Resulting primary and secondary system state points through the first 100 seconds of the accident were obtained. Two parameters that are needed to model the accident progression in the core with the code SIMULATE-3K are core pressure and core inlet temperature. Values for these two parameters are taken from the values found in Figure 2-18 and Figure 2-19.
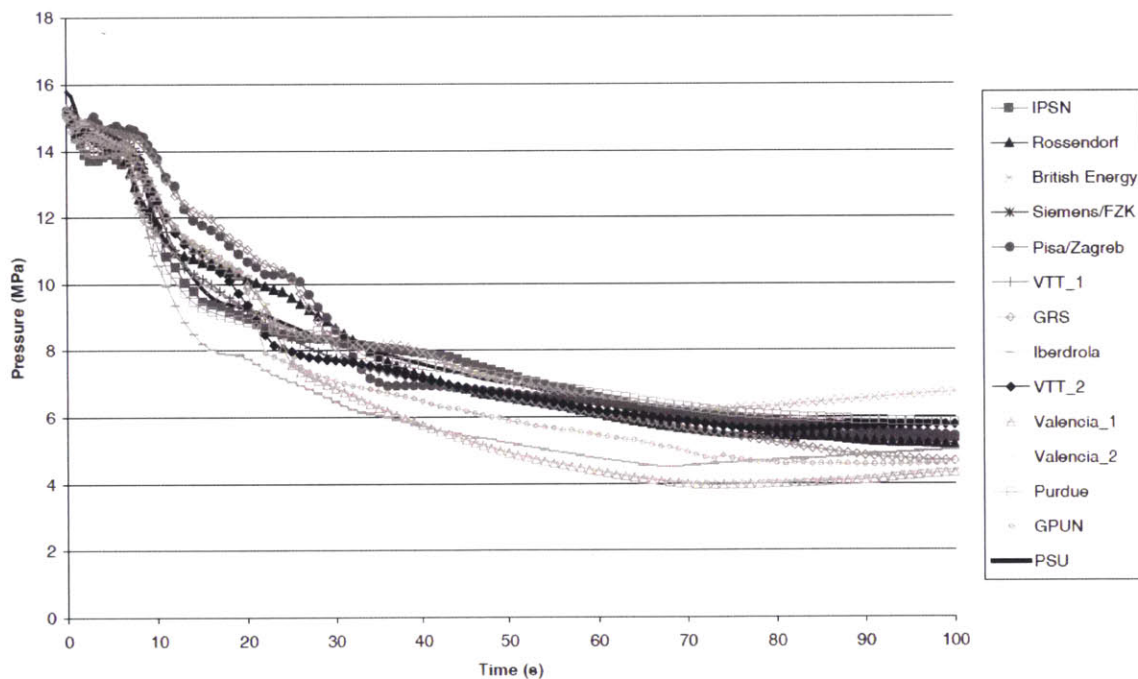
Figure 2-18: Average primary system pressure during the main steam line break transient for the TMI benchmark, showing a pressure drop over the course of the transient [Beam et. al., 2000]

75
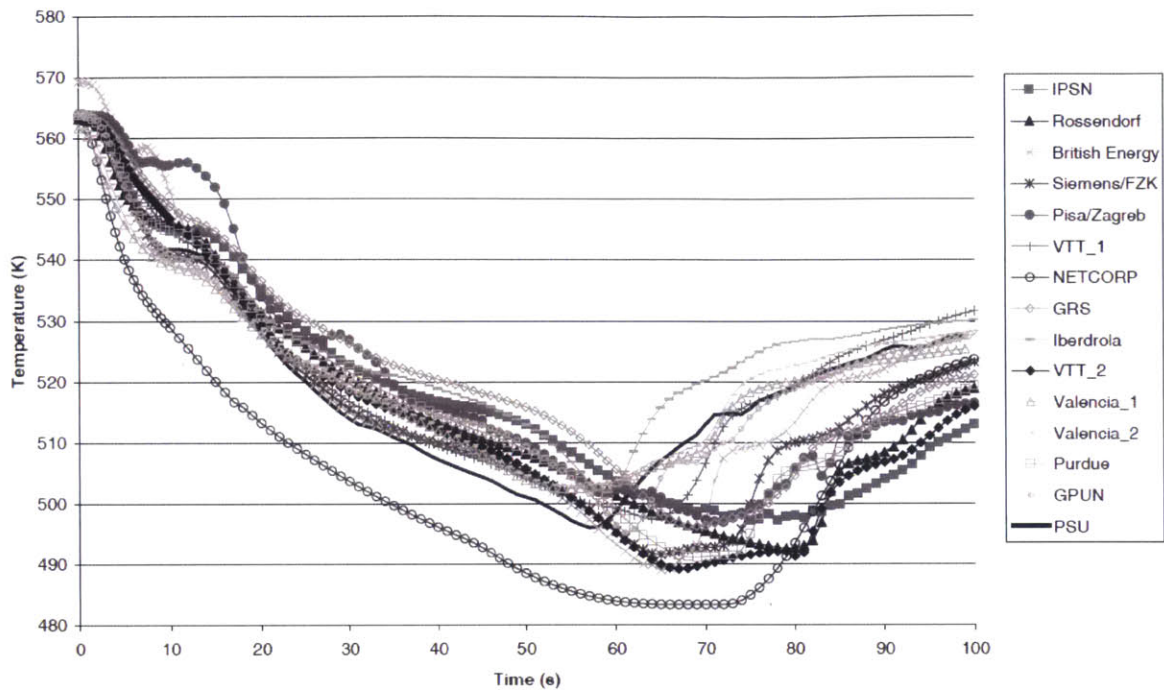
Figure 2-19: Broken cold leg temperature during the main steam line break transient for the TMI benchmark, showing initial temperature decrease and subsequent increase, when heated water from the initial power increase moves completely through the system [Beam et. al., 2000]

Core power response to the transient can be seen in Figure 2-21. It can be seen that there is a steady increase in core power for a few seconds until the overpower scram set point is reached. Immediately after this, there is a large drop in core power from the scram. The power remains low after the scram for the remainder of the transient.
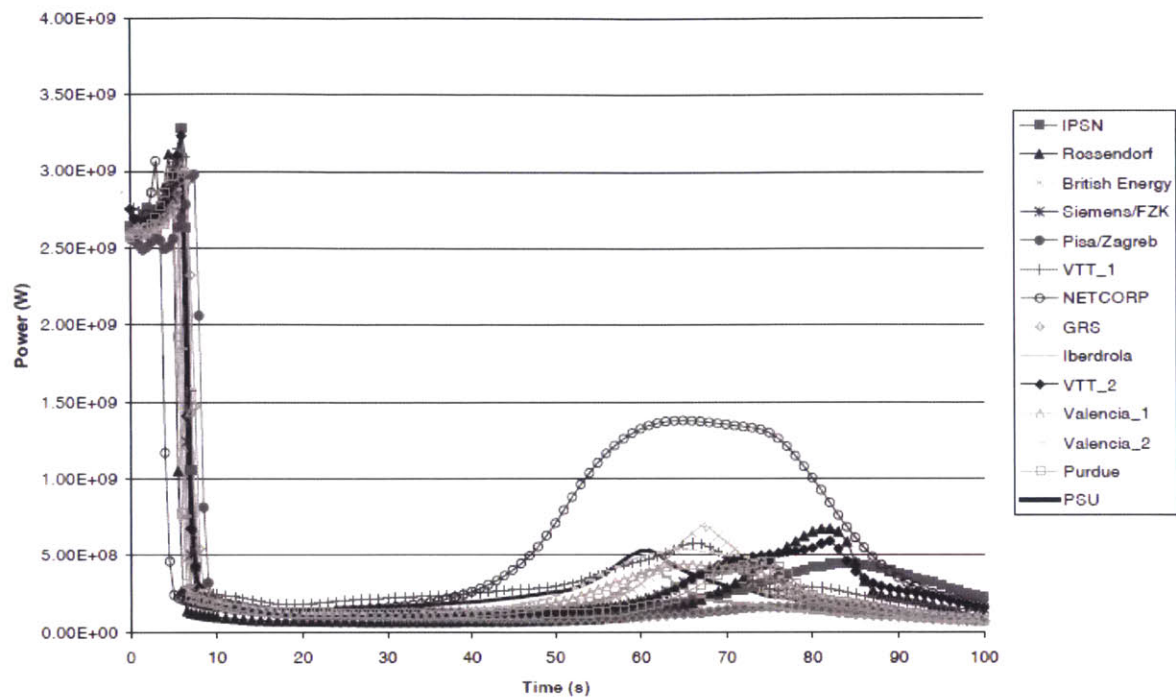
Figure 2-20: Core fission power during the main steam line break transient for the TMI benchmark, showing initial increase and then quick drop after SCRAM [Beam et. al., 2000]

77

3. Thoria-based Core Designs for Plutonium Burning

This chapter presents all thoria-plutonia fueled core designs developed. The core designs presented are for a typical 4-loop Westinghouse PWR with 193 assembly core using an 85-assembly per cycle reload scheme. Each assembly has 264 fuel pins and 25 water rods. In this analysis Zircaloy-2 was used. The fuel pins have outer diameter of 9.5 mm with a pitch of 1.26 cm as listed in Table 3-1. Spacers were modeled as being made of Inconel and are at the axial locations found in the same table. In all designs, quarter core rotational symmetry is maintained. In order to limit fuel discharge burnup, a fresh assembly is always used in the center location. This assembly is then discharged from the core. Using a fresh assembly every cycle both limits the fuel burnup of this region and maintains core symmetry. The core designs shown are all equilibrium cores with a cycle length of 492 EFPD. Separate core designs were created for three different reactivity control approaches: gadolinia, enriched IFBA and enriched soluble boron. For these cores SiC cladding was used with a thickness of 0.76 mm.

Table 3-1: Geometry of Zircaloy and "medium-thickness" SiC fuel pins for a typical 17x17 Westinghouse 4-Loop PWR fuel assembly [Westinghouse, 2014]

Geometry	Zircaloy	SiC
Fuel Pellet Outer Diameter (cm)	0.819	0.781
Cladding Inner Diameter (cm)	0.836	0.798
Cladding Outer Diameter (cm)	0.950	0.950
Fuel Rod Pitch (cm)	1.26	1.26
Clad Density (g/cm^3)	6.55	2.85
Spacer Grid Axial Locations (cm)	2.82, 64.9, 117.1, 169.3, 221.5, 273.4, 326.9	
Water Rod Inner Diameter (cm)	1.138	
Water Rod Outer Diameter (cm)	1.229	
Control Rod Outer Diameter (cm)	0.866	
Control Rod Sheath Inner Diameter (cm)	0.874	
Control Rod Sheath Outer Diameter (cm)	0.968	
Assembly Pitch (cm)	21.5	

The steady state and transient safety limits of the reactor cores are shown and described in Chapters 1 and 2. This chapter and the following two demonstrate that the cores developed meet all of the desired limits. The plutonium burning characteristics of the cores are compared to one another. Then the best design is selected based on these burning characteristics, fuel manufacturability and economic considerations. The enriched IFBA burnable poison option was selected as the best reactivity control option. For the purposes of comparison, a core using IFBA and Zircaloy cladding was also created and presented in this section. It is seen that by using SiC cladding instead of the typical Zircaloy cladding for the same extracted energy, the plutonium burning increased by roughly 3%.

3.1   Core Designs

In this section, both the geometries and material compositions of all fuel assemblies and reactor cores developed with thoria-plutonia as a fuel are described. The total height of the fueled region of an assembly is 365.76 cm. This includes a 304.8 cm region of uniform enrichment which is the assembly's primary fuel, this region contains burnable poison. On both ends of this region, there is a region of 15.24 cm with reduced enrichment fuel or the same fuel without burnable poison. Finally on both the top and bottom sections, the fissile loading is significantly reduced, to both limit peaking and conserve neutrons. The use of different burnable poisons results in altered material compositions. It also causes different thermal and neutronic conditions. These alterations therefore require different assembly designs to be created which contain different fissile loadings.

Three different burnable poison schemes were used in order to hold down the initial reactivity and meet thermal peaking requirements. The first was using gadolinia (Gd_2O_3) interspersed in the fuel pellet. This is a method commonly used for BWRs. However, there is concern about manufacturing a homogenous mixture when a ternary mixture of PuO_2, ThO_2 and Gd_2O_3 is used. [Bjork et. al. (a), 2013] The second is to use enriched boron in the coolant coupled with 1.5x IFBA. The 1.5x refers to the B-10 loading of the IFBA, where 1x is the normal loading. B-10

loading is expressed in terms of mg/cm of B-10 along the exterior of a fuel pellet, and a 1.5x IFBA has a B-10 loading of 0.927 mg/cm. This IFBA coating is 7 microns thick. The primary drawback here is the amount of boron that would need to be enriched, because of the large primary coolant volume. The third method is to use IFBA with enriched boron, increasing the B-10 loading. Here the IFBA was 4.3x, with a B-10 loading of 2.66 mg/cm and a thickness of 12 microns. A separate core design for each of these burnable poisons is presented. After analysis, the enriched IFBA design was selected to be the best. Accordingly, a version of this core design with Zircaloy cladding was created for the purposes of comparison.

In order to meet thermal design criteria, it was necessary to use two separate assembly types (i.e. enrichment patterns) for the designed cores, with the exception of the core design which used enriched boron in the coolant. These two assembly types had different fissile loadings, different burnable poison distributions and had different criticality constants accordingly. The amount of burnable poison in the assemblies is primarily driven by the need to keep the soluble boron concentration of the coolant below 1500 ppm. The fissile loadings above and below the central fuel region are chosen primarily to limit local peaking. At BOL due to reactivity hold-down in the middle axial region of the fuel and the axial neutron leakage, local power peaking often occurs at the top and bottom of the core. Local peaking can occur at the top and bottom since while they contain lower enrichment fuel, they do not have any burnable poisons.

The value of an assembly's k_{inf}, which is referenced multiple times, is calculated by CASMO4E. This value is taken assuming a concentration of 0 ppm boron in the coolant, a fuel temperature of 950 K and a moderator temperature of 585 K. Assemblies are depleted at a power density of 109.9 kW/L. These values are representative for a 2D central fuel segment with burnable poison.

3.1.1   Enriched IFBA as a Burnable Poison

In this sub-section, the core designs which use enriched IFBA as a burnable poison are presented. Two designs are shown, one with SiC cladding and one with Zircaloy cladding. All

assemblies presented use 4.3x IFBA which has a B-10 loading of 2.66 mg/cm. For comparison, a typical IFBA assembly in a nominal enriched UO_2 fueled core has 1.5x IFBA with a B-10 loading of 0.927 mg/cm or 1.0x IFBA with 0.618 mg/cm of B-10. This IFBA coating is placed on 156 of the 264 fueled pins in an assembly, roughly 58% of the fuel pins. The locations of pins with IFBA coating are based on a typical Westinghouse assembly, and were chosen to limit local pin peaking. A ray-trace plot taken from CASMO4E showing one fourth of an assembly can be seen in Figure 3-1. Fuel is shown as purple, cladding as gray and IFBA as light green. Each assembly also has 24 water rods and an instrumentation tube; these are shown as slightly larger blue rods, outlined with a black contour.
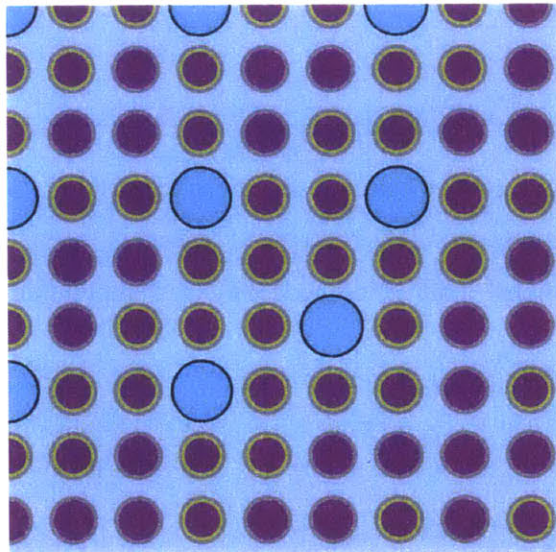
Figure 3-1: Assembly loading pattern (southeast quadrant) with thoria-plutonia fuel using SiC CMC cladding and enriched IFBA as burnable poison. Fuel is shown as purple, IFBA as light green and SiC as gray. Large blue rods are water rods.

The fissile loading of the high and low enriched assemblies used in the core designs can be found in Table 3-2. It can be seen that the SiC assemblies have larger concentration of fissile loading compared to Zircaloy assemblies. This is because of the smaller total fuel mass due to the increased thickness of the SiC cladding.

Table 3-2: Plutonium loading in wt% HM of cores using enriched IFBA as a burnable poison. Assembly designs using both SiC CMC and Zircaloy cladding are shown.

Axial Zone	SiC CMC		Zircaloy	
	Low	High	Low	High
Top Blanket	3.05	3.05	3.50	3.50
Top Fuel Region without Burnable Poison	4.09	4.09	4.09	3.50
Central Fuel Region with Burnable Poison	7.02	7.74	6.69	7.41
Bottom Fuel Region without Burnable Poison	4.09	4.09	3.50	3.50
Bottom Blanket	3.05	3.05	3.50	3.50
Average Pu Loading	6.45	7.06	6.18	6.77
Average Fissile Loading	6.07	6.45	5.82	6.37
Initial k_{inf}	1.051	1.073	1.040	1.063
# Fresh Assemblies	37	48	37	48

The k_{inf} of a 2D central segment for these assemblies can be seen in Figure 3-2. The reactivity in the low enrichment assemblies is roughly 2500 pcm less than in the high enrichment ones. Because of the higher fissile wt% , the SiC clad assemblies have a higher k_{inf} than the Zircaloy clad ones.
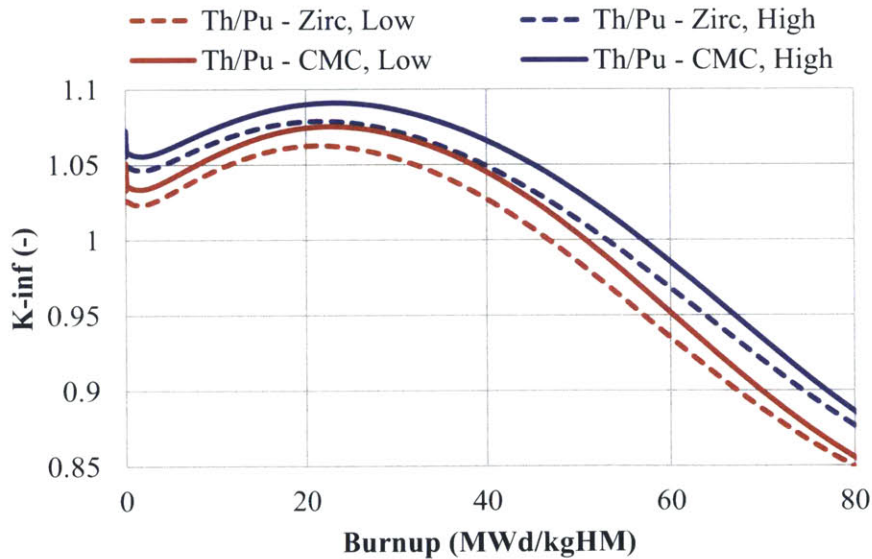
Figure 3-2: Plot of the infinite multiplication factor for both the high and low enrichment assemblies of core designs which use enriched IFBA as burnable poison

82

Using these assemblies, the core design found in Figure 3-3 was developed. This design was used for both the SiC and Zircaloy cladding cases. The numerical labels on second and third cycle assemblies indicate the location from where the assembly was moved. It can be seen that a ring of fresh fuel is located in the outside region of the core. This ring draws power from the center of the core, which has the tendency to be the hottest part of the core. To accentuate this, the higher enrichment assemblies are all in this ring (often referred to as the ring of fire). While in the central region of the core, the fresh fuel is arranged in a checkerboard pattern with once-burned fuel. Fuel that has been in the core for two cycles is exclusively on the periphery of the core. This low neutron flux region limits the doses to the fuel pins, making for more favorable fuel performance. In the design, there is no single location in the core where four fresh assemblies are next to one another. But, it is often also desirable to avoid fresh assemblies at connected flat sides of a fresh assembly. This was not applied here.
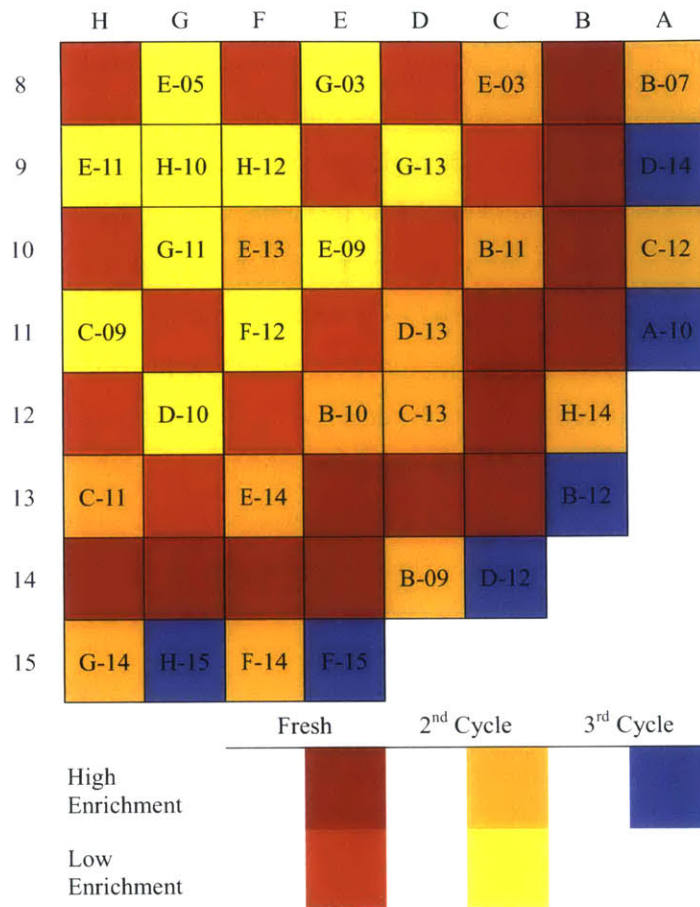
Figure 3-3: Core loading pattern (southeast quadrant) with thoria-plutonia fuel for both SiC CMC and Zircaloy cladding, labels indicate where second and third cycle fuel was shuffled from

3.1.2 Gadolinia (Gd$_2$O$_3$) as a Burnable Poison

The core loading pattern, which had gadolinia as a burnable poison is presented here. The high and low enriched assembly loading patterns are shown in Figure 3-4. In the low enrichment assembly, more reactivity is held down, so on average the fuel pellets are 1.88 wt% Gd$_2$O$_3$. In the high enrichment assembly, the pellets are 1.17 wt% Gd$_2$O$_3$ on average. These average Gd concentrations are higher than those of the assemblies currently used in BWRs, and that is due to the use of weapons-grade plutonium which has much higher initial excess reactivity.

84
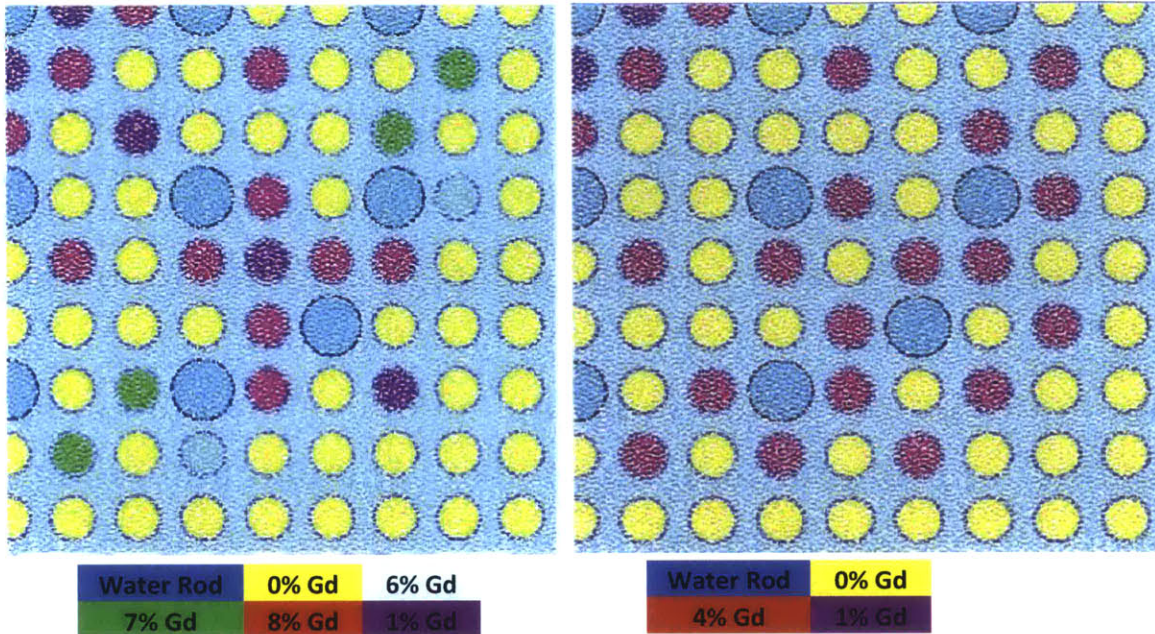
Figure 3-4: Assembly loading patterns for both the low (left) and high (right) enrichment assemblies used in the core design which use gadolinia as a burnable poison

Since the reactivity needs to be held-down for most of a cycle's length, many different concentrations of Gd are needed in an assembly. This allows minimization of peaking, and lead burnout of Gd to happen at different times for the different concentrations. For the gadolinia core, more fissile material is needed in the fuel because a portion of the fuel is displaced by gadolinia. This is reflected in Table 3-3, which contains the fissile loading of assemblies that used Gd as a burnable poison.

Table 3-3: Plutonium loading in wt% of high and low enrichment assemblies using SiC CMC cladding and gadolinia as burnable poison

Axial Zone	Low	High
Top Blanket	4.19	4.19
Top Fuel Region without Burnable Absorbers	5.09	5.09
Central Fuel Region with Burnable Absorbers	7.14	8.64
Bottom Fuel Region without Burnable Absorbers	4.19	5.09
Bottom Blanket	4.19	4.19
Average Pu Loading	6.70	7.98
Average Fissile Loading	6.31	7.52
Initial k_{inf}	1.053	1.121
# Fresh Assemblies	57	28

The resultant core loading pattern developed can be seen in Figure 3-5. It is very similar to the previously shown core in Figure 3-3. All the fresh assemblies are in the same locations. However, there are more low enrichment assemblies. The shuffling pattern of second and third cycle fuel assemblies is also different.
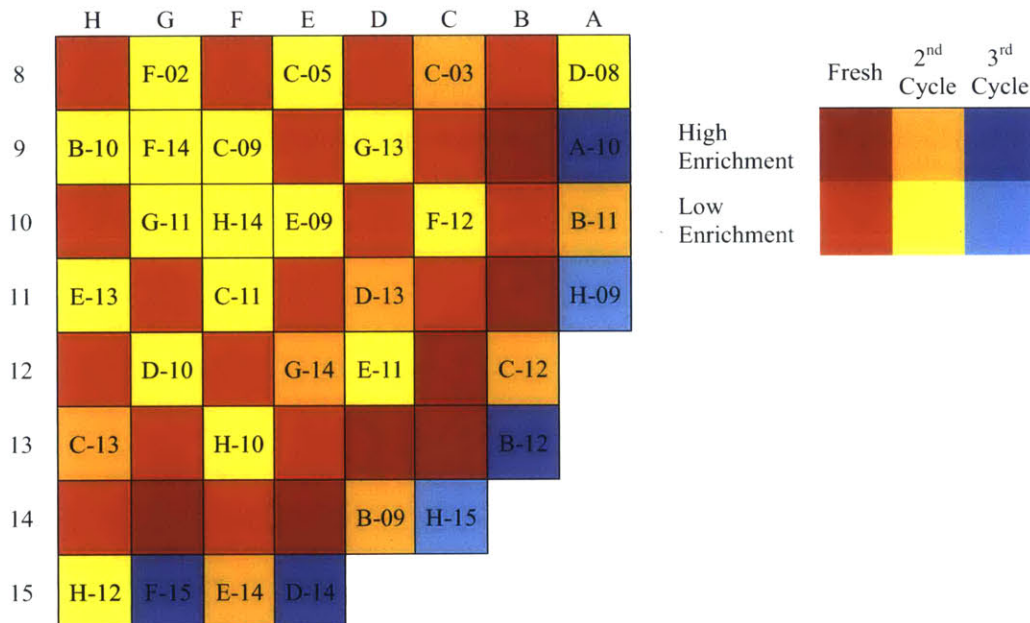
Figure 3-5: Core loading pattern (southeast quadrant) with thoria-plutonia fuel using SiC and gadolinia burnable poison, labels indicate where second and third cycle fuel was shuffled from

3.1.3 Enriched Soluble Boron as a Burnable Poison

For the enriched soluble boron core, enriched boron is used in the coolant instead of a high concentration of natural boron. Using SIMULATE3, the required initial soluble boron concentration using natural boron was found to be 3050 ppm. To limit cladding corrosion and other fuel performance issues, it is desirable to have a boron concentration in the coolant below 1400 ppm. To determine the B-10 composition of the enriched soluble boron, a pin cell comparison using the Monte Carlo code Serpent was used. The soluble boron concentration was set to 1400 ppm boron at BOL. The B-10 enrichment which gave the same BOL k_{eff} as the pin cell with a natural boron concentration of 3050 ppm was used. Accordingly the B-10 composition of the soluble boron was at 43.0 atom percent. Neutronic safety coefficients are determined based on the equivalent natural boron which was calculated in SIMULATE3. The assemblies also used 1.5x IFBA as a burnable poison with a B-10 loading of 0.927 mg B_{10}/cm. Since the core demonstrated a very flat radial power peaking profile, it was not necessary to use multiple assembly types. The plutonium loading of the chosen assembly is shown in Table 3-4.

Table 3-4: Plutonium loading in wt% HM in all assemblies using SiC cladding and enriched soluble boron as burnable poison

Axial Zone	Plutonium Loading
Top Blanket	5.09
Top Fuel Region without Burnable Absorbers	6.73
Central Fuel Region with Burnable Absorbers	6.73
Bottom Fuel Region without Burnable Absorbers	6.73
Bottom Blanket	5.09
Average Pu Loading	6.67
Average Fissile Loading	6.28
Initial k_{inf}	1.214
# Fresh Assemblies	85

Based on this assembly, a core design was developed and is shown in Figure 3-6. This design is very similar to the previous two developed cores given in Table 3-2 and Table 3-3, with the exception that only one assembly type is used.

	H	G	F	E	D	C	B	A
8		C-03		C-05		E-05		B-07
9	C-13	B-11	H-12		G-13			D-14
10		G-11	H-14	E-09		C-12		C-11
11	E-13		F-12		D-13			A-10
12		D-10		B-10	F-14		C-09	
13	E-11		E-14				B-12	
14					B-09	H-09		
15	G-14	H-15	H-10	F-15				

Fresh · 2nd Cycle · 3rd Cycle
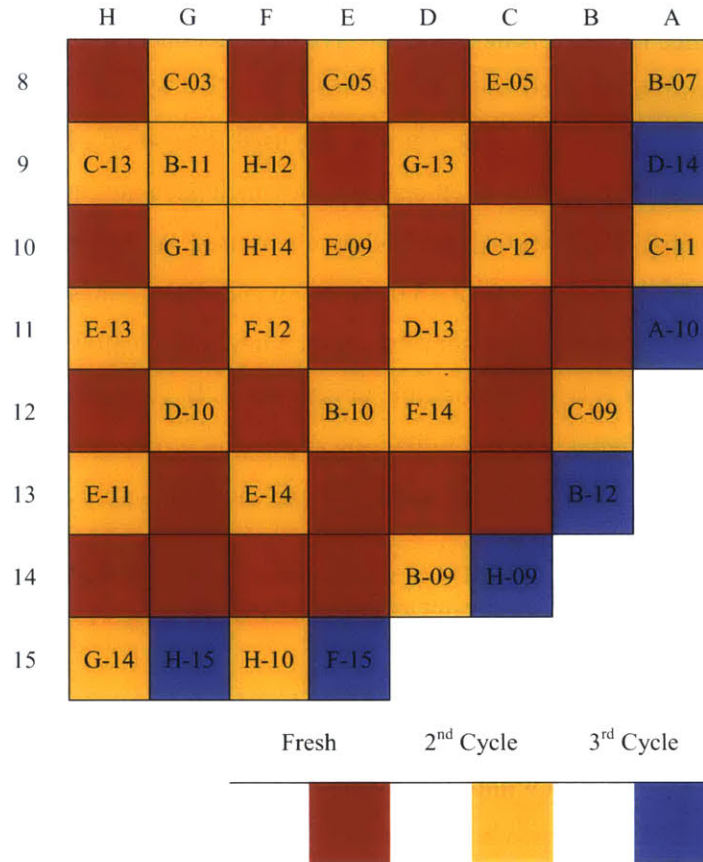
Figure 3-6: Core loading pattern (southeast quadrant) with thoria-plutonia fuel using enriched soluble boron as burnable poison, labels indicate where second and third cycle fuel was shuffled from

3.2   Steady-state and Safety Analysis

The cores developed meet all of the safety and thermal design limits. This includes the MTC, FΔH, F$_Q$ and the initial boron concentration. The coolant boron concentration for the cores developed is lower for the IFBA cores than the core with enriched soluble boron or the

88

gadolinium core. This may be because of the high amount of boron in the IFBA coating on the fuel rods. Boron letdown curves for all of the cores can be seen in Figure 3-7.
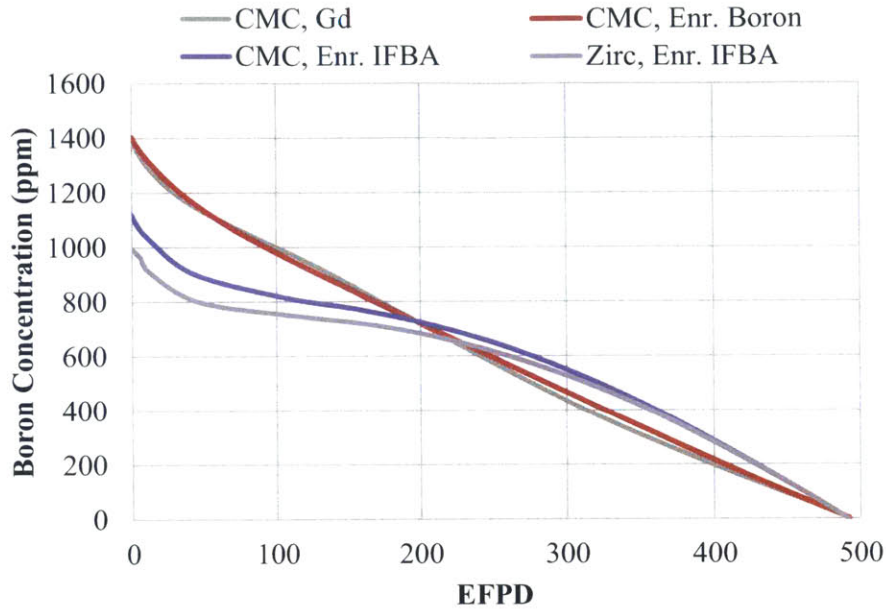
Figure 3-7: Boron letdown curve for the thoria-plutonia fuel cores developed

A comparison of the different k_{inf} values throughout the cycle length can be seen in Figure 3-8. It can be seen that the average k_{inf} of the high and low enrichment assemblies is similar for the gadolinia core and the enriched IFBA core. The core with enriched soluble boron exhibits different behavior, showing a more linear drop in reactivity throughout the cycle length. This is because the excess reactivity is not controlled on the assembly level as it is with the other two burnable poison types, but rather on a core level, which includes assemblies at wide range of burnups.
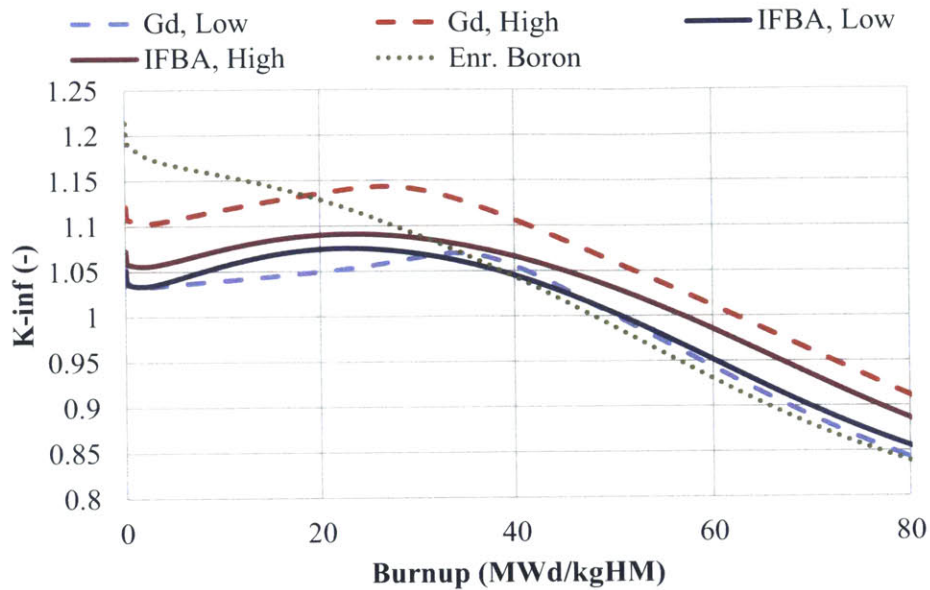
Figure 3-8: The infinite multiplication factor for all assembly designs using thoria-plutonia fuel and SiC CMC cladding

The $F_{\Delta H}$, which is indicative of pin-level hot channel peaking, and the F_Q, or nodal peaking, of the cores developed are shown in Figure 3-9. It can be seen that there is similar behavior from the enriched IFBA cores, both Zircaloy and SiC. The F_Q values of the enriched soluble boron core are much lower because axially the assemblies are more uniform, due to a reduced amount of burnable poison in the central region. This limits the amount of peaking on both the tops and bottoms of fuel pins, which have no burnable poison. This peaking on the top and bottom ends controls the value of F_Q at beginning of life. The reduced peaking at BOL also reduces peaking at EOL since the fuel pins are burned more uniformly.
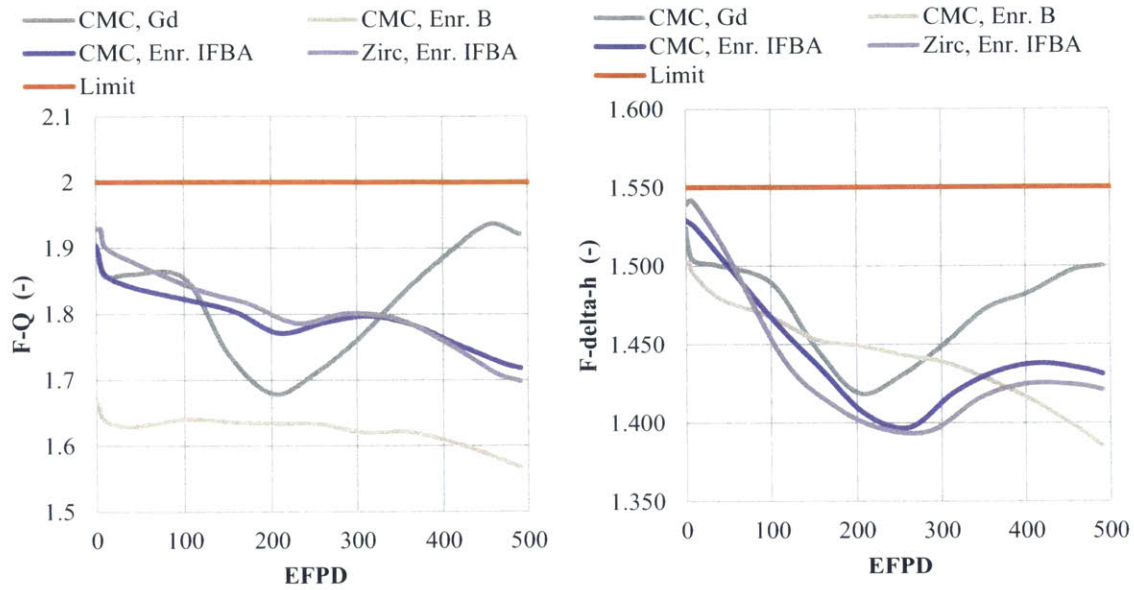
Figure 3-9: Plots of the thermal peaking parameters F_Q (left) and $F_{\Delta H}$ (right) for thoria-plutonia fueled core

The limiting values of the steady-state design parameters can be seen in Table 3-5. All of the parameters meet the licensing values with the exception of the assembly and pin exposures, which exceeded the current licensing limits for Zr clad fuel. However, it is possible that SiC will have a higher burnup limit than Zircaloy. The increased pin and assembly exposures over UO_2 cores are partly the result of the lower fuel density, and partly due to the lower amount of fuel in the core. Pin exposure may be lowered by improved assembly design and incorporating assembly rotation into final core designs. The maximum assembly burnup occurs in the central region, while the maximum pin occurs on the exterior of the core. The maximum burned assembly is from the second cycle, while the maximum pin is from third cycle fuel. The second cycle assembly exhibits the highest burnup because the k_{inf} of thoria-plutonia fueled assemblies remains above 1.0 until over 50 MWd/kg and many of the 2nd cycle assemblies are in the center of the core, where assembly powers are high for the duration of a cycle.

Table 3-5: Steady-state design parameters of thoria-plutonia fueled cores

Parameter	Gadolinia-SiC	Enriched Soluble Boron- SiC	Enriched IFBA SiC	Zircaloy
Core Cycle Burnup -MWd/kg	24.4	24.0	23.5	21.3
Max $F_{\Delta H}$	1.52	1.50	1.53	1.54
Max F_Q	1.94	1.67	1.90	1.93
Initial Boron -ppm	1405	1400	1118	993
Peak Pin Exposure- MWd/kg	85.5	73.7	82.1	75.7
Peak Assembly Exposure - MWd/kg	59.7	59.7	57.6	52.6

Safety parameters for the thoria-plutonia cores are shown in Table 3-6. It can be seen that the MTC is negative at HFP for all the cores developed. The HZP limit is also met for the cores. MTC resembles a near-straight line from BOC to EOC. When B_4C rods were used, the cores also met the required shutdown margin, which is 1300 pcm for a PWR. B_4C was used as a control rod material since it is a more effective neutron absorption than the typical AgInCd control rods typically used in a PWR. When AgInCd control rods were used in an initial core, the shutdown margin was not met.

Table 3-6: Safety parameters of thoria-plutonia fueled cores

Parameter	Reactor Condition	Gadolinia - SiC	Enriched Soluble Boron- SiC	Enriched IFBA SiC	Zircaloy
MTC at HFP $pcm/°F$	BOL	-6.71	-11.4	-18.6	-21.8
	EOL	-29.6	-30.1	-31.4	-32.7
MTC at HZP- $pcm/°F$	BOL	3.29	-0.03	-4.72	-7.91

3.3 Comparison of Designs

The plutonium burning characteristics of the cores presented in this chapter can be seen in Table 3-7. The amount of plutonium burned across all core designs are all within 2% of each other. That is understandable, since the amount of energy derived from the core is constant.

92

Additionally, the fraction of plutonium burned upon discharge is almost similar for all designs. All cores with SiC cladding burned a higher fraction Pu than the reference Zircaloy core. This is in part because the Zircaloy core has a higher initial plutonium loading due to the increased fuel volume. In a Zircaloy clad pin, there is 10% more volume for fuel than in the SiC core. Overall, there is a 4% decrease in initial plutonium loading required for the desired cycle length when SiC cladding is used, this is most likely attributed to the lower absorption cross section of SiC compared to Zircaloy.

Table 3-7: Plutonium burning characteristics of the thoria-plutonia cores developed

Parameter	Gadolinia	Enriched Soluble Boron	Enriched IFBA	
			SiC	Zircaloy
Cycle Burnup - MWd/kg	24.3	24.0	23.5	21.3
Initial Pu Loading - $wt\% HM$	7.12	6.67	6.79	6.51
Initial Pu Loading, Mass - kg	2270	2155	2246	2369
Discharge Mass Pu - kg	788	699	778	899
Net Pu Burned - kg	1482	1456	1468	1470
Percent of Initial Pu Burned - $\%$	65.3	67.6	65.4	62.0

Of the burnable poison options explored, we believe that using enriched IFBA has the least drawbacks. One possible concern when using enriched boron in IFBA is that there is a possibility that this would result in increased internal rod pressure due to increased gas release from B-10 neutron interactions. Fuel pin free volume might have to be adjusted to accommodate the He released from IFBA, in addition to the fission products. Possible ways to limit the internal pressure of the fuel rod, should this be an issue, include using annular fuel pellets at the top and bottom of the fuel rods (which creates more free volume) and slightly increasing the length of the fuel rod plenum. Additional analysis to this end needs to be performed. Using enriched boron in the coolant would require large investment in increasing the enrichment of boron in the entire primary system, which would lead to a higher cost. The gadolinia core would require a ternary mixture of Pu, Th and Gd oxides. There are doubts about the ternary oxide mixture stability in PWR operating conditions. [Bjork et. al. (a), 2013] This also results in further degradation of thermal conductivity of the fuel.

4. Comparison of Thoria to Urania for Plutonium Burning

This chapter presents a comparison of thoria-plutonia fuel to the more commonly used urania-plutonia fuel, which is traditionally considered for plutonium burning. This comparison is in three parts. First, the steady state performance of the cores is examined. Second, the safety parameters are compared. Third, the designs are evaluated for their effectiveness in burning weapons grade plutonium. For this, they are evaluated according to the content of discharged assembly of critical masses of relevant fissile materials, discharged plutonium vector and the amount and fraction of plutonium burned at discharge.

In order to perform this comparison it was necessary to develop urania-plutonia, commonly referred to as MOX, fueled core designs using both SiC and Zircaloy claddings. The cores developed have the same cycle length, cycle energy, assembly geometry, core geometry and similar loading patterns with enriched IFBA as the burnable poison. Additionally all the cores developed are equilibrium cores that were achieved after 9 reload cycles.

A conventional PWR using standard enriched uranium fuel was also developed and is presented here. This core serves as a comparison point for the safety parameters and transient analysis of thoria-plutonia fuel. The core was loaded with 4.3 wt% U-235 and used Zircaloy as the cladding.

The cores considered here utilized weapons grade plutonium as fuel. It is assumed that the core can fully accommodate urania-plutonia fuel. It should be noted that not all PWRs can accommodate a full MOX core, due to reactivity control system limitations. However, studies have shown that more modern PWRs such as EPR and AP1000 are able to allow a full MOX core. [Areva, 2015] [Westinghouse, 2015]

It was found that a design with thoria-plutonia fuel and SiC cladding is the best for plutonium disposition among all cores considered here. Using thoria-based fuel results in a smaller percentage of plutonium remaining at discharge. Additionally the discharged fuel has a better plutonium isotopic mix (or isotopic vector) and less fissile mass. A SiC cladding also results in better plutonium burning characteristics than the Zr alloy counterpart, as shown in Chapter 3.

4.1   Core Designs

The core and assembly designs presented here have the same geometry that was discussed in the previous chapter. They also meet all of the design limits previously summarized. Similar to thoria-plutonia core design, the urania-plutonia and the typical PWR cores had a high and a low enriched assembly type.

4.1.1   Uranium-Plutonium (MOX) Fueled Core

Two urania-plutonia designs are presented, one with SiC cladding and one with Zircaloy cladding. These core designs also use enriched IFBA as the burnable poison. All assemblies use 4.3x IFBA which has a B-10 loading of 2.66 mg/cm. This is the same as the thoria-plutonia design. Both use the same loading pattern developed for the thoria-plutonia core design with enriched IFBA as a burnable poison, which can be seen in Figure 3-3 in the previous chapter. The location of burnable poison rods in the assemblies used is also the same; a CASMO 4E ray-trace plot of this geometry can be seen in Figure 3-1 in the previous chapter.

Both of the core designs used two assembly types to limit local power peaking. The fissile loadings of these assemblies can be seen in Table 4-1. It can be seen that the Zircaloy core needs a lower fissile loading because of the higher fuel volume.

Table 4-1: Plutonium loading in wt% HM of high and low enrichment assemblies of urania-plutonia fuel. Both SiC CMC and Zircaloy claddings are shown.

Axial Zone	SiC CMC		Zircaloy	
	Low	High	Low	High
Top Blanket	1.91	2.31	1.91	2.31
Top Fuel Region without Burnable Absorbers	2.31	2.72	2.31	2.72
Central Fuel Region with Burnable Absorbers	5.94	6.67	5.69	6.45
Bottom Fuel Region without Burnable Absorbers	2.31	2.72	2.31	2.31
Bottom Blanket	1.91	2.31	1.91	2.31
Average Pu Loading	5.30	5.98	5.10	5.78
Average Fissile Loading	4.99	5.63	4.8	5.44
Initial k_{inf}	1.043	1.067	1.035	1.061
# Fresh Assemblies	37	48	37	48

When examining the initial k_{inf} of theses assemblies, it can be seen that they are close to those seen when using thoria-plutonia fuel. This can be seen in Figure 4-1, which shows the value of k_{inf} from BOL to a depletion of 80 MWd/kg. At BOL and at low burnups the reactivity of the thoria-plutonia fueled assemblies is higher, since there is less absorption in Th-232 than in U-238. At end of life, this trend reverses and the urania-plutonia fuel has more reactivity because of the higher amount of fissile material in the assembly. This is in part a result of Pu-239 breeding from neutron capture events in U-238.
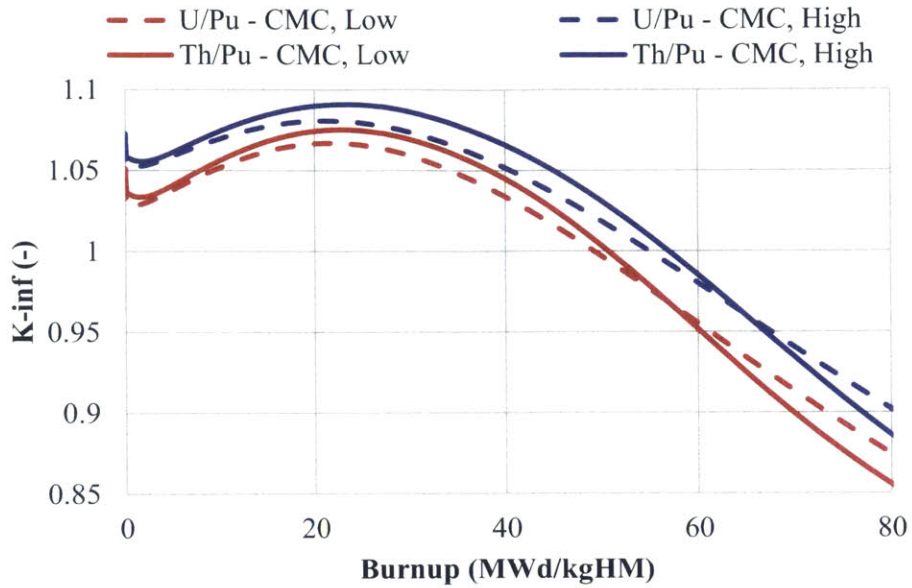
Figure 4-1: Comparison of the resultant infinite multiplication factors of both the high and low enrichment assemblies when a thoria-plutonia fuel is used instead of a urania-plutonia fuel. SiC CMC is the cladding for all cases.

This difference in reactivity can be seen in the boron letdown curve for soluble boron in the coolant of the resultant cores. It takes into account the different assembly types and burnable poisons used. In Figure 4-2, it can be seen that thorium fuel has larger excess reactivity, requiring more soluble boron to maintain core reactivity at the critical level. SiC cladding also results in needing higher boron concentration than Zircaloy cladding. Reducing enrichment to lower this value would result in a penalty to cycle length, which is held constant in this study. This is due to the smaller absorption of SiC compared to Zircaloy and the higher fissile loading of SiC assemblies.

97
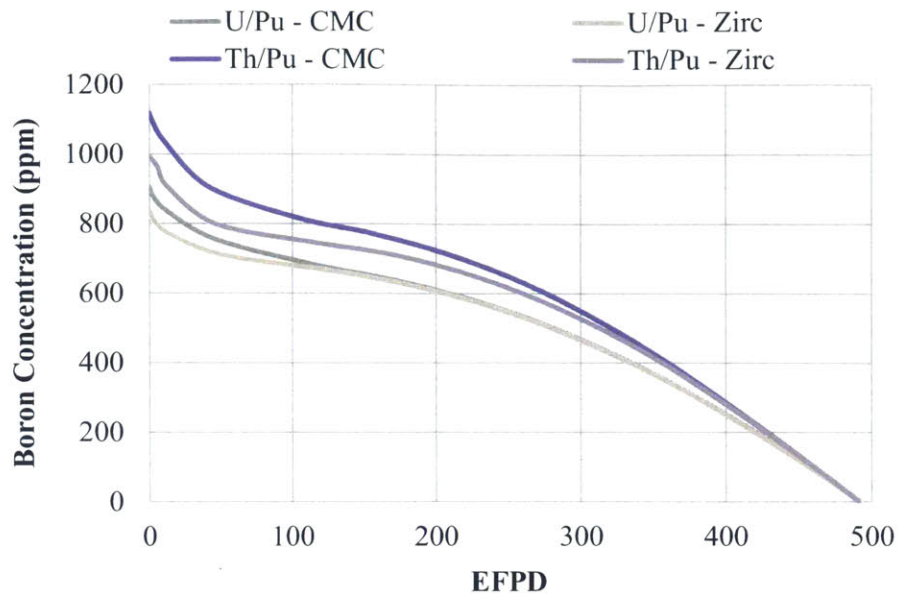
Figure 4-2: Comparison of the boron letdown curve of a thoria-plutonia to a urania-plutonia fueled core. Both SiC and Zircaloy cladding options are shown for both fuel types.

The thermal limits F_Q and $F_{\Delta H}$ are shown in Figure 4-3. While the F_Q values are similar for all designs, the urania-plutonia designs show a lower $F_{\Delta h}$ by ~0.07 than the thoria-plutonia designs. This indicates that it is easier to create a core design that meets thermal limits using uranium as a host for plutonium as opposed to thorium for typical current PWR loading patterns.
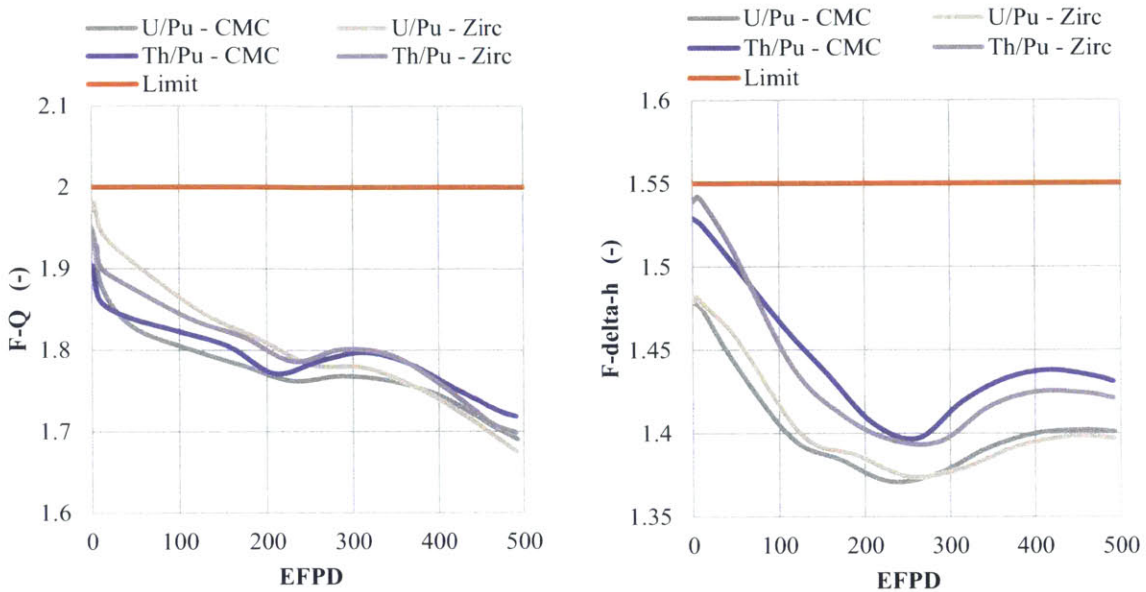
Figure 4-3: Comparison of FQ and FΔh throughout a cycle of thoria-plutonia core to a urania-plutonia fueled core. Both SiC and Zircaloy cladding for both fuel types are shown. The design limit is shown in red.

The limiting values of the design parameters can be seen in Table 4-2. All of the values meet the design limits, except for peak pin exposure. Both the assembly and peak pin exposure are higher when using thoria-plutonia as a fuel. This is mainly because of the lower density of the fuel: 10.6 g/cm for the urania-plutonia mix and 9.6 for the thoria-plutonia mix.

Table 4-2: Most limiting values of important design parameters of both thorium and uranium hosting plutonium fueled core designs

Fuel	U /Pu		Th /Pu	
Cladding	SiC CMC	Zircaloy	SiC CMC	Zircaloy
Cycle Burnup - *MWd/kg*	21.5	19.5	23.5	21.3
Max $F_{\Delta H}$	1.48	1.48	1.53	1.54
Max F_Q	1.95	1.97	1.90	1.93
Initial Boron - *ppm*	905	836	1118	993
Peak Pin Exposure *MWd/kg*	76.9	70.1	82.1	75.7
Peak Assembly Exposure *MWd/kg*	52.7	47.9	57.6	52.6

99

4.1.2 Typical PWR with Enriched Uranium Fuel

For the purposes of comparison of behavior during transient cases, a typical PWR was also developed. The core was fueled with enriched uranium and used the same 85-assembly loading pattern as the enriched IFBA cases. The assembly compositions can be seen in Table 4-3. The central assembly needed reduced enrichment so that the local power would not result in an $F_{\Delta H}$ value that was too high.

Table 4-3: U-235 loading in wt% HM of high and low enrichment assemblies using urania-plutonia fuel in zircaloy cladding

Axial Zone	Low	High	Central
Top Blanket	2.52	2.52	2.52
Top Fuel Region without Burnable Absorbers	3.53	3.53	3.53
Central Fuel Region with Burnable Absorbers	4.44	4.74	2.52
Bottom Fuel Region without Burnable Absorbers	3.53	3.53	3.53
Bottom Blanket	2.52	2.52	2.52
Average U-235 Loading	4.22	4.47	2.59
Initial k_{inf} of Center Region	1.095	1.116	0.898
# Fresh Assemblies	36	48	1

The different behavior of enriched uranium fueled assemblies compared to the plutonium cases can be seen in Figure 4-4. While the reactivity has a higher peak around beginning of life for the nominal uranium fuel case, it drops well below the plutonium-fueled cases at higher burnups. Since the plutonium-fueled cases do not drop as much at end of life, it is necessary to increase the burnable poison loading of any plutonium fueled assembly so thermal margins aren't violated because of excess local power generation. The higher value of k_{inf} later in life for plutonia-based fuels also makes reactivity hold-down at beginning of cycle harder.
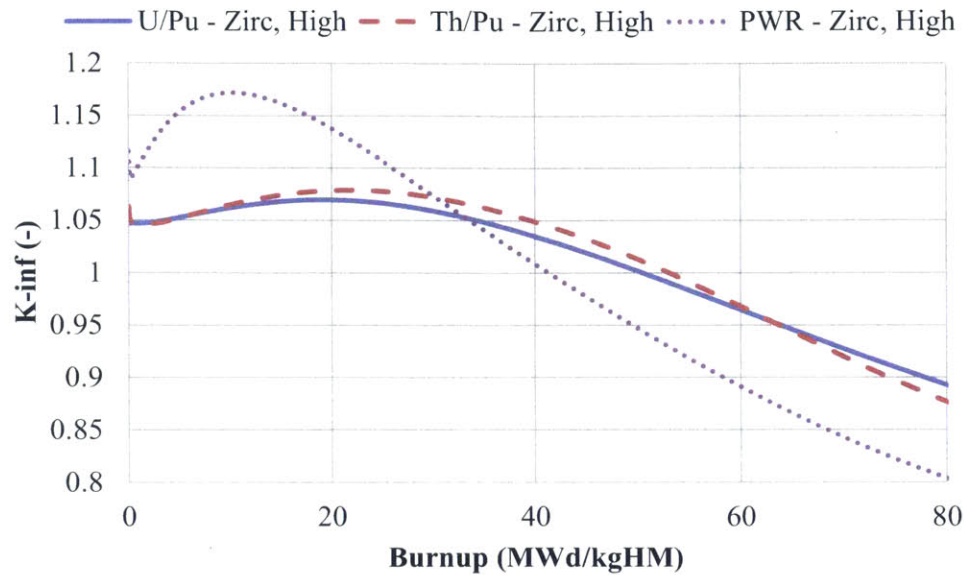
Figure 4-4: Comparison of the infinite multiplication factor of the high enrichment assemblies of different fuel types. Zircaloy is the cladding for all cases.

4.2   Safety Analysis

The safety-related parameters of both urania-plutonia and thoria-plutonia fuel is similar to that of a typical low enriched uranium fueled PWR, indicating safe behavior inferred by steady-state conditions. Additionally, it can be expected that the advanced fueled reactor plants should show similar behavior to a typical, today's vintage, PWR system during transients. The shutdown margins for the thoria-plutonia systems are higher than those of the urania-plutonia system. The fuel temperature coefficient of thoria-plutonia fuel is more negative than that of urania-plutonia fuel with similar cladding. The moderator temperature coefficient and power coefficient, however, follow an opposite trend. These trends can be seen in Table 4-4.

101

Table 4-4: Safety-related parameters of both thorium and uranium hosted, plutonium fueled core designs

Parameter	Reactor Condition	U/Pu		Th/Pu		Enriched U
		SiC	Zircaloy	SiC	Zircaloy	Zircaloy
MTC at HFP *pcm/°F*	BOL	-23.0	-25.2	-18.6	-21.8	-17.7
	EOL	-39.0	-39.6	-31.4	-32.7	-39.8
MTC at HZP *pcm/°F*	BOL	-8.64	-11.3	-4.72	-7.91	-4.61
FTC at HFP *pcm/°F*	BOL	-1.30	-1.43	-1.44	-1.62	-1.44
	EOL	-1.35	-1.53	-1.51	-1.75	-1.56
Power Coefficient at HFP *pcm/°F*	BOL	-21.5	-19.1	-19.8	-18.3	-16.2
	EOL	-29.4	-24.4	-26.2	-22.2	-23.8
SDM *pcm*	BOL	1557	1723	1882	2444	-
	EOL	1713	2054	2557	3309	-

The moderator temperature coefficient at hot full power over course of an entire equilibrium cycle can be seen in Figure 4-5 plotted against cycle EFPD. In the plot it can be seen that the MTC is less negative when thoria-plutonia fuel is used, with both thoria-plutonia cases having less negative values compared to the urania-plutonia cores. Additionally, SiC CMC cladding has a less negative MTC value. The shape of the MTC plot is more consistent between fuel types as opposed to cladding types.
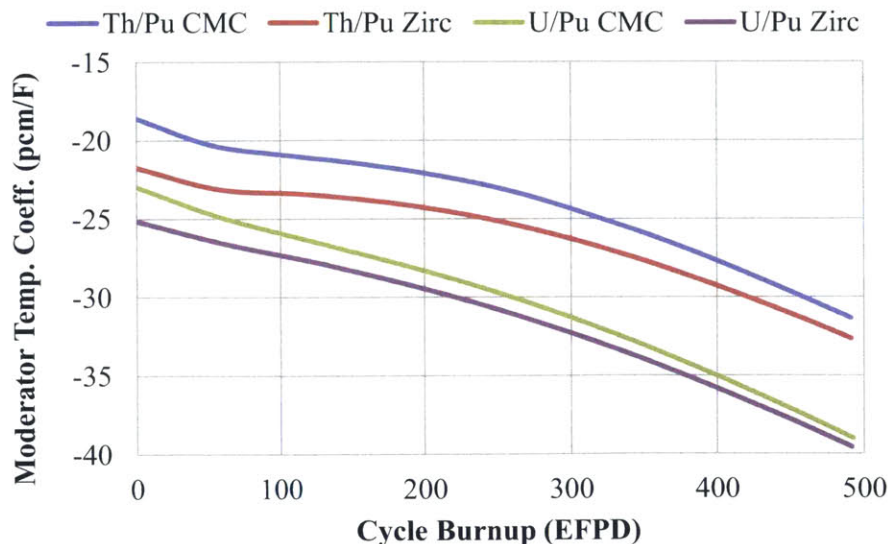
Figure 4-5: Moderator temperature coefficient as a function of core burnup for both urania and thoria cores during a single cycle

The Doppler coefficient, and fuel temperature coefficient, shows less variance than the MTC over the course of a cycle. Here the Doppler coefficient is at least 0.12 pcm/F, nearly 10%, more negative for thoria based fuel compared to urania based fuel. This can be seen in Figure 4-6.
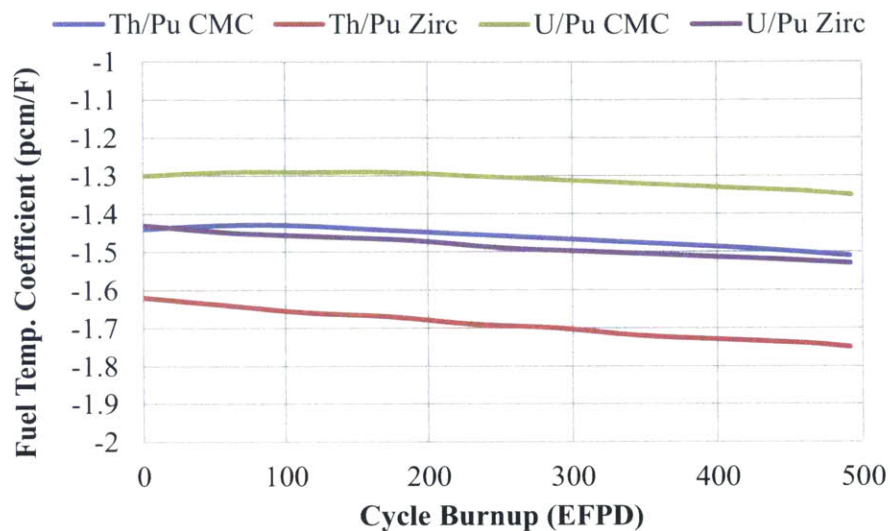
Figure 4-6: Fuel temperature coefficient as a function of core burnup for both urania and thoria cores during a single cycle

The power coefficient that is the resultant from these two coefficients can be seen in Figure 4-7. The power coefficient is more negative for SiC CMC cladding cases in comparison to Zircaloy cladding. This may be a result of both the decreased thermal conductivity and the fuel volume that lead to a higher temperature increase during a rise in power. This larger temperature rise means that there would be more Doppler feedback.
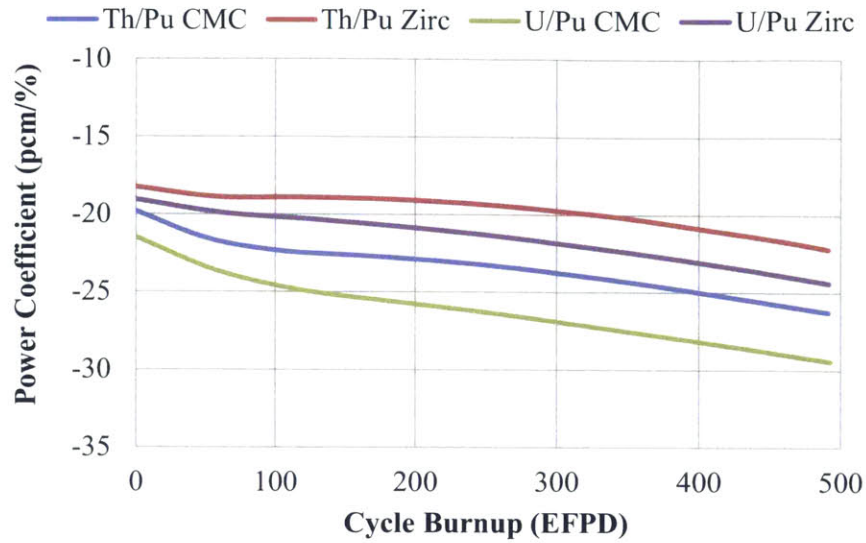
Figure 4-7: Power coefficient as a function of core burnup for both urania and thoria cores during a single cycle

The plot of core boron worth over the entire cycle length, shown in Figure 4-8, indicates that boron has more worth in thoria-plutonia systems as opposed to urania-plutonia systems. Additionally the worth is higher in SiC CMC core designs.
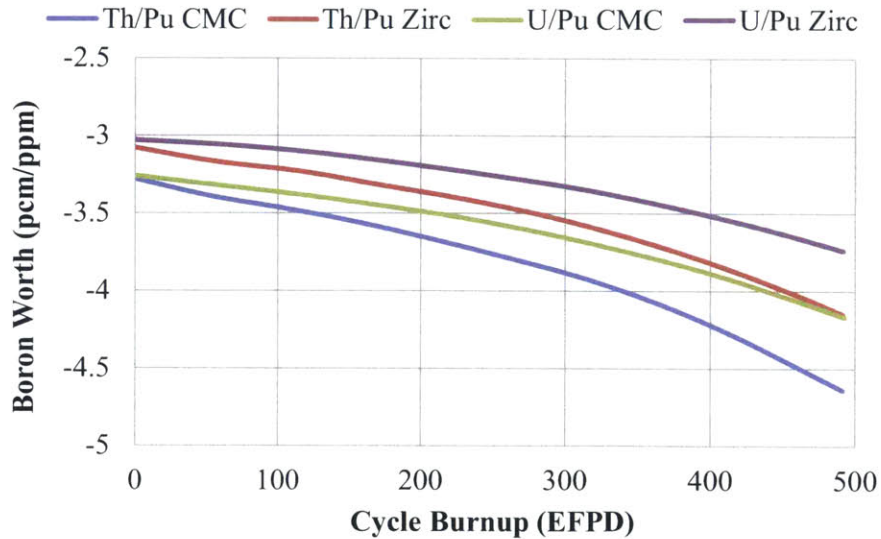
Figure 4-8: Core boron worth as a function of core burnup for both urania and thoria cores during a single cycle

4.3   Comparison of Designs

Plutonium burning characteristics of each of the reactor cores developed are displayed in Table 4-5. It can be seen that there is a benefit to using SiC as a cladding. Using SiC cladding and thoria-plutonia as a fuel resulted in the largest percentage of initial plutonium being burned. In terms of percentage, a 3% to 4% benefit is achieved by moving to SiC from Zircaloy. A 33% benefit is achieved by using thoria-plutonia instead of urania-plutonia. This large increase in the plutonium mass change is primarily due to the fact that no new plutonium is being bred in a thoria-plutonia system. This system does however breed U-233 from Th-232.

Table 4-5: Plutonium burning characteristics of different oxide fuels

Fuel	U/Pu		Th/Pu	
Cladding	SiC	Zircaloy	SiC	Zircaloy
Cycle Burnup $MWd/kgHM$	21.5	19.5	23.5	21.3
Initial Pu Loading $wt\% HM$	5.69	5.48	6.79	6.51
Initial Pu Mass Loading kg	2058	2183	2246	2369
Discharged Mass Pu - kg	1382	1554	778	899
Pu Mass Change - kg	676	630	1468	1470
Percent of Initial Pu Burned - %	32.9	28.8	65.4	62.0

Even though the plutonium enrichment is higher in SiC cores, the overall loading is likely less because of the reduced absorption cross-section of silicon carbide. The plutonium enrichment is necessarily higher in thoria-plutonia cases because of the thorium higher neutron absorption in the thermal spectrum and the fuel's reduced density.

To evaluate the effect of raising a thoria-plutonia fuel with SiC cladding to a higher burnup, a single assembly study was performed using typical core conditions, which are summarized at the beginning of Chapter 3. The results can be seen in Table 4-6. It was found that as the burnup is

105

extended, the percentage of initial plutonium remaining at discharge decreases. This indicates a more efficient system for plutonium is achieved, the higher fuel burnup can be pushed. However, as burnup increases the amount of U-233 that is bred from Th-232 absorptions increases, which counteracts some of the proliferation benefit found through plutonium burning.

Table 4-6: Effect of increased burnup on plutonium burning characteristics of the core

Max Pin Burnup *MWd/kg*	Initial Pu *wt % HM*	Remaining Pu at Discharge - %
60	6.4	38.0
80	7.9	32.9
100	9.3	27.8

The percentage of initial plutonium remaining at discharge, which is the first metric of proliferation resistance examined here, can be found in Table 4-7. It can be concluded that there is a small proliferation benefit to using SiC as a cladding material. SiC results in 3% to 4% less plutonium remaining at discharge and requires less plutonium to be loaded into the core in the first place. Additionally, a large benefit from the use of thorium instead of uranium can be seen. The U-Pu cases have higher remaining fractions of Pu, since U-238 breeds more Pu-239 in the core.

Table 4-7: Percentage of initial plutonium mass at discharge

Fuel	Clad	Percentage - %
Th/Pu	Zircaloy	38.0
	SiC CMC	34.6
U/Pu	Zircaloy	71.2
	SiC CMC	67.1

The second metric examined is the plutonium vector at discharge. A plutonium vector that contains more Pu-239 and other odd fissile isotopes is preferred for weapons activities. Table 4-8 shows the plutonium isotopic vector at core average discharge, comparing thoria to urania as host materials. It can be seen that the use of plutonia-thoria fuel results in near 20% less Pu-239 at discharge.

106

The effect of using SiC in comparison to Zircaloy as a cladding material can be seen in Table 4-8. It compares the change in percent (%) if a Zircaloy clad were used in place of SiC cladding. There is a small benefit from using SiC cladding; however it does not drastically change the characteristics of the discharged plutonium vector.

Table 4-8: Comparison of the plutonium isotopic composition of SiC CMC cladding to Zircaloy cladding at core average discharge burnup (wt%)

Isotope	Initial WG-Pu	U/Pu		Th /Pu	
		SiC CMC *wt% HM*	Zircaloy *% difference*	SiC CMC *wt% HM*	Zircaloy *% difference*
Pu-238	0.012	0.5	- 0.1	0.7	- 0.1
Pu-239	93.8	52.0	+ 4.6	32.8	+ 5.8
Pu-240	5.8	27.0	- 2.2	34.5	- 2.2
Pu-241	0.23	15.7	- 1.3	22.7	-1.6
Pu-242	0.022	3.9	- 1.0	8.0	- 1.8
Am-241	0.13	0.8	0.0	1.2	- 0.1

The heavy metal composition of a thoria-plutonia fueled core design with SiC CMC cladding can be seen in Figure 4-9. The values shown are taken from a CASMO4E assembly model with an initial plutonium composition that is the same as the average plutonium composition of all fresh assemblies in a batch. The assembly is depleted to a batch average discharge without soluble boron in the coolant or burnable poison on the fuel pellet exterior. It can be seen that plutonium is gradually depleted out of the core, while simultaneously uranium is bred from the thorium present in the core. As burnup increases, the percentage of uranium that is Pu-239 decreases, until at discharge, there is a similar amount to Pu-240 and Pu-241, which become more prevalent as burnup increases. While U-233, which is readily bred form Th-232, is the primary isotope of uranium present in the core, other uranium isotopes become more prevalent at higher burnup.
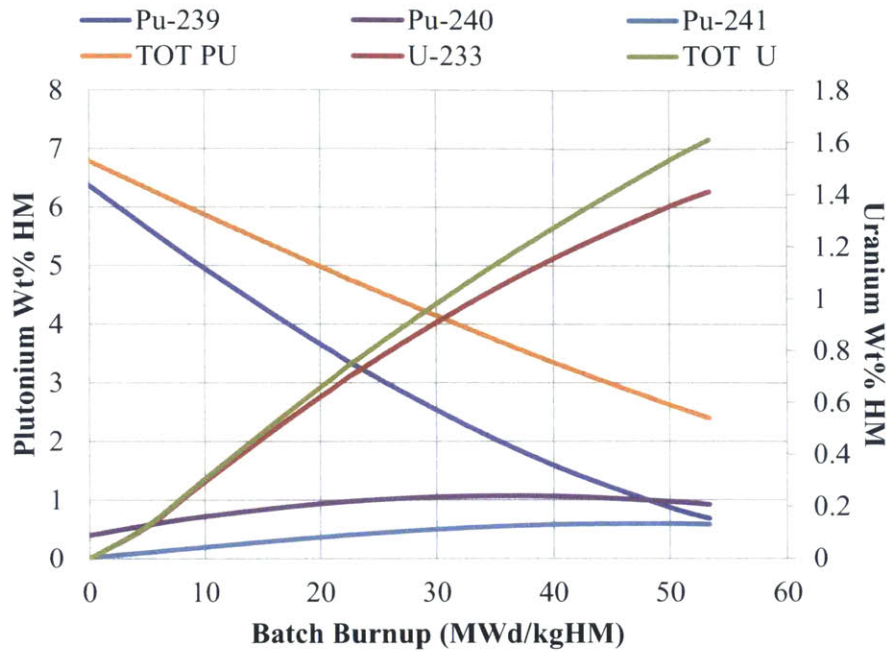
Figure 4-9: Uranium and plutonium isotopic composition of core designs with thoria-plutonia fuel with SiC CMC cladding

Similarly, the heavy metal composition of a urania-plutonia fueled core design with SiC CMC cladding can be seen in Figure 4-10. A similar assembly model is used in as in the previous case. The amount of plutonium in in a batch depletes less quickly when urania is used a host material, since Pu-239 is bred from the U-238 present in the core. The percentage of plutonium that is Pu-239 gradually decreases until is near 50% of the plutonium present. Pu-240, Pu-241 and Pu-242 are all present in increased amounts at discharge.
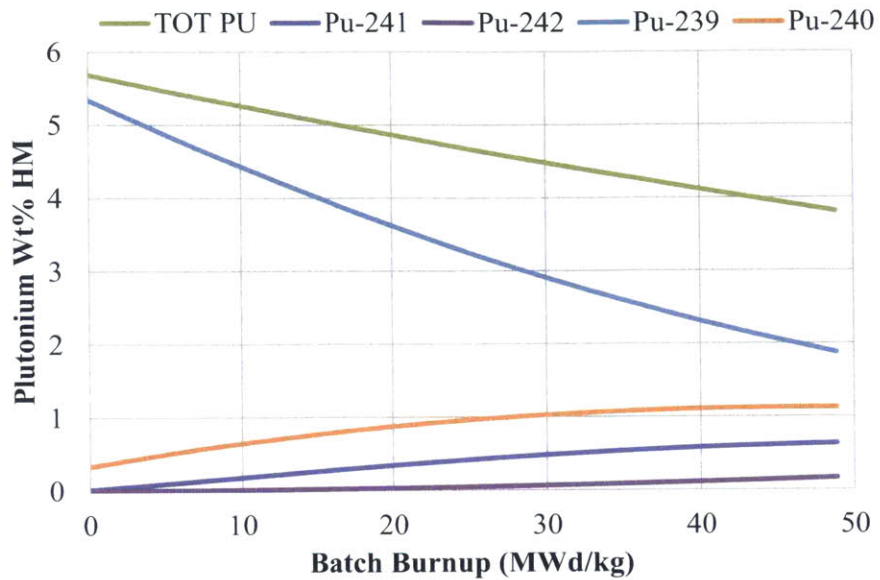
Figure 4-10: Plutonium isotopic composition of core designs with urania-plutonia fuel with SiC CMC cladding

The mass change of plutonium and uranium (for thoria cases in which U-233 is bred), both of which could be used for weapons activities, in a single assembly were calculated and are presented in Table 4-9. It can also be seen that the amount of mass discharged is less for thoria-plutonia and SiC. Using thoria instead of urania results in roughly 2.9 to 3.0 kg more mass change at discharge of materials that could be used for weapons. Using SiC instead of Zircaloy also results in a mass change 0.5 to 0.7 kg greater.

Table 4-9: Mass, both U and Pu, change from loading to discharge of a single assembly

Fuel	Clad	BOL Mass - *kg* Weapons Grade Pu	EOL Mass - *kg*	Mass Change - *kg*
Th - Pu	Zircaloy	27.9	10.3 Pu 6.4 U	-11.2
	SiC	26.4	8.8 Pu 5.9 U	-11.7
U - Pu	Zircaloy	25.7	17.6 Pu	-8.1
	SiC	24.2	15.4 Pu	-8.8

Based on the plutonium burning characteristics and proliferation resistance of the four designs presented, it is concluded that using SiC CMC cladding with a thoria-plutonia fuel was the best design for plutonium disposition. Thoria-based fuel results in a higher percentage of plutonium burned, a better plutonium vector at discharge and a lower critical mass multiple at discharge. A thoria-plutonia fueled assembly has 56% to 58% of the plutonium at discharge that a urania-plutonia fuel has. Switching from Zircaloy to SiC results in roughly 3% improvement in the percent of initial plutonium burned when SiC CMC cladding is used, even though the total amount of plutonium mass change from beginning of life to discharge is nearly identical.

4.3.1 Proliferation Figure of Merit

Another method to assess the attractiveness of a nuclear fuel for various proliferation scenarios can be found in work by Bathke (2012), which uses a figure of merit (FOM) based on three key proliferation metrics. The development of this FOM is a result of collaboration between the three DOE weapons labs, Los Alamos National Laboratory, Sandia National Laboratory and Lawrence Livermore National Laboratory. The equation for this figure of merit can be seen in Equation 4-1. First is the multiple of bare critical mass of the material in question. Second is the heat content of the fuel, and third is the dose rate of the fuel. The FOM relates these three values to accepted standards for materials that are considered unattractive: (1) threshold for low-enriched uranium of 20% U-235, (2) radioisotope thermoelectric generator Pu (>80% Pu-238) heat generation rate and (3) a self-protecting dose rate of 500 rad/h. [Bathke, 2012]

$$FOM = 1 - \log_{10}\left(\frac{M}{800} + \frac{Mh}{4500} + \frac{M}{50}\left(\frac{D}{500}\right)^{\frac{1}{\log_{10} 2}}\right) \qquad (4\text{-}1)$$

Where:

$M = bare\ critical\ mass\ (kg)$
$h = heat\ content\ (W/kg)$
$D = dose\ rate\ of\ 0.2 \times critical\ mass\ evaluated\ at\ 1\ meter\ (rad/h)$

According to this figure of merit, values over 1.0 are considered attractive as weapons, while those over 2.0 are considered highly attractive. Values below 1.0 are unattractive as weapon material, and those below 0.0 are very unattractive. The proliferation characteristics of key uranium and plutonium isotopes can be seen in Table 4-10. It can be seen that U-232 has a comparatively high dose rate and Pu-238 has a comparatively high heat generation rate. Both isotopes have a FOM near 1.0, meaning they are unattractive for use in weapons. Other isotopes, like U-233 and Pu-239 are both highly attractive with an FOM of 2.7 and 2.8 respectively. They are the most preferred isotopes for use in weapons.

Table 4-10: Proliferation characteristics of key uranium and plutonium isotopes [Bathke, 2012]

Isotope	Density g/cm^3	Critical Mass kg	Heating W/kg	Dose (D) rad/h	FOM
^{232}U	18.95	6.7	7.10E+02	0.282	1.0
^{233}U	18.95	15.3	2.81E-01	1.46E-04	2.7
^{234}U	18.95	126.1	1.79E-01	3.59E-04	1.8
^{235}U	18.95	46.5	6.00E-05	1.04E-05	2.2
^{236}U	18.95	1.00E+12	-	-	-
^{238}U	18.95	1.00E+11	-	-	-
^{238}Pu	19.84	9.7	5.68E+02	2.11E-01	0.9
^{239}Pu	19.84	10	1.92E+00	3.95E-04	2.8
^{240}Pu	19.84	37.3	7.08E+00	7.17E-03	2.0
^{241}Pu	19.84	13	3.28E+00	1.45E-03	2.6
^{242}Pu	19.84	89.1	1.17E-01	5.45E-03	1.9
^{241}Am	13.69	57.3	1.14E+02	1.22E+00	0.8

To calculate the critical mass of the relevant isotopes in an assembly at discharge, the Monte Carlo depletion code Serpent was used. A bare sphere was used to determine the critical mass. For thoria-based assemblies, both uranium and plutonium isotopes are considered for proliferation purposes. For thoria-based assemblies, both combined and separated uranium and plutonium cases are considered. This is conservative, since the large amount of U-233 in an assembly at discharge, makes it more attractive. For urania-based designs, only the plutonium present was considered. If uranium isotopes were considered, the critical mass would be much

higher because of the U-238 present. The uranium and plutonium isotopic composition for critical mass calculations at the batch average discharge assembly can be seen in Table 4-11. This discharge composition was calculated using a single assembly model with no soluble boron in the coolant and no burnable poison (IFBA) on the exterior of fuel pellets. The initial plutonium loading of the assembly model was the same as that of a fresh fuel batch. It was assumed that both uranium and plutonium were separated from other isotopes in spent fuel through reprocessing.

Table 4-11: Uranium and plutonium composition at batch average discharge for plutonium burning core designs

Isotope	U/Pu Zircaloy	U/Pu SiC CMC	Th/Pu Zircaloy	Th/Pu SiC CMC
U-232	-	-	0.1	0.2
U-233	-	-	33.9	35.2
U-234	-	-	3.6	4.0
U-235	-	-	0.7	0.7
U-236	-	-	0.0	0.1
Pu-238	0.4	0.5	0.4	0.4
Pu-239	53.4	49.2	21.0	17.0
Pu-240	27.4	29.5	22.3	22.9
Pu-241	15.4	16.6	14.0	14.5
Pu-242	3.3	4.2	4.1	5.0

Based on the vectors shown in Table 4-11, the resultant critical mass and heating for use in the FOM calculation can be seen in Table 4-12. Also included in the table are weapons grade plutonium and reactor grade plutonium for reference points. The dose rate of discharged assemblies was assumed to be the same as the reactor-grade plutonium case in Bathke (2012) at 8.42×10^{-3} rad/h. Dose rates below ~50 rad/h do not have an affect the figure of merit beyond the third decimal place, so the reported FOM is not significantly affected by this assumption. It can be seen that the FOM of all of the different assembly designs are similar. Because of the lower critical mass, the urania-plutonia fuels are slightly more attractive. Similarly this is the case with silicon carbide cladding. The FOM of discharged assemblies is roughly halfway

between that of weapons grade Pu and reactor grade Pu. The most limiting cases are those of separated uranium for thoria-plutonia fuel. However, it should be noted that all cases at discharge show a FOM above 2.0, which is highly attractive for weapons activity. The primary benefits of using thoria-based fuel is that there is less weapons useable material at discharge and more disposed of during operation.

Table 4-12: Proliferation characteristics of plutonium burning fuel designs at batch average discharge burnup compared to weapons and reactor grade plutonium

Design		Critical Mass (M) kg	Heating (Mh) W	FOM
U/Pu Zircaloy		13.8	81.13	2.45
U/Pu SiC CMC		14.4	90.51	2.42
Th/Pu - SiC CMC Combined U and Pu		16.9	99.61	2.36
Th/Pu - SiC CMC	U	17.2	51.17	2.48
Separated U and Pu	Pu	17.2	135.2	2.29
Th/Pu – Zircaloy Combined U and Pu		16.3	89.25	2.40
Th/Pu – Zircaloy	U	17.1	4.53	2.50
Separated U and Pu	Pu	16.3	117.9	2.33
Weapons Grade Pu (Initial Pu Composition)		10.5	23.9	2.73
Reactor Grade Pu at 45 MWd/kgHM [Bathke, 2012]		14.4	257	2.13

4.3.2 Isotopic Energy and Power

Using a single assembly model to approximate the behavior of a batch in the code CASMO4E the relative power and relative energy generated from each isotope were found. This single

assembly model contained no soluble boron in the coolant and no burnable poison (IFBA) on the exterior of fuel pellets. The initial plutonium loading of the assembly model was the same as that of a fresh fuel batch. For the thoria-plutonia design with silicon carbide cladding the relative power generated from plutonium and uranium can be seen in Figure 4-11. It can be seen that at beginning of life most of the power is generated from plutonium. As the burnup increases, the amount of power generated by uranium gradually increases until it generates 30% of the total power at the end of life. Nearly all of the power generated by uranium is generated by U-233. For plutonium, the amount of power generated by Pu-239 gradually decreases over time and the amount of power generated by Pu-241 increases, as it is created as the assembly is depleted.
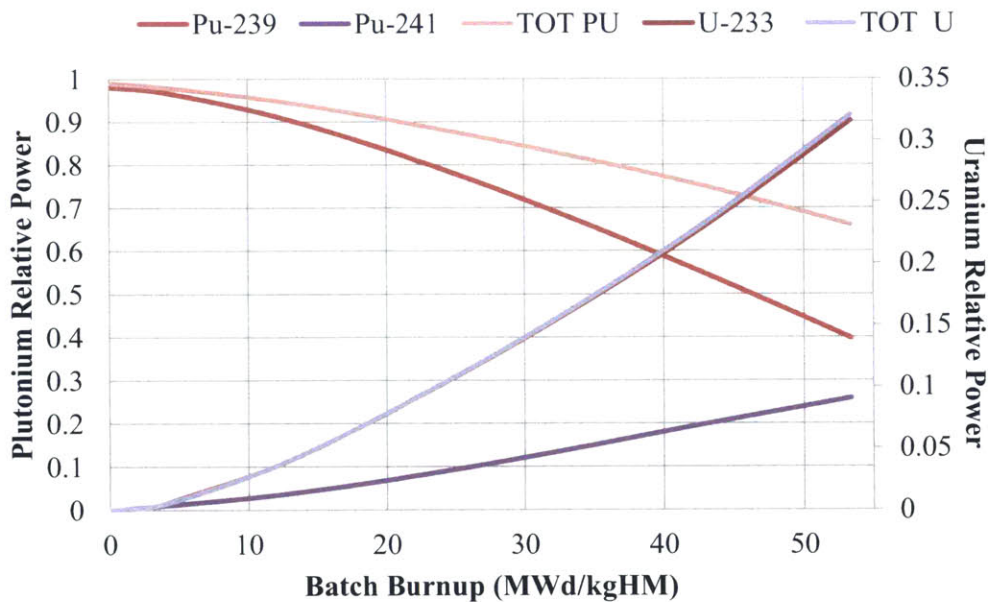
Figure 4-11: Relative amount of power generated by uranium and plutonium for thoria-plutonia fueled assemblies with silicon carbide cladding

Similarly, the total amount of energy generated by relevant isotopes for thoria-plutonia fueled assemblies with silicon carbide cladding can be seen in Figure 4-12. Like the relative amount of power generated, the total amount of energy generated by uranium, and also Pu-241, increases with time.
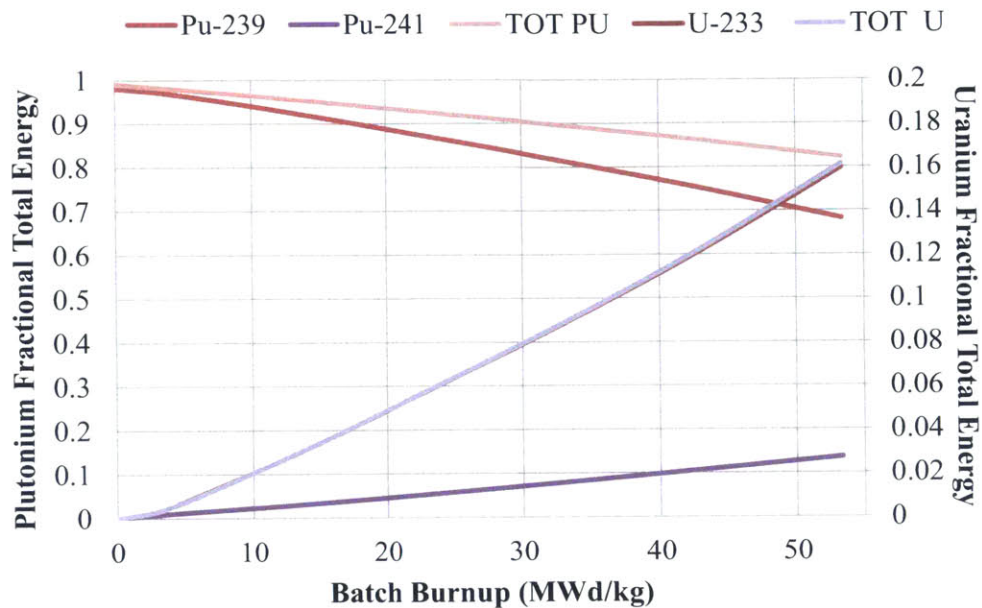
Figure 4-12: Relative amount of total energy generated by uranium and plutonium for thoria-plutonia fueled assemblies with silicon carbide cladding

For urania-plutonia fueled assemblies with silicon carbide cladding, the total amount of power generated by uranium and plutonium is nearly constant with time. Uranium power is generated by fast fissions from U-238, since the uranium is taken to be entirely of depleted enrichment. This can be seen in Figure 4-13. The amount of energy generated by Pu-239 decreases with time while the power generated by Pu-241 increases with time.
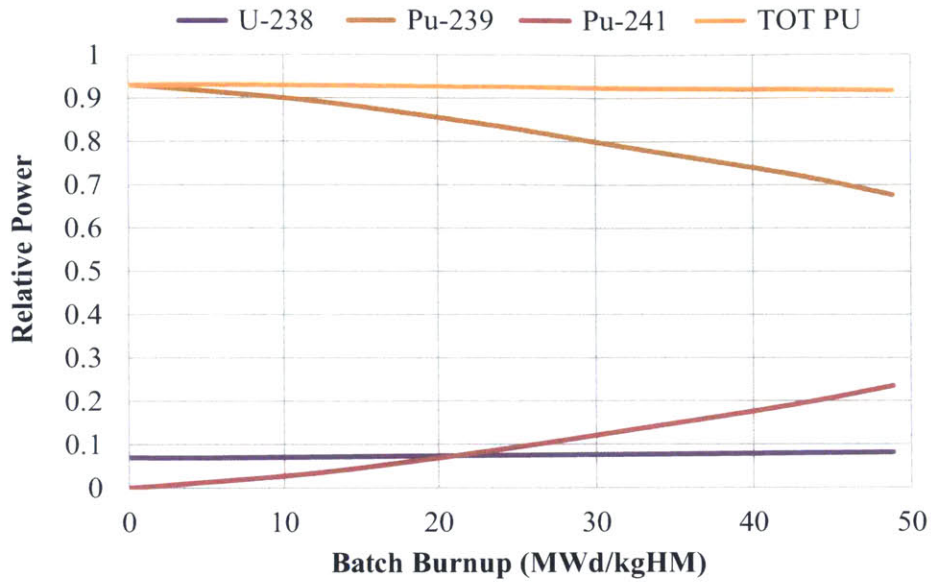
Figure 4-13: Relative amount of power generated by uranium and plutonium for urania-plutonia fueled assemblies with silicon carbide cladding

The total amount of energy generated for this case can be seen in Figure 4-14. It follows the same trends found in power. The amount of energy generated by U-238 is constant with time.
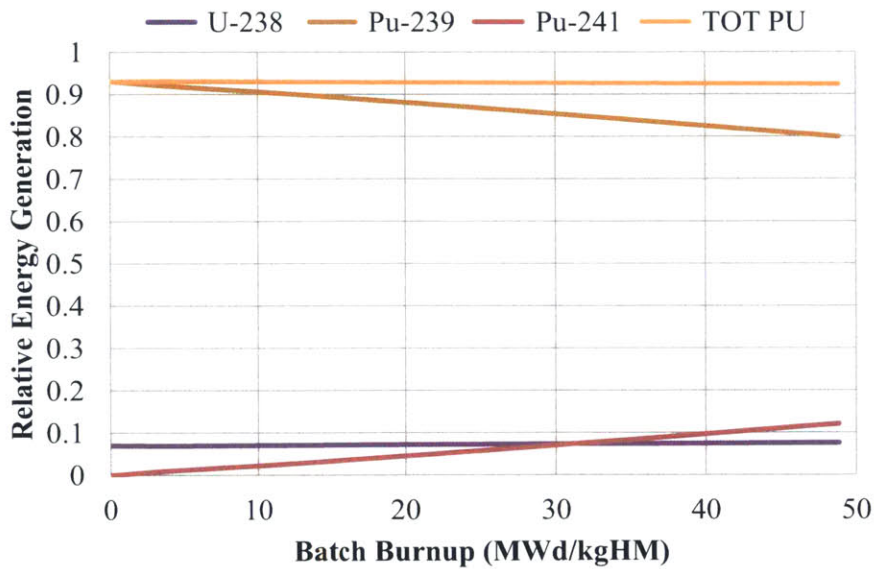
Figure 4-14: Relative amount of total energy generated by uranium and plutonium for urania-plutonia fueled assemblies with silicon carbide cladding

The relative isotopic burnup for the two separate plutonium disposition fuel options can be seen in Figure 4-15 and Figure 4-16 when silicon carbide cladding is used.
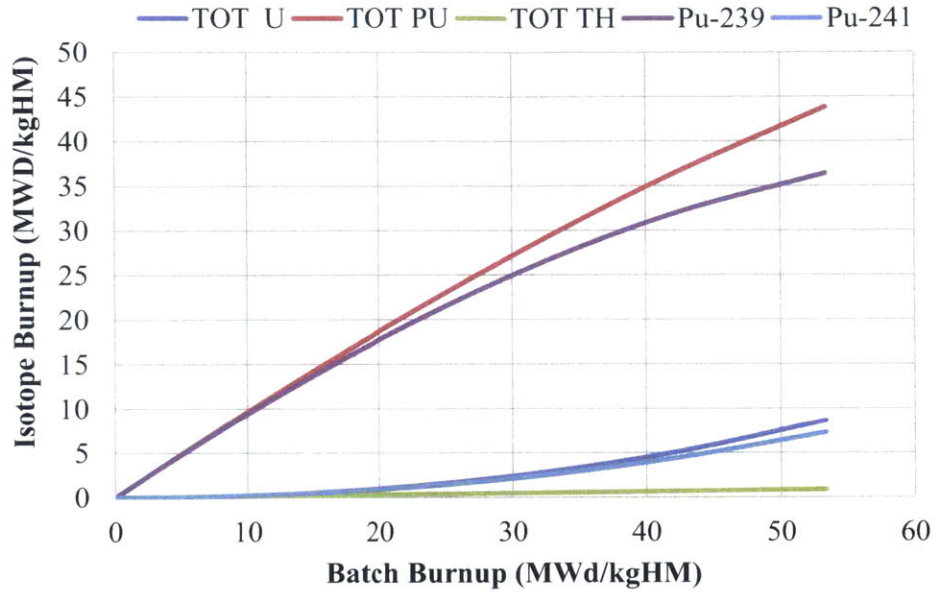
Figure 4-15: Isotopic burnup for thoria-plutonia fueled assemblies with silicon carbide cladding
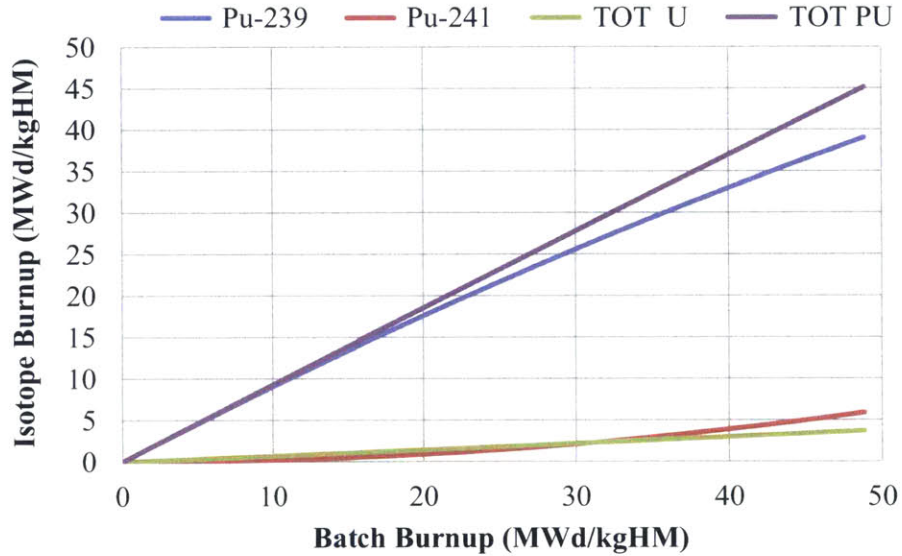
Figure 4-16: Isotopic burnup for urania-plutonia fueled assemblies with silicon carbide cladding

5. Transient Analysis of Accident Scenarios of Plutonium Burning Cores

Because of the different kinetic characteristics of thoria-plutonia fuel compared to urania-plutonia (MOX) or enriched urania fuel, it is necessary to perform transient analyses of the reactor core designs during design-basis accident scenarios. Of particular interest are rapid reactivity insertion accidents, since they are highly dependent on the fuel used. Different values of the delayed neutron fraction, prompt neutron lifetime and thermal conductivity all lead to different behavior in transient accidents. Two accident scenarios that are important for core design basis accident assessment and indicative of the different fuel type behavior are rod ejection and main steam line break. The progressions of both accidents are discussed in Sections 2.5.1 and 2.5.2. In any transient, it is necessary for the core to maintain safe behavior. This includes maintaining a safe mDNBR, fuel temperature and core power response. For these analysis, the code SIMULATE3K was used, which is the transient version of SIMULATE3. Typically, for licensing analysis, many conservative factors and assumptions are applied to the transient simulation. Since the primary motivation behind this analysis is to present the relative different performance of each fuel type, no additional conservatism is taken into account.

In transient analysis, the delayed neutron fraction is one of the driving factors behind core behavior. This value is dependent on the isotopes in the system. The values of relevant plutonium and uranium isotopes can be seen in Table 5-1 for both fast and thermal neutron energies. It can be seen that the delayed neutron fraction for both U-233 and Pu-239 are significantly lower than those for U-235 and U-238. This indicates that cores which use these as the primary fuel will respond to reactivity insertion accidents significantly faster.

Table 5-1: Delayed neutron fraction for both fast and thermal fissions [Shultis and Faw, 2008]

Isotope	Fast Fission	Thermal Fissions
^{235}U	0.0064	0.0065
^{233}U	0.0026	0.0026
^{239}Pu	0.0020	0.0021
^{241}Pu	-	0.0049
^{238}U	0.0148	-
^{232}Th	0.0203	-
^{240}Pu	0.0026	-

The thermal conductivity of the different cladding and fuels was inputted into SIMULATE3K as a function of burnup and temperature. The thermal conductivity of thoria-plutonia fuel can be seen in Figure 5-1. Along the same lines, the thermal conductivity of urania-plutonia can be seen in Figure 5-2. Compared to thoria-polutonia fuel, the thermal conductivity of urania plutonia-fuel increases and is therefore higher at high temperatures. For both types of fuel, the thermal conductivity decreases as the burnup increases. The behavior of enriched urania fuel can be seen in Figure 5-3. It exhibits similar behavior to urania-plutonia fuel, with a higher initial thermal conductivity.
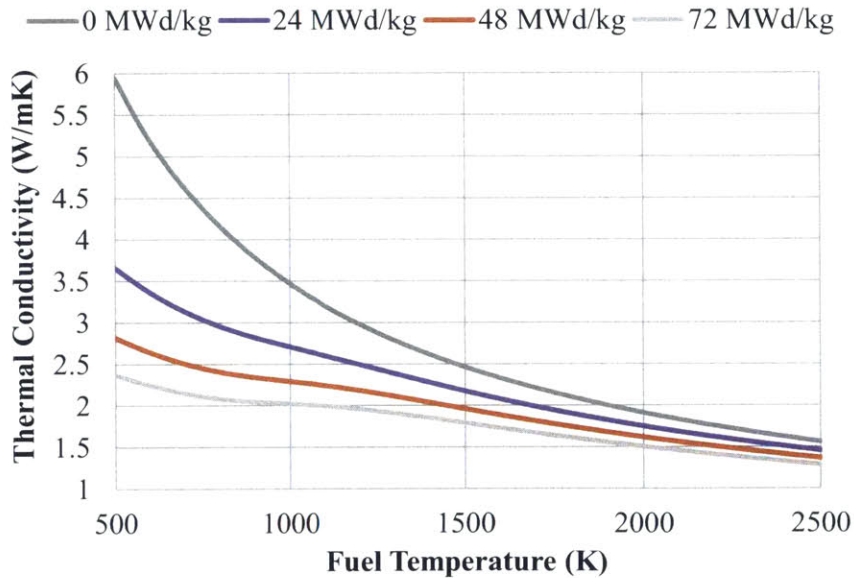
Figure 5-1: Thermal conductivity of thoria-plutonia fuel

119
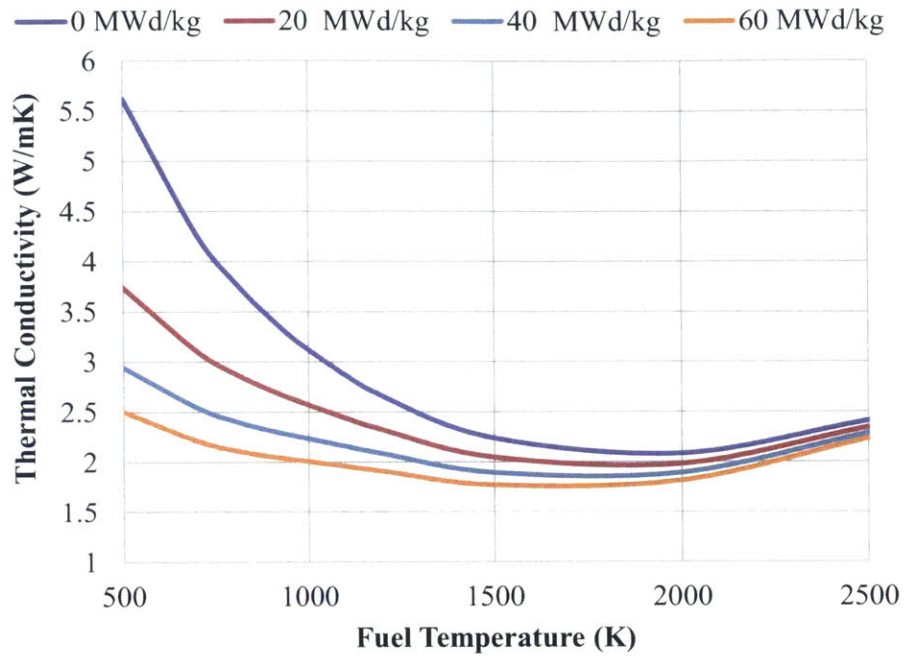
Figure 5-2: Thermal conductivity of urania-plutonia fuel
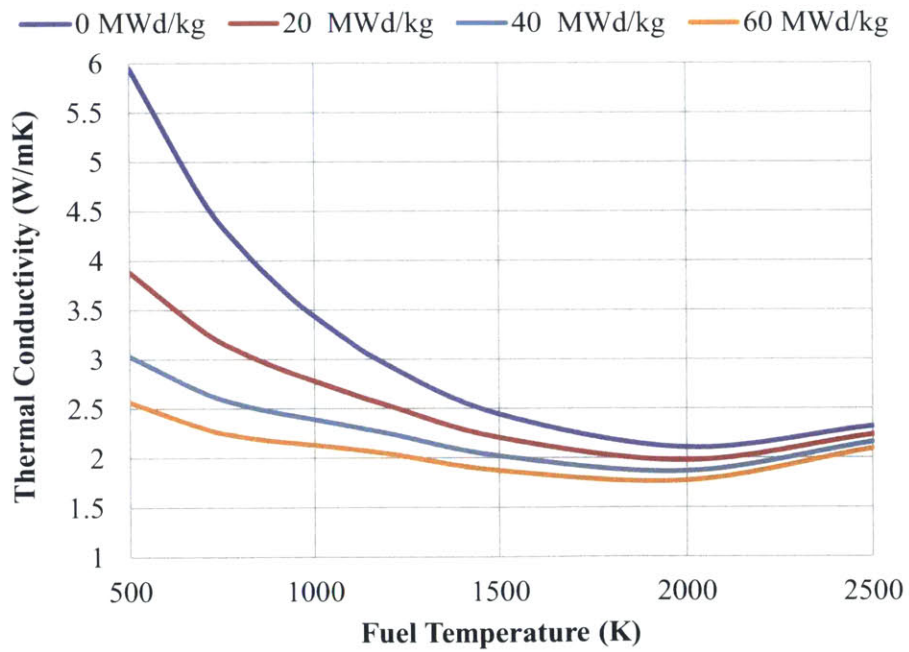
Figure 5-3: Thermal conductivity of enriched UO₂ fuel

120

5.1   Rod Ejection

The first reactivity insertion accident examined is a control rod ejection. In this simulation, the reactor was simulated at the most limiting condition, HZP, at both BOC and EOC. The core model is run at a steady-state condition for 1.0 seconds. Then at 1.0 seconds, the control rods in an assembly, which results in the most increase in core reactivity, is ejected. The progression of this accident and the design limits are covered in detail in Section 2-5. The rods used in the core are AgInCd for the nominal urania-Zircaloy PWR case but are made of B_4C for all other cases.

The ejected rod cluster was chosen as the one which gives the highest reactivity insertion into the core. This does not always correspond to the rod with the highest worth, so reactivity insertion by all high worth rods need to be simulated. A typical rod worth map can be seen in Figure 5-4, which shows the ejected rod worth of each control and safety rod in the southeast corner of the core. Only one rod cluster was ejected from the core, and not one in each quadrant.

```
08   579.           575.           309.           40.

09                                        142.

10   575.           843. *                       46.

11                                        147.

12   309.                          303.           13.

13           140.           146.

14   40.            45.            13.

15
      H      G      F      E      D      C      B      A
```
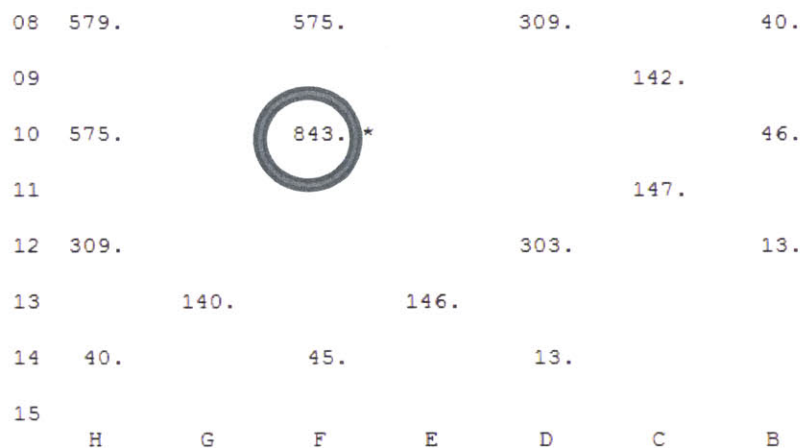
Figure 5-4: Control and safety rod worth map of the southeast corner of the core at BOC for the thoria-plutonia core with SiC CMC as a cladding. The maximum rod cluster is shown at F-10.

Since the reactor is in a different condition at BOC compared to EOC, both conditions need to be simulated. A second rod worth map is given for the same core at EOC in Figure 5-5. It can be seen that, in comparison to the BOC worth map, that at EOC the highest worth rods are near the edge of the core and not concentrated in the center. However, other cores have different rod worth maps and high worth rods at BOC or EOC may be at different locations.

121

```
08   315.           513.           492.           186.

09                                          382.

10   515.           738.                          286.

11                                   666.

12   493.                      881.               69.

13          376.        667.

14   183.           287.           67.

15
     H      G      F      E      D      C      B      A
```
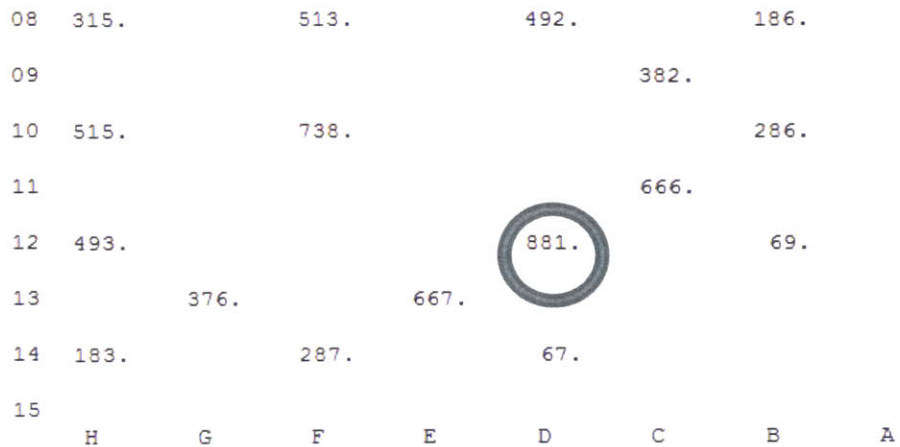
Figure 5-5: Control and safety rod worth map (in pcm) of the southeast corner of the core at EOC for the thoria-plutonia core with SiC CMC as a cladding. The maximum rod cluster is shown at D-12.

The locations of the most limiting rod ejection can be seen in Table 5-2, also shown in the table are the rod ejection worth ($) and the delayed neutron fraction of the core. The ejection worth is higher at BOC as opposed to EOC for all cases. At EOC the delayed neutron fraction is higher for both U/Pu and Th/Pu cases, since at EOC there is less plutonium-239 in the core, which has a low delayed neutron fraction compared to the other fissile isotopes in the systems. Because the typical low enriched urania PWR core has a higher delayed neutron fraction, the ejection worth (in terms of dollars) is significantly higher for urania-plutonia and thoria-plutonia cores. This ejection worth determines the magnitude of the core power spike.

Table 5-2: Rod location and ejection worth of maximum

Fuel	Clad	Time in Cycle	Rod Ejection Location	Ejection Worth - $	Delayed Neutron Fraction - β
Typical PWR Enriched UO_2	Zircaloy	BOC	F-10	1.31	0.00606
		EOC	D-12	1.30	0.00517
U/Pu	Zircaloy	BOC	F-10	2.19	0.00335
		EOC	F-10	1.88	0.00362
	SiC CMC	BOC	F-10	2.24	0.00322
		EOC	F-10	1.90	0.00363
Th/Pu	Zircaloy	BOC	F-10	2.62	0.00294
		EOC	D-12	2.15	0.00341
	SiC CMC	BOC	F-10	2.59	0.00294
		EOC	D-12	2.42	0.00345

The ejection worths shown are higher than those found in the PWR MOX/UO_2 rod ejection benchmark performed by Kozlowski and Downar (2007). There is significantly more plutonium in the cores developed in this study than in the benchmark. This leads to a lower core-wide delayed neutron fraction and a faster transient response. The maximum enthalpy, which is the design limit, contained in the highest enthalpy node is given in Table 5-3. It can be seen that none of the ejected rods exceeded the limits shown in Figure 2-10, which shows a minimum limit of 120 cal/g. At BOC, the maximum enthalpy of a rod ejection was 66.1 cal/g, for the U/Pu case with SiC-CMC cladding. At EOC, the maximum enthalpy of 49.3cal/g may not be acceptable for Zr. Furthermore, there are no definite limits for SiC at this time.

Table 5-3: Maximum enthalpy of highest worth rod ejection

Fuel	Clad	Time in Cycle	Max Enthalpy - *cal/g*
Typical PWR Enriched UO_2	Zircaloy	BOC	39.6
		EOC	33.8
U/Pu	Zircaloy	BOC	58.3
		EOC	45.8
	SiC CMC	BOC	63.2
		EOC	49.3
Th/Pu	Zircaloy	BOC	60.6
		EOC	46.2
	SiC CMC	BOC	66.1
		EOC	56.0

In relation to Zircaloy cladding, SiC CMC cladding resulted in an enthalpy that was higher at both BOC and EOC, with BOC being 4.9 to 5.5 cal/g higher. It can also be seen that BOC rod ejection is 12.5 to 19.6 cal/g higher than rod ejection at EOC for both U/Pu and Th/Pu fuel. For the two different fuel types there was no discernable trend and the results for the same cladding at the same condition were within 3.0 cal/g for all cases. Plots showing the behavior of the different core designs are shown in the next two subsections. Included are reactivity, core power and maximum fuel enthalpy

5.1.1 Beginning of Cycle

The core power resultant from the rod ejection transient at BOC can be seen in Figure 5-6 for the full duration of the transient, and in Figure 5-7 for time when core power is at its maximim. The transient begins at 1.0 second, after a full second to develop a steady-state. At this point the rod is fully ejected over 0.1 seconds. The core power rises exponentially over the course of this 0.1 second ejection, peaking near 1.1 seconds. At this point, Doppler feedback drives core reactivity,

124

and also power, back down. The core power rise is slightly faster for the SiC CMC cases in relation to the Zircaloy cases.
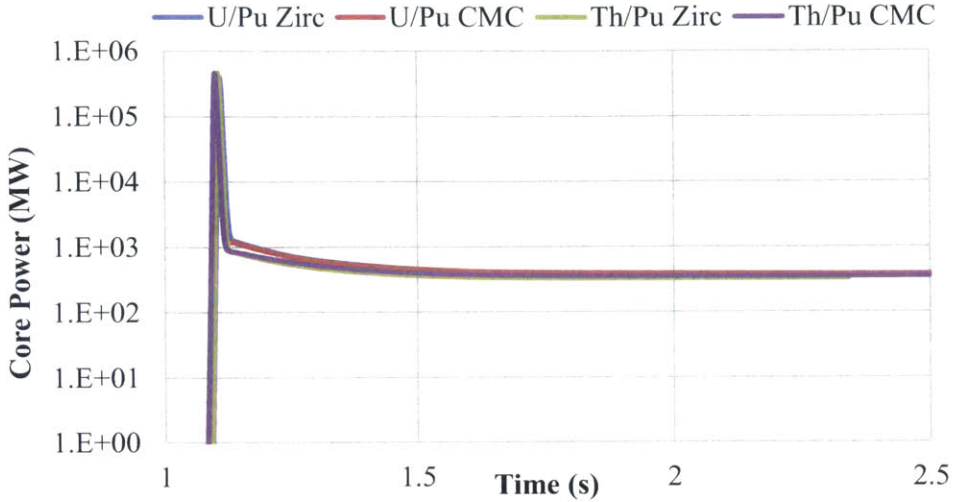
Figure 5-6 : Core power as a function of time during a rod ejection accident at BOC, showing both thoria and urania fueled cores
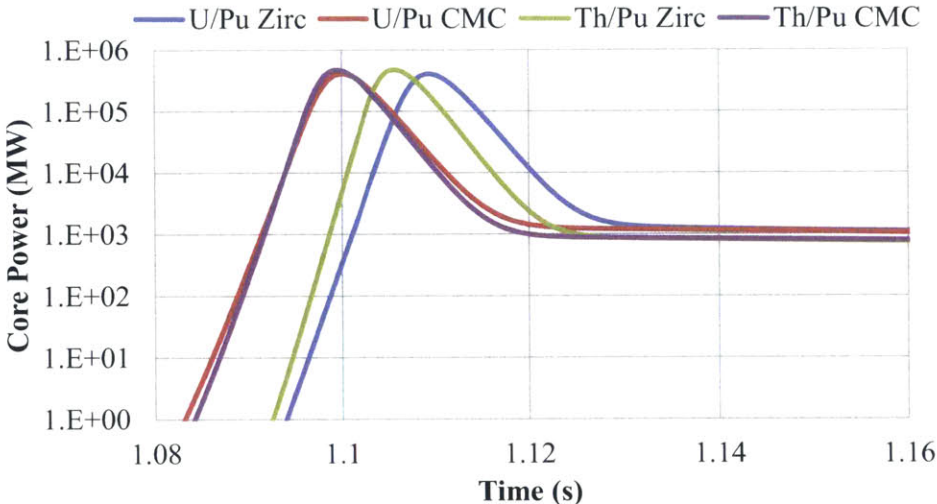
Figure 5-7: Core power as a function of time during a rod ejection accident at BOC, showing both thoria and urania fueled cores, short time

While the core power rises to a value significantly higher than what it is operationally permissible, the overall pulse width is actually very small, with the time when the reactor is above full power only being ~0.02 seconds. This means that the overall amount of energy

deposited is very small, and is likely to be well below the limits established. The maximum enthalpy in a single fuel node can be seen in Figure 5-8. Like the core power, a peak is seen near 1.1 seconds, when the rod is fully ejected and Doppler feedback begins to dominate.
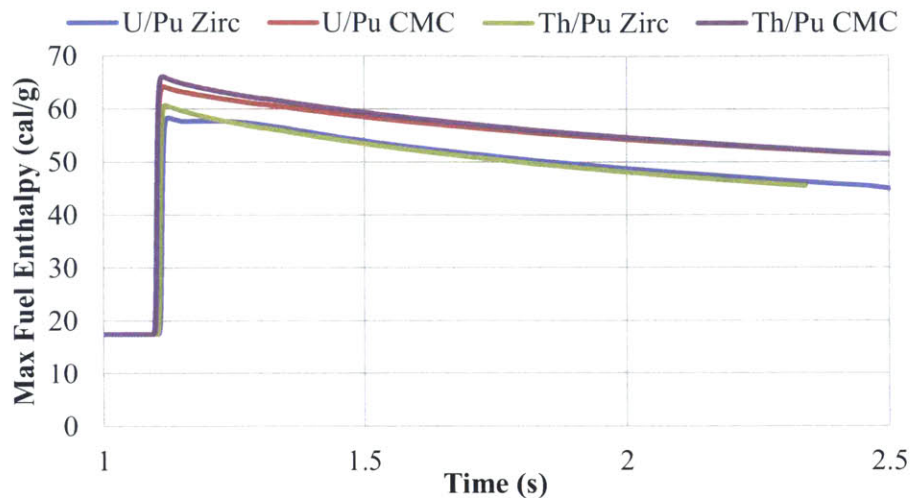
Figure 5-8: Maximum fuel enthalpy as a function of time during a rod ejection accident at BOC, showing both thoria and urania fueled cores

The core reactivity resultant from the control rod ejection can be seen in Figure 5-9 and in Figure 5-10. The reactivity rises roughly linearly from 1.0 to 1.1 seconds as the control rod is ejected. At the rise in fuel temperature that is associated with a rise in core power, leads the core reactivity to rapidly decrease. As the reactivity drops and becomes negative, this serves as a driver for the core power drop at the same time. Core reactivity then continues to remain negative because of the increased fuel and moderator temperature from the power rise. In these reactivity plots, it can be seen that the overall amount of reactivity added is less for urania-plutonia fuel than thoria-plutonia fuel.
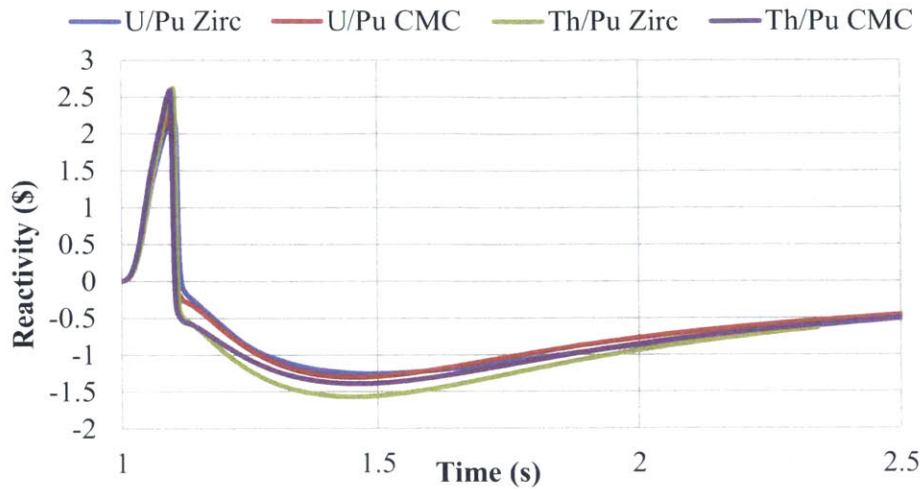
Figure 5-9: Core reactivity as a function of time during a rod ejection accident at BOC, showing both thoria and urania fueled cores
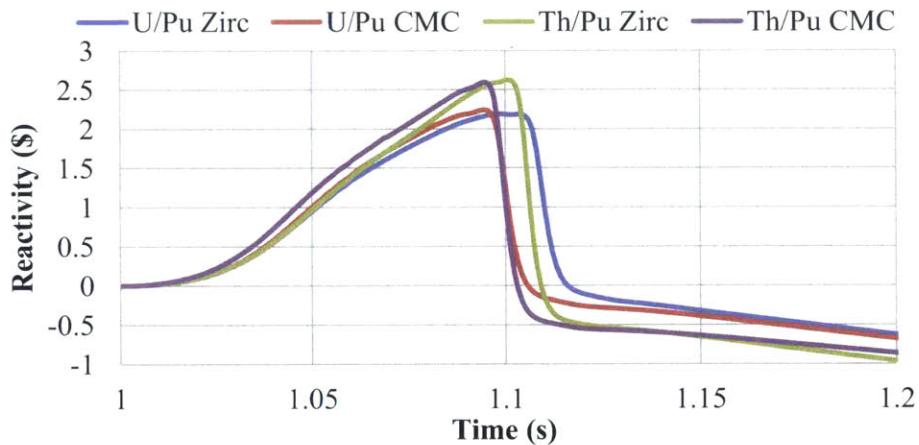
Figure 5-10: Core reactivity as a function of time during a rod ejection accident at BOC, showing both thoria and urania fueled cores, short time

5.1.2 End of Cycle

The same trends seen the core power rise from a rod ejection at BOC can also be seen at EOC. This is shown in Figure 5-11. Core power rises faster for SiC CMC in relation to Zircaloy. At EOC the maximum core power is lower than at BOC, this is a result of the decreased rod ejection worth of the cases shown and summarized in Table 5-2. The time of the maximum power is ~0.05 seconds delayed from the BOC transient.
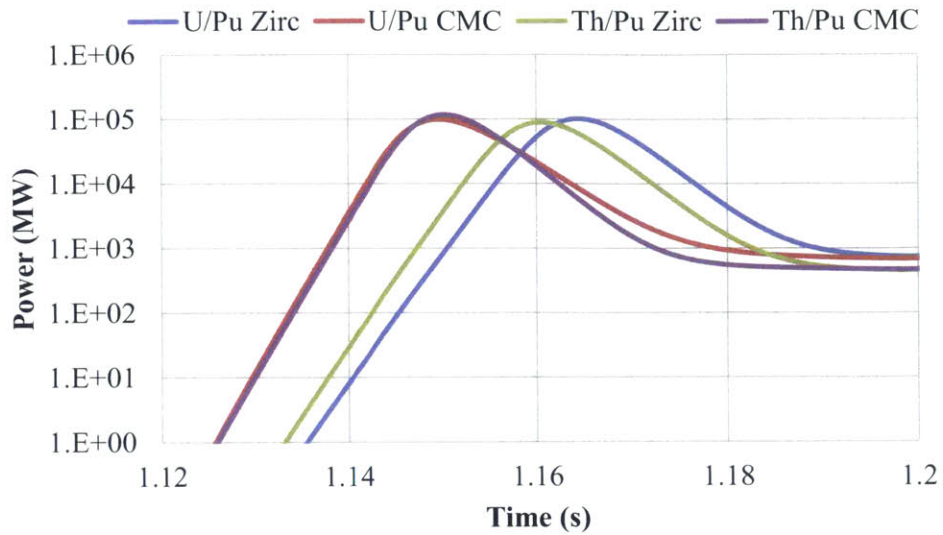
Figure 5-11: Core power as a function of time during a rod ejection accident at EOC, showing both thoria and urania fueled cores, short time

This delayed maximum power, and the associated fuel temperature rise, results in the core reactivity maintaining its maximum value for roughly 0.05 seconds. This "flat" period in core reactivity can be seen in Figure 5-12, from the times of 1.1 to 1.15 seconds. All four cases shown demonstrate this behavior.
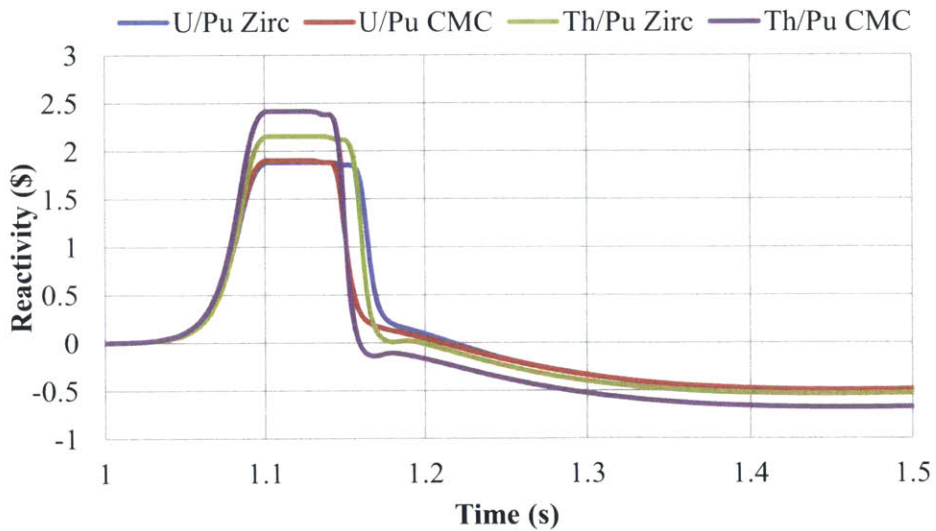
Figure 5-12: Core reactivity as a function of time during a rod ejection accident at EOC, showing both thoria and urania fueled cores, short time

The maximum fuel enthalpy occurs for EOC cases near 1.15 seconds, corresponding to the point when core power is at its highest and right before the point when core reactivity drops. This behavior can be seen in Figure 5-13.
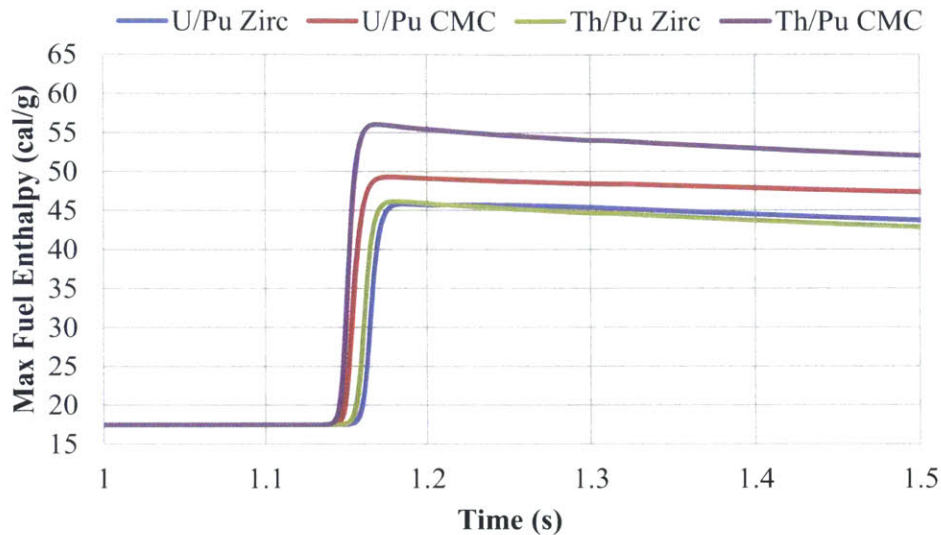
Figure 5-13: Maximum fuel enthalpy as a function of time during a rod ejection accident at EOC, showing both thoria and urania fueled cores, short time

5.2   Main Steam Line Break (MSLB)

The second reactivity insertion accident examined is a main steam line break (MSLB). Like the rod ejection accident, this analysis needs to be performed at both BOC and EOC. To ensure the reactor's safe behavior, the reactor scram is required to keep core in a subcritical state. The mDNBR is also monitored to ensure the coolant is able to remove sufficient heat from the core during the transient. A full description of the event and the expected core behavior is presented in Section 2.5.2.

For the purposes of this analysis, it is sufficient to model only the core region itself. To do this the two driving variables, core pressure and core inlet coolant temperature are used as boundary conditions. These values are taken from the TMI OECD/NEA benchmark and approximated

based on Figure 5-14 and Figure 5-15. The core pressure transient response can be seen in Figure 5-14. Increased cooling by the secondary system leads to a drop in the core inlet temperature, which is associated with an increase in the coolant density. As density increases, the system pressure drops, due to more volume becoming available for the vapor. However, after some time, the cooling in the secondary system decreases, and the core inlet temperature starts to increase.
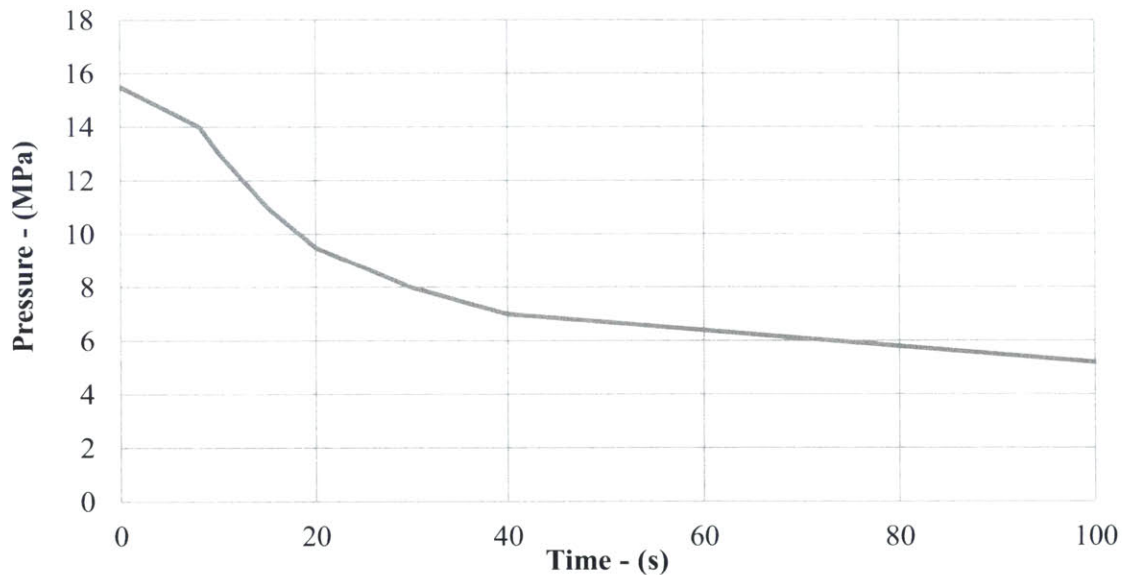
Figure 5-14: Core pressure behavior during the MSLB transient

The inlet coolant temperature response can be seen in Figure 5-15. Initially, the increased boiling and lower pressure by the secondary system leads to a drop in core inlet temperature. The temperature increase, later in the transient, is a result of the initial power increase, which comes about because of lower coolant temperature and higher density that causes increase in moderation. The increase is delayed following the initiation of the accident, since the water needs to circulate through the system.
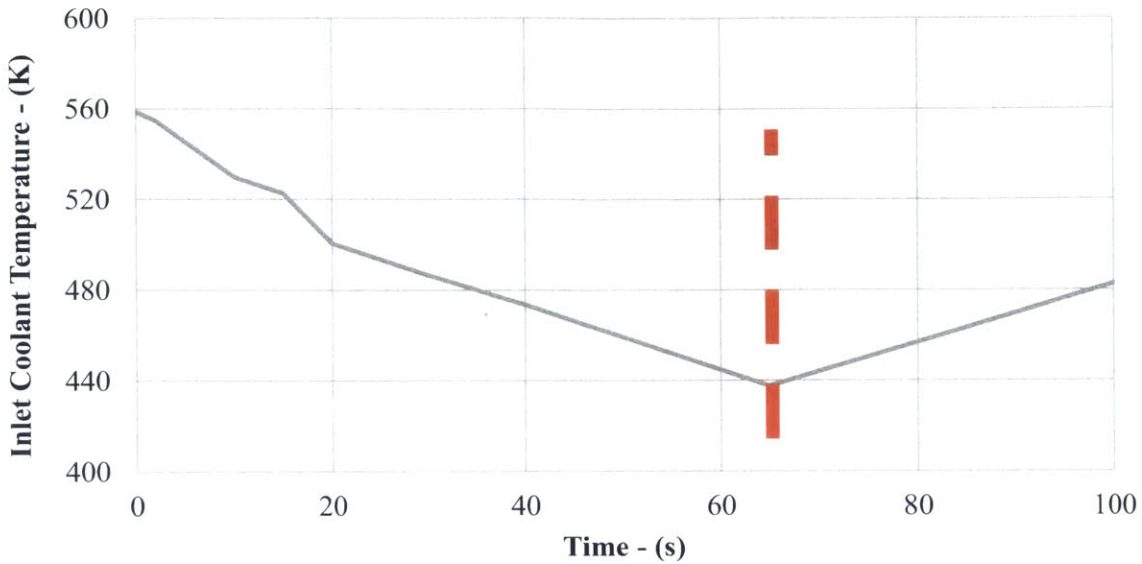
Figure 5-15: Core pressure behavior during the MSLB transient

5.2.1 Beginning of Cycle

In a MSLB accident the two main core parameters that must be monitored are the core power response and the DNBR of the core. The core power must not rise too quickly in the transient and the minimum DNBR needs to remain above a value of 2.17, as calculated using the Westinghouse W-3 Correlation. Accordingly, these parameters are shown along with the core reactivity and fuel temperature. While the transient is simulated up to 100 seconds, the plots shown go only to 20 seconds, since the values after the reactor scram are near constant for the parameters plotted. The core power response to 20 seconds is shown in Figure 5-16. Both the initial core power rise due to the decreased core inlet coolant temperature and the subsequent SCRAM at over power are shown in the plot. After the scram, the core power does not rise again. It can be seen in the plot that the core power remains low after the scram.
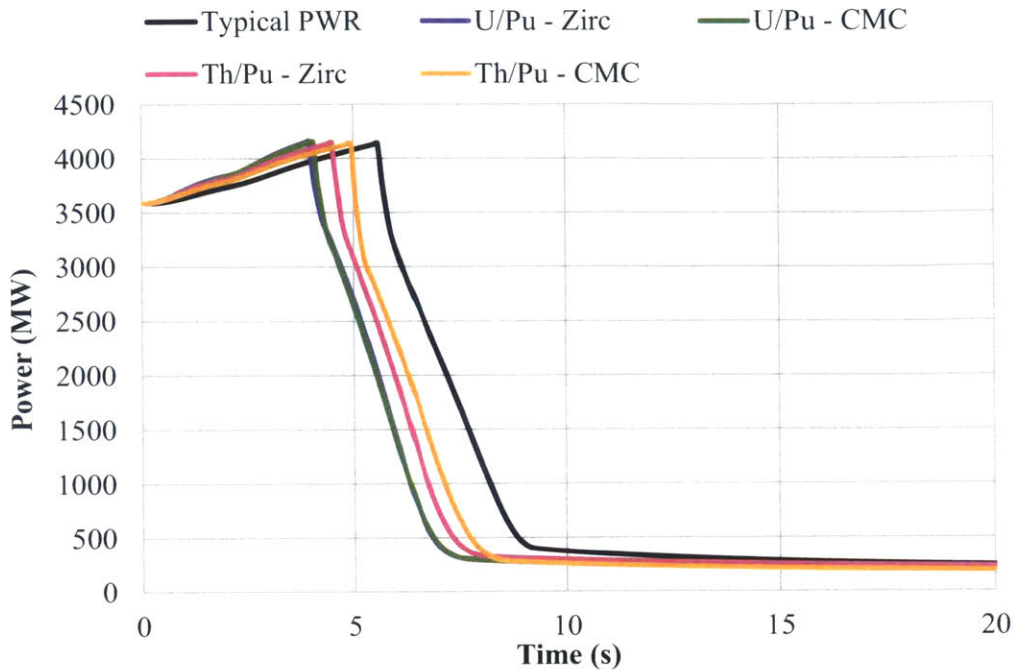
Figure 5-16: Core power response during MSLB transient at BOC

To get a better look at what is occurring at during an MSLB at the beginning of cycle one needs to look at the behavior from 3 to 6 seconds, which is plotted in Figure 5-17. It can be seen that the PWR scram occurs at the latest time. The thoria-plutonia cores take longer to SCRAM than the corresponding urania-plutonia cores. Using SiC cladding results in a later SCRAM compared to Zircaloy cladding. This can be seen in both instances. The relative rate of increase in core power is influenced by a combination of two main factors: the first is the moderator temperature coefficient which dictates how much reactivity is added to the core as the inlet temperature decreases. The second is the delayed neutron fraction - the smaller the value the slower the core power increases. The typical PWR case has the largest delayed neutron fraction and thus the most gradual core power rise. Urania-plutonia fuel has a more negative MTC than thoria-plutonia fuel, which leads to more reactivity being inserted as the inlet temperature decreases and thus the power increases more rapidly.

132
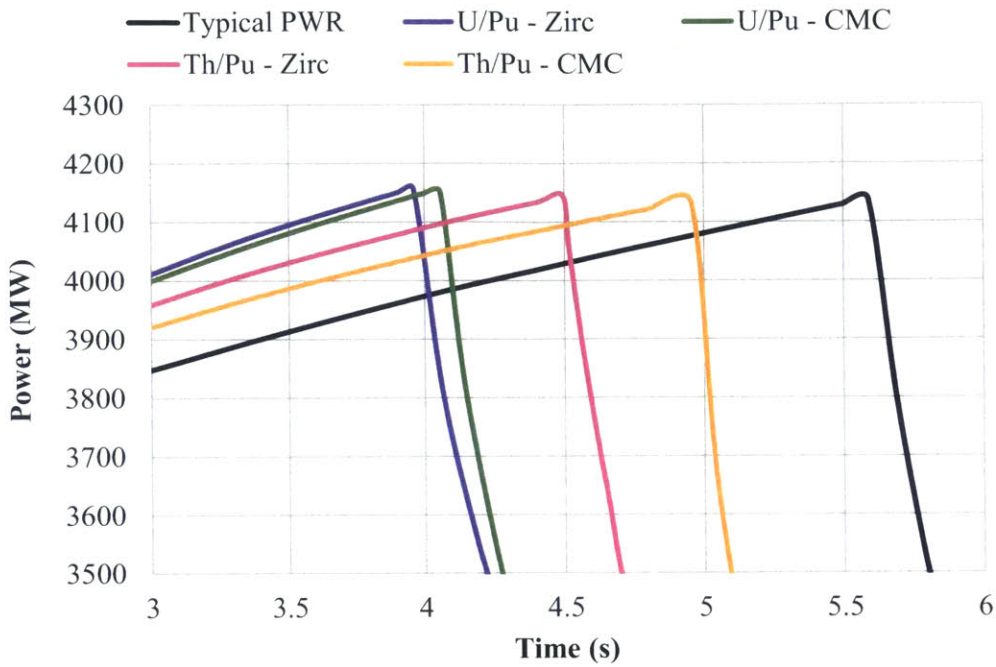
Figure 5-17: Core power response during MSLB transient at BOC, short time

The mDNBR during the transient is given in Figure 5-18. It can be seen that the behavior for all cases is similar and the minimum DNBR value is well above the limit for the transients' duration. A large increase in the value occurs right after the SCRAM, as core power drops.
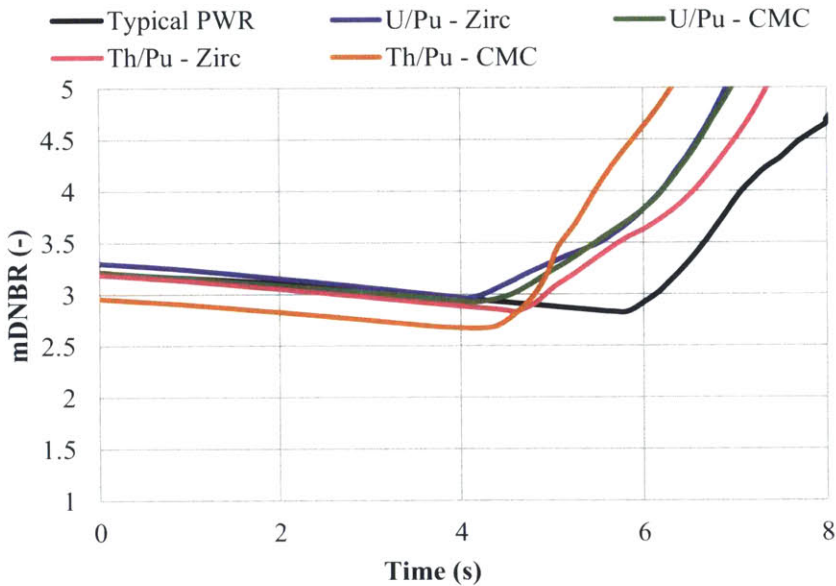
Figure 5-18: mDNBR during MSLB transient at BOC, short time

133

Core reactivity can be seen in Figure 5-19, from 0 to 20 seconds. The figure shows a large drop in core reactivity after the SCRAM is initiated. The typical PWR case has a much lower rod worth than the plutonium burning cases when the reactivity is expressed in terms of dollars, due to the small Pu delayed neutron fraction. While the rod worths are the same in terms of pcm, the much smaller fuel delayed neutron fraction increases the worth in terms of dollars involved. To observe the reactivity increase from the coolant temperature drop, a look at the conditions at 6 seconds of the transient is necessary, shown in Figure 5-20. The reactivity increases to 0.08 $ and then scrams in each case. The same trends are seen here as in core power.
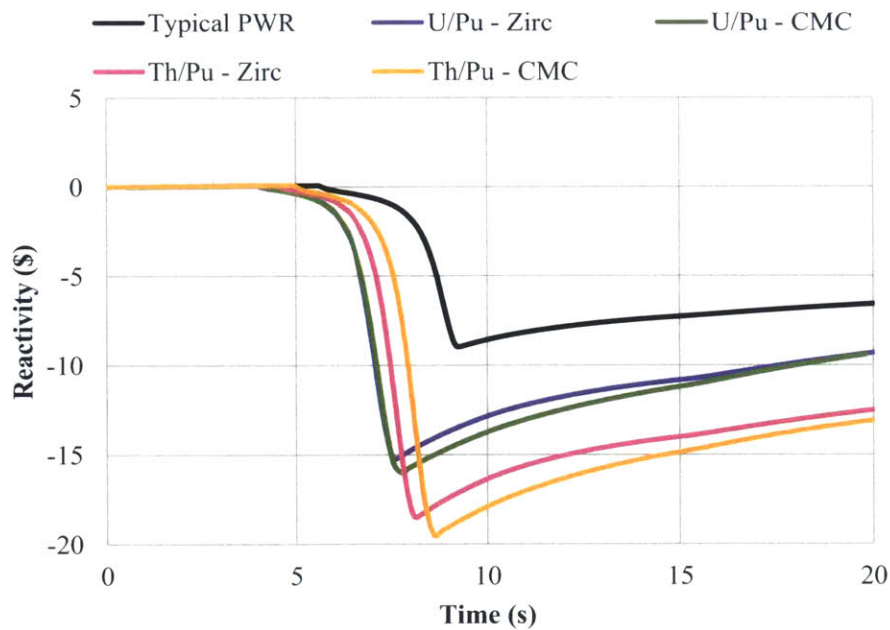
Figure 5-19: Core reactivity during MSLB transient at BOC
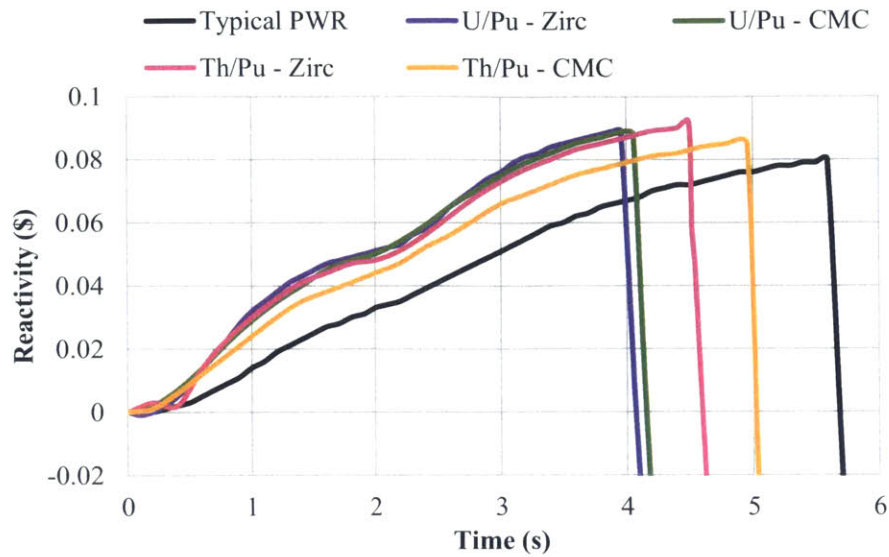
Figure 5-20: Core reactivity during MSLB transient at BOC, short time

The fuel temperature during the transient can be seen in Figure 5-21. It rises during the transient as the core power increases and then sharply declines after the reactor scram. It can be seen that there is only a small increase in fuel temperature during the transient.
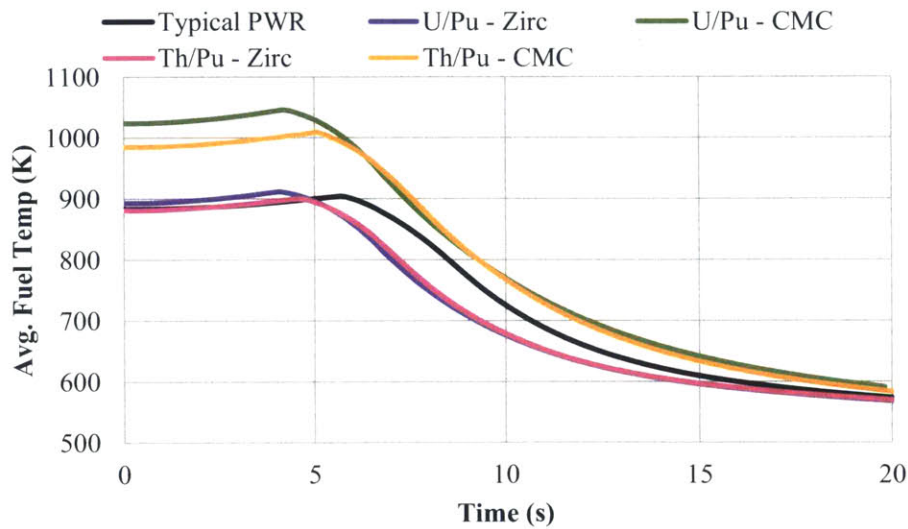
Figure 5-21: Core average fuel temperature during MSLB transient at BOC

135

The relative difference in average fuel temperature among the different cladding and fuel options can be seen in Figure 5-22. Silicon carbide cladding results in an elevated fuel temperature of over 100 K higher than that of Zircaloy cladding. The increased thermal conductivity and gap conductance of thoria-plutonia also results in a lower fuel temperature than urania-plutonia.
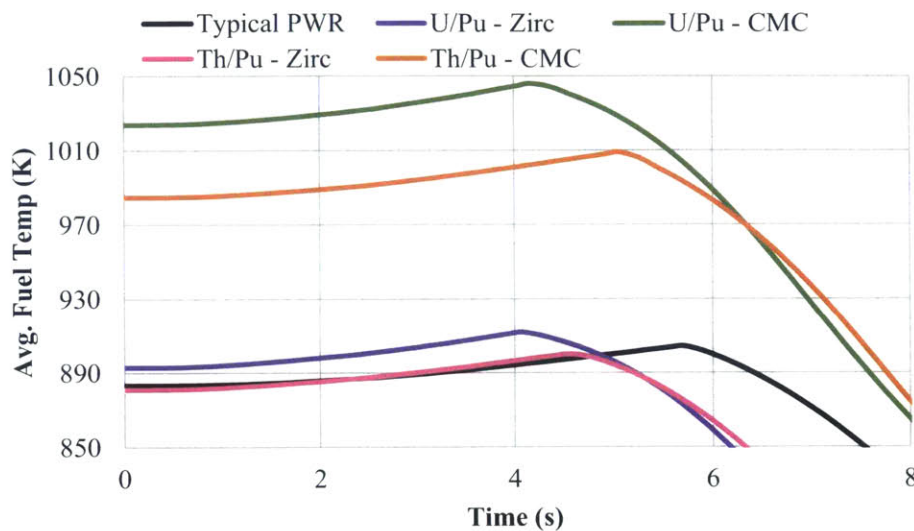
Figure 5-22: Core average fuel temperature during MSLB transient at BOC, short time

Based on these plots and interpretation, it can be said that all of the cores simulated showed safe behavior in the transient. The behavior was also similar to that of a typical PWR. It should however be noted here that the transient modeled used expected core conditions. When licensing analysis is performed, more conservative conditions are imposed that lead to higher power peaking parameters.

5.2.2   End of Cycle

At end of cycle the behavior of the core during the MSLB transient exhibits very similar behavior as it does at beginning of cycle. The core power response can be seen in Figure 5-23, showing roughly similar core power increases followed by a SCRAM from 3 to 3.5 seconds into the transient. Similar trends are seen as in the BOL case with the exception of the thoria-plutonia

136

cores taking longer for the core power to rise. As expected, the mDNBR remains well above the limit for all cases, which can be seen in Figure 5-24. However, the behavior of the typical PWR of today's vintage is slightly different, showing more similarity to the thoria-plutonia CMC cladding case than other MOX cases as it did at BOL.
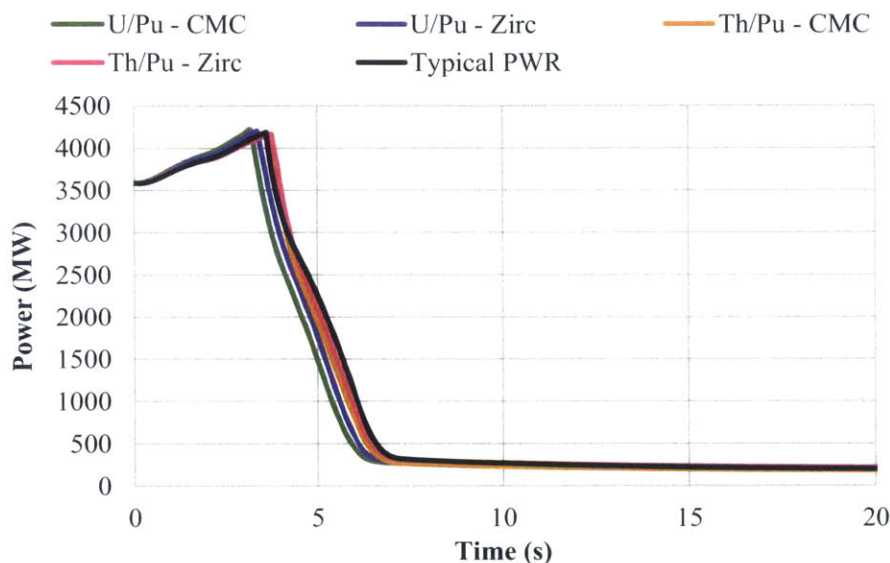
Figure 5-23: Core power response during MSLB transient at EOC
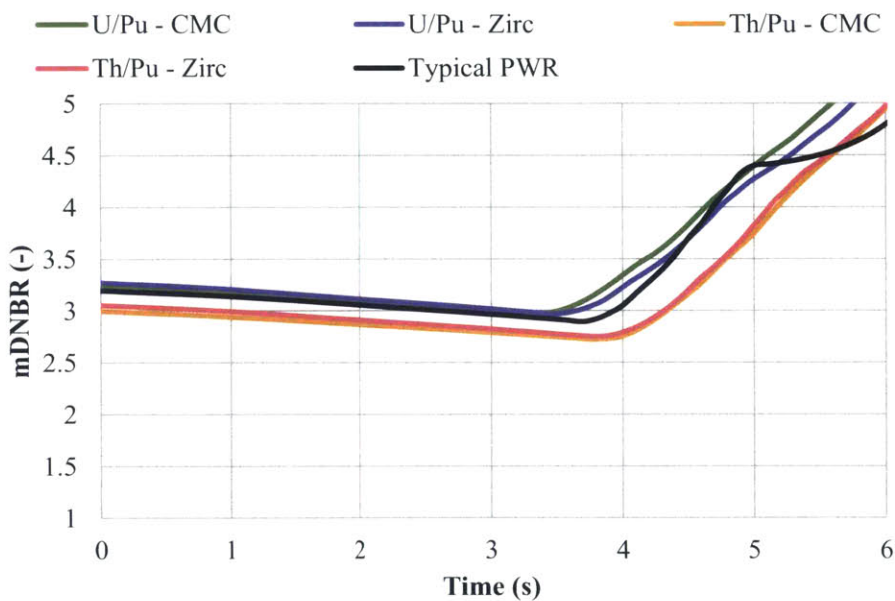
Figure 5-24: Core power response during MSLB transient at EOC, short time

137

Based on these plots and interpretation, it can be said that all of the cores simulated showed safe behavior in the transient. The behavior was also similar to that of a typical PWR. It should also be noted here that the transient modeled used expected core conditions. When licensing analysis is performed, more conservative values for the reactor operating conditions are applied to lead to a more conservative power peaking parameters.

6. Economic Analysis of Accident Tolerant Fuel Cladding Options

If an accident tolerant fuel cladding is to replace the zirconium alloys, it will have to be economically viable for nuclear electric utilities. Four proposed materials are examined as cladding options: Stainless steel (SS), FeCrAl alloy, molybdenum (Mo) tri-layer composite and silicon carbide ceramic matrix composite (SiC CMC), each having its own development time and costs. The thickness of each cladding was assumed to reflect the approximate strength of the material and its manufacturing constraints. The UO_2 enrichment savings or penalty was calculated for each cladding option relative to zirconium, given unit costs from recent market conditions. In this analysis, natural zirconium is used to represent zirconium-based alloys which are currently used in operating reactors like Zircaloy-2, Zircaloy-4, ZIRLO and M5. The accident tolerant fuel (ATF) cladding is assumed to be capable of preventing reactor loss and radioactivity release in a Fukushima-type event.

Since Fukushima, there has been increased interest in ATF as a way to prevent both reactor loss and the large early release of fission products in case of severe accidents. An economic assessment of the benefit to the nuclear industry from different ATF cladding materials has been performed, based on the net present value (NPV) of any future fuel cladding changes. The changes in the cladding dimensions and materials will have an effect on the neutron balance in the core, and thus will have consequences to the cost of the fuel needed for operation. A cost analysis was performed that accounted for the changes in the needed enrichment, and fuel pin size, assuming the reactor operated at the same power level and same power cycle. For this analysis, recent (2014) fuel cycle component prices and a constant discount rate of 6% are adopted. In order to determine the overall cost of any fuel cladding changes, the cladding development cost, development time and resultant enrichment savings or increases were considered.

In addition, the economic savings from preventing future severe accidents are evaluated using a probabilistic approach. Two different accident scenarios were taken into account, the first involving total reactor loss but with the non-gaseous fission products being contained (i.e not released to the environment) and the second with some fission products being released outside

139

the containment. These two accident types are representative of the events at Three Mile Island (TMI) and Fukushima, respectively.

Many different ATF claddings have been proposed, but only four different options are addressed in this work. Three metallic cladding options were examined: stainless steel (SS), an alloy of iron, chromium and aluminum (FeCrAl) and a tri-layer zirconium, molybdenum and FeCrAl composite (Zr-Mo-FeCrAl). [Cheng, 2013] [George, 2015] Additionally, the ceramic silicon carbide with a ceramic composite (SiC-CMC), which was assumed to be a three layer composite, was also examined. [Lee, 2013] Materials properties of the materials of interest can be seen in Table 6-1.

Table 6-1: Fuel cladding material properties candidate accident tolerant fuel materials near room temperature

Parameter	Zirconium [Azom, 2015]	SiC CMC [Mielsoyzk, 2015]	FeCrAl [Thermalloys, 2015] [HMwire, 2015]	Stainless Steel [Efunda, 2015]	Molybdenum* [Goodfellow, 2015] [Azom, 2015]
Yield Strength *MPa*	230	***	460 or Higher	240	415 or Higher
Young's Modulus - *GPa*	94.5	***	220	196	330
Thermal Conductivity *W/mK*	16.7	~9.5 (unirradiated) ~2.2 (irradiated)	11.0	16.1	138
Density *g/cm³*	6.5	2.85	7.1	7.9	10.3
Cladding Thickness - *mm*	0.57	0.76	0.40	0.40	0.075/0.20/0.125

*Molybdenum properties given for Mo alone, not the tri-layer composite, which also contains FeCrAl and Zirconium.
***Yield strength and Young's Modulus for SiC CMC is not displayed, since the material is a tri-layer composite, see the Ph.D. thesis of Mielosyzk (2015) for more complete information on SiC properties

Given the number of light water reactors operating worldwide (estimated at roughly 440 reactors with an average age of 30 years in operation), a core damage frequency for LWRs, based on the three core damage events at Fukushima and the one at Three Mile Island (TMI), of 2.96E-04 per year is assumed. [Lahoda, 2014] Other possible values for the core damage (severe accident) frequency were explored in the parametric study as bounding options. This was used to

determine the probability of annual cost of severe accidents. The cost of the TMI accident was taken to be $10.6 billion, while the cost of the Fukushima accident was taken to be $137 billion. [Lahoda, 2014] On a per reactor basis, the cost of the Fukushima accident was about $34 billion, since four reactors were lost in the course of the accident (though there were only three core damage events). For 100 reactors in the US, this gives a probable cost of $3.1 million per year per reactor for an event of reactor loss and no adverse release and a cost of $10.2 million per year per reactor with reactor loss and adverse radioactive release. If an ATF cladding can successfully prevent either a severe accident that results in a reactor loss or fission product release, it is effectively saving the industry the risk of losing this amount of money per year.

Two separate cases were examined to represent the US conditions. In the first, there are approximately 100 reactors that deploy a single ATF option and operate for the next 60 years, while in the second their number tapers to 75 reactors in 60 years. Two uranium pricing scenarios were also looked at, the first with historically high 2010 prices and the second with the lower values taken from July 2014.

6.1   Model Assumptions

In this analysis, a Westinghouse 17x17 PWR fuel assembly design was used for all calculations. All of the cladding designs maintained an outer diameter of 0.95 cm, so that the hydraulic diameter of the assembly remained constant. Both stainless steel and FeCrAl were allowed a thin clad thickness of 0.4 mm, reflecting their higher strength at expected temperatures. The fuel-cladding gap in these rods was taken to be of equal value to today's fuel, and thus larger UO_2 pellets are used. The zirconium thickness was set to a value of 0.57 mm, common to PWRs of today. SiC CMC is assumed to be 0.76 mm thick, the thickest cladding option due to manufacturing constraints. [Lee, 2013] [George, 2014] In this case the fuel pellet had to shrink to keep the gap at a constant value. The tri-layer Zr-Mo-FeCrAl had 0.4 mm as total thickness, with the inner Zr layer 0.075 mm thick and the outer FeCrAl layer 0.125 mm thick. [Cheng, 2013] Fuel pin geometries are presented in Table 6-2.

Table 6-2: Fuel pin geometries for modeled cladding materials

Parameter	Zirconium	SiC CMC	FeCrAl	Stainless Steel	Molybdenum Tri-layer
Cladding Thickness - *mm*	0.57	0.76	0.40	0.40	0.075/0.20/0.125
Pellet Outer Diameter - *cm*	.819	0.781	0.853	0.853	0.853
Cladding Inner Diameter - *cm*	0.836	0.798	0.870	0.870	0.870
Cladding Outer Diameter - *cm*	0.950	0.950	0.950	0.950	0.950
Pin Pitch - *cm*	1.26	1.26	1.26	1.26	1.26

Each cladding needs different development time and has different development cost. As mentioned before, to extract the same amount of energy out of a given fuel assembly, different enrichments are required and were calculated using standard industry tools. The reload enrichment needed takes into account both the differences in the amount of UO_2 in the core and the parasitic absorptions in the cladding materials.

The cost and benefit values of the different cladding options were assessed using the net present value approach, calculated as shown in Equation 7-1

$$NPV(i, N) = \sum_{t=0}^{N} \frac{R_t}{(1+i)^t} \qquad (7\text{-}1)$$

where i is the discount cost of money, R_t is the annual required payment, t is the number of years from now, and N is the total expected years of operation. The fuel cost relative to Zirconium and the potential accident prevention benefit were calculated using this equation. This value was assessed using the net present value for each operating year from the present until 60 years in the future.

Note that only the direct fuel cost was considered here, no carrying charges on fuel purchases prior to the time of its use were considered.

The development costs and timelines for each of the four cladding types examined (SS, FeCrAl, a Mo tri-layer composite, SiC) were approximated based on previous experience with each cladding type and technological readiness. Stainless steel was assumed to have the shortest development time and cost at 6 years and $200 million, and SiC CMC the longest and most expensive development at 16 years and $600 million. The development times and costs assumed for all options are shown in Table 6-3. The development costs are the total development cost spread over the whole development timeframe. It should be kept in mind that only the United States effort is considered here, and that the current budget for the ATF program at DOE is under $50M/yr, supporting the investigation of all options (for fuels and for claddings) supported by about $10M/yr as industry investment.

Table 6-3: Assumed ATF cladding options development times and costs

Cladding	Development Time Years	Development Cost $ Millions
SiC CMC	16	600
SS	6	200
FeCrAl	12	300
Zr/Mo/FeCrAl	12	300

Two separate uranium price scenarios were examined. The first used a relatively low recent (2014) price for U_3O_8, conversion to UF_6 and separative work units (SWU). The second used the short-lived peak in prices that occurred in 2010. These values can be seen in Table 6-4. It can be observed that both the U_3O_8 and SWU costs were ~70% higher in 2010 than in 2014, which is close to where they are now. [Ux Consulting Company, 2015] Ideally, an ATF option would still be economically viable in both pricing cases.

Table 6-4: Recent (2014) uranium prices and uranium prices in 2010 [Ux Consulting Company, 2015]

	2014 Prices	2010 Prices
U_3O_8 Cost - $/lb	28.25	48
Conversion Cost - $/kgU	7.5	7.0
SWU - $/SWU	95	165

Using the Monte Carlo code Serpent, an assembly-level model was "depleted out" to the point when an identical amount of energy was extracted from each of the fuel-cladding combinations. This method is intended to ensure that all assemblies are evaluated on the basis of an identical fuel cycle length. The assembly model examined can be seen in Figure 6-1.
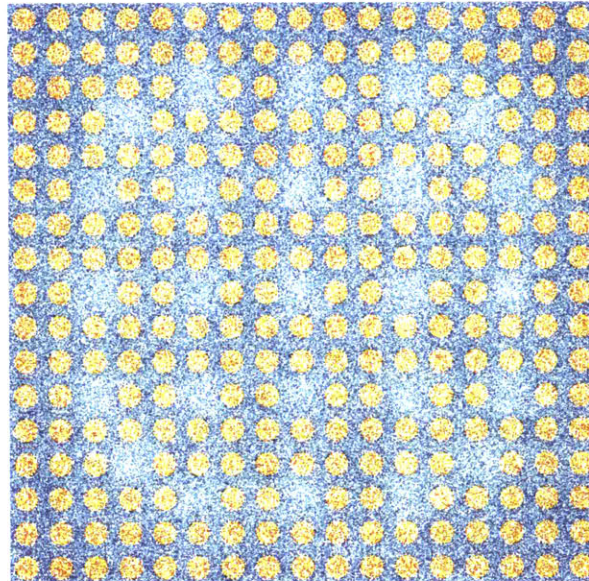
Figure 6-1: Serpent-generated reaction rate results plot for a 17x17 Westinghouse Assembly

The modeled assembly had 0 ppm of soluble boron in the coolant, an average fuel temperature of 900 K and a moderator temperature of 600 K. Assembly depletions were performed at a specific power of 50 kW/kgHM. A core leakage of 3.3% was used, to better reflect real reactor conditions. This leakage number is based on the full core typical PWR calculations shown earlier in Chapter 4. The assembly model had reflective boundary conditions axially and radially. In order to calculate the required enrichment for the different cladding typed two separate enrichment cases were performed using Serpent. Then, linear reactivity was used to interpolate

144

between the lines and determine the necessary enrichment. This method is shown in Figure 6-2. The batch burnup at discharge was taken to be that corresponding to k_{eff} of 1.033. The Monte Carlo depletion code Serpent was run using 20,000 neutrons per cycle. 200 total cycles were run and the first 40 were discarded starting from a uniform initial source. The maximum uncertainty for k_{eff} for any point in an assembly depletion was 61 pcm.
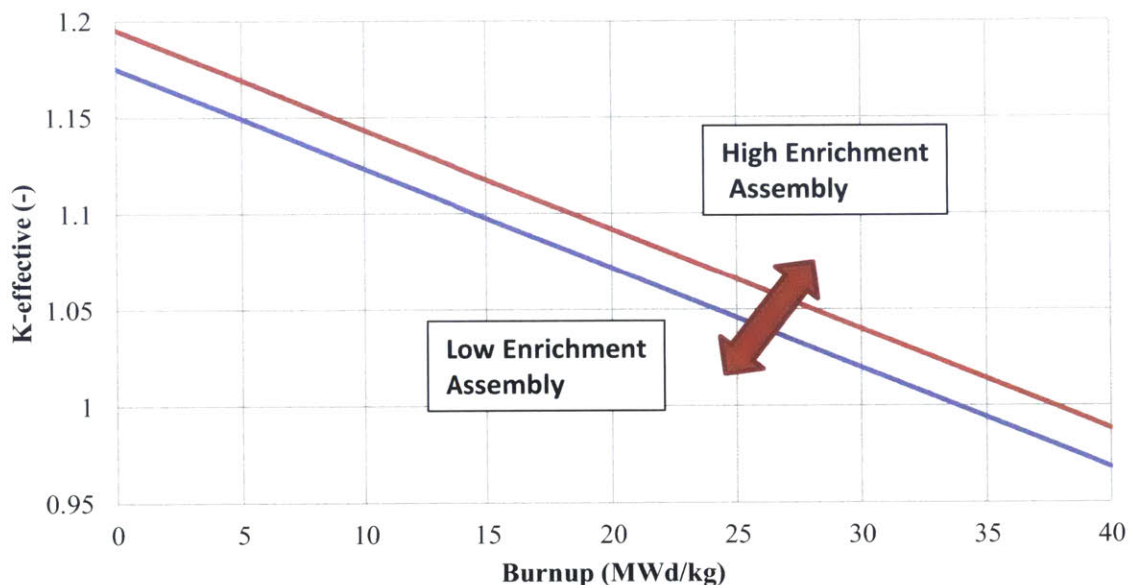
Figure 6-2: High and low enrichment curves for Zr/Mo/FeCrAl tri-layer cladding, showing how linear reactivity allows interpolation to find required enrichments

The resultant enrichment required for equal cycle lengths can be found in Table 6-5. Shown in Figure 6-3 is the mass of U^{235} found in a typical pin. All alternative metallic cladding options require more than 5% enrichment; any additional fuel cycle costs beyond the cost of the fuel itself are not addressed in this work.

Table 6-5: Required fuel enrichments and single batch discharge burnups for different claddings including Zirconium to achieve the same cycle length

Cladding	Enrichment *wt% HM*	Single batch discharge burnup *MWd/kgHM*
Zirconium	4.74	35.8
SiC CMC	4.98	39.3
SS	5.67	32.9
FeCrAl	5.31	32.9
Zr/Mo/FeCrAl	5.85	32.9

In addition to enrichment, total fuel mass is another important factor in determining the total cost of the uranium required. The uranium-235 mass per pin for the different cladding options can be seen in Figure 6-3. The increased enrichment and fuel volume in alternative metallic cladding lead to a significantly higher fissile loading compared to zirconium. Silicon carbide, while requiring a slightly higher enrichment requires a lower fissile loading because of the decreased fuel area.
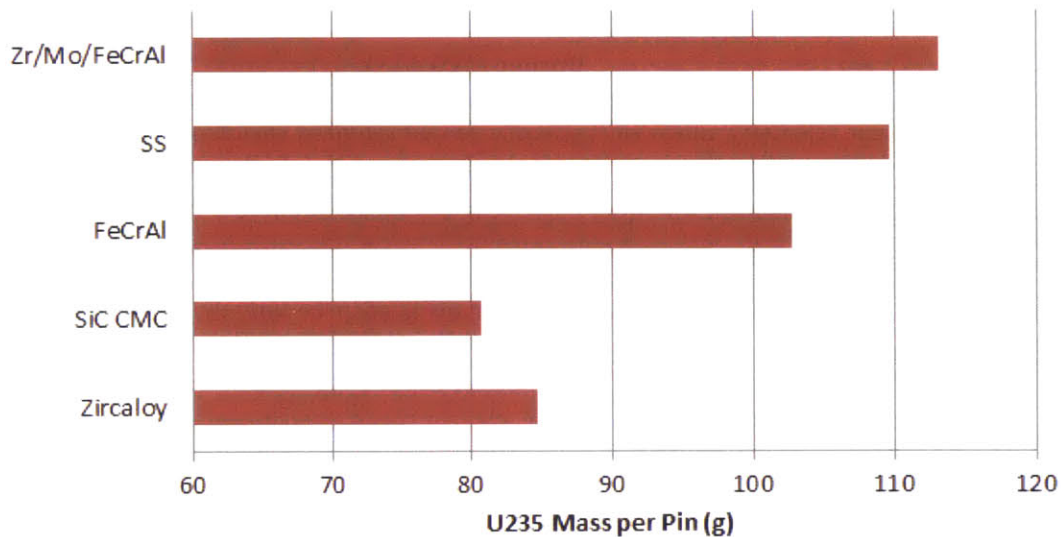
Figure 6-3: Uranium-235 mass per pin for different cladding types

6.2   Total Fuel Development Costs

The resultant enriched fuel cost, in terms of dollars per kilogram of end user product ($/kgEUP), and the fuel rod (and assembly) fabrication cost have been considered. These two numbers are used to determine the fuel cost in terms of $/MWhe. Then, fuel cost changes for the fleet relative to present day zirconium alloys are determined, assuming that there are 100 reactors operating and generating 999,324,000 MWhe/yr. The reactors were assumed to have an average output of 1200 MWe and an availability of 95%. [Lahoda, 2014]

The ore, enrichment and conversion costs were calculated using the web based UxC Fuel Quantity and Cost Calculator and the fabrication cost was estimated based on current experience. For common metals it was taken as 200 $/kgU and for the three layer Mo cladding and the SiC-CMC, it was taken as 400 $/kgU. The resultant fuel costs can be seen in Table 6-6 for the recent (July 2014 fuel) costs. To better reflect uranium usage in a typical core, the single batch discharge burnup calculated using Serpent was converted using linear reactivity theory to a 2.33 batch discharge burnup. The thermodynamic efficiency of the power cycle system (i.e thermal to electrical power conversion efficiency) was taken to be 33%.

Table 6-6: ATF fuel costs at 2014 prices using different claddings as well as Zirconium

Cladding	Zirconium	SiC CMC	SS	FeCrAl	Zr/Mo/FeCrAl
Ore/Enrichment/ Conversion - *$/kgEUP*	1492	1583	1844	1707	1912
Fabrication - *$/kgU*	200	400	200	200	400
Fuel Cost - *$/MWhe*	4.27	4.55	5.59	5.22	5.85
Fleet Cost Increase/yr *$ Millions*	-	$283	$1,324	$949	$2,057

Note that the cost of enrichment per kg of the SiC fuel is higher than that of Zirconium but the fuel volume is smaller. Thus, the difference of the net cost of the fuel per unit energy is more dependent on the assumed cost of fabrication of the cladding.

147

Using the higher 2010 prices, the same fleet cost changes were calculated. Due to the higher cost of both SWU and U_3O_8 found in 2010, the fuel costs are estimated to be over 60% higher than for the 2014 prices. This can be seen in Table 6-7. Because a smaller amount of total uranium mass is required for the SiC CMC cladding than for Zirconium, the increase in fleet cost is less when higher uranium prices are used.

Table 6-7: ATF fuel costs at 2010 prices using different cladding options

Cladding	Zirconium	SiC CMC	SS	FeCrAl	Zr/Mo/FeCrAl
Ore/Enrichment/ Conversion - *$/kgEUP*	2506	2659	3100	2869	3215
Fuel Cost - *$/MWhe*	6.83	7.02	9.03	8.40	9.89
Fleet Cost Increase above Zirconium *$ Millions/yr*	-	195	2,201	1,570	3,063

A comparison of the additional cost resulting from the two pricing scenarios can be seen in Figure 6-4, for all of the claddings examined. It can be seen that the 2010 prices result in a larger economic penalty relative to Zirconium for metallic claddings. However, the penalty is less for silicon carbide because less fissile mass in required. Furthermore, since the SiC fuel mass needed is actually smaller that than of the fuel needed with Zr, the increase with the 2010 unit prices is less than that with the 2014 prices.

148
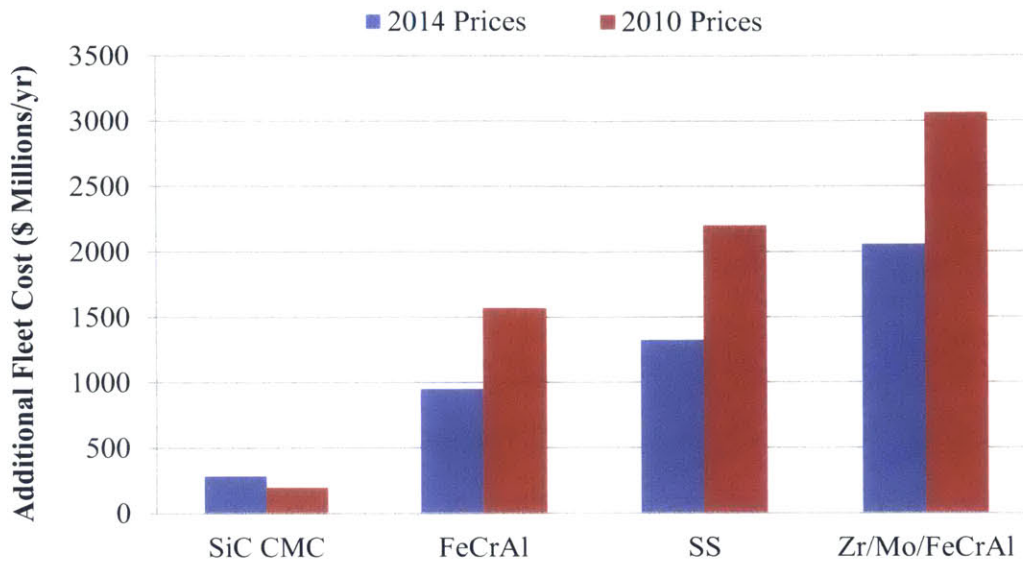
Figure 6-4: Comparison of additional fleet fuel costs for 2014 and 2010 uranium pricing scenarios

6.3 Avoided Costs of Severe Accidents

In this section, three separate analyses are shown. The first two show a scenario with 100 reactors operating in the United States for 60 years; one considering the 2014 unit prices and other the 2010 prices. The third assumes that there are only 75 reactors operating after 60 years, with the total number decreasing linearly from 100 between now and then. For this analysis, the 2014 prices were used. No case was considered with a larger number of reactors in the US. The projected number of reactors in 2050 by the Energy Information Administration has been fluctuating over the years, and it is not certain how many new reactors will be built in the future.

The net present value (NPV) integrated over time of the additional cost of ATF cladding options, and of avoiding the two types of severe accidents discussed above are shown in Figure 6-5.
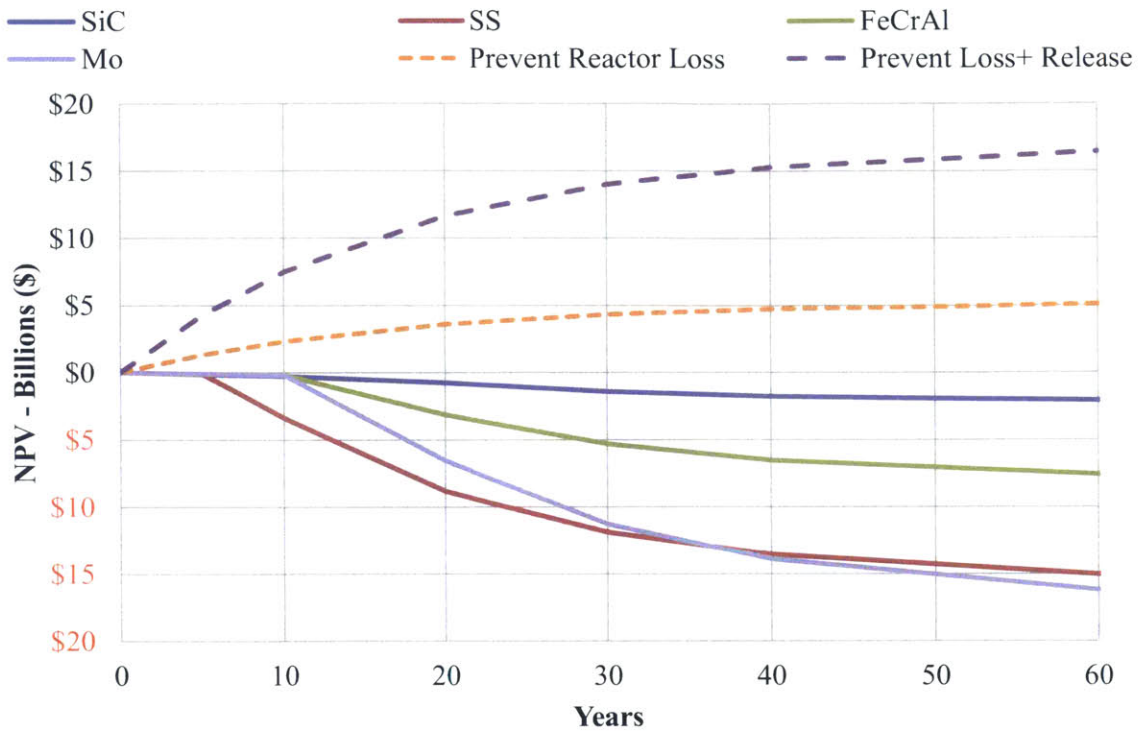
Figure 6-5 : Net present value of ATF cladding relative to zirconium compared to the NPV of preventing reactor loss and release

It can be seen that the added cost from SiC cladding is significantly less than that from metallic claddings. Stainless steel and molybdenum are the most expensive, though isotopic tailoring can reduce the U235 enrichment penalty by removing the isotopes with the highest neutron absorption. This cost saving has to be balanced against the added cost of isotopic enrichment of the metallic elements. [Richard, 2012] The added cost of the SiC has some uncertainties beyond the feasibility of withstanding the stresses encountered during operation. Both the cost of manufacturing and the final possible thickness of the cladding are not known at present. In a separate evaluation of the effect of thickness on SiC cladding performance in the core, it was found that if the extra thickness of the cladding can be taken from the coolant side, the enrichment needed would be less and the effect on the pumping power needs would be small. [Sukjai, 2014] [Shirvan, 2014]

150

The annual overall cost for the SiC cladding is given in Figure 6-6, and shows the development costs, additional fuel costs and the accident prevention benefit from the cladding. It can be seen that the investment in development of SiC is a net negative benefit for the first 16 years, and then the net benefit becomes positive after the cladding is implemented in the operating reactors (here assumed in all reactors at once).
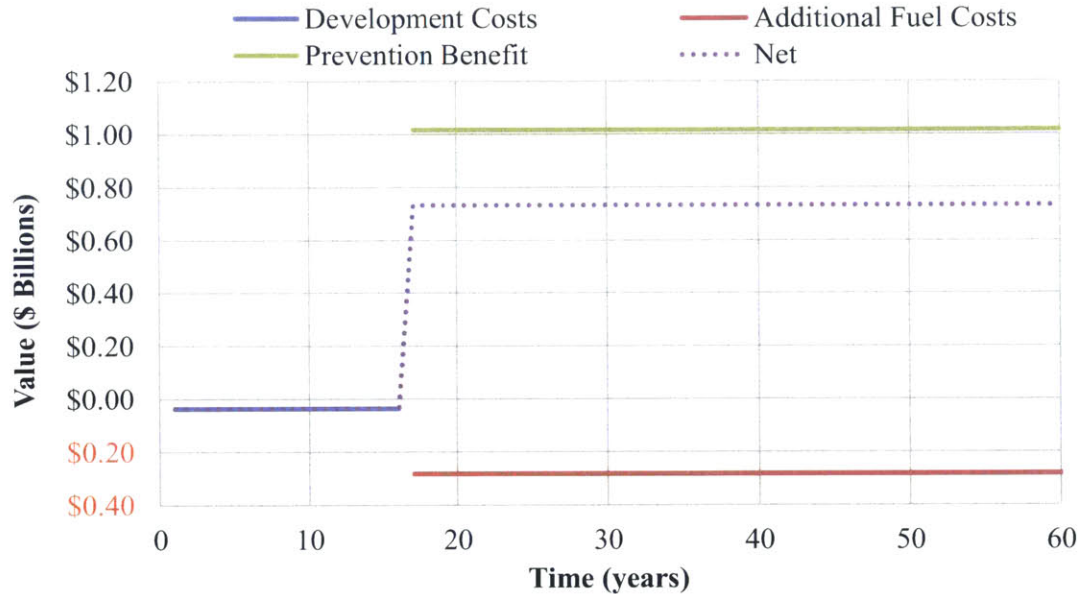
Figure 6-6: Yearly cost of SiC CMC fuel over the course of 60 years, assuming 100 reactors operating at 60 years

Similarly, the yearly costs of FeCrAl cladding are plotted in Figure 6-7. While the accident prevention benefit is the same, the net economic benefit that can be garnered is significantly less because of the increased fuel cost associated when switching to the fuel. It can be seen that fuel net value is slightly above the breakeven point. This of course assumes that the cladding will be able to prevent the accident, which is yet to be demonstrated.

151
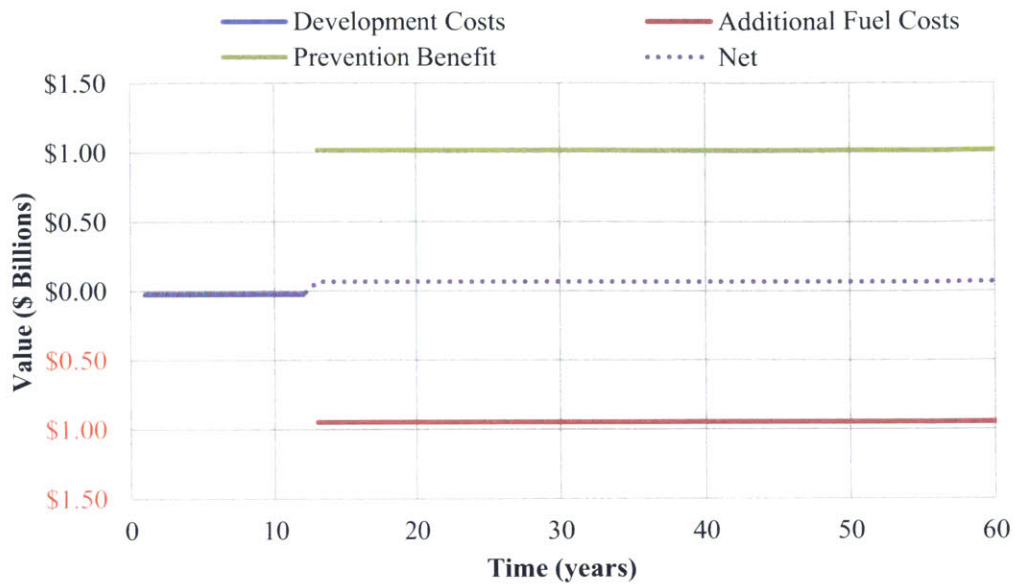
Figure 6-7: Yearly cost of FeCrAl fuel cladding over the course of 60 years, assuming 100 reactors operating at 60

Combining the economic benefit from preventing a severe accident resulting in reactor loss and fission product release with the cost of implementing different ATF claddings, we arrive at Figure 6-8. The NPV remains near zero during the development time since the development cost when spread over the development time is small compared to the cost of uranium or that of an accident that ruins the reactor. After the fuel development time ends, both the accident prevention benefit and the change in uranium cost are applied. While there is a clear economic benefit to using SiC cladding, the benefit of FeCrAL may be equal to the cost. But the economic benefit that can be garnered by using other metallic ATF is in fact negative. Thus, the increased cost to the fuel cycle is not recovered from avoiding the risk of a severe accident of this type. This result should be tempered by the doubts about whether a metallic fuel can avoid an accidental release of non-gaseous fission products in case of a severe accident. The SiC maintains its strength up to 2000 °C, and may avoid fission gas release from the fuel, and the threat to containment since its reactions with steam at high temperatures are two orders of magnitude smaller than zirconium and not exothermic. [Lee, 2013] [Terrani, 2014] The iron based alloys' reactions with steam may be less severe than with zirconium, but the melting point at which the fuel can release fission products in the containment are not favorable. Mo remains uncertain in its impact on severe accidents, as it was reported in the past that one of the oxides

formed when reacting with steam has a very low volatilization point. [DeVan, 1961]
[Gulbransen, 1963] However, recent experiments funded by EPRI have reported high stability of
molybdenum in dry steam. [Cheng, 2013]
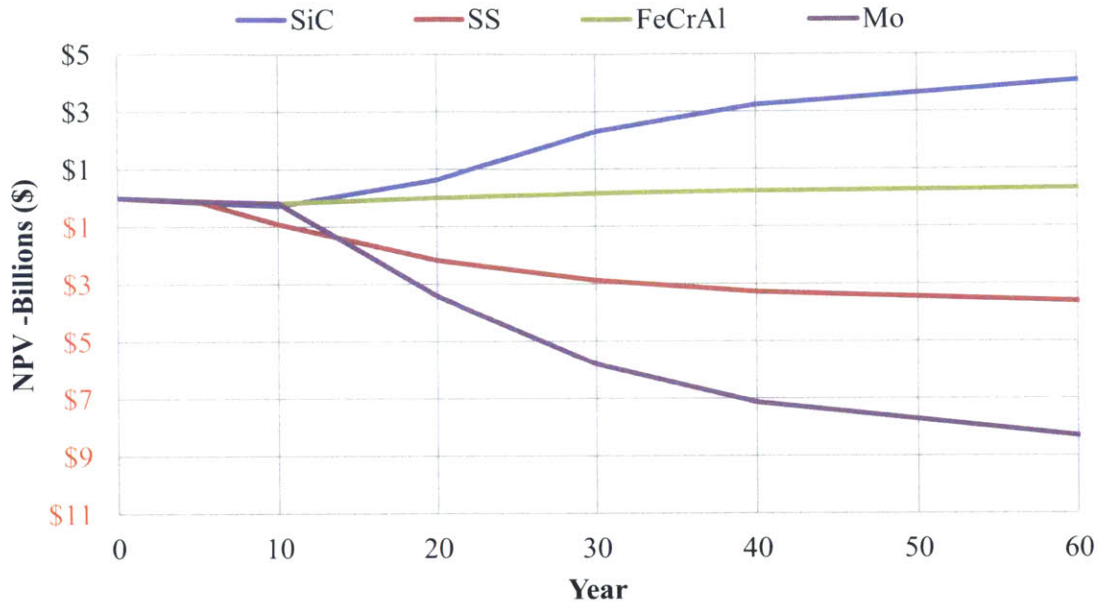
Figure 6-8: Net present value of ATF cladding relative to zirconium for preventing reactor loss and fission product release, using 2014 uranium prices. It is assumed that there are 100 reactors operating for the full 60 years.

When examining the benefit that could be garnered from preventing a TMI-type accident, which would result in reactor loss but no significant non-gaseous fission product release, there is only a minimal loss for using SiC cladding and a large loss from using a metallic ATF cladding including stainless steel. This can be seen in Figure 6-9. This indicates that SiC may be beneficial if it can save both reactor and prevent negative externalities that may insure if there is a meltdown event at a reactor in the United States.
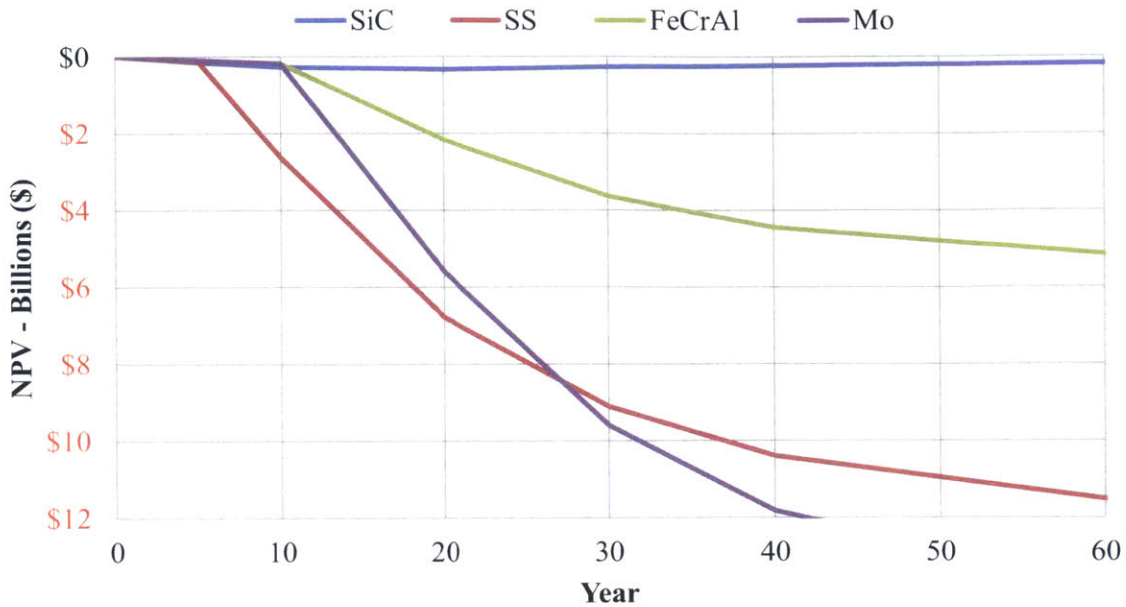
Figure 6-9: Net present value of ATF cladding relative to zirconium for preventing reactor loss, using 2014 uranium prices. It is assumed that there are 100 reactors operating for the full 60 years.

A larger benefit can be garnered from preventing reactor loss and fission product release when there are more reactors operating. As the number of operating reactors decreases due to expected shutdowns without being replaced, this benefit decreases. If the more expensive 2010 uranium prices are used, then economic benefits of preventing severe accidents turn to losses, with the exception of SiC, which is slightly more economically beneficial. These results are shown in Figure 6-10 and Figure 6-11.
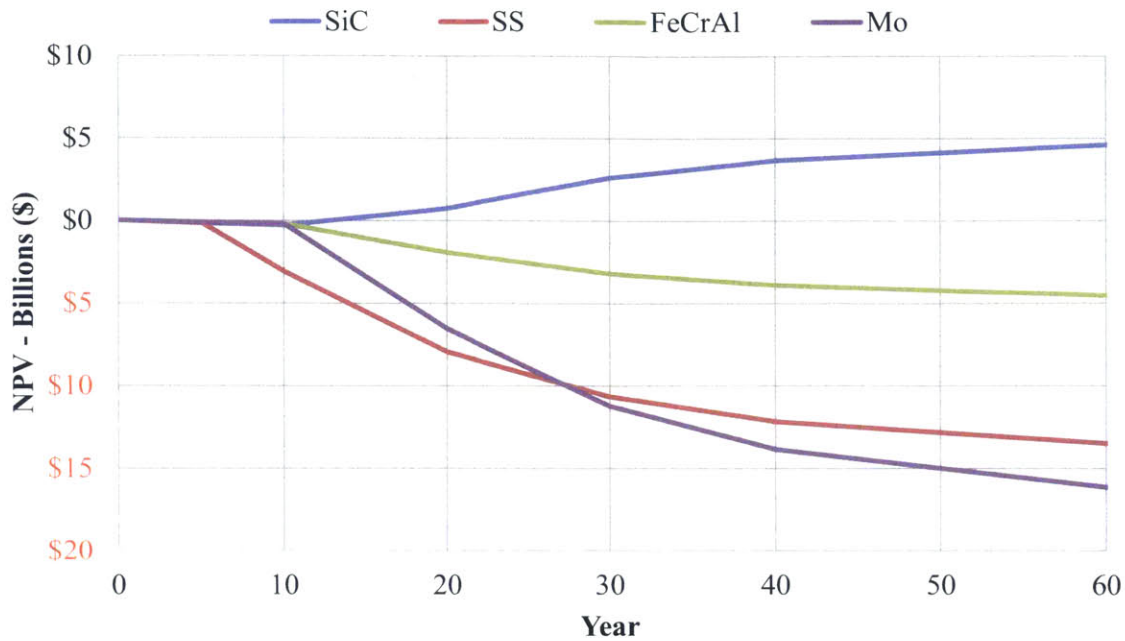
Figure 6-10: Net present value of ATF cladding relative to zirconium for preventing reactor loss and fission product release, using 2010 uranium prices. It is assumed that there are 100 reactors operating for the full 60 years.
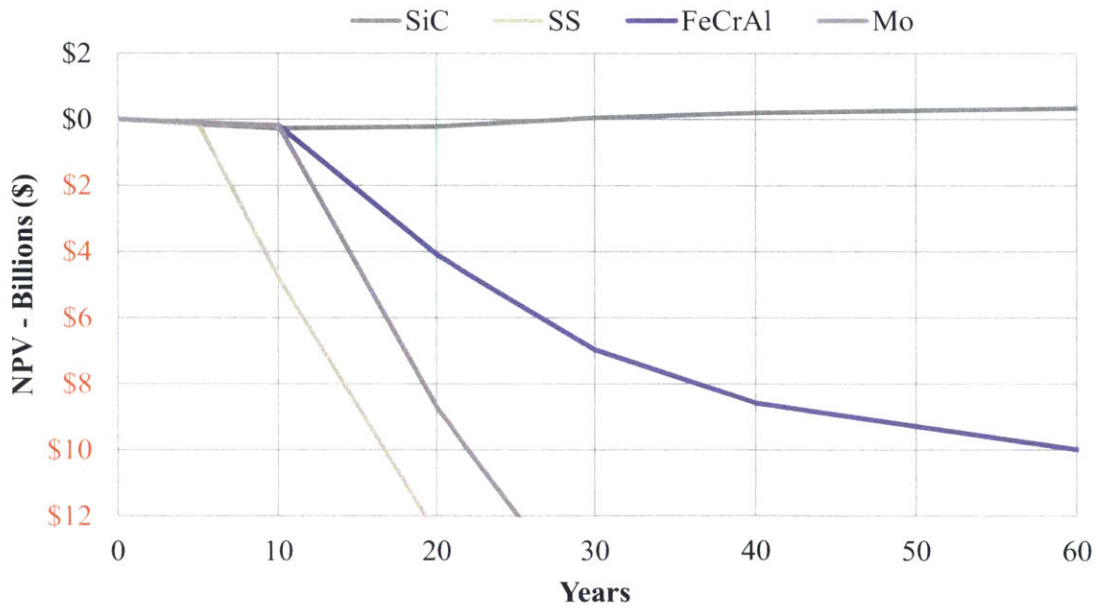
Figure 6-11: Net present value of ATF cladding relative to zirconium for preventing reactor loss, using 2010 uranium prices. It is assumed that there are 100 reactors operating for the full 60 years.

155

The third scenario examined used the lower 2014 uranium and enrichment costs, while also assuming that the number of operational reactors dropped linearly to 75 in 60 years. This results in lower overall fuel costs to the reactor fleet, but also less economic benefit from accident prevention. The annual costs of this scenario can be seen in Figure 6-12 for SiC CMC cladding.
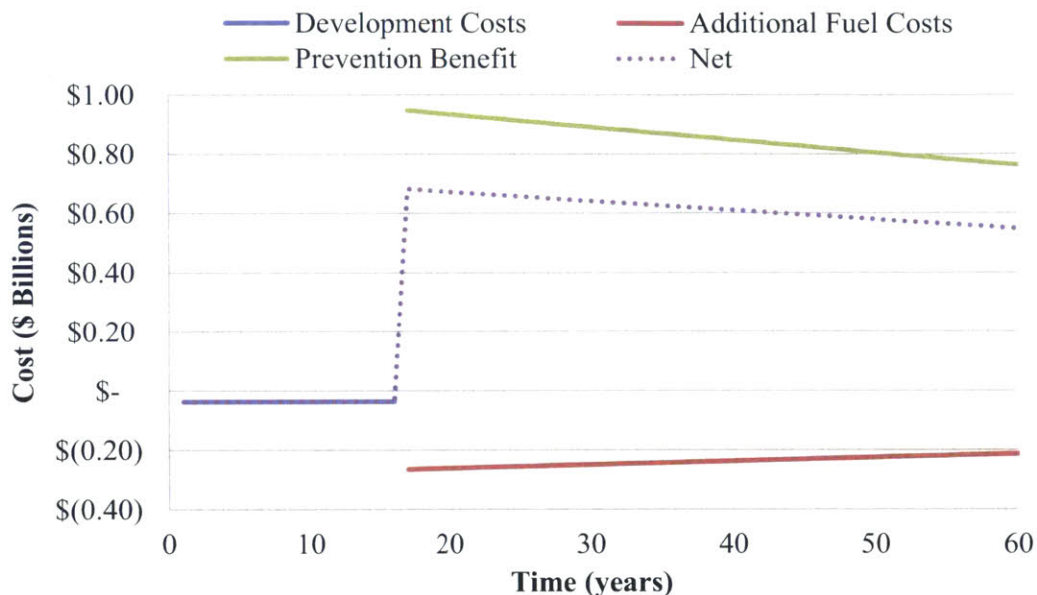
Figure 6-12: Yearly cost of SiC CMC fuel over the course of 60 years, assuming 75 reactors operating at 60 years

This leads to less overall economic benefit for the case of reactor loss and release prevention, as shown in Figure 6-13. Additionally, it shows that the SiC case, which was previously shown to result in an economic benefit for reactor loss if higher 2010 uranium prices are used, no longer shows an economic benefit. This can be seen in Figure 6-14.
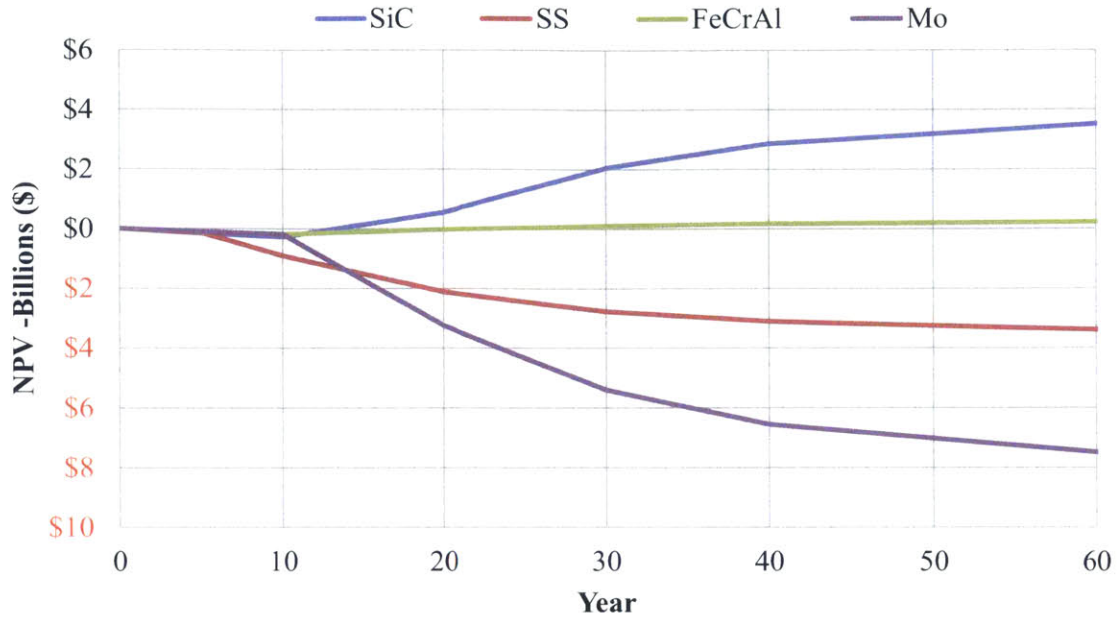
Figure 6-13: Net present value of ATF cladding relative to zirconium for preventing reactor loss and fission product release, using 2014 uranium prices. It is assumed that there are 75 reactors operating at the end of 60 years.
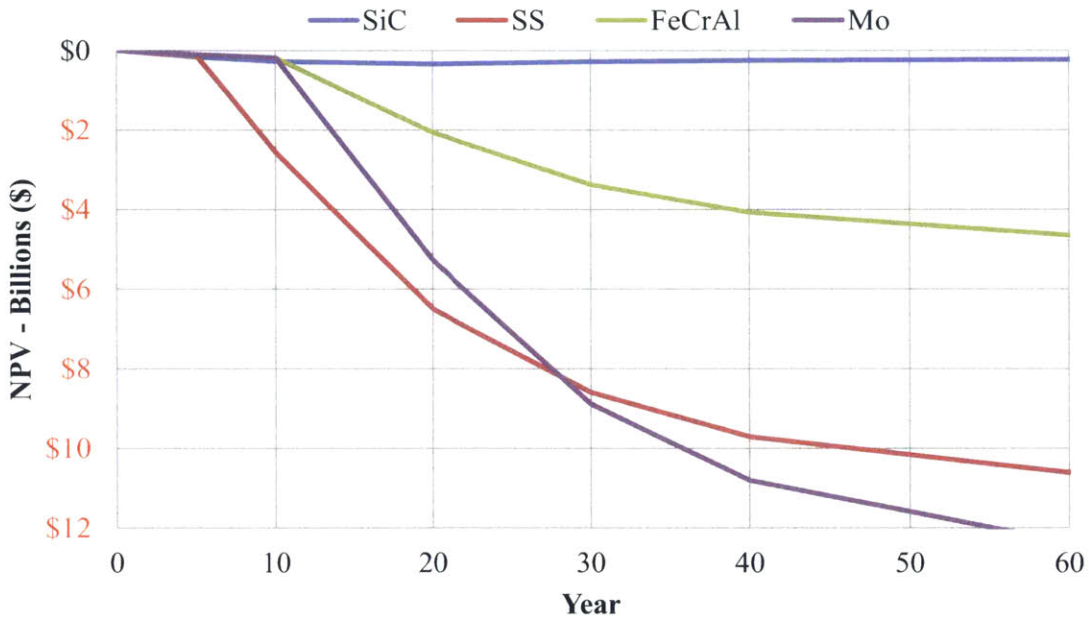
Figure 6-14: Net present value of ATF cladding relative to zirconium for preventing reactor loss, using 2014 uranium prices. It is assumed that there are 75 reactors operating at the end of 60 years.

In all three cases it can be seen that there is an economic benefit in preventing reactor loss and radioactivity release using SiC. That is, accounting for the risk of severe accidents and the reactor loss prevention, SiC leads to positive net present value, and may be more beneficial as the number of operating reactors increases. This is assuming that new reactors would have similar core damage frequencies (CDF) to those assumed in this work. Yet, if the CDF were significantly lower, such as those found in an AP1000, then there may be no financial benefit in applying advanced cladding types in this reactor. However, it appears that there is little benefit and perhaps a significant added cost from using metallic ATF claddings. This is compounded by the doubt about whether or not metallic claddings can prevent significant reactor loss and release events like Fukushima.

The above analyses had many assumptions about the ATF that may not prove right, even if their feasibility is shown to be technically attainable. For example, the cost of manufacturing of the advanced cladding may turn out to be much more than was assumed here. The discount rate used for estimating the present value may be off as well. Finally, the burden of the accident losses is in reality shared by the insurance pool, all the nuclear fleet and the government of the US. However, the fuel cost changes are borne by the utility customers. Thus, for an individual utility, the cost-benefit analysis of the introduction of any ATF option will be based on assumptions that are suitable for their own fleet.

6.4   Parametric Studies of Economic Parameters

The overall economic value of accident tolerant fuel is highly dependent on the parameters used in the economic assessment. Accordingly, several of the most important factors in the economic analysis presented thus far in this chapter were examined for their impact on the overall economics of the system. The total accident cost, discount rate and estimated core damage frequency for both SiC CMC and FeCrAl claddings are considered in this section.

158

6.4.1 Accident Costs

Five separate accident cost scenarios were examined for the reactor loss and containment breach accident. These separate cases can all be seen in Table 6-8. Case 3 is near the nominal value of $34 billion used for this study. Two cases with costs above and below this value are also examined at alternative accident costs, since the costs of the Fukushima-Daiichi accident are not fully clear yet. Each sequential case is incremented $10 billion from the last.

Table 6-8: Alternative total costs for a Fukushima-type accident

Case	Total Accident Cost Billion ($)/Reactor
Cost 1	15
Cost 2	25
Cost 3	35
Cost 4	45
Cost 5	55

The resultant net present value of each case, taking into account fuel costs and accident prevention benefits, for both SiC CMC cladding and FeCrAl cladding are shown in Figure 8-15 and Figure 8-16 respectively.
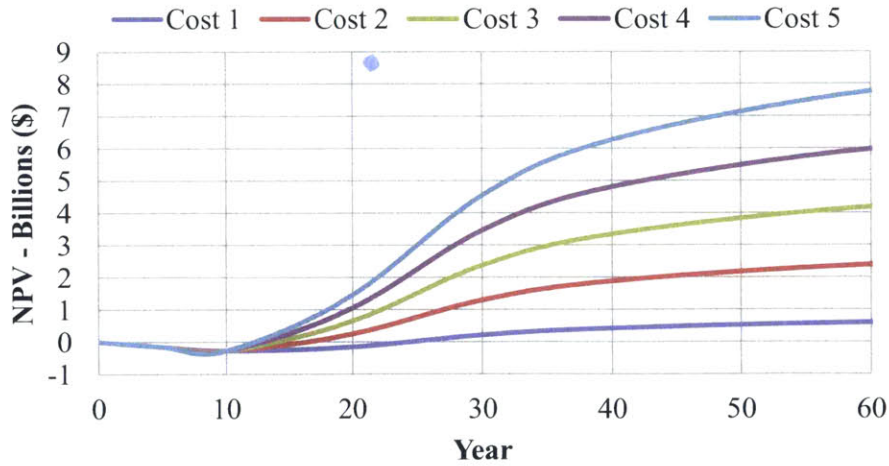
Figure 6-15: Parametric study of total accident cost for SiC CMC cladding during a Fukushima-type accident

159
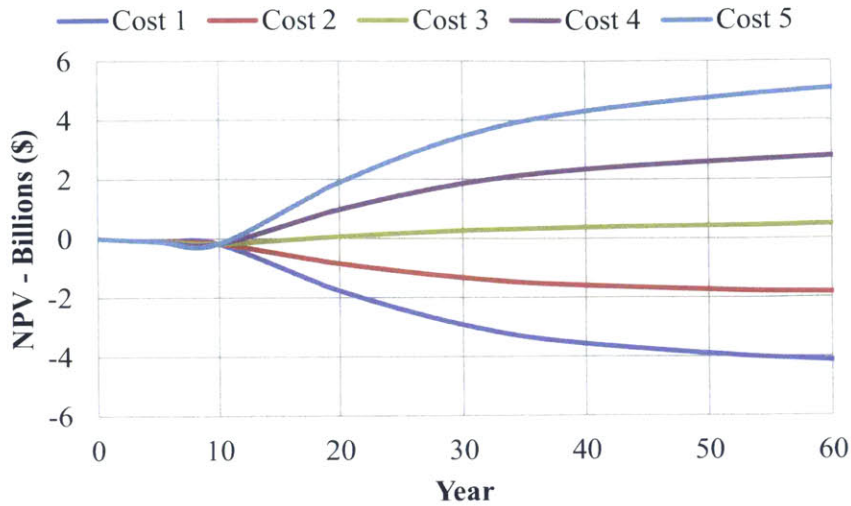
Figure 6-16 : Parametric study of total accident cost for FeCrAl cladding during a Fukushima-type accident

By looking at the NPV of different assumed total accident costs, it is possible to determine the total accident cost at which each of the cladding becomes economically beneficial. SiC CMC demonstrates a positive NPV even in lower accident cost events, while FeCrAl cladding begins to demonstrate a positive return on investment near the nominal value of $35 billion. However, for FeCrAl to have a large long term financial benefit, it appears that the cost of the accident must be even higher.

6.4.2 Discount Rate

The second economic parameter examined is the discount rate of money. A good understanding of the impact of the discount rate is necessary to fully understand the long term economic implications of any cladding option. For this analysis the discount rate was the same for both fuel costs and accident prevention benefits. A more realistic discount rate would take into account the different players involved in both the implementation of a new fuel and the cleanup of an accident event such as the federal government, the utility and the vendor.

160

To explore the impact of potential discount rates, values from two to ten percent were considered. The effect of the discount rate on the reactor loss with containment breach accident was examined for both FeCrAl and SiC CMC. The effects of the different discount rates can be seen in Figure 8-17 for SiC CMC cladding. It can be seen that as the discount rate decreases, the overall return that can be gained from switching to a SiC cladding increases. As the discount rate increases, the return becomes smaller and smaller, eventually approaching zero when the discount rate is near ten percent.
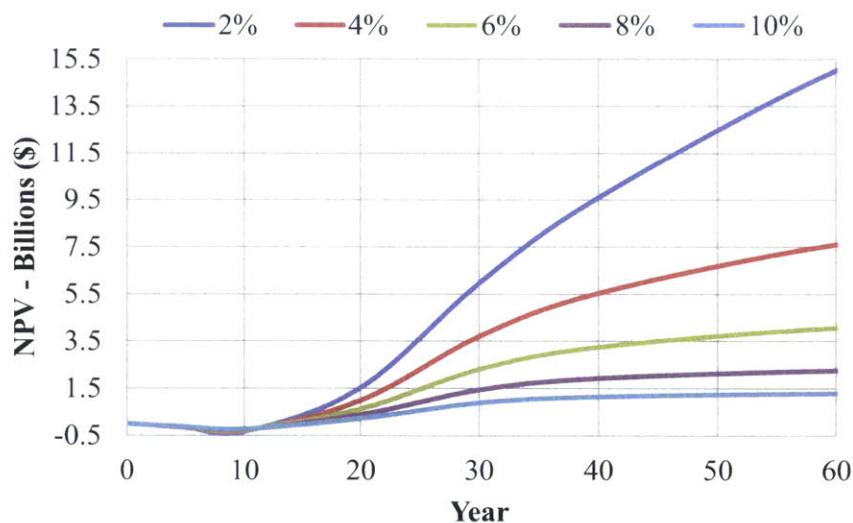
Figure 6-17: Parametric study of discount rate for SiC CMC cladding during a Fukushima-type accident

The effect of different discount rates on FeCrAl can be seen in Figure 8-18. Since the positive economic benefit after the development time period is less, the NPV of the cladding does not increase by the same magnitude, however the relative increase is similar to the case of the CMC cladding.
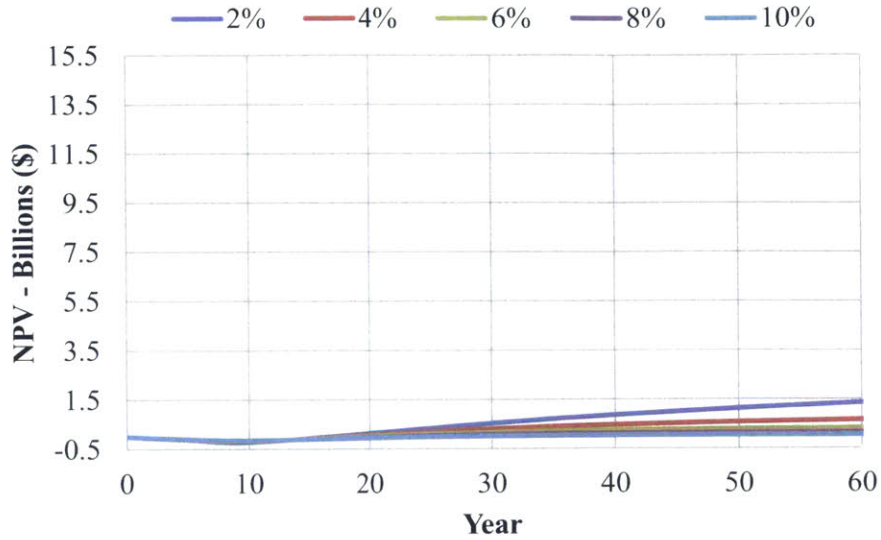
Figure 6-18: Parametric study of discount rate for FeCrAl cladding during a Fukushima-type accident

6.4.3 Core Damage Frequency

The final parameter examined is the core damage frequency. Accordingly, five separate core damage frequencies were examined, two higher and two lower than the value used in the main study. These separate cases can all be seen in Table 6-9. Case 3 is near the nominal value of 2.96E-04 events/year. They were selected as possible bounding cases and have no inherent significance.

Table 6-9: Alternative core damage frequencies for a Fukushima-type accident

Case	Core Damage Frequency *events per year*
CDF1	3.33E-05
CDF2	1.00E-04
CDF3	3.00E-04
CDF4	6.00E-04
CDF5	9.00E-04

The accident was taken to be a reactor loss and containment breach event and the cost was kept at the nominal value of $34 billion per event for all of the cases. The resultant net present value of each of the core damage frequencies can be found in Figure 6-19 for the SiC CMC cladding. It can be seen that as the CDF increases, the total benefit that can be achieved by changing the cladding increases. Similar trends are followed when a FeCrAl cladding is examined. This can be seen in Figure 6-20.
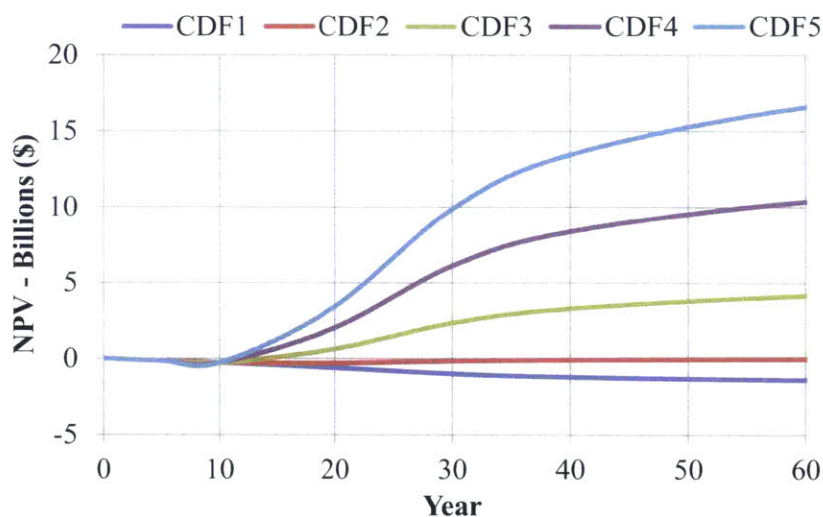
Figure 6-19: Parametric study of core damage frequency for SiC CMC cladding during a Fukushima-type accident
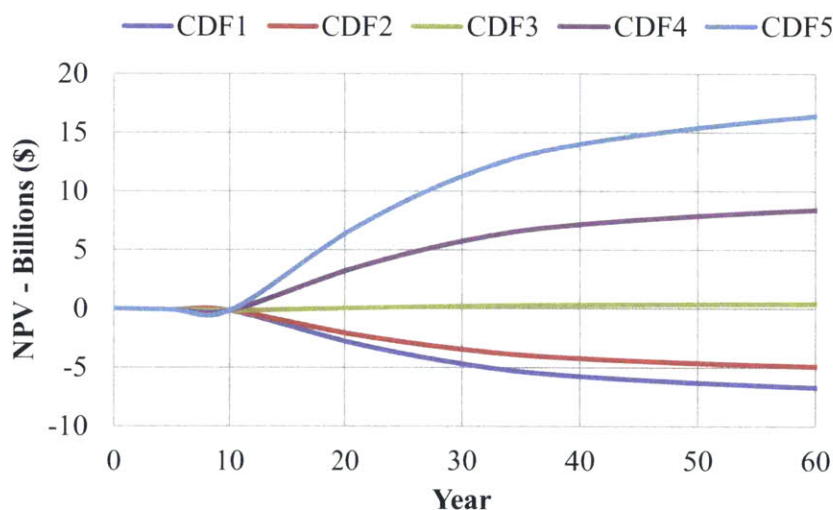
Figure 6-20: Parametric study of core damage frequency for FeCrAl cladding during a Fukushima-type accident

Current power plants, have a probabilistic risk assessment (PRA) calculated rate of core damage frequency close to 5×10^{-5}/reactor-yr for a plant with active safety systems. [Gorgemans, 2011] This value does not take into account beyond design basis accidents, like those at Fukushima-Daiichi. Typical PRA values for an advanced reactor are significantly lower, for an AP1000 CDF is 5.1×10^{-7}/reactor-yr. [Gorgemans, 2011] Neither of these numbers takes into account beyond design basis accidents. However it is can be assumed that the AP1000 would have a frequency of severe accidents with release events significantly lower than currently operating reactors light water reactors. This would make the economic case for ATF less viable, unless the overall cost of an accident were higher than presented in this study.

6.5   Conclusions

Three separate metallic cladding options and and the SiC CMC cladding proposed as ATF options were examined according to their impact on fuel cost. For each cladding considered, different development time and cost was assumed, and the enrichment penalty in relation to zirconium was calculated. This does not imply any judgment about the technical feasibility of each concept. It was found that the least cost option is SiC. Avoiding severe accidents is considered a significant economic benefit that could be realized with SiC. However, this economic advantage was not realized when metallic claddings were examined, since their enrichment penalty was higher than that of SiC.

If the present value of avoiding such large reactor accident with a large radioactivity release is estimated using past experience for LWR severe accidents, there is a definite net economic benefit relative to typical zirconium cladding only in using SiC CMC as a cladding material. Because of the high enrichment costs relative to accident costs, there is only at best a marginal economic benefit in using SiC in current commercial LWRs to prevent a core-only loss without

164

radioactivity release (TMI-type) accident and a large economic loss using metallic ATF concepts.

The parametric sensitivity study showed that the analysis conclusions are sensitive to assumed parameters, such as the total cost of a severe accident or the money discount rate. It is also important to note that for this analysis it was assumed that all claddings prevented the accidents in question. The effectiveness of the claddings examined in the prevention of core damage events is not explored in this work, and have yet to be confirmed experimentally.

7. Design of Uranium Nitride Fueled Tight-Lattice PWR for Breeding

The concept of a light water reactor (LWR) breeder reactor has been examined for a long period of time, with extensive research going back into the 1970s. While the thorium-uranium fuel cycle was the main choice in the 1970s, currently, there is more interest in reduced moderation boiling water reactors (BWR) based on uranium-plutonium. Multiple investigations from Japanese industry and research establishments have addressed breeding BWR reactors. In the past, much more research was performed in the US into the possibility of using a pressurized water reactor (PWR) in order to breed new fissile materials. However, in the last few years, US Department of Energy (DOE)-sponsored university research programs appeared to focus on the reduced moderation BWR concept.

This chapter examines the possibility of using uranium nitride (UN) fuel instead of the MOX fuel in a PWR breeder. Since the heavy metal density of nitride is higher than the oxide, the hydrogen to heavy metal (H/HM) ratio is decreased in the core, even if nothing else was changed. This skews the energy spectrum to a higher energy, making breeding easier. This is further enhanced by going to a tighter fuel array. For comparison, the H/HM ratio of a typical PWR is near 3.0, whereas for the work here, the value is 1.1 at a maximum.

Similar examination of a BWR breeder was performed by Feng (2011). Feng (2011) also provided a preliminary analysis of a nitride-fueled PWR breeder. However, the simulation was performed primarily for the purpose of scoping one design. The conditions of the simulation were not the same as an operating PWR. The simulation had the core geometry of a reduced moderation boiling water reactor (RBWR) assembly and had single phase liquid water as the coolant at 7.2 MPa. [Feng, 2011] In contrast to this, the present work maintains the conditions of an operating PWR core. The coolant temperature, pressure and density are the same as an operating reactor.

Using enrichments similar to those in the RBWR and reduced moderation pressurized water reactor designs, the FIR of the assembly modeled by Feng (2011) shows an initial FIR increase at beginning of life, followed by a decrease below 1.0 near a burnup of 20 MWd/kgHM. A plot

of the FIR of both an RBWR mixed oxide assembly (RBWR-MOX) and a 95% theoretical density uranium nitride, single phase water RBWR assembly (RBWR-MN-SP-95) can be seen in Figure 7-1.
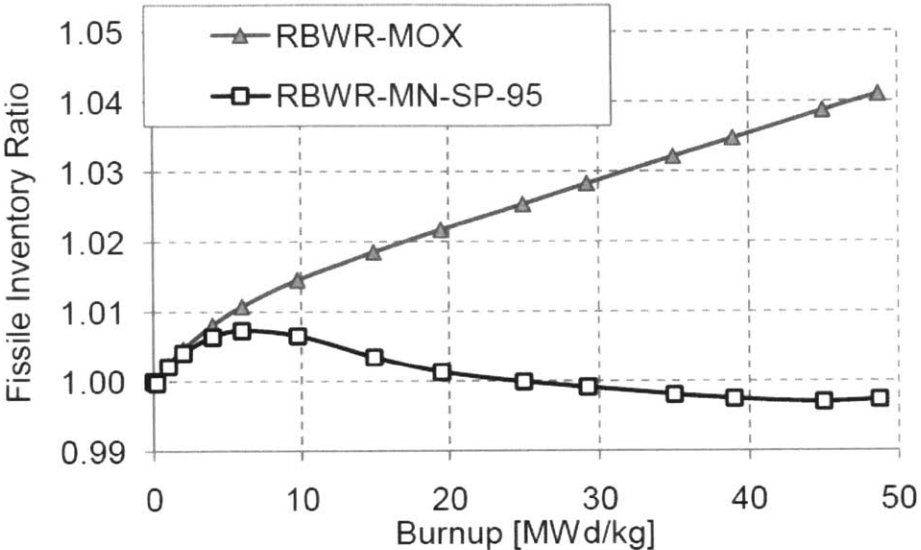
Figure 7-1: Fissile inventory ratio versus burnup for RBWR assemblies with

By reducing the average fissile plutonium enrichment of the assembly from 5.06 to 4.67 wt% HM, Feng (2011) was able to achieve an FIR above 1.0 at higher burnups. However, this came with a penalty to fuel cycle length and burnup. It should also be noted that the work by Feng (2011) did not include thermal hydraulic or safety analysis of nitride fueled PWR assemblies. It also did not explore how the breeding characteristics changed when a switch to an 85% theoretical density UN fuel was made. Both safety analysis and effect of theoretical density are addressed in the present work.

This chapter discusses the selection of a design for a comparison between nitride and oxide fuel for use in a reduced moderation PWR. The selected design is then used to provide a basis for comparative neutronic, thermal hydraulic and safety study. In the thermal hydraulics, the mDNBR, pressure drop and vibration ratio are all calculated. Based on the previous mDNBR correlation examination, the KfK correlation is used for the purpose. For the vibration ratio, the Paidoussis correlation is used. For friction losses, the Cheng and Todreas correlation for pressure

167

loss in wire-wrapped hexagonal assemblies is used. [Dalle, 2005] [Todreas and Kazimi, 2011] For neutronics, the Monte Carlo depletion code Serpent is used.

7.1   Assembly Designs

A summary of previous breeding PWR designs has been given by Feng (2011). In order to harden the spectrum, all designs shift from a traditional fuel rod square array to a tight hexagonal array. Additionally, these designs utilize different characteristics to obtain a conversion ratio near or above one. The principal method of doing this is to introduce heterogeneity into the core by allowing a zone of low-enriched fuel within the high fissile zones. This can be done both axially and radially on the core level or on an assembly level. The heterogeneity makes fuel manufacturing and core management more difficult. Therefore, one of the key parameters in the selection of a design is fuel assembly simplicity. Ideally, there should be a minimal level of heterogeneity, a minimal level of reprocessing and a minimal number of fuel pin types. Based on these criteria, the reduced moderation water reactor - PWR (RMWR-PWR) is the reactor design selected to be examined in this paper. [Shelley, 2003] For this design, the Conversion Ratio (CR) was found to be 1.0 through Monte-Carlo depletion calculations performed with MVP-BURN. [Okumura, 2005] [Shelley, 2003] The core design uses a sandwich model axially; from bottom to top there are five zones of enrichment: blanket-seed-blanket-seed-blanket. [Feng, 2011]

A variation on this design was also explored. The design of voided thimble tube cell locations was made, and not filled with water and fuel pins. This modification reduced the amount of moderator in the assemblies, while keeping the amount of fuel constant. This lowers the H/HM ratio, as desirable for a higher conversion ratio.

168

7.1.1 Initial Design

The design chosen for this analysis contained both axial and radial blanket regions in an assembly. The assembly height of 2.95 m was optimized in the work by Shelley et al. (2003), which also showed that an internal blanket was necessary in addition to the external blanket. The design also has axial blankets on the top and bottom ends of the seed regions. The core height is less than the current PWR active core height of 3.66m. An axial diagram of the assembly design selected for examination can be seen in Figure 7-2.
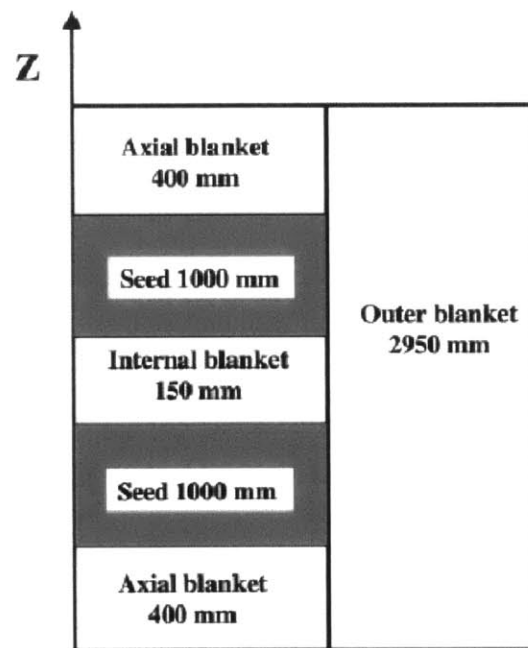
Figure 7-2: Axial composition of RMWR-PWR fuel assembly [Shelley, 2003]

The axial region definitions can be seen in Table 7-1. When the core design is modeled, it needs to include a plenum region and a lower reflector region. On the lower end of all fuel pins is a B_4C reflector. Below that is a water reflector, which fills the entire radial region. On top of the fuel pellets in the fuel pins is a plenum region. In addition, both axial ends are bounded by a black absorber.

169

Table 7-1: Axial regions of seed pins

Region	Height _cm_
Upper Simulation Boundary (Non-Reflective)	-
Upper Plenum Region	30
Upper Axial Blanket	40
Upper Fissile Region	100
Inner Blanket	15
Lower Fissile Region	100
Lower Axial Blanket	40
Lower B4C Layer	7
Lower Water Reflector	23
Lower Simulation Boundary (Non-Reflective)	-

The assembly design contains 14 rows of inner seed pins and 4 rows of external blanket pins. Accordingly the assembly contains 505 seed pins and 366 blanket pins surrounding the seed. [Shelley, 2003] The seed pins can be seen in the center of Figure 7-3, while the blanket pins can be seen on the outer region. The dark pins are seed and the light pins are blanket.

Each of the five axial regions (two fissile, three blankets) was split into three different axial regions, leading to 15 simulated axial fuel regions. Blanket pins are treated separately from seed pins for each axial slice, this leads to 30 total simulated fuel regions. Each of the pins is additionally simulated using three radial regions of equal volume. Thimble tube regions can also be seen as water in between the pins. On each of the corners of the assembly is a tie rod, which is not fueled and is modeled as zirconium.
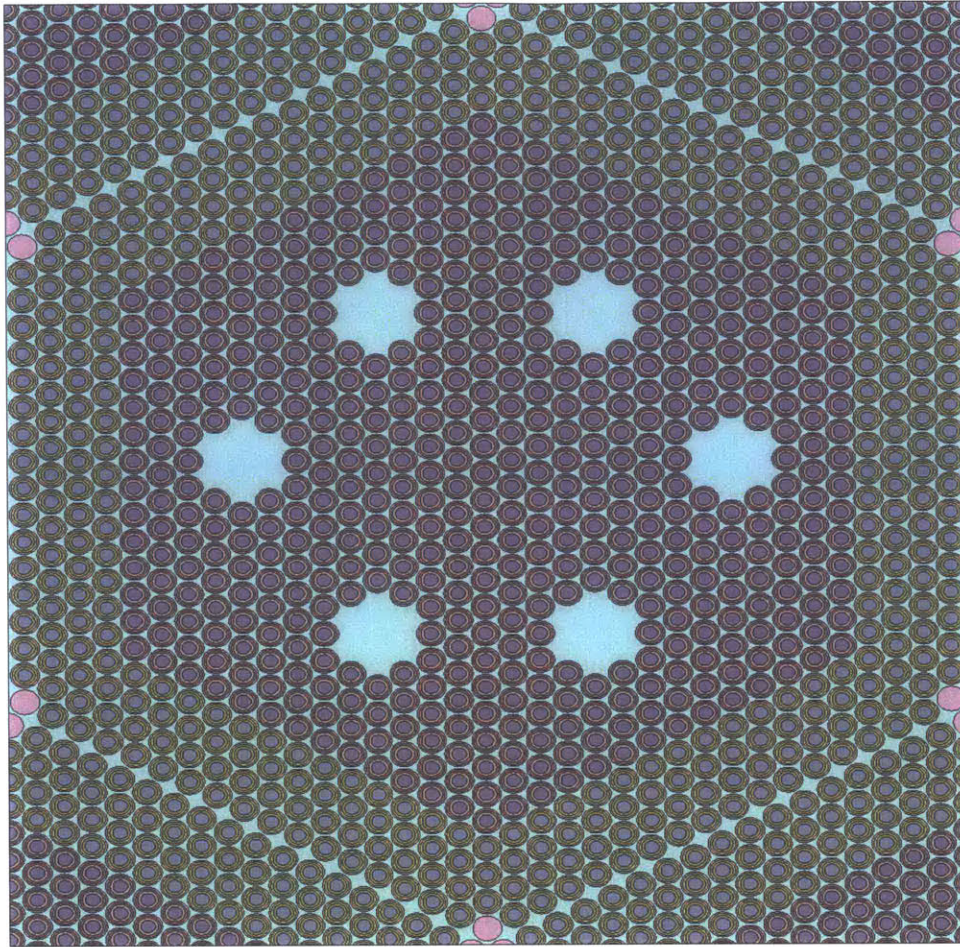
Figure 7-3: Full assembly geometry plot generated by Serpent, showing the seed region, blanket region and thimble tubes

A radial flux plot at both 0.0 MWd/kgHM (BOL) and 25.0 MWd/kgHM (EOL) is shown in Figure 7-4. This plot is produced directly by Serpent, with brighter colors indicating a higher neutron flux and darker colors indicating a lower neutron flux. Figure 6-4 (a) shows the assembly at BOL, and Figure 6-4 (b) shows the assembly at EOL. The flux is relatively higher in the seed region at BOL in comparison to EOL, because no plutonium has been bred in the blanket region yet. This is in line with expectations and indicates that the model is working correctly. Additionally, the pins next to the thimble tube are higher in flux at both BOL and EOL. This is because of the increased moderation that occurs in the middle of the thimble tubes, which can also be seen in the plots.

171
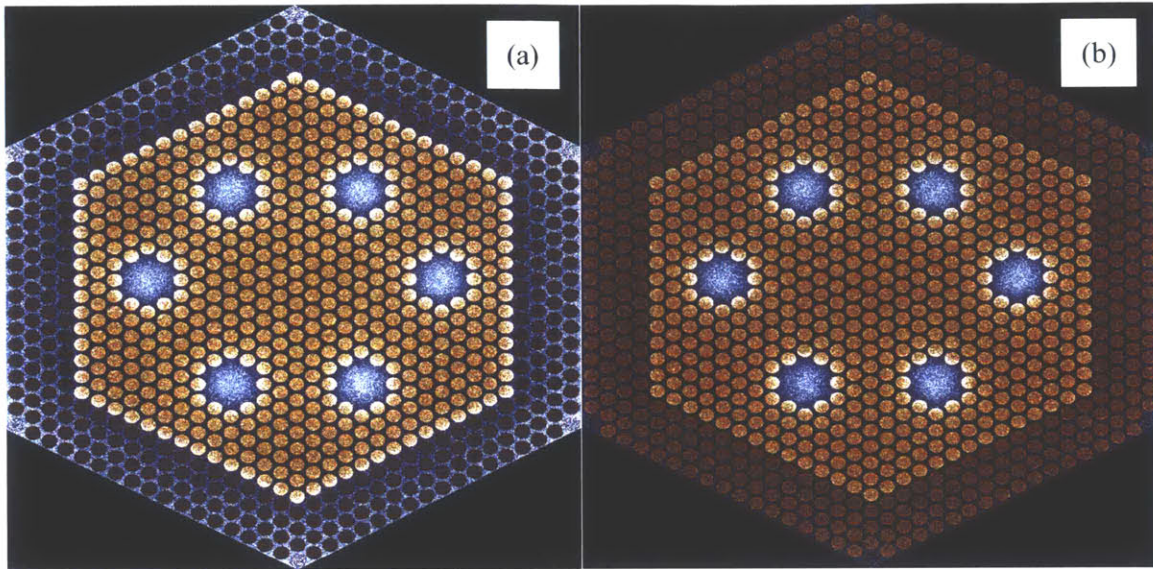
Figure 7-4: Radial relative reaction rate plot of the modeled assembly at (a) BOL and (b) EOL

The same plot was produced axially at both burnups of 0.0 MWd/kgHM (BOL) and 25.0 MWd/kgHM (EOL). This can be seen in Figure 7-5, which shows expected trends of higher flux in the fueled regions as opposed to the blanket regions. Similar power distributions can be seen in both the upper and lower fissile regions. These results are also peaked in the center, which is as expected. As the depletion proceeds from BOL shown in Figure 6-5 (a) to EOL shown in Figure 6-5 (b), the power spreads out from the fissile regions to the edges of the blanket regions. A significantly higher proportion of the total power is generated in the blankets at EOL in comparison to BOL. At beginning of life, the two axial seed regions, including their surrounding radial blankets, generate nearly 98% of the total power. Blankets are included in the analysis, even though they generate a small amount of power because they are where most plutonium breeding occurs, and are therefore needed to correctly asses the breeding characteristics of a design.

172
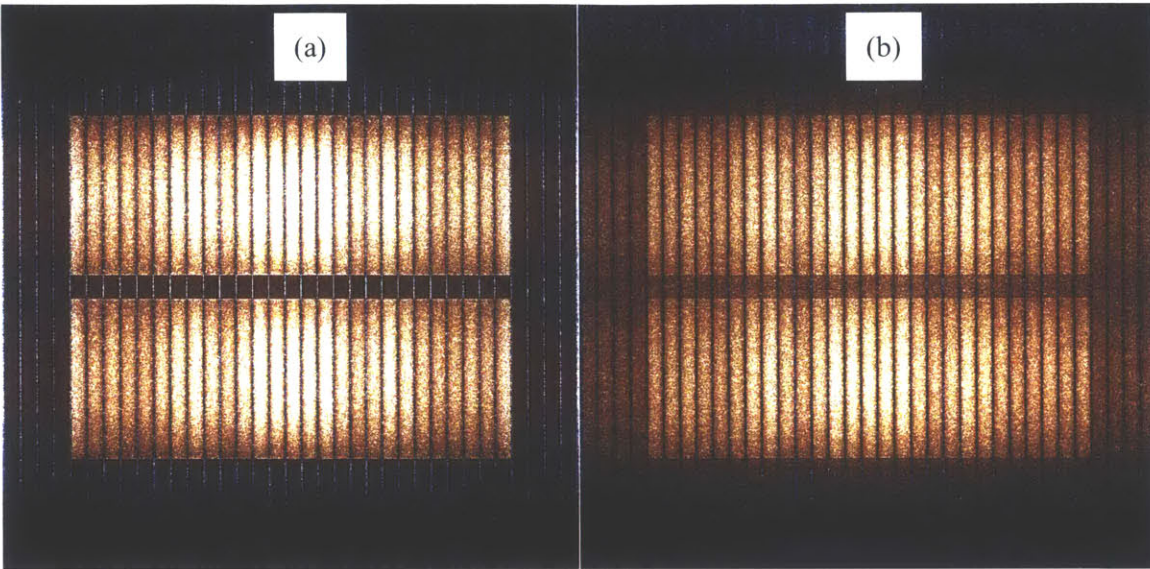
Figure 7-5: Relative axial reaction rates of the modeled assembly at (a) BOL and (b) EOL

7.1.2   Thimble Tube Alteration

The first explored alteration to this design was changing the material filling the thimble tube cells to void. This provides an upper bound for the conversion ratio that could be obtained by reducing the moderation through scattering with the material in the thimble tube region. The geometry for this alteration can be seen in Figure 7-6. The voided thimble tubes can be seen in black. Like in the previous design iteration, the inner seed region is darker than the outer blanket region. Additionally, within each pin there are three burnable regions.
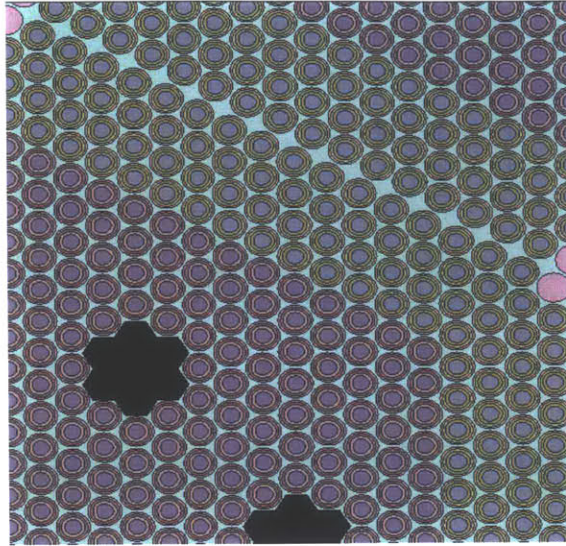
Figure 7-6: Serpent generated output for the voided assembly tube cases, northeast quarter of the assembly shown

Since the radial geometry was altered, a radial flux plot is shown in Figure 7-7 at burnups of both 0.0 MWd/kgHM (BOL) and 25.0 MWd/kgHM (EOL). The peaking that was present in the pins near the thimble tubes is now absent, since there is decreased moderation in that region. Like in the previous cases, the power profile evens out as the burnup increases; this can be seen in the differences between the BOL and EOL cases. Like the original case, there is still a peak in pin power at the edge of the seed region at beginning of life, so the problem of high local peaking factors is not eliminated by this alteration. The axial flux plot is not included, since it did not change appreciably, this is as expected since the axial make-up of the assembly did not change.
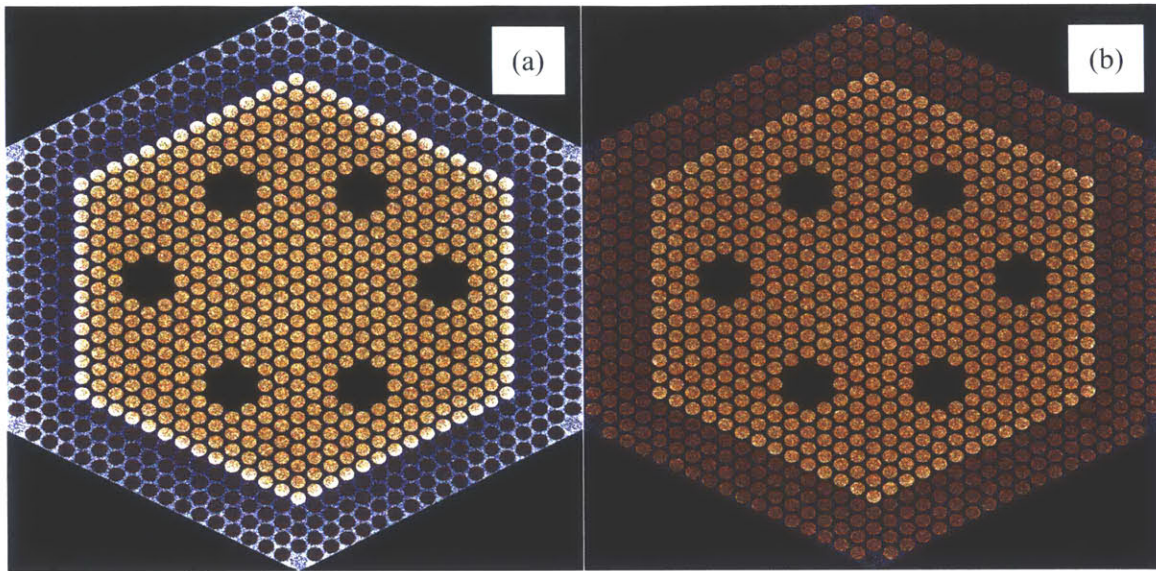
Figure 7-7: Radial relative reaction rate plot of the modeled assembly with voided thimble regions at (a) BOL and (b) EOL

7.2   Modeling Parameters

The modeled assembly was set to a power level corresponding to the thermal hydraulic limits, which resulted in an average linear heat rate in the seed region near 20 kW/m, as will be discussed further in the upcoming sections. This rate is from neutronic calculations within one assembly, and does not take into account any core radial assembly peaking factors. Maximum assembly powers were determined based on the pressure drop, vibration ratio (y/D) and the minimum departure from nucleate boiling ratio (MDNBR) limits. Maximum assembly powers for the six variations examined can be seen in Table 7-6. Depletion was performed to a maximum burnup of 25 MWd/kgHM. This burnup refers to the mass of heavy metal in the whole assembly, not just in the fissile regions. The boundary conditions for the calculation were reflective radially and vacuum axially. For this neutronic analysis 20,000 particles per cycles were used. A total of 90 cycles were run, with the first 20 being thrown away starting from a uniform source distribution. The basis for these parameters is taken from Shelley (2003). In order to obtain more accurate results, future studies should run more particles additional cycles and

175

throwing away additional cycles. The core power will be associated with a lower assembly-average linear heat rate in the seed region, to allow for the radial power distribution in the core.

7.2.1 Pin Geometry

Fuel pin specifications can be seen in Table 7-2. The diameter of the fuel pins is 12 mm and the minimum gap width between pins is 1 mm. A large fuel pin diameter and a small gap both serve to lower the H/HM ratio, which results in a raised conversion ratio. It is also desirable to increase the blanket pin diameter, but due to complexity of manufacturing and flow distribution, the blanket fuel pin is kept the same as the fuel pin. The cladding for all of fuel pins is Zircaloy.

Table 7-2: Fuel pin specifications for RMWR-PWR [Shelley, 2003]

Parameter	Specification
Rod Pitch - *mm*	13
Cladding outer diameter - *mm*	12
Cladding inner diameter - *mm*	10.48
Pellet diameter - *mm*	10.38
Material of seed fuel rod	$(Pu, U)O_2$ or $(Pu, U)N$
Material of blanket fuel rod	Depleted UO_2 or UN
Cladding Material	Zirconium

7.2.2 Material Properties

The density and temperature of the materials modeled in Serpent are shown in Table 7-3. Water conditions are taken to be core average values of 580 K temperature and at 15.5 MPa pressure. Cladding was modeled as natural zirconium. The boron carbide reflectors used in the core are

176

modeled to have 90% B-10, enriched from the natural composition. They are also at the same temperature as the coolant. All fuel in the core is modeled at 900K.

Table 7-3: Density and temperature of materials used in tight-lattice assembly modeling

Material	Properties
Water	0.7108 g /cm^3 580 K
Zirconium	6.5 g /cm^3 626 K
90% Enriched B$_4$C	2.394 g /cm^3 580 K
Fuel	900 K

The fuels simulated were MOX, 95% theoretical density nitride (N-95) or 85% theoretical density uranium nitride (N-85). The motivation behind analyzing the 85% nitride is to reduce volume swelling by allowing for larger fission gas release in the nitride vs. oxide fuels. [Feng, 2011] Fuel characteristics are summarized in Table 7-4.

Table 7-4: Fuel characteristics of the fissile and seed regions [Feng, 2011] [Shelley, 2003]

	Seed Region			Blanket Region		
Fuel	(U,TRU)O$_2$	(U,TRU)N	(U,TRU)N	UO$_2$	UN	UN
% Theoretical Density	95	95	85	95	95	95
Fuel Density g/cm^3	10.5	13.62	12.18	10.5	13.585	13.585
Uranium Density g/cm^3	9.26	12.78	11.45	9.26	12.78	12.78

The plutonium vector for the seed region can be seen in Table 7-5. The reactor grade plutonium vector is taken from Shelley (2003); it was kept consistent so that a better comparison with previous work could be made.

177

Table 7-5: Reactor grade plutonium vector used in tight-lattice uranium nitride examinations [Shelley, 2003]

Isotope	Reactor Grade *wtHM%*
Pu-238	2.7
Pu-239	47.9
Pu-240	30.3
Pu-241	9.6
Pu-242	8.2
Am-241	1.0

Blanket regions contained only depleted uranium with 0.25% U-235. Seed regions contained depleted uranium mixed with 12.75 wt% HM plutonium. The heavy metal composition of both the fissile and blanket regions can be seen in Table 7-6.

Table 7-6: Isotopic composition (in %HM) of both the fissile and blanket regions [Shelley, 2003]

Isotope	Seed	Blanket
U-235	0.0019	0.0025
U-238	0.7763	0.9975
Pu-238	0.0060	-
Pu-239	0.1062	-
Pu-240	0.0672	-
Pu-241	0.0213	-
Pu-242	0.0188	-
Am-241	0.0022	-

It is also important to note that the nitride itself needs to be enriched to 99.5% to 99.9% N-15 in order to limit parasitic absorption by N-14, which has a prohibitively high neutron cross section. Naturally nitrogen is only 0.37% N-15. In comparison to N-14, N-15 is virtually transparent to neutrons. Using only N-15 also limits the amount of radioactive C-14 that is formed from the absorption of neutrons in N-14. [Feng, 2011] Accordingly, the nitrogen used was assumed to be 100% N-15, though the actual enrichment for a real design would be near 99.9%. This assumption is made to maintain consistency with the work by Feng (2011).

7.3   Analysis and Results

7.3.1   T/H Analysis

An evaluation of DNB was performed on a pin by pin basis, using the pin peaking factors outputted by Serpent for the entire assembly, and assembly peaking factors based on typical PWR values. For this analysis, the KfK DNB correlation was used, since it was determined to be the most appropriate correlation for use in tight lattice calculations. [Dalle, 2005] The EPRI-I, EPRI-B&W, WSC-2 and W-3 DNB correlations had also been examined for suitability. [Akiyama, 1991] [Bowring, 1979] [Reddy, 1981] [Uotinen, 1981] The KfK correlation showed the least scatter between the correlation-predicted DNB heat flux and the actual DNB heat flux in a range of experiments. The MDNBR depends greatly on the coolant mass flux through the assembly and the power of the assembly. An assembly maximum pressure drop of 400 kPa was used to determine the maximum allowable mass flux. This pressure drop is more than a factor of 2 higher than in typical PWRs, but is thought to be tolerable from a mechanical design stand point (enhanced hold-down mechanisms and increased pumping power are drawbacks). For this analysis, the Cheng and Todreas correlation for wire-wrapped rods was used for frictional losses. [Todreas and Kazimi, 2011] Gravity and form losses were also taken into account.

Additionally, the calculated mass flux was used to determine the vibration magnitude of the fuel rods. For this evaluation, the Paidoussis correlation was used, and a maximum y/D value of 0.021 was obtained. [Paidoussis, 1998] The maximum assumed void fraction value in the assembly for this analysis was 0.40, similar to a standard PWR hot channel outlet. Once the maximum allowable mass flux was determined, this value was used to determine the maximum power allowed in the assembly to meet a MDNBR value of 1.44. The MDNBR shown is the minimum value of all pins in the assembly at all axial locations. This analysis was only performed at beginning of life (BOL), since the most severe peaking seen in the assembly occurs at BOL and not at end of life (EOL). The parameters for the analysis can be seen in Table 7-7.

Table 7-7: Thermal-hydraulic analysis parameters

Parameter	Value
Pressure	15.5 MPa
Inlet Temperature	569 K
Hydraulic Diameter	3.5 mm
Hot Assembly Peaking Factor	1.45
Heat remaining in subchannel after generation	100%
Wire-wrap axial pitch	40 cm
Coeff. of expansion pressure loss	1.0
Coeff. of contraction pressure loss	0.5

However, there are a number of conservative assumptions which are not normally applied in the model. For this analysis, a single channel model was used. Whereas in a subchannel analysis, not all of the heat generated in a subchannel remains there. There is heat transfer, mass transfer and momentum transfer between adjacent subchannels and assemblies. Such lateral mass and energy exchange is not modeled here. It is also unclear if the hot assembly peaking factor of 1.45 applied is accurate, since this is a value taken from typical PWRs. This hot assembly peaking factor is applied on top of the pin peaking factor. Since the mean free path of neutrons is greater in this design, the core radial peaking factor could be less than typical PWRs. The core radial peaking factor is additionally affected by leakage for which the current model does not account. The most limiting fuel pin was used, which was based on pin peaking. To determine this, all of the pins in the modeled assemblies were examined. One trend that can clearly be seen is that the nitride cases provide more margin than the oxide cases at all flow rates.

It would be logical to conclude that there would be less peaking in the assembly as the switch in the fuel is made. The resultant mass flux for an assembly in this analysis was 6221 kg/m^2s and the resultant vibration ratio magnitude was 0.007. The resultant average assembly powers can be seen in Table 7-8. The pin peaking in Table 7-8 is within the assembly. It does not include the 1.45 assembly radial peaking factor used in the DNB analysis.

Table 7-8: Maximum allowable assembly power and pin peaking for tight-lattice assemblies

Fuel	Thimble Cell	Average Assembly Power - MW	Pin Peaking at BOL
MOX		19.4	2.63
N-85	Water	19.5	2.49
N-95		20.1	2.45
MOX		17.6	2.94
N-85	Void	19.0	2.53
N-95		20.1	2.52

7.3.2 Neutronic and Breeding Analysis

The results for the fissile inventory ratio obtained from the assembly model can be seen in Table 7-9. The Monte Carlo depletion code Serpent was run using 20,000 neutrons per cycle. 90 total cycles were run and the first 20 were discarded. The average statistical uncertainty on k_{eff} at BOL was 71 pcm; this decreased as burnup increased. The maximum statistical uncertainty for k_{eff} for these assembly studies was 83 pcm, however these values do not account for propagation of nuclide composition uncertainties between depletion steps. In the same table are single-batch discharge burnups (B_1). It can be seen that in comparison to the base oxide case, which has an FIR of 0.974 at 35 MWd/kgHM burnup, the nitride is able to boost the FIR slightly. Since the nitride cases also showed that the FIR is less than one, the assemblies were altered so that the water in the thimble tubes was replaced with void. The altered cases were much more effective at breeding than the base cases. The altered cases with void in the thimble tubes all have FIR values greater than 1.0. Similar FIRs were obtained for the alterations made, regardless of whether the fuel is nitride or oxide. However, if the burnup curve is extended to the k_{eff}=1.0 line, then the FIR for the nitride cases is higher at this point. The use of nitride allows for a much longer cycle length than the traditional oxide fuel. This is indicated by the much higher single batch burnup.

Table 7-9: Summary of the fissile inventory ratio (FIR) and single batch burnup results

Fuel	Thimble Cell	Average Assembly Power - *MW*	FIR at 35 *MWd/kgHM*	Bu_1 *MWd/kgHM*	H/HM Ratio
MOX		19.4	0.974	19.2	1.10
N-85	Water	19.5	0.979	25.0	0.83
N-95		20.1	0.987	31.3	0.74
MOX		17.6	1.027	15.6	0.91
N-85	Void	19.0	1.029	24.5	0.69
N-95		20.1	1.033	32.2	0.61

As a function of burnup, the value of k_{eff} for the designs examined can be seen in Figure 7-8. The burnup shown in the plots and tables in this section is the assembly average burnup and not the peak burnup.
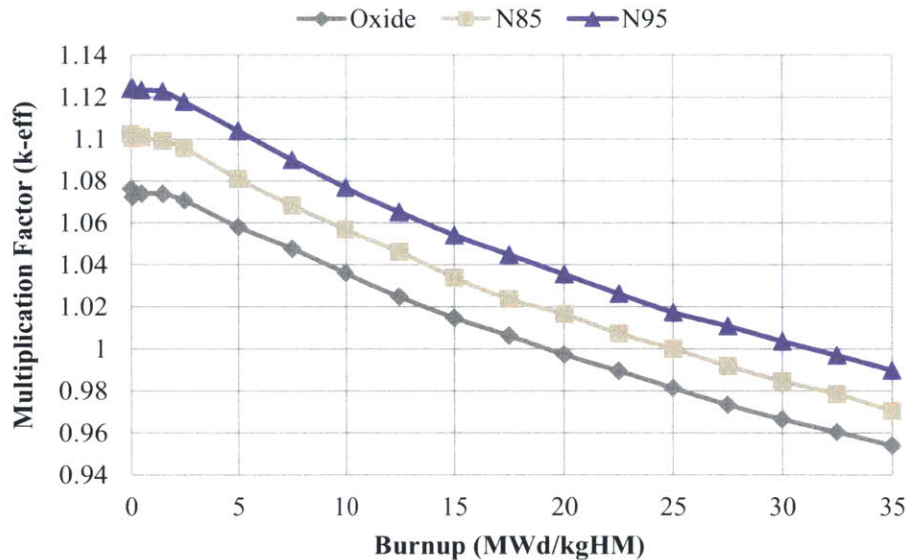
Figure 7-8: k_{eff} history for cases with water in the thimble tube region

Figure 7-9 contains a plot of the FIR as a function of burnup for cases with void in the thimble tube region. It can be seen that there is a small improvement in the FIR when uranium nitride fuel is used instead of uranium oxide. This benefit would increase if the cycle length of the uranium nitride and uranium oxide were matched. At the same cycle lengths there would be less

plutonium in a uranium nitride assembly relative to uranium-238. Accordingly, the FIR would be boosted further.
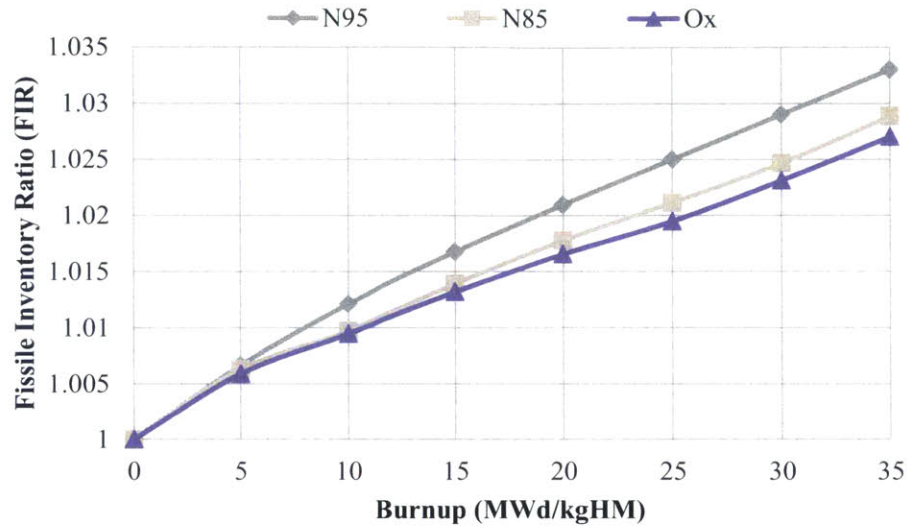
Figure 7-9: Fissile inventory ratio for cases with void in the thimble tube region

Several analyses were performed to determine the behavior of the assembly and the distribution of fissile isotopes within it. To highlight the change in the fissile isotope distribution in the assembly, the BOL and EOL fission isotope composition is shown in Figure 7-10 for the oxide fuel case in the inner seed region. Figure 7-11 provides a similar plot for the outer blanket region. Similar trends were seen in the nitride cases, so they were not shown here.
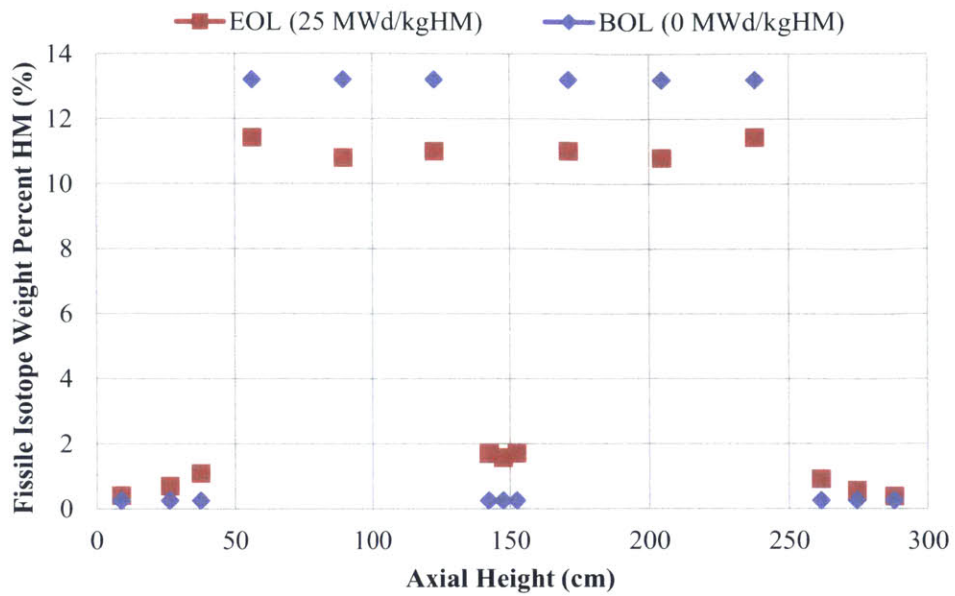
Figure 7-10: Fissile isotope weight percent HM in the seed region of the oxide fuel assembly
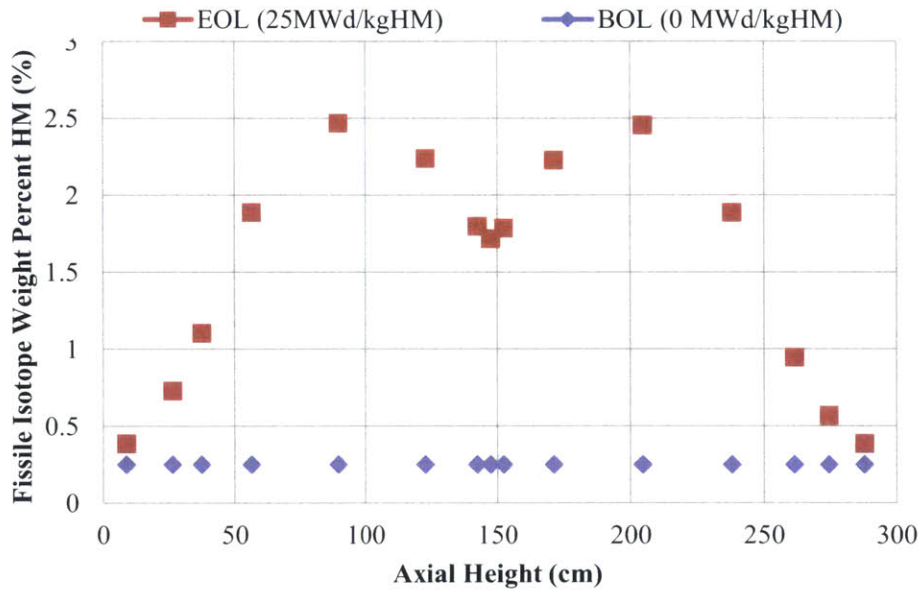
Figure 7-11: Fissile isotope weight percent HM in the blanket region of the oxide fuel assembly

184

7.3.3 Moderator Density and Power Coefficient Analysis

In order to evaluate the safety features of the reactor in off-normal conditions, the moderator density coefficient of reactivity was calculated. It is imperative that this value be positive, to help limit any increase in the power to flow ratio. Otherwise the formation of vapor in the core could cause it to become unsafe. In order to determine the coefficient, the value of k_{eff} was determined when the density of the moderator is altered from the nominal value of 711 kg/m^3 to a value 10% less than this (641 kg/m^3). So that the change in density could be isolated from a change in moderator temperature, the moderator temperature was kept constant at the value originally used in all core calculations, 580 K. The coefficient calculated is a core average value. [Shelley, 2003] For this neutronic analysis 40000 particles per cycles were used. In these runs, 90 cycles were run, with the first 20 thrown away. For this analysis the average statistical uncertainty for the original k_{eff} was 32 pcm and the average altered density uncertainty was 33 pcm. The density coefficient of assembly designs can be seen in Table 7-10 and Table 7-11.

Table 7-10: Associated values of k_{eff} for density coefficient analysis at BOL

Fuel	Thimble Tube	Original k_{eff}	Uncertainty	Altered Density k_{eff}	Uncertainty
MOX	Water	1.07527	0.00031	1.07179	0.00038
N85	Water	1.10153	0.00039	1.09962	0.00029
N95	Water	1.12524	0.00024	1.12396	0.00030
MOX	Void	1.04968	0.00033	1.04837	0.00035
N85	Void	1.07666	0.00034	1.07750	0.00032
N95	Void	1.10302	0.00032	1.10428	0.00033

Table 7-11: Density coefficient at BOL

Fuel	Thimble Tube	$\Delta\rho$ pcm	Density Coefficient $pcm/(kg/m^3)$	Uncertainty $pcm/(kg/m^3)$
MOX	Water	-302	4.25	0.64
N85	Water	-158	2.22	0.62
N95	Water	-101	1.42	0.48
MOX	Void	-119	1.67	0.64
N85	Void	72.4	-1.02	0.61
N95	Void	103	-1.45	0.59

Four of the six cases have a positive density coefficient. However, the N85 and N95 fuel returned negative density coefficients when voided thimble cells were used. Additionally, when the voided thimble tubes are used, the density coefficient became less than when water thimble tubes are used. This leads to a conclusion that the more moderator there is in the core, the more positive the density coefficient is. However, it needs to be asserted that this value would change when radial leakage is taken into account, with a potential for a more positive coefficient due to increased leakage upon voiding.

While it is preferable for a reactor to have a negative void coefficient, it is not necessary. CANDU reactors currently operate with a positive void coefficient and in the past many fast reactors operated with positive void coefficients, including FFTF, EBRII, PHOENIX, and Superphénix. For all of these reactors the power coefficient of reactivity was used to demonstrate the design's safety response. The power coefficient reflects the net reactivity feedback from the fuel temperature change, moderator temperature change and moderator density change. Accordingly, a 50% increase in assembly power was simulated. Based on this 50% increase in core power, higher moderator and fuel temperatures were calculated. Based on the new coolant temperature and operating pressure, a new moderator density was also found. The fuel temperature increased from a nominal value of 900 K to 1065 K, the moderator temperature increased from a nominal value of 580 K to 585 K and the moderator density was changed from a nominal value of 712 kg/m^3 to a value of 700.5 kg/m^3. Results of this analysis can be seen in

Table 7-12 and Table 7-13; for these cases the average uncertainty in k_{eff} was 50 pcm. It can be seen that the power coefficient of reactivity is negative for all of the cases examined.

Table 7-12: Associated values of k_{eff} for power coefficientat BOL

Fuel	Thimble Tube	Original k_{eff}	Uncertainty	Altered Power k_{eff}	Uncertainty
MOX		1.07527	0.00031	1.06952	0.00049
N85	Water	1.10153	0.00039	1.09653	0.00052
N95		1.12524	0.00024	1.12045	0.00050
MOX		1.04968	0.00033	1.04436	0.00049
N85	Void	1.07666	0.00034	1.07262	0.00047
N95		1.10302	0.00032	1.09896	0.00053

Table 7-13: Power coefficient at BOL

Fuel	Thimble Tube	$\Delta\rho$ pcm	Power Coefficient pcm/(% power)	Uncertainty pcm/(% power)
MOX		-500	-7.03	0.76
N85	Water	-414	-5.82	0.83
N95		-380	-5.34	0.70
MOX		-485	-6.83	0.79
N85	Void	-350	-4.92	0.76
N95		-335	-4.71	0.79

7.4   Conclusion

Since the oxide fuel is found to be more inherently safe, judging by the density coefficient analysis, and the nitride fuel provides a more reasonable MDNBR value, we need to examine other parameters to provide a full assessment of these two fuels. Nitride fuels offer significantly improved thermal conductivity over oxide fuel, reducing the amount of stored energy in the fuel. Conversely, nitride fuel could under-go more hydrogen pickup, mainly due to a much higher burnup compared to the oxide. This is in addition to the effect of the harder spectrum. An

187

increase in hydrogen pickup would lead to increased clad embrittlement. If, within the same core volume, it is possible to extract more energy from the nitride fuel, it will be a more economically favorable fuel than the oxide. However, this may require increased coolant flow, to allow the MDNBR to remain at the same level as in present PWRs.

The economics of the nitride fuel are potentially far superior to the oxide fuel, because of the significantly increased single batch discharge burnup. If the current PWR core shroud diameter is used, then 66 assemblies could fit into the pressure vessel, leading to a core power of 1326 MWth for 95% TD nitride compared to 1162 MWth for oxide. This core power is significantly lower than currently operating PWRs, which operate near 3500 MW_{th}. This decrease in core power is a result of the increase in peaking factors over a current PWR and the decrease in the rod gap, which limits coolability. This large decrease in power puts this assembly design's economic viability in question. However, the concept itself is validated. An alternative assembly design with a lower pin peaking factor would be much more appealing.

This analysis indicates that a higher FIR can be achieved at the same burnup for higher theoretical density nitride. This, coupled with nitride's other advantages, makes it a better choice for a breeder.

However, while the neutronic and T/H characteristics of UN fuel could be viewed as favorable. The fuel performance of UN fuel is still of concern. In particular, nitride fuel has increased swelling in relation to uranium oxide. To address this, seed region of any core should not exceed a theoretical density of 85% to maintain fuel survivability. [Feng, 2011] Another concern is that when heated water vapor comes into contact with the UN, ammonia, UO_2 and hydrogen gas are formed. [Sunder, 1998] Another concern that remains is the economics of using uranium nitride instead uranium oxide. While the cost of the uranium itself may be similar, there is an additional cost of enriching nitride for use. Because of the large neutronic penalty when using N-14 in the fuel it is necessary to enrich nitride to 99.5% to 99.9%. It is unclear how expensive this would be on an industrial scale.

8. Summary, Conclusions and Future Work

This work examined specific knowledge gaps in the use of alternative fuel and cladding combinations in a pressurized water reactor environment. This included thoria and urania in conjunction with silicon carbide cladding for the disposition of weapons grade plutonium. In this analysis, it was found that thoria when used as a fuel matrix presents a benefit in both the amount of plutonium burned and the initial plutonium disposal percentage.

Secondly, the economics of accident tolerant fuel claddings were examined. The costs of fuel cycle changes that would be incurred in this switch were evaluated against the economic benefit of preventing severe accidents. The reactor was assumed to retain its operating characteristics, including the fuel cycle length and batch size. Two cases were considered, one with the fleet of 100 reactors remain operating for 60 years and the other had only 60 reactors operating by the end of 60 years. It was found that SiC CMC cladding offered a significant economic benefit in the prevention of reactor loss and release events, similar to Fukushima-Daiichi.

Finally the neutronic and thermal hydraulic characteristics of a uranium nitride fueled tight-lattice pressurized water reactor design for breeding were examined. By breeding plutonium from U-238, the total amount that can be extracted from fuel is increased. It was found that uranium nitride offered improved economics and slightly improved breeding characteristics. While the density coefficient of reactivity was not positive for uranium nitride, the power coefficient was.

8.1   Plutonium Burning in Thorium and Uranium

The core designs developed are for a typical 4-loop Westinghouse PWR with 193 assembly core using an 85-assembly per cycle reload scheme. Each assembly has 264 fuel pins and 25 water rods. The fuel pins have outer diameter of 9.5 mm with a pitch of 1.26 cm. The core designs created are all equilibrium cycle cores with a cycle length of 492 EFPD. For this analysis the

Studsvik light water reactor analysis package was used. Using the lattice physics code CASMO4E, assembly designs were created. These assembly designs were then used to develop full core designs with the nodal diffusion code SIMULATE3. These cores were then used for accident calculations in the code SIMULATE3K.

Using a thoria-plutonia fuel mix and SiC CMC cladding separate core designs were created for three different reactivity control approaches: gadolinia, enriched IFBA and enriched soluble boron. For these cores SiC cladding was used with a thickness of 0.76 mm, compared to the typical Zircaloy thickness of 0.57 mm, while maintaining the clad outer radius and gap size. The amount of plutonium burned across all core designs are all within 2% of each other. All cores with SiC cladding burned a higher fraction Pu than the reference Zircaloy core. This is in part because the Zircaloy core has a higher initial plutonium loading due to the increased fuel volume. In a Zircaloy clad pin, there is 10% more volume for fuel than in the SiC core. However, there is only a 4% decrease in initial plutonium loading required for the desired cycle length.

Of the burnable poison options explored, it is believed that using enriched IFBA has the least drawbacks. While enriched boron would be used in the IFBA, this is already something that is done with current operating fuel. Fuel pin free volume might have to be adjusted to accommodate the He released from IFBA, in addition to the fission products. Using enriched boron in the coolant would require large investment in increasing the enrichment of boron in the entire primary system, which would lead to a higher cost. The gadolinia core would require a ternary mixture of Pu, Th and Gd oxides. There are doubts about the ternary oxide mixture stability in PWR operating conditions. [Bjork et. al. (a), 2013]

Thoria-plutonia fuel was then compared to the urania-plutonia fuel, which has been traditionally considered for plutonium burning. For this, they are evaluated according to the content of discharged assembly, discharged material proliferation risk and the amount and fraction of plutonium burned at discharge. Accordingly, it was necessary to develop urania-plutonia fueled core designs using both SiC and Zircaloy claddings. The cores developed have the same cycle length, cycle energy, assembly geometry, core geometry and similar loading patterns with enriched IFBA as the burnable poison. Additionally all the cores were compared based on their

equilibrium characteristics. A conventional PWR using standard enriched uranium fuel was also developed and is presented here. This core serves as a comparison point for the safety parameters and transient analysis of thoria-plutonia fuel.

It was found that a design with thoria-plutonia fuel and SiC cladding is the best option for plutonium disposition. Using thoria-plutonia based fuel results in a smaller percentage of initial plutonium at discharge. The discharged fuel has a better plutonium isotopic mix (or isotopic vector) and less fissile mass. A SiC cladding results in better plutonium burning characteristics than a Zr alloy counterpart.

The reactor cores showed acceptable behavior in the two reactivity insertion transients modeled, rod ejection at hot zero power and main steam line break. To maintain shutdown margin, it was necessary to use B_4C control rods instead of the AgInCd control rods currently used. During main steam line break accidents at both BOC and EOC, these rods were sufficiently worthy to decrease core power when scrammed and to prevent any power rise as the core cooled down. During the transient, the mDNBR limit was not violated for any case. Rod ejection transients of the highest worth rod failed to exceed the maximum allowable enthalpy in any single fuel node.

8.2   Economics of Accident Tolerant Fuel

Since the Fukushimi-Daichi accident there has been increased interest in the implementation of accident tolerant fuel (ATF) options. Three separate metallic claddings (Stainless steel (SS), FeCrAl alloy and molybdenum (Mo) tri-layer composite) proposed as accident tolerant fuel options and SiC CMC were examined according to their effect on fuel cost. The tri-layer Mo composite contained an inner Zr layer, a middle Mo layer and an outer FeCrAl layer.

These four claddings had different development times and costs, based on the technological challenges facing each. Using the Monte Carlo depletion code Serpent the enrichment penalty of each of these cladding options was found. The thicknesses of each candidate cladding was based

on the different strengths of the materials examined. SiC was taken to be 0.76 mm, FeCrAl and stainless steel were both 0.40 mm. The tri-layer Mo composite had layer thicknesses of 0.075 mm, 0.020 mm and 0.0125 mm respectively. Enrichment penalties ranged from 0.24% for SiC cladding to 1.11% for the Mo tri-layer.

With the calculated enrichment penalties, the increased fuel costs were found for two separate uranium pricing scenarios: a lower one from summer 2014 and a higher one from summer 2010. Of the new claddings examined, silicon carbide was found to be the least costly option. This increase in fuel cycle cost was then compared to the economic benefit of preventing two types of severe accident. The first is a reactor loss event, like the TMI event. The other is a reactor loss and radioactivity release event, like the Fukushima-Daiichi event. The costs of these accidents were calculated based on the probability of such accidents on a per year basis so they could be compared to the per year fuel cycle increased costs. Then, using net present evaluation, the overall economics of the ATF options were evaluated considering sixty years into the future for the entire United States reactor fleet.

If the present value of avoiding a large reactor accident with a large radioactivity release is estimated using past experience for LWR large accidents, there is a definite net economic benefit relative to typical Zircaloy cladding only in using SiC CMC as a cladding material, since it is capable of preventing reactor loss and radioactivity release in a Fukushima-type event. Because of the high enrichment costs relative to accident costs, there is only a marginal benefit in using SiC to prevent a core-only loss without radioactivity release (TMI-type) accident and a large economic loss using metallic ATF concepts.

A sensitivity study showed that the conclusions are sensitive to assumed parameters such as the total cost of a severe accident or the discount rate, but the general trends remained. It is also important to note that for this analysis it was assumed that all the claddings prevented the accidents in question. The effectiveness of the claddings examined in the prevention of core damage events is not explored in this work.

8.3 Breeding in a PWR with Uranium Nitride Fuel

An optimized PWR breeder design was considered for analysis after a significant literature review, which was based on the work by Feng (2011). According to the primary criteria of simplicity, ease of modeling and safety, the design by Shelley et. al. (2003) was selected for further analysis. This design featured an inner seed region of 14 rows and an outer blanket of 4 rows in each hexagonal assembly. The core was homogenous in that only one type of fuel assembly is necessary. Neutronic analysis with the depletion Monte Carlo code Serpent indicated that the initial assembly design could not reach an FIR greater than 1.0, even with a switch to nitride fuel, with the as-specified dimensions. However, if the thimble tubes, which were originally modeled at water, were switched to voided, streaming regions, then the FIR would be boosted above 1.0 to nearly 1.02 (at 25.0 MWd/kgHM) for all fuel types. Nitride fuel was found to have a much longer single batch discharge burnup than oxide fuel. This indicated that much longer cycles, resulting in higher capacity factors, could be run.

This work also evaluated the EPRI-1, EPRI B&W, WSC, W-3 and KfK correlations for use in a tight lattice PWR core against a range of experiments performed. After this analysis, the KfK correlation was determined to be the most appropriate correlation for use with tight lattice fuel assemblies. It returned a mean CHF ratio prediction of experiments of 0.981 with a standard deviation of 0.074. Other correlations had a less accurate mean and a larger standard deviation. Accordingly, this correlation was applied to the assembly design selected for analysis in the work to calculate the DNBR. In addition to the mDNBR of the assembly design, the vibration ratio and pressure drop were also calculated using the Paidoussis correlation for vibration ratio the Cheng and Todreas correlation for friction pressure drop.

A density coefficient analysis indicated that nitride fuel would have positive coefficient values in the voided thimble tube cases. However, when the power coefficient of the designs analyzed was performed, all of the designs presented a negative value. Oxide fuel gave a more negative, and thus a more desirable value for the power coefficient.

Based on the analysis of density coefficients, oxide fuel seems more inherently safe. On the other hand, nitride fuel provides a more reasonable mDNBR value. Therefore, more parameters need to be examined to provide a full assessment of these two fuels. Nitride fuel offers significantly improved thermal conductivity over oxide fuel, reducing the amount of stored energy in the fuel. Conversely, the harder spectrum caused by nitride fuel may induce more hydrogen pickup in the cladding, which would lead to increased embrittlement. Since the same fuel volume is involved, it is possible to extract more energy via the nitride fuel, and thus it is economically more favorable fuel than the oxide.

The economics of the nitride fuel are far superior to the oxide fuel, because of the significantly increased single batch discharge burnup. This analysis indicates that a higher FIR can be achieved at the same burnup for the higher theoretical density nitride. This, coupled with nitride's other advantages makes it a better choice for a breeder. The stability of uranium nitride in water is an issue that needs to be considered. When heated water vapor comes into contact with the UN, ammonia, hydrogen gas and UO_2 are formed. Work along these lines has been performed at national labs.

8.4   Future Work

8.4.1   Plutonium Burning in Thorium and Uranium with SiC CMC Cladding:

1. This study considered only the fixed geometry of a Westinghouse assembly design of today's vintage. Future work can address optimization of this assembly geometry to improve its plutonium burning potential.

2. A similar analysis of a full-core equilibrium cycle boiling water reactor should also be of interest. It would evaluate the benefits of thorium relative to uranium as a fuel matrix and assess the benefits of silicon carbide vs Zircaloys. It would also provide information for a comparison between burning using thorium in a BWR compared to a PWR.

3. The burnable poison IFBA, which was selected as the best burnable poison in this study, releases helium into the fuel plenum when the ^{10}B present in it absorbs a neutron. This presents a challenge for fuel performance. The increased internal rod pressure induces cladding creep over time. It would be very beneficial to explore other burnable poison options such as using erbium as a fuel pellet coating. It would also be beneficial to continue work on the core design which used gadolinia as a burnable poison.

4. An increased knowledge of both thorium nuclear data and the fuel performance data on thorium would be very beneficial to reducing uncertainties in the system. Of particular interest are increased understanding of the nuclear cross sections, thermal conductivity and fission gas release behavior.

8.4.2 Economics of Accident Tolerant Fuel

1. All of the cladding options examined in this work used enriched UO_2 as a fuel. When moving to an ATF, the fuel material itself may change. Of particular interest are uranium nitride and uranium silicide. Both provide increased uranium density. This increased uranium density may make it possible for fuel to be enriched to less than 5% when used in combination with accident tolerant cladding options.

2. The increased cost of fuel enrichment and the fuel development and manufacturing were examined in this work. It is necessary to better understand how implementing accident tolerant fuel would impact the whole fuel cycle. Among the questions to be answered is whether enrichments above 5% would impact fuel manufacturing and transport infrastructure, as only GE Silex is commercially licensed to enrich above 5%. The cost of providing higher enrichments' infrastructure is an added cost that may negate the benefit of the accident prevention. .

3. The isotopic compositions of the different accident tolerant claddings examined were based on natural abundance. It is possible to isotopically tailor many different isotopes in

195

order to limit neutron absorption in the cladding. Of particular interest is the isotopic tailoring of Mo, which has multiple isotopes that are large absorbers.

4. Better characterization of accident and their costs would provide a more accurate estimate of the economics of the system. Of interest are better understanding of the costs of replacement power and long term cleanup costs.

5. Fuel performance studies on each of the cladding options examined need to be performed to determine the optimal pin geometry, such as cladding thickness, for steady state operations, transients and potential accidents.

8.4.3 UN-Fueled Tight Lattice PWR for Breeding

1. The size of the assembly analyzed in this work is much larger than those currently used in pressurized water reactors. It would be beneficial to explore the design space to reduce the size of the assembly, while still maintaining the ease of manufacturability and a simple design.

2. Some initial work on duplex fuel pellets, indicated they can provide more favorable breeding characteristics than homogenous pellet designs. Further exploring assembly designs and the safety characteristics of such assemblies in relation to ones which use solid cylindrical fuel pellets is of interest.

3. One step that would provide much more accurate results is the creation of a full core model. This would allow one to better determine the values of rod peaking, density coefficients and criticality values. It would reduce the uncertainly on assembly peaking, rod peaking and eliminate the radially reflective boundary condition.

4. The use of voided regions in the areas once occupied by water filled thimble tubes is feasible, but more work needs to be done to determine the ratio of moderator to void in

these regions. In this analysis, the cooling of the safety/control rods needs to be taken into account. It may be possible to cool the rods with steam, because they would not be as hot as fuel pins. It may also be possible that not all six thimble tubes present in the assembly are required to provide shutdown margin.

5. Rod gaps less than 1.0 mm could be used, which would boost breeding characteristics of the design. However, the appropriate DNB correlation for wire wrapped rods would need to be applied. The use of wire wraps is itself something that needs to be examined. But, given that a CR>1.0 can be obtained with 1.0 mm rod gaps, this modification may not actually be beneficial.

6. An examination of the behavior of a tight-lattice PWR assembly and/or core in several design basis accidents, including large and small break loss of coolant accidents and a loss of flow accident, would be of particular interest. This would provide demonstration of safe behavior in design-basis accidents, even with a positive void coefficient.

Works Cited

Contained is the references used in the analysis performed in this paper.

3M Incorporated. "3M™ Enriched Boron Oxide." Product Description, Quapaw, OK, 2014.

Akie, H., H. Takano, T. Muromura, and N. Nitani. "A New Idea of Excess Plutonium Once-Through Burning in Light Water Reactor." *Progress in Nuclear Energy*, 1995: 345-352.

Akiyama, Y., K. Hori, and S. Tsuda. "DNB experiments for high-conversion PWR core design." *Nuclear Engineering and Design* 126 (1991): 167-275.

Azo Materials. *Molybdenum - Mechanical Properties And Material Application.* June 11, 2013. http://www.azom.com/article.aspx?ArticleID=7637 (accessed May 24, 2015).

—. *Zirconium - Mechanical Properties And Material Applications.* June 11, 2013. http://www.azom.com/article.aspx?ArticleID=7645 (accessed May 24, 2015).

Bathke, Charles G., et al. "The Attractiveness of Materials in Advanced Nuclear Fuel Cycles for Various Proliferation and Theft Scenarios." *Nuclear Technology*, 2012: 5-30.

Beam, T., K. Ivanov, B. Taylor, and A. Barreta. *PRESSURIZED WATER REACOTR MAIN STEAM LINE BREAK (MSLB) BENCHMARK.* NEA/NSC/DOC(2000)21, University Park, PA: US NRC, NEA, OECD, 2000.

Bjork, K. I., C. Wah Lau, H. Nylen, and U. Sandberg. "Study of Thorium-Plutonium Fuel for Possible Operating Cycle Extension in PWRs." *Science and Technology of Nuclear Installations*, 2013: Article ID 867561.

Bjork, K. I., S. Mittag, R. Nabbi, A. Rineiski, O. Schitthelm, and B. Vezzoni. "Irradiation of a thorium-plutonium rodlet: Experiment and benchmark calculations." *Progress in Nuclear Energy*, 2013: 73-79.

Bloore, D. A. *Reactor Physics Assesment of Thick Silicon Carbide Clad PWR Fuels.* PhD Thesis, Cambridge, MA: Massachusetts Institute of Technology, 2013.

Bowring, R. W. "AEEW-R 983." 1979.

Broeders, C. H. M., E. Kiefhaber, and H. W. Wiese. "Burning transuranium isotopes in thermal and fast reactors." *Nuclear Engineering and Design*, 2000: 157-172.

Cheng, X., and U. Muller. "Critical heat flux and turbulent mixing in hexagonal tight lattice rod bundles." *International Journal of Multiphase Flow* 24 (1998): 1245-1263.

Chidambaram, R., and C. Ganguly. "Plutonium and thorium in the Indian nuclear programme." *Current Science*, 1996: 21-35.

Chodak, P. *DESTRUCTION OF PLUTONIUM USING NON-URANIUM FUELS IN PRESSURIZED WATER REACTOR PERIPHERAL ASSEMBLIES.* PhD Thesis, Cambridge: MASSACHUSETTS INSTITUTE OF TECHNOLOGY, 1996.

Dalle Donne, M., and W. Hame. *Nuclear Technology* 71, no. 111 (1985).

Diamond, D., B. Bromley, and A. Aronson. *Studies of the Rod Ejection Accident in a PWR.* Technical Report W-6382 1/22/02, Upton, NY: Brookhaven National Laboratory, 2002.

Dziadosz, D., T. N. Ake, M. Saglan, and J. J. Sapyta. "WEAPONS-GRADE PLUTONIUM-THORIUM PWR ASSEMBLY DESIGN AND CORE SAFETY ANALYSIS." *Nuclear Technology*, 2004: 69-83.

eFunda, Inc. *AISI Type 316N.* n.d. http://www.efunda.com/materials/alloys/stainless_steels/show_stainless.cfm?ID=AISI_T ype_316N&prop=all&Page_Title=AISI%20Type%20316N (accessed May 24, 2015).

Eurosafe Tribune: Ensuring Long-term Nuclear Fuel Safety. November 2009. http://www.eurosafe-forum.org/eurosafe-tribune/tribune-016 (accessed December 15, 2014).

Feng, Bo, Mujid Kazimi, and Benoit Forget. *Feasibility of Breeding in Hard Spectrum Boiling Water Reactors with Oxide and Nitride Fuels, MIT-NFC-TR-124.* Cambridge MA: Center for Advanced Nuclear Energy Systems , 2011.

Fridman, E., and S. Kliem. "Pu recycling in a full Th-MOX PWR core. Part I: Steady state analysis." *Nuclear Engineering and Design*, 2011: 193-202.

Goodfellow. *Molybdenum: Material Information.* n.d. http://www.goodfellow.com/E/Molybdenum.html (accessed May 24, 2015).

Haas, D., and D. J. Hamilton. "Fuel cycle strategies and plutonium management in Europe." *Progress in Nuclear Energy*, 2007: 574-582.

Herring, J. S., P. E. MacDonald, and K. D. Weaver. "THORIUM-BASED TRANSMUTER FUELS FOR LIGHT WATER REACTORS." *Nuclear Technology*, 2004: 84-101.

HM Wire International Inc. *Alloy 815 - FeCrAl Alloy.* 2011. http://litz-wire.com (accessed May 24, 2015).

Internation Panel on Fissile Materials. *Fissile Material Stocks.* n.d. http://fissilematerials.org/ (accessed 12 15, 2014).

International Atomic Energy Agency. *Potential of thorium based fuel cycles to constrain plutonium and reduce long lived waste toxicity.* IAEA-TECDOC-1349, Vienna: International Atomic Energy Agency, 2003.

International Atomic Energy Agency. *Safe Handling and Storage of Plutonium.* SAFETY REPORTS SERIES No. 9, Vienna: INTERNATIONAL ATOMIC ENERGY AGENCY, 1998.

Ivanov,, K. N., T. Beam, A. Baratta, A. Irani, and N. Trikouros. *PRESSURISED WATER REACTOR MAIN STEAM LINE BREAK (MSLB) BENCHMARK: Volume I.* NEA/NSC/DOC(99)8, University Park, PA: US NRC, NEA, OECD, 1999.

Iwamura, T., H. Watanabe, and Y. Murao. "Critical heat flux experiments under steady-state and transient conditions and visualization of CHF phenomenon with neutron radiography." *Nuclear Engineering and Design* 149 (1994): 195-206.

Iwamura, Takamichi, Hinori Watanabe, Tsutomu Okubo, Fumimasa Araya, and Yoshio Murao. "CHF Experiments under Steady-State and Transient Conditions for Tight Lattice Core with Non-Uniform Axial Power Distribution." *Journal of Nuclear Science and Technology* 30, no. 5 (1993): 413-424.

Iwamura, Takamichi, Tsutomu Okubo, Yoshio Murao, Takayuki Suemura, and Fijio Hiragi. "Evaluation of DNBR under Operational and Accident Conditions for Double-Flat-Core Type HCLWR." *Journal of Nuclear Science and Technology* 28, no. 1 (1991): 45-58.

Janis 4.0. n.d. http://www.oecd-nea.org/janis/ (accessed May 24, 2015).

Jeong, J., W. J. Lee, and B. D. Chung. "Simulation of a main steam line break accident using a coupled ''system thermal-hydraulics, three-dimensional reactor kinetics, and hot channel analysis'' code." *Annals of Nuclear Energy*, 2006: 820-828.

Kang, J., and F. N. von Hippel. "U-232 and the Proliferation-Resistance of U-233 in Spent Fuel." *Science & Global Security*, 2001: 1-32.

Kloosterman, J. L., and P. M. G. Damen. "Reactor physics aspects of plutonium burning in inert matrix fuels." *Journal of Nuclear Materials*, 1999: 112-119.

Kozloeski, T., and T. J. Downar. *PWR MOX/UO2 Core Transient Benchmark: Final Report.* NEA/NSC/DOC(2006)20, Purdue University, USA: US NRC, OECD NEA, 2007.

Ledergerber, G., C. Degueldre, P. Heimgartner, M. A. Pouchon, and U. Kasenmeyer. "Inert matrix fuel for the utilisation of plutonium." *Progress in Nuclear Energy*, 2001: 301-308.

Lee, C. B., Y. S. Yang, Y. M. Kim, D. H. Kim, and Y. H. Jung. "IRRADIATION BEHAVIOR OF THORIA-URANIA FUEL IN A PWR." *Nuclear Technology*, 2004: 140-148.

Leppänen, Jaako. *Serpent - a Continuous-energy Monet Carlo Reactor Physics Burnup Calculation Code.* VTT Technical Research Centre of Finland, 2012.

Liu, Wei, Masatoshi Kureta, and Hajime Akimoto. "Critical Power in 7-Rod Tight Lattice Bundle." *JSME International Journal* 47, no. 2 (2004): 299-305.

Liu, Wei, Masatoshi Kureta, Hiroyuki Yoshida, Akira Ohnuki, and Hajime Akimoto. "An Improved Critical Power Correlation for Tight-Lattice Rod Bundles." *Journal of Nuclear Science and technology* 44, no. 4 (2007): 558-571.

Lombardi, C., and A. Mazzola. "EXPLOITING THE PLUTONIUM STOCKPILES IN PWRs BY USING INERT MATRIX FUEL." *Progress in Nuclear Energy*, 1996: 1117-1126.

Lombardi, C., L. Luzzi, E. Padovani, and F. Vettraino. "Inert matrix and thoria fuels for plutonium elimination." *Progress in Nuclear Energy*, 2001: 395-398.

Long, Y. *Modeling the Performance of High Burnup Thoria and Urania PWR Fuel.* PhD Thesis, Cambridge, MA: Massachusetts Institute of Technology , 2002.

Mittag, S., and S. Kliem. "Burning plutonium and minimizing radioactive waste in existing PWRs." *Annals of Nuclear Energy*, 2011: 98-102.

NRC, US. *The Pressurized Water Reactor (PWR)*. March 29, 2012. http://www.nrc.gov/reading-rm/basic-ref/students/animated-pwr.html (accessed January 13, 2015).

Okumura, Keisuke, Yasunobu Nagaya, and Takamasa Mori. *MVP-BURN: Burn-up Calculation Code Using A Continuous-energy Monte Carlo Code MVP*. Tokai, Japan\: Japan Atomic Energy Agency, 2005.

Olson, G. L., R. K. McCardell, and D. B. Illum. *Fuel Summary Report: Shippingport Light Water Breeder Reactor*. INEEL/EXT-98-00799, Idaho Falls, ID: Idaho National Engineering and Environmental Laboratory, 2002.

Paidoussis, M. P. "Fluid-Structure Interactions." *Academic Press, Inc.* 2 (1998-c2004): 868-870.

Reddy, D. G., et. al. "EPRI-NP-2609 vol. 2." 1983.

Ronen, Y. *High Converting Light Water Reactors* . Boca Raton, FL: CRC Press, 1990.

Safety and Regulatory Issues of the Thorium Fuel Cycle. NUREG/CR-7176, ORNL/TM-2013/543, Rockville, MD: US NRC, 2013.

Saglam, M., J. J. Saptya, S. W, Spetz, and L. A. Hassler. "CORE DESIGNS AND ECONOMIC ANALYSES OF HOMOGENEOUS THORIA-URANIA FUEL IN LIGHT WATER REACTORS." *Nuclear Technology*, 2003: 8-19.

Shelley, Afroza, Soichiro Shimada, Teruhiko Kugo, Tsutomu Okubo, and Takamichi Iwamura. "Optimization of seed-blanket type fuel assembly for reduced-moderation water reactor." *Nuclear Engineering and Design* 224 (2003): 265-278.

Shultis, J. K., and Richard E. Faw. *Fundamentals of Nuclear Science and Engineering*. Boca Raton, FL: CRC Press, 2008.

Shwageraus, E., and H. Feinroth. "Potential of Silicon Carbide Cladding to Extend Burnup of Pu-Th Mixed Oxide Fuel." *American Nuclear Society Annual Meeting*. American Nuclear Society, 2011.

Shwageraus, E., P. Hejzlar, and M. S. Kazimi. "USE OF THORIUM FOR TRANSMUTATION OF PLUTONIUM AND MINOR ACTINIDES IN PWRs." *Nuclear Technology*, 2003: 53-68.

Studsvik. "CASMO-4E User's Manual: Extended Capability CASMO-4." PROPRIETARY SSP-09/442-U Rev 0, 2009.

Studsvik Scandpower. "CASMO-E User's Manual: A Fuel Assembly Burnup Program." PROPRIETARY SSP-09/443-U Rev 0, 2009.

Studsvik Scandpower. "CMS-LINK: User's Manual." PROPRIETARY SSP-09/444-U Rev 0, 2009.

Studsvik. "SIMULATE-3 User's Manual: Advanced Three-Dimensional Two-Group Reactor Analysis Code." PROPRIETARY SSP-09/447 - U Rev 0, 2009.

Studsvik. "SIMULATE-3: Kinetics Input Specification." Proprietary SSP-98/12 Rev. 13, 2009.

Sunder, S., and N. H. Miller. "XPS and XRD studies of corrosion of uranium nitride by water." *Journal of Alloys and Compounds* 271-273 (1998): 568-572.

Thermalloys AB. *Chemical composition and properties of FeCrAl alloys.* 2012. http://www.thermalloys.com/index.php/en/alloys/fecralalloys.html (accessed May 24, 2015).

Todorova, N., B. Taylor, and K. Ivanov. *PRESSURISED WATER REACTOR MAIN STEAM LINE BREAK (MSLB) BENCHMARK: Volume III.* NEA/NSC/DOC(2002)12, University Park, PA: US NRC, NEA, OECD, 2002.

Todorova, N., K. Ivanov, and B. Taylor. *PRESSURISED WATER REACTOR MAIN STEAM LINE BREAK (MSLB) BENCHMARK: Volume IV.* NEA/NSC/DOC(2003)21, University Park, PA: US NRC, NEA, OECD, 2003.

Todreas, Neil, and Mujid Kazimi. *Nuclear Sustems Volume 1.* CRC Press, 2011.

Uotinen, V. O., et. al. "EPRI-NP-1833." 1981.

US NRC. *Standard Review Plan for the Review of Safety Analysis Reports for Nuclear Power Plants: LWR Edition (NUREG-0800, Formerly issued as NUREG-75/087) .* n.d. http://www.nrc.gov/reading-rm/doc-collections/nuregs/staff/sr0800/ (accessed December 15, 2014).

Westinghouse Electric Company. *Westinghouse RFA-2 Design.* 2014. http://westinghousenuclear.com/Portals/0/Flysheets/NF-FE-0005%20RFA-2_PWR.pdf (accessed December 15, 2014).

World Nuclear Association. *Nuclear Fuel Fabrication.* 2014. http://www.world-nuclear.org/info/Nuclear-Fuel-Cycle/Conversion-Enrichment-and-Fabrication/Fuel-Fabrication/ (accessed December 15, 2014).

Worrall, A., and C. Grove. *Comparison of thorium and uranium fuel cycles.* NNL (11) 11593 Issue 5, National Nuclear Laboratory Ltd., UK, 2012.

Yamamoto, Tasushi, Miyuki Akiba, Shinicki Morooka, Kenetsu Shirakawa, and Nobuaki Abe. "Thermal Hydraulic Performance of Tight Lattice Bundle." *JSME International Journal* 49, no. 2 (2006): 334-342.

Yang, R., R. Montgomery, and N. Waeckel. *REVISED REACTIVITY INITIATED ACCIDENT ACCEPTANCE CRITERIA FOR HIGH BURNUP FUEL.* EPRI, ANATECH Corp., Electricitie de France, n.d.

Yoshimoto, Yuichiro, et al. "Critical Power Experiments of Tight Fuel Rod Lattice for Light Water Reactors." *Journal of Nuclear Science and Technology* 30, no. 11 (1993): 1120-1120.

Appendix A: Sample Input Files for Codes Used

Appendix A.1: Sample CASMO4E Input Files

High enriched assembly using thoria-plutonia fuel and SiC CMC cladding with IFBA as a burnable poison

```
TTL * Th/Pu SiC, IFBA

PDE 109.926 'KWL'
PRE 155.130
TFU 950
TMO 585
BOR 600
VOI 000

PWR 17.00 1.26  21.50

PIN 1 0.3905 0.3917 0.3988 0.4750 /'1' 'BP3' 'AIR' 'CAN'
PIN 2 0.3905 0.3988 0.4750 /'1' 'AIR' 'CAN'
PIN 3 0.5690 0.6147 /'MOD' 'BOX'
PIN 4 0.5690 0.6147 /'MOD' 'BOX'
PIN 4 0.4331 0.4369 0.4839 0.5690 0.6147
    /'B4C' 'AIR' 'CRS' 'MOD' 'BOX'
    //1 'RCC' 'ROD'

* Fuel Composition Parameters 7.38
PU1  0.012 93.8 5.8 0.23 0.022 0.13
FUE 1  9.60 / 00.00 94000=6.81 90232=81.00 8000=12.18 92238=00.00

CAN 02.85 1.0E-06 / 14000=70.00 6000=30.00
MI1 1.159E-03 / 2003=1.3E-05
SPA 10.81934 1.800E-05 ,, 8.154 / 718=84.59 347=15.41
BP3 // 5010=2.66

LPI
3
1 1
1 2 2
4 1 1 4
1 2 2 1 1
1 2 1 1 1 4
4 1 1 4 1 1 1
1 1 2 1 1 2 2 2
2 2 2 1 2 2 1 2 1

DEP , -100
SIM , 'casenrifba4'
S3C
STA

END
```

Low enriched assembly using urania-plutonia fuel and Zircaloy cladding with IFBA as a burnable poison

TTL * U/Pu Zirc, IFBA

PDE 109.926 'KWL'
PRE 155.130
TFU 950
TMO 585
BOR 600
VOI 000

PWR 17.00 1.26 21.50

PIN 1 0.4096 0.4108 0.418 0.4750 /'1' 'BP3' 'AIR' 'CAN'
PIN 2 0.4096 0.418 0.4750 /'1' 'AIR' 'CAN'
PIN 3 0.5690 0.6147 /'MOD' 'BOX'
PIN 4 0.5690 0.6147 /'MOD' 'BOX'
PIN 4 0.4331 0.4369 0.4839 0.5690 0.6147
    /'B4C' 'AIR' 'CRS' 'MOD' 'BOX'
    //1 'RCC' 'ROD'

* Fuel Composition Parameters
PU1 0.012 93.8 5.8 0.23 0.022 0.13
FUE 1 10.44 / 00.00 94000=5.702

CAN 6.55/302=100.0
MI1 1.159E-03 / 2003=1.3E-05
SPA 10.81934 1.800E-05 ,, 8.154 / 718=84.59 347=15.41
BP3 // 5010=2.66

LPI
3
1 1
1 2 2
4 1 1 4
1 2 2 1 1
1 2 1 1 1 4
4 1 1 4 1 1 1
1 1 2 1 1 2 2 2
2 2 2 1 2 2 1 2 1

DEP , -100
SIM , 'casenrifba2'
S3C
STA

END

Sample thoria-plutonia fueled assembly with SiC CMC cladding with gadolinia as a burnable poison

TTL * Th/Pu Gd BP SiC Clad

PDE 109.926 'KWL'
PRE 155.130
TFU 950
TMO 585

VOI 000

PWR 17.00 1.26 21.50

PIN 1 0.3905 0.3988 0.4750 /'1' 'AIR' 'CAN'
PIN 2 0.3905 0.3988 0.4750 /'2' 'AIR' 'CAN'
PIN 3 0.5690 0.6147 /'MOD' 'BOX'
PIN 4 0.5690 0.6147 /'MOD' 'BOX'
PIN 4 0.4331 0.4369 0.4839 0.5690 0.6147
    /'B4C' 'AIR' 'CRS' 'MOD' 'BOX'
    //1 'RCC' 'ROD'
PIN 8 0.3905 0.3988 0.4750 /'8' 'AIR' 'CAN'

* Fuel Composition Parameters
PU1 0.012 93.8 5.8 0.23 0.022 0.13
FUE 1 9.36 / 00.00 94000=7.58 90232=79.80 8000=12.18 92238=00.00 64000=0.43   * .5percetn
FUE 2 9.36 / 00.00 94000=7.62 90232=80.21 8000=12.18 92238=00.00
FUE 8 9.36 / 00.00 94000=7.31 90232=77.00 8000=12.22 92238=00.00 64000=3.47 * 4 percent

CAN 02.85 1.0E-06 / 14000=70.00 6000=30.00
MI1 1.159E-03 / 2003=1.3E-05
SPA 10.81934 1.800E-05 ,, 8.154 / 718=84.59 347=15.41
BP3 // 5010=2.66

LPI
3
1 8
8 2 2
4 2 2 4
2 8 2 8 2
2 2 2 2 8 4
4 2 8 4 8 2 8
2 8 2 8 2 8 2 2
2 2 2 2 2 2 2 2 2

DEP , -100
SIM , 'casgd43'
STA

END

Enriched UO$_2$ fueled assembly with zircaloy cladding

TTL * Typical PWR, IFBA

PDE 109.926 'KWL'
PRE 155.130
TFU 950
TMO 585

VOI 000

PWR 17.00 1.26 21.50

PIN 1 0.4096 0.4103 0.418 0.4750 /'1' 'BP3' 'AIR' 'CAN'
PIN 2 0.4096 0.418 0.4750 /'1' 'AIR' 'CAN'
PIN 3 0.5690 0.6147 /'MOD' 'BOX'
PIN 4 0.5690 0.6147 /'MOD' 'BOX'
PIN 4 0.4331 0.4369 0.4839 0.5690 0.6147
    /'AIC' 'AIR' 'CRS' 'MOD' 'BOX'
    //1 'RCC' 'ROD'

* Fuel Composition Parameters
FUE 1 10.41 / 4.740

CAN 6.55/302=100.0
MI1 1.159E-03 / 2003=1.3E-05
SPA 10.81934 1.800E-05 ,, 8.154 / 718=84.59 347=15.41
BP3 // 5010=.927

LPI
3
1 1
1 2 2
4 1 1 4
1 2 2 1 1
1 2 1 1 1 4
4 1 1 4 1 1 1
1 1 2 1 1 2 2 2
2 2 2 1 2 2 1 2 1

DEP , -100
SIM , 'casenrifba4'

STA
END

Urania-plutonia fueled assembly with no burnable poison used in proliferation study

TTL * U/Pu SiC Proliferation Study, No BP

PDE 109.926 'KWL'
PRE 155.130
TFU 950
TMO 585
VOI 000

PWR 17.00 1.26 21.50

PIN 1 0.3905 0.3988 0.4750 /'1' 'AIR' 'CAN'

PIN 2 0.3905 0.3988 0.4750 /'1' 'AIR' 'CAN'

PIN 3 0.5690 0.6147 /'MOD' 'BOX'
PIN 4 0.5690 0.6147 /'MOD' 'BOX'
PIN 4 0.4331 0.4369 0.4839 0.5690 0.6147
     /'B4C' 'AIR' 'CRS' 'MOD' 'BOX'
     //1 'RCC' 'ROD'

* Fuel Composition Parameters
PU1 0.012 93.8 5.8 0.23 0.022 0.13
FUE 1 10.44 / 00.00 94000=5.69

CAN 02.85 1.0E-06 / 14000=70.00 6000=30.00
MI1 1.159E-03 / 2003=1.3E-05
SPA 10.81934 1.800E-05 ,, 8.154 / 718=84.59 347=15.41

LPI
3
1 1
1 2 2
4 1 1 4
1 2 2 1 1
1 2 1 1 1 4
4 1 1 4 1 1 1
1 1 2 1 1 2 2 2
2 2 2 1 2 2 1 2 1

DEP , -48.84
SIM , 'casenrifba2'
STA

TIT
RES,, 48.84
SDC 0.0007 0.0048 0.008 0.025 0.1 1.0 4.0 10.0/'Y'
STA

END

Appendix A.2: Sample CMSLINK Input File

```
'COM' 'CMS-Link Input File'/
'NEW' '/home/nandrews/weap/liball.lib'/
'MOX' 'ON'/

'CAS' '/home/nandrews/weap/casred1.cax'/
'STA' /
'CAS' '/home/nandrews/weap/casred2.cax'/
'STA' /
'CAS' '/home/nandrews/weap/casred3.cax'/
'STA' /
'CAS' '/home/nandrews/weap/casred4.cax'/
'STA' /
'CAS' '/home/nandrews/weap/casenrbor.cax'/
'STA' /
'CAS' '/home/nandrews/weap/casenrbor_b.cax'/
'STA' /
'CAS' '/home/nandrews/weap/casenrifba.cax'/
'STA' /
'CAS' '/home/nandrews/weap/casenrifba2.cax'/
'STA' /
'CAS' '/home/nandrews/weap/casenrifba3.cax'/
'STA' /
'CAS' '/home/nandrews/weap/casenrifba4.cax'/
'STA' /

'CAS' '/home/nandrews/weap/REFTOP.cax',,,'TOP'/
'STA' /
'CAS' '/home/nandrews/weap/REFRAD.cax',,,'RAD'/
'STA' /
'CAS' '/home/nandrews/weap/REFBOT.cax',,,'BOT'/
'STA' /

'END'/
```

Appendix A.3: Sample SIMULATE3 Input Files

Sample full core input file for first 10 cycles for Th/Pu fueled core with SiC CMC cladding and IFBA burnable poison

'COM' Th/Pu SiC Clad, IFBA

'DIM.PWR' 15/
'DIM.CAL' 24 2 2/
'DIM.DEP' 'EXP' 'SAM' 'HTMO' 'HBOR' 'HTFU' 'PIN' 'EBP'/

'TIT.CAS' 'Cycle 01'/

'LIB' '/home/nandrews/weap/liball.lib'/

'COR.SYM' 'ROT'/
'COR.DAT' 21.5 365.76 109.926 751.53/
'COR.STM' 0/

'PWR.OPT' 'ON'/
'PWR.CTP' 0 25 50 75 100/
'PWR.TIN' 557 557.4 557.8 558.2 558.6/

'REF.LIB' , 01 'REFBOT'/
        , 02 'REFRAD'/
        , 03 'REFTOP'/
'SEG.LIB' , 04 'casenrifba'/
        , 05 'casenrifba2'/
        , 06 'casred3.inp'/
        , 07 'casgd4'/
        , 08 'casred2'/
        , 09 'casred1'/
        , 10 'casred4.inp'/
        , 11 'casgd5'/
        , 12 'casgd6'/
        , 13 'casgd7'/
        , 14 'casgd42'/
        , 15 'casgd43'/
        , 16 'casgd44'/
        , 17 'casenrifba3'/
        , 18 'casenrifba4'/

'SEG.TFU' 0 0 345.47 -14.34/

'TAB.TFU' 1, 0, 'EXP', 8, 'POW', 1
      000.0 005.0 007.2 021.5 045.0 054.0 064.0 069.0
001.0   005.0 118.0 123.0 136.0 135.0 129.0 140.0 145.0 /

'FUE.ZON' , 01 1 'b4cREFRAD' 01 0.0 02 365.76 03/
        , 02 1 'refcasb4c' 01 0.00 06 15.24 08 30.48 05 335.28 08 350.52 06 365.76 03/
        , 03 1 'refcasb4c' 01 0.00 06 15.24 05 30.48 04 335.28 05 350.52 06 365.76 03/
        , 04 1 'refcasb4c' 01 0.00 06 15.24 05 30.48 04 335.28 05 350.52 06 365.76 03/
        , 05 1 'refcasb4c' 01 0.00 06 15.24 05 30.48 04 335.28 05 350.52 06 365.76 03/

209

```
            , 06 1 'refcasb4c' 01 0.00 06 15.24 08 30.48 18 335.28 08 350.52 06 365.76 03/
'FUE.GRD' 'ON'   2.82 3.36 'INC'
            64.87 3.36 'INC'
           117.07 3.36 'INC'
           169.27 3.36 'INC'
           221.46 3.36 'INC'
           273.66 3.36 'INC'
           325.86 3.36 'INC'/
'FUE.TYP' 1
       2 2 2 2 2 2 2 2 1
       2 2 2 2 2 2 2 2 1
       2 2 2 2 2 2 2 2 1
       2 2 2 2 2 2 2 2 1
       2 2 2 2 2 2 2 1 1
       2 2 2 2 2 2 2 1 0
       2 2 2 2 2 2 1 1 0
       2 2 2 2 1 1 1 0 0
       1 1 1 1 1 0 0 0 0/

'FUE.NEW' 'TYPE01' 'A01' 16 02,,,1,,20 24
       1 24*48 7 24*0.704 9 24*600/
'FUE.NEW' 'TYPE01' 'A17' 16 03,,,1,,20 24
       1 24*48 7 24*0.704 9 24*600/
'FUE.NEW' 'TYPE01' 'A33' 20 04,,,1,,20 24
       1 24*48 7 24*0.704 9 24*600/
'FUE.NEW' 'TYPE01' 'A53' 16 05,,,1,,20 24
       1 24*48 7 24*0.704 9 24*600/
'FUE.NEW' 'TYPE01' 'A69' 16 06,,,1,,20 24
       1 24*48 7 24*0.704 9 24*600/

'FUE.NEW' 'TYPE01' 'B01' 16 02,,,1,,20 24
       1 24*24 7 24*0.704 9 24*600/
'FUE.NEW' 'TYPE01' 'B17' 16 03,,,1,,20 24
       1 24*24 7 24*0.704 9 24*600/
'FUE.NEW' 'TYPE01' 'B33' 20 04,,,1,,20 24
       1 24*24 7 24*0.704 9 24*600/
'FUE.NEW' 'TYPE01' 'B53' 16 05,,,1,,20 24
       1 24*24 7 24*0.704 9 24*600/
'FUE.NEW' 'TYPE01' 'B69' 16 06,,,1,,20 24
       1 24*24 7 24*0.704 9 24*600/

'FUE.NEW' 'TYPE01', 'C01', 16, 02,,,1/
'FUE.NEW' 'TYPE01' 'C17' 16, 03,,,1/
'FUE.NEW' 'TYPE01' 'C33' 20, 04,,,1/
'FUE.NEW' 'TYPE01' 'C53' 16, 05,,,1/
'FUE.NEW' 'TYPE01' 'C69' 16, 06,,,1/

'FUE.SER' 4/
01 1            B30  B31  B15  B82  B40  B60  B08
02 1        B29  B14  C51  C30  C81  C52  C07  C21  C08  B42  B38
03 1      B48  C65  C32  C66  C49  C13  B51  C06  C75  C76  C23  C57  B21
04 1      B52  C31  C67  B65  B49  A31  B32  B05  B58  B73  C59  C24  B06
05 1  B16  C16  C84  B81  A16  C50  A30  A29  B59  B76  A08  B57  C58  C41  B22
06 1  B68  C29  C83  B66  B84  A15  C68  B83  C38  A07  C40  B39  C39  C22  B23
```

```
07 1  B50 C15 C14 B13 B67 C48 A14 C82 A06 C60 A22 A23 C05 C73 B07
08 1  B78 C47 B46 B28 A25 B79 C78 A01 C74 B75 A21 B24 B41 C42 B74
09 1  B11 C77 C09 A27 A26 C64 A10 C70 A02 C33 B55 B01 C02 C03 B35
10 1  B27 C26 C44 B44 C45 A11 C43 B71 C56 A03 B72 B54 C71 C17 B56
11 1  B26 C46 C62 B61 A12 B80 B63 A17 A18 C35 A04 B69 C72 C04 B04
12 1    B10 C28 C63 B77 B62 B09 B20 A19 B34 B53 C55 C19 B37
13 1    B25 C61 C27 C80 C79 C10 B36 C01 C34 C54 C20 C53 B33
14 1      B43 B47 C12 C25 C11 C37 C69 C18 C36 B02 B17
15 1        B12 B64 B45 B70 B03 B19 B18
0 0

'RES' 'NEWFUEL'/

'HYD.ITE' /

'BAT.LAB' 1,'CYC-1'/
'FUE.INI','JILAB'/
'BAT.EDT' 'ON' 'ARPF' 'AEXP' 'AKIN' '3PIN' '3XPO' /

'ITE.BOR' 2500/
'ITE.SRC' 'SET' 'EOLEXP',,0.001,,,'KEF' 1.000 0.00001 'MINBOR'/

'DEP.CYC' 'CYCLE01' 0.0 01/
'DEP.STA' 'AVE' 0.0 0.15 0.25 0.5 -0.5 28/
'PRI.STA' '2EXP' '2RPF'/
'SUM' '/home/nandrews/weap/refsimb4c_01.sum'/
'WRE' '/home/nandrews/weap/refsimb4c_01.res' 20000/

'STA'/
'END'/

'DIM.PWR' 15 15 15 0/
'DIM.CAL' 24 2 2/
'DIM.DEP' 'EXP' 'SAM' 'HTMO' 'HBOR' 'HTFU' 'PIN' 'EBP'/
'COR.SYM' 'ROT'/

'TIT.CAS' 'Cycle 02'/

'INC.FIL' 'loadifba.txt'/
'FUE.NEW','TYPE01','U200', 37, 02 ,,, 2 /
'FUE.NEW','TYPE02','H200', 48, 06 ,,, 2 /


'RES' '/home/nandrews/weap/refsimb4c_01.res' 20000/
'BAT.LAB' 2 'CYC-2' /

'ITE.BOR' 2500/
'ITE.SRC' 'SET' 'EOLEXP',,0.001,,,'KEF' 1.000 0.00001 'MINBOR'/

'DEP.CYC' 'CYCLE02' 0.0 02/
'DEP.STA' 'AVE' 0.0 0.15 0.25 0.5 -0.5 28/
'FUE.INI' 'JILAB'/
'PRI.STA' '2EXP' '2RPF'/
'SUM' '/home/nandrews/weap/refsimb4c_02.sum'/
```

'WRE' '/home/nandrews/weap/refsimb4c_02.res' 20000/

'STA'/
'END'/

'DIM.PWR' 15/
'DIM.CAL' 24 2 2/
'DIM.DEP' 'EXP' 'SAM' 'HTMO' 'HBOR' 'HTFU' 'PIN' 'EBP'/
'COR.SYM' 'ROT'/
'TIT.CAS' 'Cycle 03'/

'INC.FIL' 'loadifba.txt'/

'FUE.NEW','TYPE01','U300', 37, 02 ,,, 3 /
'FUE.NEW','TYPE02','H300', 48, 06 ,,, 3 /

'RES' '/home/nandrews/weap/refsimb4c_02.res' 20000/
'BAT.LAB' 3 'CYC-3' /

'ITE.BOR' 2500/
'ITE.SRC' 'SET' 'EOLEXP',,0.001,,,'KEF' 1.000 0.00001 'MINBOR'/

'DEP.CYC' 'CYCLE03' 0.0 03/
'DEP.STA' 'AVE' 0.0 0.15 0.25 0.5 -0.5 28/
'FUE.INI' 'JILAB'/
'PRI.STA' '2EXP' '2RPF'/
'SUM' '/home/nandrews/weap/refsimb4c_03.sum'/
'WRE' '/home/nandrews/weap/refsimb4c_03.res' 20000/

'STA'/
'END'/

'DIM.PWR' 15/
'DIM.CAL' 24 2 2/
'DIM.DEP' 'EXP' 'SAM' 'HTMO' 'HBOR' 'HTFU' 'PIN' 'EBP'/

'TIT.CAS' 'Cycle 04'/
'COR.SYM' 'ROT'/

'INC.FIL' 'loadifba.txt'/

'FUE.NEW','TYPE01','U400', 37, 02 ,,, 4 /
'FUE.NEW','TYPE02','H400', 48, 06 ,,, 4 /

'RES' '/home/nandrews/weap/refsimb4c_03.res' 20000/
'BAT.LAB' 4 'CYC-4' /

'ITE.BOR' 2500/
'ITE.SRC' 'SET' 'EOLEXP',,0.001,,,'KEF' 1.000 0.00001 'MINBOR'/

'DEP.CYC' 'CYCLE04' 0.0 04/
'DEP.STA' 'AVE' 0.0 0.15 0.25 0.5 -0.5 28/
'FUE.INI' 'JILAB'/

'PRI.STA' '2EXP' '2RPF'/
'SUM' '/home/nandrews/weap/refsimb4c_04.sum'/
'WRE' '/home/nandrews/weap/refsimb4c_04.res' 20000/

'STA'/
'END'/

'DIM.PWR' 15/
'DIM.CAL' 24 2 2/
'DIM.DEP' 'EXP' 'SAM' 'HTMO' 'HBOR' 'HTFU' 'PIN' 'EBP'/
'COR.SYM' 'ROT'/
'TIT.CAS' 'Cycle 05'/

'INC.FIL' 'loadifba.txt'/

'FUE.NEW','TYPE01','U500', 37, 02 ,,, 5 /
'FUE.NEW','TYPE02','H500', 48, 06 ,,, 5 /

'RES' '/home/nandrews/weap/refsimb4c_04.res' 20000/
'BAT.LAB' 5 'CYC-5' /

'ITE.BOR' 2500/
'ITE.SRC' 'SET' 'EOLEXP',,0.001,,,'KEF' 1.000 0.00001 'MINBOR'/

'DEP.CYC' 'CYCLE05' 0.0 05/
'DEP.STA' 'AVE' 0.0 0.15 0.25 0.5 -0.5 28/
'FUE.INI' 'JILAB'/
'PRI.STA' '2EXP' '2RPF'/
'SUM' '/home/nandrews/weap/refsimb4c_05.sum'/
'WRE' '/home/nandrews/weap/refsimb4c_05.res' 20000/

'STA'/
'END'/

'DIM.PWR' 15/
'DIM.CAL' 24 2 2/
'DIM.DEP' 'EXP' 'SAM' 'HTMO' 'HBOR' 'HTFU' 'PIN' 'EBP'/
'COR.SYM' 'ROT'/
'TIT.CAS' 'Cycle 06'/

'INC.FIL' 'loadifba.txt'/

'FUE.NEW','TYPE01','U600', 37, 02 ,,, 6 /
'FUE.NEW','TYPE02','H600', 48, 06 ,,, 6 /

'RES' '/home/nandrews/weap/refsimb4c_05.res' 20000/
'BAT.LAB' 6 'CYC-6' /

'ITE.BOR' 2500/
'ITE.SRC' 'SET' 'EOLEXP',,0.001,,,'KEF' 1.000 0.00001 'MINBOR'/

'DEP.CYC' 'CYCLE06' 0.0 06/
'DEP.STA' 'AVE' 0.0 0.15 0.25 0.5 -0.5 28/
'FUE.INI' 'JILAB'/

'PRI.STA' '2EXP' '2RPF'/
'SUM' '/home/nandrews/weap/refsimb4c_06.sum'/
'WRE' '/home/nandrews/weap/refsimb4c_06.res' 20000/

'STA'/
'END'/

'DIM.PWR' 15/
'DIM.CAL' 24 2 2/
'DIM.DEP' 'EXP' 'SAM' 'HTMO' 'HBOR' 'HTFU' 'PIN' 'EBP'/
'COR.SYM' 'ROT'/
'TIT.CAS' 'Cycle 07'/

'INC.FIL' 'loadifba.txt'/

'FUE.NEW','TYPE01','U700', 37, 02 ,,, 7 /
'FUE.NEW','TYPE02','H700', 48, 06 ,,, 7 /

'RES' '/home/nandrews/weap/refsimb4c_06.res' 20000/
'BAT.LAB' 7 'CYC-7' /

'ITE.BOR' 2500/
'ITE.SRC' 'SET' 'EOLEXP',,0.001,,,'KEF' 1.000 0.00001 'MINBOR'/

'DEP.CYC' 'CYCLE07' 0.0 07/
'DEP.STA' 'AVE' 0.0 0.15 0.25 0.5 -0.5 28/
'FUE.INI' 'JILAB'/
'PRI.STA' '2EXP' '2RPF'/
'SUM' '/home/nandrews/weap/refsimb4c_07.sum'/
'WRE' '/home/nandrews/weap/refsimb4c_07.res' 20000/

'STA'/
'END'/

'DIM.PWR' 15/
'DIM.CAL' 24 2 2/
'DIM.DEP' 'EXP' 'SAM' 'HTMO' 'HBOR' 'HTFU' 'PIN' 'EBP'/
'COR.SYM' 'ROT'/
'TIT.CAS' 'Cycle 08'/

'INC.FIL' 'loadifba.txt'/

'FUE.NEW','TYPE01','U800', 37, 02 ,,, 8 /
'FUE.NEW','TYPE02','H800', 48, 06 ,,, 8 /

'RES' '/home/nandrews/weap/refsimb4c_07.res' 20000/
'BAT.LAB' 8 'CYC-8' /

'ITE.BOR' 2500/
'ITE.SRC' 'SET' 'EOLEXP',,0.001,,,'KEF' 1.000 0.00001 'MINBOR'/

'DEP.CYC' 'CYCLE08' 0.0 08/
'DEP.STA' 'AVE' 0.0 0.15 0.25 0.5 -0.5 28/
'FUE.INI' 'JILAB'/

'PRI.STA' '2EXP' '2RPF'/
'SUM' '/home/nandrews/weap/refsimb4c_08.sum'/
'WRE' '/home/nandrews/weap/refsimb4c_08.res' 20000/

'STA'/
'END'/

'DIM.PWR' 15/
'DIM.CAL' 24 2 2/
'DIM.DEP' 'EXP' 'SAM' 'HTMO' 'HBOR' 'HTFU' 'PIN' 'EBP'/
'COR.SYM' 'ROT'/
'TIT.CAS' 'Cycle 09'/
'INC.FIL' 'loadifba.txt'/
'FUE.NEW','TYPE01','U900', 37, 02 ,,, 9 /
'FUE.NEW','TYPE02','H900', 48, 06 ,,, 9 /
'RES' '/home/nandrews/weap/refsimb4c_08.res' 20000/
'BAT.LAB' 9 'CYC-9' /
'ITE.BOR' 2500/
'ITE.SRC' 'SET' 'EOLEXP',,0.001,,,'KEF' 1.000 0.00001 'MINBOR'/
'DEP.CYC' 'CYCLE09' 0.0 09/
'DEP.STA' 'AVE' 0.0 0.15 0.25 0.5 -0.5 28/
'FUE.INI' 'JILAB'/
'PRI.STA' '2EXP' '2RPF'/
'SUM' '/home/nandrews/weap/refsimb4c_09.sum'/
'WRE' '/home/nandrews/weap/refsimb4c_09.res' 20000/
'STA'/
'END'/

'DIM.PWR' 15/
'DIM.CAL' 24 2 2/
'DIM.DEP' 'EXP' 'SAM' 'HTMO' 'HBOR' 'HTFU' 'PIN' 'EBP'/
'COR.SYM' 'ROT'/
'TIT.CAS' 'Cycle 10'/
'INC.FIL' 'loadifba.txt'/
'FUE.NEW','TYPE01','U1000', 37, 02 ,,, 10 /
'FUE.NEW','TYPE02','H1000', 48, 06 ,,, 10 /
'RES' '/home/nandrews/weap/refsimb4c_09.res' 20000/
'BAT.LAB' 10 'CYC-10' /
'ITE.BOR' 2500/
'ITE.SRC' 'SET' 'EOLEXP',,0.001,,,'KEF' 1.000 0.00001 'MINBOR'/
'DEP.CYC' 'CYCLE10' 0.0 10/
'DEP.STA' 'AVE' 0.0 0.15 0.25 0.5 -0.5 28/
'FUE.INI' 'JILAB'/
'PRI.STA' '2EXP' '2RPF'/
'SUM' '/home/nandrews/weap/refsimb4c_10.sum'/
'WRE' '/home/nandrews/weap/refsimb4c_10.res' 20000/
'STA'/
'END'/

Sample full core input file for equilibrium cycle for Th/Pu fueled core with SiC CMC cladding and IFBA burnable poison

```
'COM' Th/Pu SiC Clad, IFBA

'DIM.PWR' 15/
'DIM.CAL' 24 2 2/
'DIM.DEP' 'EXP' 'SAM' 'HTMO' 'HBOR' 'HTFU' 'PIN' 'EBP'/
'COR.SYM' 'ROT'/
'TIT.CAS' 'Equilibrium Cycle'/

'INC.FIL' 'loadifba.txt'/
'FUE.NEW','TYPE01','U1100', 37, 02 ,,, 11 /
'FUE.NEW','TYPE02','H1100', 48, 06 ,,, 11 /

'RES' '/home/nandrews/weap/refsimb4c_10.res' 20000 /
'FUE.INI' 'JILAB'/

'CRD.GRP' 1
4*0         00 00 00 00 00 00 00        4*0
2*0     00 9 00 3 00 2 00 3 00 9 00    2*0
 0   00 00 00 6 00 8 00 8 00 7 00 00 00   0
 0    9 00 1 00 00 00 5 00 00 00 1 00 9   0
   00 00 7 00 00 00 00 00 00 00 00 00 6 00 00
   00 3 00 00 00 2 00 4 00 2 00 00 00 3 00
   00 00 8 00 00 00 00 00 00 00 00 00 8 00 00
   00 2 00 5 00 4 00 1 00 4 00 5 00 2 00
   00 00 8 00 00 00 00 00 00 00 00 00 8 00 00
   00 3 00 00 00 2 00 4 00 10 00 00 00 3 00
   00 00 6 00 00 00 00 00 00 00 00 00 7 00 00
 0    9 00 1 00 00 00 5 00 00 00 1 00 9   0
 0   00 00 00 7 00 8 00 8 00 6 00 00 00   0
2*0     00 9 00 3 00 2 00 3 00 9 00     2*0
4*0         00 00 00 00 00 00 00        4*0/
'CRD.ZON' 1 1 'ARO' 0 0.0 0 365.76/
'CRD.ZON' 2 1 'AIC' 0 0.0 0 7.57 10 365.76/
'CRD.DAT' 226 1.585/
'CRD.TYP' 1
4*0         1 1 1 1 1 1 1        4*0
2*0     1 02 1 02 1 02 1 02 1 02 1    2*0
 0   1 1 1 02 1 02 1 02 1 02 1 1 1   0
 0   02 1 02 1 1 1 02 1 1 1 02 1 02   0
   1 1 02 1 02 1 1 1 1 1 02 1 02 1 1
   1 02 1 1 1 02 1 02 1 02 1 1 1 02 1
   1 1 02 1 1 1 1 1 1 1 1 1 02 1 1
   1 02 1 02 1 02 1 02 1 02 1 02 1 02 1
   1 1 02 1 1 1 1 1 1 1 1 1 02 1 1
   1 02 1 1 1 02 1 02 1 02 1 1 1 02 1
   1 1 02 1 02 1 1 1 1 1 02 1 02 1 1
 0   02 1 02 1 1 1 02 1 1 1 02 1 02   0
 0   1 1 1 02 1 02 1 02 1 02 1 1 1   0
2*0     1 02 1 02 1 02 1 02 1 02 1    2*0
```

```
4*0        1 1 1 1 1 1 1      4*0/
'CRD.SEQ'  1  000 000 000 000 115 226 226 226 226 226/
'CRD.SEQ'  2  000 000 000 115 226 226 226 226 226 226/
'CRD.SEQ'  3  000 000 115 226 226 226 226 226 226 226/
'CRD.SEQ'  4  000 115 226 226 226 226 226 226 226 226/
'CRD.SEQ'  5  226 226 226 226 226 226 226 226 226 226/
'CRD.SEQ'  6  226 226 226 226 226 226 226 226 226 226/
'CRD.SEQ'  7  226 226 226 226 226 226 226 226 226 226/
'CRD.SEQ'  8  226 226 226 226 226 226 226 226 226 226/
'CRD.SEQ'  9  226 226 226 226 226 226 226 226 226 226/
'CRD.SEQ' 10  226 226 226 226 226 226 226 226 226 226/
'CRD.PAS' 10 6/

'PIN.EDT' 'ON' 'SUMM' '2PIN' '2EXP' 'AEXE'/

'ITE.BOR' 2500/
'ITE.SRC' 'SET' 'EOLEXP',,0.001,,,'KEF' 1.000 0.00001 'MINBOR'/

'DEP.CYC' 'CYCLE11' 0.0 11/
'DEP.STA' 'AVE' 0.0 0.15 0.25 0.5 -0.5 28/
'WRE' '/home/nandrews/weap/refsimeqeqb4c.res' 0 0.15 0.25  0.5 1 1.5 2 2.5 3 3.5 4 4.5 5 5.5 6 6.5 7 7.5 8 8.5 9 9.5
10 10.5 11 11.5 12 12.5 13 13.5 14 14.5 15 15.5 16 16.5 17 17.5 18 18.5 19 19.5 20 20.5 21 21.5 22 22.5 23 23.5 24
24.5 25 25.5 26 26.5 27 27.5 28/
'BAT.EDT' 'ON' 'QPIN' 'QXPO' /
'PRI.ISO' 'ON' /
'KIN.EDT' 'ON' '1-D'/
'STA'/


'END'/
```

Sample loading pattern input file

```
'FUE.LAB',6/
 1  1                                 K-01   H-06   H-01   J-02   B-04   E-03   F-01
 2  1                      H-07   P-07   TYPE01 TYPE01 TYPE01 TYPE01 TYPE01 TYPE01 TYPE01 G-03     D-02
 3  1             P-04   TYPE01 TYPE01 TYPE01 L-02   TYPE01 L-05   TYPE01 D-03     TYPE01 TYPE01 TYPE01 G-08
 4  1             N-07   TYPE01 K-02   P-06   TYPE01 M-06   TYPE01 C-07   TYPE01 C-04     B-06     TYPE01 G-02
 5  1 R-06   TYPE01 TYPE01 M-03   TYPE01 K-04   TYPE01 L-03   TYPE01 G-05     TYPE01 F-02     TYPE01 TYPE01 A-06
 6  1 N-05   TYPE01 N-04   TYPE01 L-07   H-02   J-05   TYPE01 D-08   B-08     D-06     TYPE01 B-05     TYPE01 F-08
 7  1 M-02   TYPE01 TYPE01 J-03   TYPE01 H-04   P-05   N-03   E-02     E-07     TYPE01 F-04     TYPE01 TYPE01 A-08
 8  1 P-09   TYPE01 L-11   TYPE01 N-11   TYPE01 N-13   TYPE01 C-03     TYPE01 C-05     TYPE01 E-05     TYPE01 B-07
 9  1 R-08   TYPE01 TYPE01 K-12   TYPE01 L-09   L-14   C-13   B-11     H-12     TYPE01 G-13     TYPE01 TYPE01 D-14
10  1 K-08   TYPE01 P-11   TYPE01 M-10   P-08   M-08   TYPE01 G-11     H-14     E-09     TYPE01 C-12     TYPE01 C-11
11  1 R-10   TYPE01 TYPE01 K-14   TYPE01 J-11   TYPE01 E-13   TYPE01 F-12     TYPE01 D-13     TYPE01 TYPE01 A-10
12  1             J-14   TYPE01 P-10   N-12   TYPE01 N-09   TYPE01 D-10     TYPE01 B-10     F-14     TYPE01 C-09
13  1             J-08   TYPE01 TYPE01 TYPE01 M-13   TYPE01 E-11   TYPE01 E-14     TYPE01 TYPE01 TYPE01 B-12
14  1                      M-14   J-13   TYPE01 TYPE01 TYPE01 TYPE01 TYPE01 TYPE01 TYPE01 B-09     H-09
15  1                                 K-15   L-13   P-12   G-14   H-15   H-10   F-15
 0  0
```

Appendix A.4: Sample S3K Input Files

Rod ejection accident for a typical PWR at BOC

```
'DIM.PWR' 15/
'DIM.CAL' 24 4 2/


'TIT.CAS' 'Rod Ej'/
'RES' '/home/nandrews/PWR2/refsimeqeqb4c.res' 10000 /
'COM' '/home/nandrews/PWR2/refsimb4c_3k.res' 10000 /
'COR.OPE' 0./
'LIB' '/home/nandrews/PWR2/liball.lib'/

'CRD.GRP' 1
4*0          00 00 00 00 00 00 00          4*0
2*0      00  9 00  3 00  2 00  3 00  9 00     2*0
 0    00 00 00  7 00  8 00  8 00  7 00 00 00     0
 0     9 00  1 00 00 00  5 00 00 00  1 00  9    0
   00 00  7 00 00 00 00 00 00 00 00 00  7 00 00
   00  3 00 00 00  2 00  4 00  2 00 00 00  3 00
   00 00  8 00 00 00 00 00 00 00 00 00  8 00 00
   00  2 00  5 00  4 00  1 00  4 00  5 00  2 00
   00 00  8 00 00 00 00 00 00 00 00 00  8 00 00
   00  3 00 00 00  2 00  4 00 10 00 00 00  3 00
   00 00  7 00 00 00 00 00 00 00 00 00  7 00 00
 0     9 00  1 00 00 00  5 00 00 00  1 00  9    0
 0    00 00 00  7 00  8 00  8 00  7 00 00 00     0
2*0      00  9 00  3 00  2 00  3 00  9 00     2*0
4*0          00 00 00 00 00 00 00          4*0/
'CRD.ZON' 1 1 'ARO' 0 0.0 0 365.76/
'CRD.ZON' 2 1 'AIC' 0 0.0 0 7.57 10 365.76/
'CRD.DAT' 226 1.585/
'CRD.TYP' 1
4*0          1  1  1  1  1  1  1          4*0
2*0      1 02  1 02  1 02  1 02  1 02  1     2*0
 0    1  1  1 02  1 02  1 02  1 02  1  1  1    0
 0    02  1 02  1  1  1 02  1  1  1 02  1 02    0
   1  1 02  1  1  1  1  1  1  1  1  1 02  1  1
   1 02  1  1  1 02  1 02  1 02  1  1  1 02  1
   1  1 02  1  1  1  1  1  1  1  1  1 02  1  1
   1 02  1 02  1 02  1 02  1 02  1 02  1 02  1
   1  1 02  1  1  1  1  1  1  1  1  1 02  1  1
   1 02  1  1  1 02  1 02  1 02  1  1  1 02  1
   1  1 02  1  1  1  1  1  1  1  1  1 02  1  1
 0    02  1 02  1  1  1 02  1  1  1 02  1 02    0
 0    1  1  1 02  1 02  1 02  1 02  1  1  1    0
2*0      1 02  1 02  1 02  1 02  1 02  1     2*0
4*0          1  1  1  1  1  1  1          4*0/
'CRD.BNK' 4*0 5*0 0/
'ITE.KEF' 0.92/
'HYD.CND' 1 0.4096 0.418 0.4750 /
'HYD.CND' 2 0.4096 0.418 0.4750 /
```

'HYD.EPN' 0 'FTC' 'FTC' /

'HYD.EPT' 'FTC' 8 7

	0	10	20	30	40.000000	50	6.00E+01	7.00E+01
500	1.07E-01	8.35E-02	6.98E-02	6.08E-02	5.45E-02	4.98E-02	4.61E-02	4.32E-02
700	8.28E-02	6.83E-02	5.90E-02	5.26E-02	4.79E-02	4.43E-02	4.14E-02	3.90E-02
800	7.44E-02	6.29E-02	5.53E-02	4.98E-02	4.57E-02	4.25E-02	3.99E-02	3.78E-02
900	6.75E-02	5.87E-02	5.24E-02	4.78E-02	4.42E-02	4.14E-02	3.90E-02	3.70E-02
1000	6.18E-02	5.50E-02	5.00E-02	4.61E-02	4.30E-02	4.05E-02	3.84E-02	3.65E-02
1200	5.29E-02	4.89E-02	4.56E-02	4.28E-02	4.05E-02	3.85E-02	3.68E-02	3.53E-02
1500	4.40E-02	4.17E-02	3.97E-02	3.79E-02	3.64E-02	3.49E-02	3.37E-02	3.25E-02 /

'KIN.POS'   10 3 0 0
             1 0
             1.1 226 /

'CMS.EDT' 'SCA' /
'KIN.CHF', 'W-3' /
'KIN.TIM' 0.1 1.0 0.005 2.5 0.1/

'KIN.PRI', 1 0 'ELAPT', 'APOW' , 'RHO$','TFUAVE','TMOAVE','CPGMX','RHOPRT' /
'STA'/

'END'/

Main steam line break accident for a Typical PWR at BOC

'DIM.PWR' 15/
'DIM.CAL' 24 2 2/

'TIT.CAS' 'Rod Ej'/
'RES' '/home/nandrews/PWR2/refsimeqeqb4c.res' 10000 /
'COM' '/home/nandrews/PWR2/refsimb4c_3k.res' 10000 /
'COR.OPE' 100./
'LIB' '/home/nandrews/PWR2/liball.lib'/

'CRD.GRP' 1
4*0   00 00 00 00 00 00 00   4*0
2*0   00 9 00 3 00 2 00 3 00 9 00   2*0
 0   00 00 00 7 00 8 00 8 00 7 00 00 00   0
 0   9 00 1 00 00 00 5 00 00 00 1 00 9   0
   00 00 7 00 00 00 00 00 00 00 00 00 7 00 00
   00 3 00 00 00 2 00 4 00 2 00 00 00 3 00
   00 00 8 00 00 00 00 00 00 00 00 00 8 00 00
   00 2 00 5 00 4 00 1 00 4 00 5 00 2 00
   00 00 8 00 00 00 00 00 00 00 00 00 8 00 00
   00 3 00 00 00 2 00 4 00 2 00 00 00 3 00
   00 00 7 00 00 00 00 00 00 00 00 00 7 00 00
 0   9 00 1 00 00 00 5 00 00 00 1 00 9   0
 0   00 00 00 7 00 8 00 8 00 7 00 00 00   0

```
2*0    00 9 00 3 00 2 00 3 00 9 00    2*0
4*0       00 00 00 00 00 00 00      4*0/
'
CRD.ZON' 1 1 'ARO' 0 0.0 0 365.76/
'CRD.ZON' 2 1 'AIC' 0 0.0 0 7.57 10 365.76/
'CRD.DAT' 226 1.585/
'CRD.TYP' 1
4*0       1 1 1 1 1 1 1       4*0
2*0    1 02 1 02 1 02 1 02 1 02 1    2*0
 0   1 1 1 02 1 02 1 02 1 02 1 1 1    0
 0   02 1 02 1 1 1 02 1 1 1 02 1 02    0
   1 1 02 1 1 1 1 1 1 1 1 1 02 1 1
   1 02 1 1 1 02 1 02 1 02 1 1 1 02 1
   1 1 02 1 1 1 1 1 1 1 1 1 02 1 1
   1 02 1 02 1 02 1 02 1 02 1 02 1 02 1
   1 1 02 1 1 1 1 1 1 1 1 1 02 1 1
   1 02 1 1 1 02 1 02 1 02 1 1 1 02 1
   1 1 02 1 1 1 1 1 1 1 1 1 02 1 1
 0   02 1 02 1 1 1 02 1 1 1 02 1 02    0
 0   1 1 1 02 1 02 1 02 1 02 1 1 1    0
2*0    1 02 1 02 1 02 1 02 1 02 1    2*0
4*0       1 1 1 1 1 1 1      4*0/
'CRD.BNK' 10*226/
'HYD.CND' 0 0.4096 0.418 0.4750 /


'HYD.EPN' 0 'FTC' 'FTC' /


'HYD.EPT' 'FTC' 8 7
          0       10      20      30      40.000000       50      6.00E+01 7.00E+01
500     1.07E-01 8.35E-02 6.98E-02 6.08E-02 5.45E-02 4.98E-02 4.61E-02 4.32E-02
700     8.28E-02 6.83E-02 5.90E-02 5.26E-02 4.79E-02 4.43E-02 4.14E-02 3.90E-02
800     7.44E-02 6.29E-02 5.53E-02 4.98E-02 4.57E-02 4.25E-02 3.99E-02 3.78E-02
900     6.75E-02 5.87E-02 5.24E-02 4.78E-02 4.42E-02 4.14E-02 3.90E-02 3.70E-02
1000    6.18E-02 5.50E-02 5.00E-02 4.61E-02 4.30E-02 4.05E-02 3.84E-02 3.65E-02
1200    5.29E-02 4.89E-02 4.56E-02 4.28E-02 4.05E-02 3.85E-02 3.68E-02 3.53E-02
1500    4.40E-02 4.17E-02 3.97E-02 3.79E-02 3.64E-02 3.49E-02 3.37E-02 3.25E-02 /


'CMS.EDT' 'SCA' /


'KIN.CHF', 'W-3' /

'KIN.OPR' 8  0   0
        8  -219
        10 -364
        15 -655
        20 -872
        30 -1090
        40 -1235
        100 -1496 /

'KIN.TIN' 10 0   558.6
        2   554.6
        10  529.6
```

```
    15  522.6
    20  500.6
    30  486.6
    40  473.6
    50  461.6
    65  437.6
   100 482.6 /
```

'KIN.TRP' 'COR', 114.0 , , 0.5 /

'KIN.SCM' 'TRP' 95.,0.1,98.,10. /

'KIN.TIM' 0.1 20.0 /

'KIN.PRI', 1 0 'ELAPT', 'MDNBR' 'APOW' 'CPWR', 'RHO$','TFUAVE','TMOAVE','RHOPRT'/
'STA'/

'END'/

Appendix A.5: Serpent Input Files

Typical PWR assembly

set title "FeCrAl PWR Assembly"

--- Geometry Definitions

Pin Definitions:
```
pin 1     # Z1 Blanket
fuel      0.4266
void       0.4350
clad       0.475
water

pin 2    # Zone 1
fuel      0.4266
void       0.4350
clad       0.475
water

pin 3    # Z1 Seed
water              0.5747
clad               0.6147
water

pin 4    # Z1 Seed
water              0.5747
clad               0.6147
water
```

lat 110 1 0.0 0.0 17 17 1.26

1	2	1	2	2	1	2	2	2	2	2	1	2	2	1	2	1
2	2	2	2	1	1	2	1	1	1	2	1	1	2	2	2	2
1	2	1	1	1	4	1	1	4	1	1	4	1	1	1	2	1
2	2	1	4	1	1	1	2	1	2	1	1	1	4	1	2	2
2	1	1	1	1	1	2	2	1	2	2	1	1	1	1	1	2
1	1	4	1	1	4	1	1	4	1	1	4	1	1	4	1	1
2	2	1	1	2	1	2	2	1	2	2	1	2	1	1	2	2
2	1	1	2	2	1	2	1	1	1	2	1	2	2	1	1	2
2	1	4	1	1	4	1	1	3	1	1	4	1	1	4	1	2
2	1	1	2	2	1	2	1	1	1	2	1	2	2	1	1	2
2	2	1	1	2	1	2	2	1	2	2	1	2	1	1	2	2
1	1	4	1	1	4	1	1	4	1	1	4	1	1	4	1	1
2	1	1	1	1	1	2	2	1	2	2	1	1	1	1	1	2
2	2	1	4	1	1	1	2	1	2	1	1	1	4	1	2	2
1	2	1	1	1	4	1	1	4	1	1	4	1	1	1	2	1
2	2	2	2	1	1	2	1	1	1	2	1	1	2	2	2	2

```
      1    2    1    2    2    1    2    2    2    2    2    1    2    2    1    2    1
% --- Water with 550 ppm boron:
mat water 7.088200E-02 moder lwtr 1001
1001.06c 4.7240E-02
8016.06c 2.3620E-02


mat clad  -7.1  tmp 626        # Fuel Clad - Zircaloy
25055.06c       -1.7E-03
14000.06c       -2.1E-03
24000.06c       -2.2E-01
26000.06c       -0.724
13027.06c       -5.3E-02
39089.06c       -3.00E-04
40000.06c       -5.00E-04

mat fuel  -10.5  tmp 900 burn 3 vol 50.312
8016.09c   -1.185E-01
92235.09c  -4.760E-02
92234.09c  -3.319E-04
92238.09c  -8.336E-01

mat bp  -6.036  tmp 900
Zr-nat.03c  -0.75815
5010.09c    -2.41850E-01

####################### Assembly Geometry ##########################

% --- -assembly ("unit 100"):

surf 1000 sqc 0.0 0.0 10.69
cell 100 0 fill 110 -1000
cell 101 0 outside 1000

# cell 1 0 fill 1 -1
# cell 99 0 outside 1

# --- Assembly cells

# --- Thermal Scattering Data (take all at 600K)
therm lwtr lwe7.12t

####################### Control Information ########################


# Neutron population and criticality cycles

set pop 20000 200 40

# Cross section library file path:

set acelib "/opt/serpent/xsdata/endfb7/sss_endfb7.xsdata"

#added by : decay data path
```

```
set declib "/opt/serpent/xsdata/endfb7/sss_endfb7.dec"

#added by : fission yeild data path
set nfylib "/opt/serpent/xsdata/endfb7/sss_endfb7.nfy"

#added by :
% Options for burnup calculation:

set pcc     1 % Predictor-corrector calc
set xscalc  1 % Cross section from transport
set printm  1 % Material compositions

% --- Isotope list for inventory:
set inventory
541350
922350
922380
942390
942400
942410

# periodic boundary conditions (radial only)
set bc 2

# turn on full unresolved resonance sampling
set ures 1 92235.09c 92238.09c 93237.09c 94238.09c 94239.09c 94240.09c 94240.09c 94241.09c 94242.09c
95241.09c 94242.09c 95241.09c 95342.09c 95243.09c 96244.09c 96245.09c 26426.09c

# Group Constant Homogenization
# set gcu 101 102 103 104 105 106 107 108 109 110 111 112 113 114 115 116 117 118
set nfg 2 0.625e-6
ene egrid 1 1.E-10 0.625E-6 15.0

# random number seed
set seed 1300652262

% Cut-offs:

set fpcut    1E-9
set stabcut  1E-12
set xsfcut   1E-6
% Options for burnup calculation:

set bumode  2 % CRAM method
set pcc     1 % Predictor-corrector calc
set xscalc  1 % Cross section from transport
set printm  1 % Material compositions

set powdens 0.05

dep butot
 0.100
 0.500
 1.000
```

2.000
3.000
4.000
5.000
6.000
7.000
8.000
9.000
10.000
11.000
12.500
15.000
17.500
20.000
22.500
25.000
27.500
30.000
32.500
35.000
37.500
40.000

Bare sphere for critical mass calculations

set title "bare sphere for Th/Pu SiC CMC Clad"

--- Geometry Definitions

mat fuel -19.482 tmp 600
  92232.06c -0.00153
  92233.06c -0.35229
  92234.06c -0.04049
  92235.06c -0.00736
  92236.06c -0.00056
  94238.06c -0.00400
  94239.06c -0.16991
  94240.06c -0.22900
  94241.06c -0.14456
  94242.06c -0.05030
% 95241.06c   -1.30E-03

####################### Assembly Geometry ###########################

% --- -assembly ("unit 100"):

% --- sphere:
surf 1 sph 0.000 0.000 0.000 5.92

cell 1 0 fuel -1 % plutonium inside surface 1
cell 2 0 outside 1 % outside world

################### Control Information #########################

Neutron population and criticality cycles
set pop 100000 200 40

Cross section library file path:
set acelib "/opt/serpent/xsdata/endfb7/sss_endfb7.xsdata"

#: decay data path
set declib "/opt/serpent/xsdata/endfb7/sss_endfb7.dec"

fission yeild data path
set nfylib "/opt/serpent/xsdata/endfb7/sss_endfb7.nfy"

% Options for burnup calculation:

set pcc   1 % Predictor-corrector calc
set xscalc 1 % Cross section from transport
set printm 1 % Material compositions

% --- Isotope list for inventory:
set inventory
541350
922350
922380
942390
942400
942410

periodic boundary conditions (radial only)
set bc 1

turn on full unresolved resonance sampling
set ures 1 92235.09c 92238.09c 93237.09c 94238.09c 94239.09c 94240.09c 94240.09c 94241.09c 94242.09c
95241.09c 94242.09c 95241.09c 95342.09c 95243.09c 96244.09c 96245.09c 26426.09c

Group Constant Homogenization
set gcu 101 102 103 104 105 106 107 108 109 110 111 112 113 114 115 116 117 118
set nfg 2 0.625e-6
ene egrid 1 1.E-10 0.625E-6 15.0

random number seed
set seed 1300652262

% Cut-offs:

set fpcut   1E-9
set stabcut 1E-12
set xsfcut   1E-6

Appendix B: Duplex Fuel Pellets for Breeding in a UN-Fueled PWR

The primary limitation of the tight-lattice PWR breeder design explored in this work is pin peaking, which leads to a violation of the mDNBR safety criterion. The primary contributors to this large pin-peaking are the presence of a blanket pins that generate essentially no power and the internal axial blanket, which also has very low power. In order to limit this pin-peaking an alternative fuel pellet design was examined. In this "duplex" design, the outer part of the fuel pellet is entirely plutonium, while the interior is entirely depleted uranium.

The assembly modeled contained 91 pins of 95% theoretical density uranium nitride with the same geometry used in the analysis in Chapter 7. This design contains six rows in a hexagonal tight-lattice assembly, compared to the 18 used previously. This smaller assembly size is also a benefit. The axial breakdown of the assembly can be seen in Table B-1.

Table B-1: Axial regions of 91-pin fuel tight-lattice UN fuel assembly with duplex fuel pellets

Region	Height cm
Upper Simulation Boundary (Non-Reflective)	-
Upper Plenum Region	30
Upper Axial Blanket	30
Fissile Region	290
Lower Axial Blanket	30
Lower B4C Layer	7
Lower Water Reflector	23
Lower Simulation Boundary (Non-Reflective)	-

Only a scoping neutronic study was performed. This was done to demonstrate the feasibility of a uniform assembly with only duplex fuel pellets in maintaining an FIR above 1.0. For this study 200 cycles of 10,000 neutrons were run, with the first 20 being discarded. The depletion was performed at 1.9 MW of assembly power, which was based on a scaling of the maximum allowable power of the other designs explored in this work. The FIR of the design at a burnup of

20 MWd/kgHM was found to be 1.0069. This indicates that this design should see further analysis to explore its viability for breeding. In the future, T/H and safety analysis will need to be performed. The uniformity of the design is projected to allow for a higher overall core power than other tight-lattice breeding designs. Axial and radial reaction rate plots for this assembly can be seen in Figure B-1.
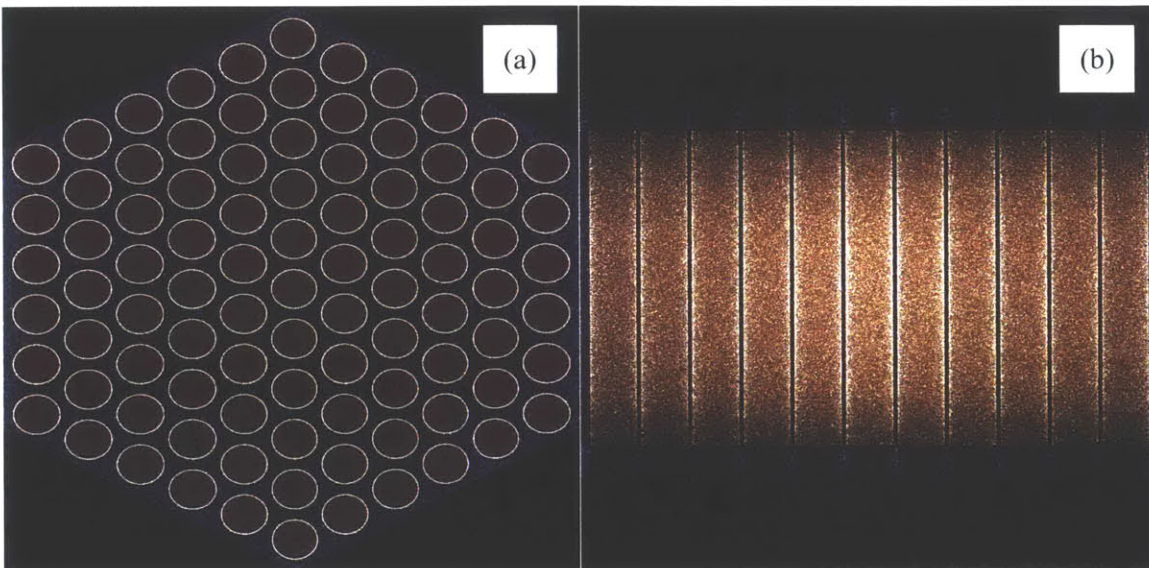

Figure B-1: (a) Radial and (b) axial reaction rate plot of 91 pin hexagonal tight-lattice assembly with duplex fuel pellets

The primary drawback to using a duplex fuel pellet is the fact that nearly all of the fuel pin degradation from increased burnup occurs in the outer fueled region. In future analyses, a maximum allowable burnup of this region will need to be determined.

Appendix C: Isotopics of Plutonium-burning Oxide Fuel after 10 Years of Cooling

After fuel is discharged from a reactor, it must undergo a cooling period before it can be transported. During this cooling period, the isotopic composition of the fuel changes due to nuclear interactions and decay. The resultant plutonium and uranium composition after this cooling period of the different designs examined can be seen in Table C-1. The compositions at discharge, which are presented in Chapter 4, are once again shown for comparison purposes in Table C-2. It can be seen that there is more Pu-239 and U-233, while less Pu-241 after cooling.

Table C-1: Uranium and plutonium composition at batch average discharge after 10 years of cooling for plutonium burning core designs

Isotope	U/Pu Zircaloy	U/Pu SiC CMC	Th/Pu Zircaloy	Th/Pu SiC CMC
U-232	-	-	0.1	0.1
U-233	-	-	37.3	38.9
U-234	-	-	3.8	4.2
U-235	-	-	0.7	0.8
U-236	-	-	0.1	0.1
Pu-238	0.6	0.7	0.5	0.6
Pu-239	56.8	52.5	21.6	17.4
Pu-240	29.0	31.5	22.9	23.6
Pu-241	10.1	10.8	8.9	9.1
Pu-242	3.5	4.5	4.2	5.2

Table C-2: Uranium and plutonium composition at batch average discharge for plutonium burning core designs

Isotope	U/Pu Zircaloy	U/Pu SiC CMC	Th/Pu Zircaloy	Th/Pu SiC CMC
U-232	-	-	0.1	0.2
U-233	-	-	33.9	35.2
U-234	-	-	3.6	4.0
U-235	-	-	0.7	0.7
U-236	-	-	0.0	0.1
Pu-238	0.4	0.5	0.4	0.4
Pu-239	53.4	49.2	21.0	17.0
Pu-240	27.4	29.5	22.3	22.9
Pu-241	15.4	16.6	14.0	14.5
Pu-242	3.3	4.2	4.1	5.0